Lecture Notes in Civil Engineering

Boominathan Adimoolam
Subhadeep Banerjee *Editors*

Soil Dynamics and Earthquake Geotechnical Engineering

IGC 2016 Volume 3

Springer

Lecture Notes in Civil Engineering

Volume 15

Lecture Notes in Civil Engineering (LNCE) publishes the latest developments in Civil Engineering - quickly, informally and in top quality. Though original research reported in proceedings and post-proceedings represents the core of LNCE, edited volumes of exceptionally high quality and interest may also be considered for publication. Volumes published in LNCE embrace all aspects and subfields of, as well as new challenges in, Civil Engineering. Topics in the series include:

- Construction and Structural Mechanics
- Building Materials
- Concrete, Steel and Timber Structures
- Geotechnical Engineering
- Earthquake Engineering
- Coastal Engineering
- Hydraulics, Hydrology and Water Resources Engineering
- Environmental Engineering and Sustainability
- Structural Health and Monitoring
- Surveying and Geographical Information Systems
- Heating, Ventilation and Air Conditioning (HVAC)
- Transportation and Traffic
- Risk Analysis
- Safety and Security

To submit a proposal or request further information, please contact the appropriate Springer Editor:

- Mr. Pierpaolo Riva at pierpaolo.riva@springer.com (Europe and Americas);
- Ms. Swati Meherishi at swati.meherishi@springer.com (India);
- Ms. Li Shen at li.shen@springer.com (China);
- Dr. Loyola D'Silva at loyola.dsilva@springer.com (Southeast Asia and Australia/NZ).

More information about this series at http://www.springer.com/series/15087

Boominathan Adimoolam
Subhadeep Banerjee
Editors

Soil Dynamics and Earthquake Geotechnical Engineering

IGC 2016 Volume 3

Springer

Editors
Boominathan Adimoolam
Department of Civil Engineering
Indian Institute of Technology Madras
Chennai, Tamil Nadu
India

Subhadeep Banerjee
Department of Civil Engineering
Indian Institute of Technology Madras
Chennai, Tamil Nadu
India

ISSN 2366-2557 ISSN 2366-2565 (electronic)
Lecture Notes in Civil Engineering
ISBN 978-981-13-0561-0 ISBN 978-981-13-0562-7 (eBook)
https://doi.org/10.1007/978-981-13-0562-7

Library of Congress Control Number: 2018941216

Printed on acid-free paper

This Springer imprint is published by the registered company Springer Nature Singapore Pte Ltd.
part of Springer Nature
The registered company address is: 152 Beach Road, #21-01/04 Gateway East, Singapore 189721, Singapore

Foreword

The Indian Geotechnical Society (IGS) was started as the Indian National Society of Soil Mechanics and Foundation Engineering in the year 1948, soon after the Second International Conference on Soil Mechanics and Foundation Engineering held at Rotterdam. The Society was affiliated to the International Society in the same year, and since then, it has strived to fulfil and promote the objectives of the International Society. In December 1970, the name 'Indian Geotechnical Society (IGS)' was adopted.

The Society conducted several symposia and workshops in different parts of India since its inception in 1948. In the year of 1983, the Indian Geotechnical Society organized its first annual conference IGC 1983 in Indian Institute of Technology Madras.

Several local chapters of the Society were established over the years, and gradually, the annual conferences were held in different cities under the leadership of the respective local chapters. The conferences were well utilized as the venue for showcasing the research works and the case studies on geotechnical engineering and geoenvironmental engineering, and the papers presented during the deliberations were being published as conference proceedings volume.

The annual conferences IGC 1996 and IGC 2006 were organized by IGS Chennai Chapter, and the papers were published as printed volumes. The practice of printing the volumes was later discontinued in view of large expenditure involved and also because of the easy access to the electronic storage media. The papers then became not accessible to the rest of the geotechnical community.

The responsibility of organizing the annual conference of 2016 was taken up by IGS Chennai Chapter, and the conference was held during 15–17 December 2016. It was felt necessary to publish selected papers for the benefit of the entire geotechnical engineering community as well as of the contributing authors. The Chapter approached Springer with a request to take up this responsibility, and with the great help of Springer, about 150 selected papers are being published in four volumes under the series 'Lecture Notes in Civil Engineering'. The selected papers are distributed among these volumes depending upon the topic of discussion.

Volume 1: Geotechnical Characterisation and Geoenvironmental Engineering
Volume 2: Ground Improvement Techniques and Geosynthetics
Volume 3: Soil Dynamics and Earthquake Geotechnical Engineering
Volume 4: Geotechnical Applications

I am thankful to all the general editors and the reviewers of these papers who provided valuable review comments for the betterment of the papers published in these volumes. The support provided by the former President of the Indian Geotechnical Society, the late Prof. Sreerama Rao, and the former Honorary Secretary of IGS, Shri Jai Bhagwan, is gratefully acknowledged here.

Bringing out these volumes under the banner of prestigious publishers, Springer will immensely improve the visibility of these conference proceedings volumes. The Chennai Chapter of the Indian Geotechnical Society places on record its acknowledgement of the efforts put forth by Springer for bringing out these volumes for the benefit of the geotechnical engineering community.

Chennai, India

Prof. Boominathan Adimoolam
Chairman, Indian Geotechnical
Conference 2016
Department of Civil Engineering IIT Madras

Preface to Volume 3

There are about 29 papers in this volume covering various aspects of *Soil Dynamics and Earthquake Geotechnical Engineering*. India has a wide variety of natural features and is under a constant risk of being hit by disasters involving dynamic loadings such as earthquakes, winds, man-made blasting, waves, traffic loadings. Recent events like the Sikkim earthquake in 2011 and the Nepal earthquake in 2015 had catastrophic effects on the region, resulting in a high death toll and loss of public property. India has seen a booming development in infrastructure in the recent years. Though measures have been taken to strike a balance between nature and development, unavoidably some disasters have been accelerated by these developments. Moreover, in India, there are numerous types of geological and geotechnical conditions encountered. For example, most of the major cities in India are concentrated near or along the coastline. The coastal plains of India consist of predominantly marine clays ranging in thickness of 2–10 m. As a result, many important inland and offshore structures such as bridges, port and harbours, tall structures like liquid storage tanks and chimneys in those areas are built overlying soft to medium stiff marine clay. In such situations, the behaviour of those structural systems under earthquake loading is an important factor affecting the integrity of infrastructures. On the other hand, the entire Indo-Gangetic plain comprises of fine silts and sands which are extremely vulnerable against liquefaction. All these reasons warrant the relevance of the theme of the present volume which includes a wide range of studies on seismic response of dams, foundation–soil systems, natural and man-made slopes, reinforced earth walls, base isolation systems. Moreover, there are papers reporting some of the allied issues such as landslide risk assessments, liquefaction mitigation, dynamic analysis of mechanized tunnelling, advanced seismic soil–structure interaction analysis. In summary, the present volume covers length and breadth of the area of *Soil Dynamics and Earthquake Geotechnical Engineering*.

We thank the technical committee of IGC 2016 for giving us the responsibility to be editors for this volume of the Springer Proceedings.

Chennai, India

Dr. Boominathan Adimoolam
Dr. Subhadeep Banerjee
General Editors

Contents

About the Editors

Prof. Boominathan Adimoolam received his Ph.D. in soil dynamics from Moscow Civil Engineering Institute in 1986. He worked as a CSIR Scientific Pool Officer at the Ocean Engineering Centre, Indian Institute of Technology (IIT) Madras, in 1987. Since 1988, he has been a faculty member of the Geotechnical Engineering Division at the Indian Institute of Technology Madras. His fields of specialization include soil dynamics and earthquake engineering, foundation engineering and ground improvement. He has long since been actively involved in the area of site-specific seismic hazard assessment, which includes seismological, geophysical and geotechnical considerations. He has completed nine sponsored research projects worth roughly Rs. 1.5 crores and is currently coordinating major research projects funded by the Ministry of Earth Sciences of Government of India and the Nuclear Power Corporation of India (NPCIL), Mumbai, in the area of seismic soil–structure interaction and base isolation using geoisolators. He has authored and co-authored over 130 scientific papers and serves as an editorial board member of Journal of Earthquake and Tsunami. He was part of a working group of experts in the Geohazards programme of the National Disaster Management Authority (NDMA), Government of India. He received the IGS-Shri M. S. Jain Biennial Prize in 2004 and IGS-Prof. C. S. Desai Biannual Prize in 2012.

Dr. Subhadeep Banerjee is an associate professor of geotechnical engineering in the Department of Civil Engineering, Indian Institute of Technology Madras. He received his Ph.D. in civil engineering from the National University of Singapore. His research interests include cyclic behaviour of geomaterials, seismic soil–structure interactions and finite element analysis of complex dynamic problems. In addition, he is an expert for constitutive modelling of soils, with a special focus on transient dynamic behaviour. At the IIT Madras, he has formed three research groups to study the following attributes: (i) cyclic characterization of various types of natural soils, improved ground, landfills, etc., (ii) development of constitutive

models of soils, with an emphasis on their performance under seismic loadings and (iii) application of fundamentals of dynamics to various complex soil–structure problems such as tunnelling, base isolation techniques, plate anchors, retaining walls.

Part I
Soil Dynamics and Earthquake Geotechnical Engineering

Effect of Dynamic Loading on Properties of Saturated Sand

D. Devi Priyanka, Deepak Rathi and G. K. Kumar

Abstract Liquefaction has become one of the most important and interesting topics in the field of geotechnical earthquake engineering. Also, its study became a part and parcel of seismic microzonation considering its severity. The devastation brought by it due to earthquakes of Niigata (Japan), Bhuj (India), Nepal has turned the spotlight on the seriousness with which this hazard has to be considered. So, in the present study, a comprehensive experimental program was undertaken in which a series of strain-controlled cyclic triaxial tests were performed to evaluate the liquefaction resistance of local sand in Warangal. Tests were carried out at relative densities, i.e., 35, 50, and 65%, and reduction in pore pressure with increase in relative density was observed. Similarly, confining pressures of 100 and 150 kPa for amplitudes ranging from 0.08 to 1% were also considered. From the results, it was also observed that higher confining pressures resulted in decrease in pore pressure whereas higher amplitude of loading resulted in a rise in pore pressure. This proved that densification or increasing confining pressure improves resistance against liquefaction which can be considered as the cheapest soil improvement technique to mitigate liquefaction hazards in unconstrained areas.

Keywords Liquefaction · Cyclic triaxial test · Strain-controlled Pore pressure ratio

D. Devi Priyanka (✉)
Department of Civil Engineering, Indian Institute of Technology Hyderabad, Hyderabad, India
e-mail: devipriyanka422@gmail.com

D. Rathi · G. K. Kumar
Department of Civil Engineering, National Institute of Technology, Warangal, India
e-mail: deepakrathi.mmec@gmail.com

G. K. Kumar
e-mail: kalyan@nitw.ac.in

B. Adimoolam and S. Banerjee (eds.), *Soil Dynamics and Earthquake Geotechnical Engineering*, Lecture Notes in Civil Engineering 15,
https://doi.org/10.1007/978-981-13-0562-7_1

1 Introduction

Construction of structures like buildings, foundations on loose granular soils (like sands) has become a tough task in earthquake-prone areas. This is due to the fact that behavior of soil under static loading is different from dynamic loading. Several areas in India such as Kashmir, Himalayas, Bihar, Northeast region are frequently prone to earthquakes. Moreover, the recent earthquakes like Bhuj, 2001 and Nepal earthquake (2015) which were the most destructive earthquakes in India in the last 50 years had caused huge damage. The reconnaissance carried by many people showed that those earthquakes were characterized by widespread liquefaction that caused sand volcanoes, ground cracking, lateral spreading, etc. Not only these, there are many other cases also in the past where severe havoc was seen due to induced liquefaction during earthquakes (Seed and Idriss 1967; Sitharam et al. 2004; Boulanger et al. 1997). This resulted in evaluation of liquefaction potential by several researchers either by stress-based (Seed and Idriss 1971; Seed 1979) or strain-based (Sitharam et al. 2012) approaches. The advantage in adopting a strain-based approach is the total or partial replacement of parameters influencing soil properties like method of sample preparation, lateral earth pressure coefficient by the shear modulus in calculation of shear strains (Dobry et al. 1982). A field measurement of shear modulus (G_{max}) automatically incorporates many of the soil characteristics which are necessary for pore pressure buildup during earthquakes. Thus, this approach decreases the need for a detailed knowledge of the site which is essential in the stress-based approach. There are many ways to mitigate liquefaction of which densification is the cheapest technique (Menard and Broise 1975; Lyman 1942). So, in the present work, an attempt is made in the laboratory to study the liquefaction potential of locally available sand in Warangal and determine the effect of parameters like amplitude of loading, confining pressure, and relative density on dynamic soil behavior.

2 Experimental Program

2.1 Soil Sampling

The sand used in this study was collected from the surroundings of Warangal, Telangana, India. Tests were performed as per IS code to obtain the basic index properties as listed in Table 1. The gradation curve of the soil is shown in Fig. 1. It is clear from the properties that sand under consideration is poorly graded.

Table 1 Index properties of sand

Property	Value
Specific gravity	2.63
Maximum void ratio	0.98
Minimum void ratio	0.62
D10 (mm)	0.2
D30 (mm)	0.32
D60 (mm)	0.43
Coefficient of uniformity (Cu)	2.15
Coefficient of curvature (Cc)	1.19
Soil classification	SP

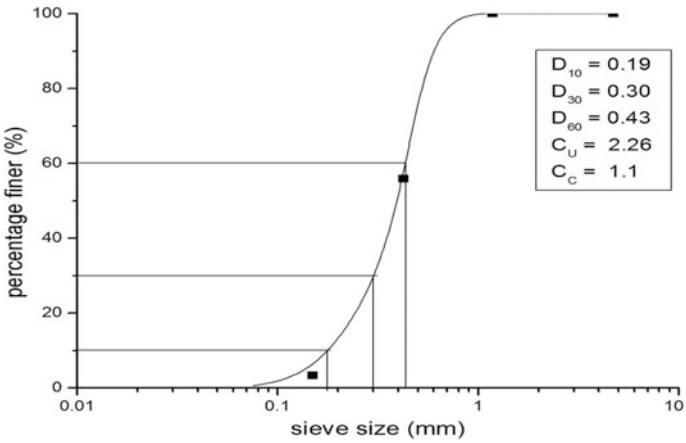

Fig. 1 Grain size distribution of sand used

2.2 *Test Methodology*

Specimens of 7.5 cm diameter and 15 cm height were reconstituted in the laboratory as explained below, and a series of strain-controlled tests were carried as listed in Table 2 for evaluation of liquefaction potential and also to determine effect of various parameters. Basically, each test comprises of three segments, i.e., saturation followed by sample preparation, consolidation, and testing stage.

2.2.1 Saturation

A calculated amount of clean dry soil was taken based on considered relative density for the preparation of sample using water sedimentation technique (Ishihara 1996).

Table 2 List of tests performed

Test no.	Dr (%)	Strain (%)	B	Eff. confining pressure (kPa)
1	50	0.02	0.95	100
2	50	0.06	0.96	100
3	50	0.20	0.95	100
4	50	0.50	0.95	100
5	50	1.00	0.96	100
6	50	0.06	0.96	150
7	50	0.20	0.94	150
8	50	0.50	0.95	150
9	50	1.00	0.95	150
10	35	0.50	0.95	100
11	65	0.50	0.96	100

Later, drainage lines are connected and saturation was carried with the aid of back pressure by maintaining initial net effective stress on the specimen. Full saturation was assumed to be achieved for B values (= $\Delta u/\Delta\sigma_c$) of 0.96 or higher. After attaining it, consolidation stage was initiated. Time taken for this saturation depends on degree of denseness of sample which increases with density of sample.

2.2.2 Consolidation

During consolidation, initially both confining and back pressure valves were closed and test pressures were given maintaining required net effective stress. Later, volume change was allowed which initiates the process of consolidation and is recorded with time. A constant line in volume change versus time graph after some time indicates the completion of consolidation stage.

2.2.3 Cyclic Loading (ASTM D5311)

After consolidation, test was carried at certain frequency (*f*), amplitude for a given number of cycles (*N*). All the tests were carried at a frequency 1 Hz as suggested by ASTM D5311. As test is being carried under strain approach, amplitude of loading is given in mm. Test was stopped after noticing a pore pressure almost equal to confining pressure as it indicates the stage of liquefaction. Then, results were analyzed and compared with other tests for conclusions.

3 Results and Discussion

A series of undrained triaxial tests were performed as listed in Table 2. Result of test performed on a specimen subjected to 0.5% strain (ε) for 100 cycles is as shown in Fig. 2. It indicates that with increase in number of cycles, pore pressure builds up and results in decrease of shear stress and stiffness of the specimen which can be noticed by flattening of hysteresis loop. Complete flattening of loop indicates that soil cannot take load anymore which shows that soil is liquefied.

3.1 Effect of Shear Strain and Number of Cycles

With an assumption that soil under consideration possess a Poisson's ratio (v) of 0.3 at a 50% relative density (D_r), tests were conducted at strains of 0.06, 0.2, 0.5, and 1% which corresponds to cyclic shear strains (γ_c) of 0.07, 0.26, 0.65, and 1.3% and results were analyzed. To better evaluate the effect of strain, excess pore pressure ratio (r_u) versus shear strain is considered for different loading cycles (N). These curves illustrate generation of pore pressure by each loading cycle and are called pore pressure generation curves. They also showed that r_u is a function of γ_c and N which can be seen in Figs. 3 and 4 at different consolidation stresses. The difference between the r_u values of first and last cycles shows the influence of loading cycles on pore pressure and indicates potential of pore pressure that could develop at a given shear strain. Once liquefaction triggers, the curve flattens and this difference decreases. At lower strains ($\gamma_c < 0.03\%$), pore pressure difference

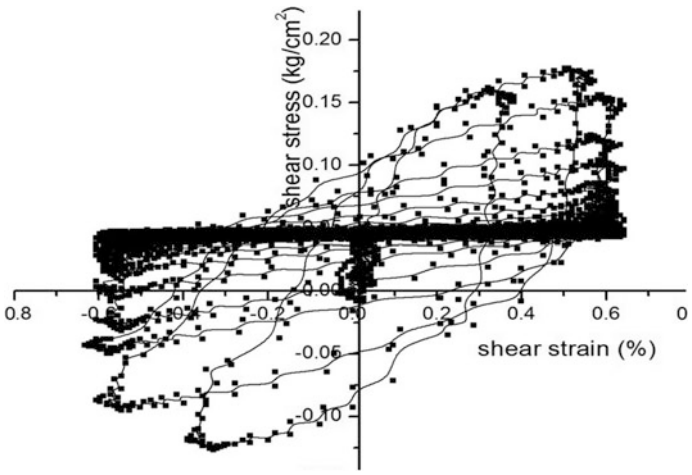

Fig. 2 Variation shear stress versus shear strain for a test at $\varepsilon = 0.5\%$, f = 1 Hz, D_r = 50%, σ_c' = 100 kPa

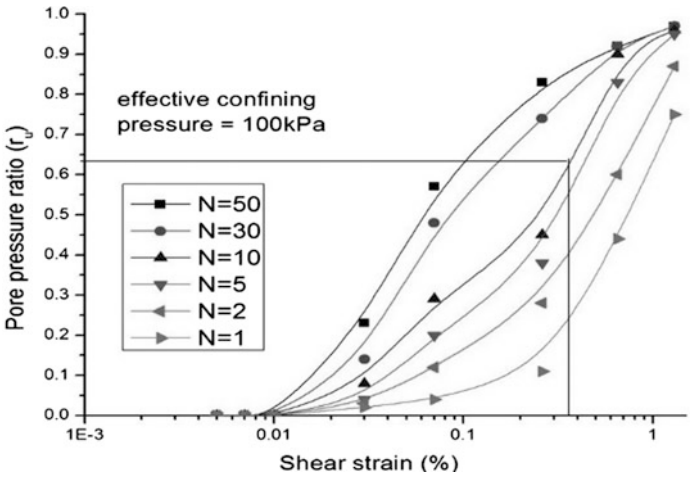

Fig. 3 Variation of r_u with γ_c at σ_c' = 100 kPa, relative density of 50%, and frequency 1 Hz

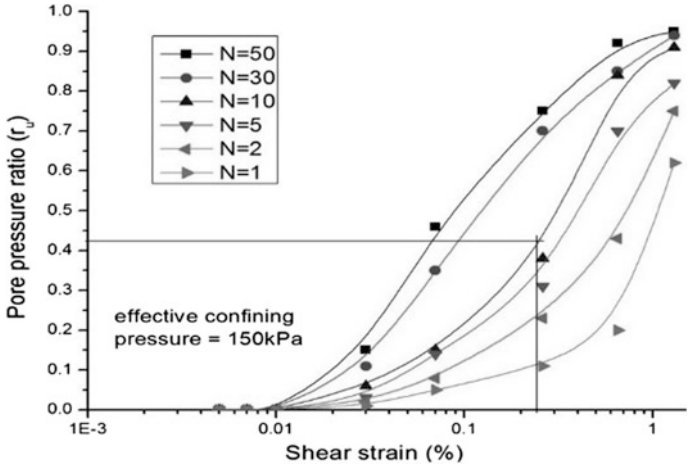

Fig. 4 Variation of pore pressure ratio with cyclic shear strain at σ_c' = 150 kPa, D_r of 50%, and frequency 1 Hz

between first and last cycles is smaller. With increase in γ_c, there is significant rise in pore pressure generation for the specimen consolidated to 100 kPa (Fig. 3), and the largest difference was observed at γ_c of 0.1%, whereas at 150 kPa, the influence region shifted to higher strains, as shown in Fig. 4 implying that the number of cycles is more influential for pore pressure buildup at high strains.

3.2 *Effect of Confining Pressure*

In the field, each depth corresponds to different consolidation stresses. So, it is essential to know the effect of confining pressure in the laboratory which accounts for depth effect in the field. For present work, two different consolidation stresses (100, 150 kPa) were considered. Dobry, 1985 performed similar tests on various sands using different specimen preparation techniques, relative densities, confining stresses and provided upper and lower bounds as shown in Fig. 5. From our present work, at a confining pressure of 100 kPa and 10 cycles, it is noticed that there is a reasonable agreement between the results obtained with the lower bound curve. Results also showed that significant pore pressure development for $\gamma_c < 0.01\%$, suggesting a threshold shear strain of 0.01%, which agrees with Dobry's results for clean sands. Similarly, tests were performed at 150 kPa and results are presented (Fig. 6), which shows 10% deviation in r_u for a smaller increment of σ_c', i.e., 50 kPa. At higher increments, more decrease in r_u can be noticed.

Moreover, the influence of the consolidation stress on pore pressure ratio is not very significant at lower ($\gamma_c < 0.03\%$) and higher ($\gamma_c > 1\%$) strain levels. More reduction in pore pressure was seen in the middle range strains. It is important to note that specimens consolidated to 150 kPa also did not produce any excess pore pressure for $\gamma_c < 0.01\%$ showing that threshold shear strain is not influenced by σ_c' between 100 and 150 kPa.

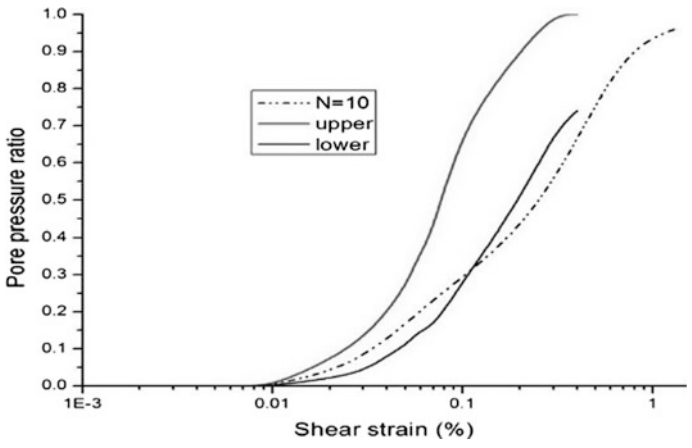

Fig. 5 Variation of pore pressure with shear strain at σ_c' = 100 kPa, D_r of 50%, and frequency 1 Hz for ten cycles

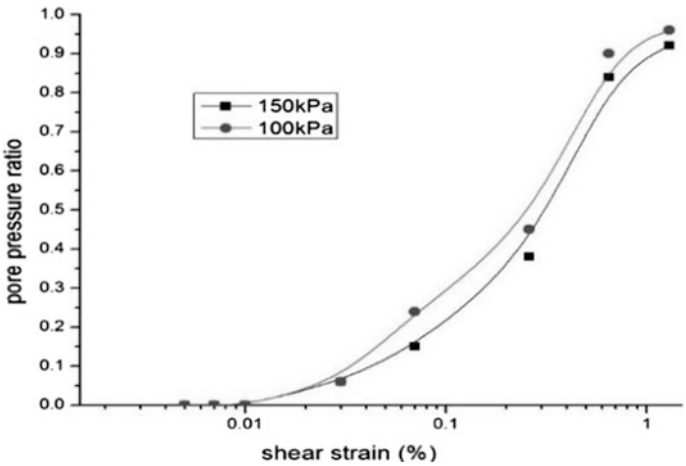

Fig. 6 Variation of pore pressure ratio with shear strain at different consolidation stresses for ten cycles

3.3 Effect of Relative Density

Tests were also carried out on samples at relative densities of 35, 50, and 65% by varying strains. Each test was terminated after reaching initial liquefaction and analyzed for results. The comparison of pore pressure generated for loose and medium dense specimens at a γ_c of 0.65% with number of cycles is as shown in Fig. 7. This showed that specimens prepared at lower densities generate higher pore

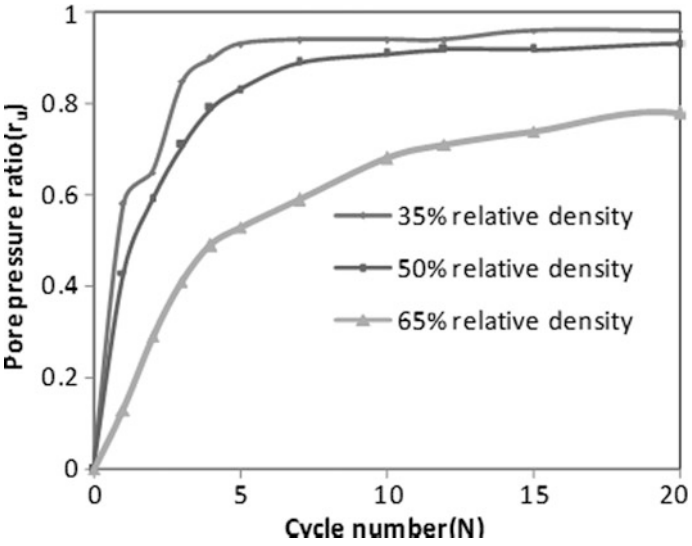

Fig. 7 Variation of pore pressure ratio with cycles at different relative densities

pressure compared to medium dense specimens indicating that liquefaction potential for looser sand deposits is high. This is due to the fact that loose specimens possess more voids filled with water which under load application in undrained conditions results in high pore pressure generation.

4 Conclusions

The following conclusions were drawn based on the investigations carried on saturated sands.

- In cases where site-specific data is incomplete, strain-based approach can be used comfortably.
- Increase in confining pressure results in reduction in excess pore pressure development during cyclic loading. But for strains less than 0.03%, no clear development of pore pressures was observed over the confining pressure range of 100–150 kPa.
- As amplitude of loading or number of cycles increases, the excess pore pressure also raises resulting in the loss in shear strength and stiffness of specimen and leading to failure by liquefaction.
- Threshold shear strain is not influenced by effective confining pressure in a range of 100–150 kPa.
- The higher the relative density more will be liquefaction resistance suggesting densification as one of the methods to mitigation liquefaction hazards.

References

ASTMD5311 M-13. (2013). Standard test method for load controlled cyclic triaxial strength of soil, pp. 1–11.

Boulanger, R., Meija, L., & Idriss, I. (1997). Liquefaction at moss landing during Loma Prieta earthquake. *Journal of Geotechnical and Geoenvironmental Engineering, ASCE, 123,* 453–467.

Dobry, R., Ladd, R. S., Yokel, F. Y., Chung, R. M., & Powell, D. (1982), Prediction of pore water pressure buildup and liquefaction of sands during earthquakes by the cyclic strain method. *National Bureau of Standards Building Science Series 138*, pp. 150.

Ishihara, K. (1996). *Soil behavior in earthquake geotechnics* (1st ed., p. 350). Oxford: Clarendon Press.

Lyman, A. K. B. (1942). Compaction of cohesion less foundation soils by explosives. *Transactions ASCE*, pp. 1330–1348.

Menard, L., & Broise, Y. (1975). Theoretical and practical aspects of dynamic consolidation. *Géotechnique, 15,* 3–18.

Seed, H. B., & Idriss, I. M. (1967). Analysis of soil liquefaction: Niigata earthquake. *Journal of the Soil Mechanics and Foundation Division ASCE, 93,* 83–108.

Seed, H. B., & Idriss, I. M. (1971). Simplified procedure for evaluating soil liquefaction potential. *Journal of the Soil Mech and Foundations Division, ASCE, 97*(9), 1249–1273.

Seed, H. B. (1979). Soil liquefaction and cyclic mobility evaluation for level ground during earthquakes. *Journal of the Geotechnical Engineering Division, ASCE, 105*(GT2), 201–255.

Sitharam, T. G., Govinda Raju, L., & Srinivasa Murthy, B. R. (2004). Cyclic and monotonic undrained shear response of silty sand from Bhuj region in India. *ISET Journal of Earthquake Technology, 41*(2–4), 249–260, paper 450.

Sitharam, T. G., Ravishankar, B. V., & Patil, S. M. (2012). Liquefaction and pore water pressure generation in sand: Cyclic strain controlled triaxial tests. *IJGEE, 3*(1), 57–85.

A Study on Mitigation of Tilting Problems in Liquefiable Soil

Puja Dutta and Ashim Kanti Dey

Abstract Tilting of foundations during liquefaction of soil is one of the primary concerns for stability of structures constructed in saturated sand in seismically active areas. Niigata earthquake resulted in tilting of a number of buildings. Once tilted, the structure is to be dismantled. Tilting also results in loss of life and property. The main aim of this study is to restrict tilting and allow the structure to float on liquefied soil. During a high-magnitude earthquake, the structure may not float for a long time, but may sink instead of tilting. Archimedes principle has been applied in the present study. The shape of conventional rectangular footing is changed to spherical and trapezoidal section. Shake table tests were performed at different frequencies like 0.5, 1 and 1.5 Hz. Comparisons of tilting and sinking of all the three types of footings were performed. Accelerations imposed on the footings were also measured. Results showed a positive response for a footing with spherical cross sections.

Keywords Liquefaction · Tilting of foundation · Shake table test

1 Introduction

A lot of studies have been carried out on seismic performance of shallow foundations resting on saturated sand (Liu and Dobry 1997; Knappett et al. 2004; Dunga et al. 2006, and so on). Post-liquefaction deformations have also been reported (Shamoto et al. 1996). Most of these deformations result in tilting of buildings. Once tilted, the structure cannot be reverted back to its original position. However, no study has been reported to withstand the tilting deformation during liquefaction

P. Dutta (✉) · A. K. Dey
Civil Engineering Department, National Institute of Technology, Silchar 788010, India
e-mail: puja.dutta11121990@gmail.com

A. K. Dey
e-mail: ashim_kanti@yahoo.co.in

B. Adimoolam and S. Banerjee (eds.), *Soil Dynamics and Earthquake Geotechnical Engineering*, Lecture Notes in Civil Engineering 15,
https://doi.org/10.1007/978-981-13-0562-7_2

of soil. The present study consists of laboratory model tests on specially designed footings to withstand the deformations. One-dimensional shake table tests were conducted to observe the deformations of the footings at different frequencies. It is observed that sinking of footings could not be avoided at higher frequency but tilting deformation could be avoided. Uniform settlement can be accepted like most of the buildings in Mexico City.

2 Methodology

The basic concept consists of modifying the geometrical shape of footing so that during liquefaction of soil the modified footing displaces enough liquefied soil for floating stability. This is achieved by designing the bottom surface of the footing in the form of spherical or trapezoidal. In order to reduce the self-weight of the footing, the midsection of the footing is kept void. Three footings of identical plan area were considered for the present study—conventional rectangular cross section, top flat and bottom spherical cross section, top flat and bottom trapezoidal cross section. Although all the tests were carried out in the laboratory, for designing the shape of the models, a prototype plan of length = 5.5 m and width = 2.1 m was considered initially.

For designing a spherical section in both directions, first a spherical surface was generated along transverse direction. The surface equation was considered to be parabolic, i.e.

$$f(x) = ax^2 + c \tag{1}$$

The surface equation was obtained considering Archimedes principle for floating stability. Theoretically, for any submerged body, the Metacentric height is calculated as,

$$\mathrm{GM} = \mathrm{BM} - \mathrm{BG} \tag{2}$$

where G is the centre of gravity of the submerged body, M is the Metacentric position, and B is the centre of buoyancy.

BM = Ratio of moment of inertia of the cross-sectional area of the submerged body at the liquid surface about its longitudinal axis and volume of liquid displaced by the submerged body.

$$\mathrm{BM} = \mathrm{I}/\mathrm{V} \tag{3}$$

where I (Moment of inertia of the body at liquid surface of spherical section) = $1/12 \times 5.5 \times 2.1^3 = 4.244\ \mathrm{m}^4$.

For a structure to be in stable equilibrium, GM > 0.

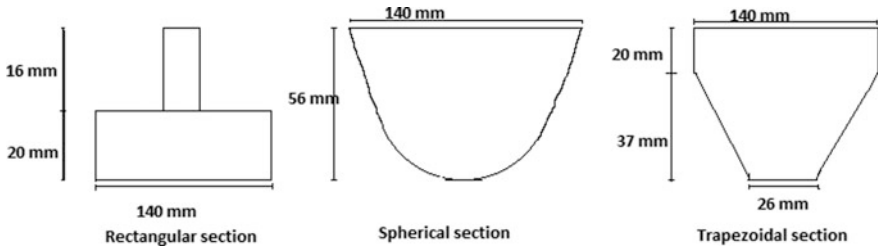

Fig. 1 Cross sections of model footings

And moreover, it was assumed that weight of the fluid displaced by spherical section is more than the rectangular section.

Weight of fluid displaced = Unit weight of fluid × volume of fluid displaced. The unit weight of fluid considered in this work is 14 kN/m^3. The unit weight of fluid is higher than water, because during liquefaction the density of the liquid is more than that of water.

It was proposed to maintain volume of fluid displaced by modified footing > volume of fluid displaced by the conventional rectangular footing.

Satisfying the above equations, a parabolic surface has been achieved for spherical footing: $f(x) = 0.581x^2 - 0.845$ (x in metres), along the transverse direction. Along the longitudinal direction, the depth of footing remains constant till 2.328 m from the centre on both sides and then depth starts decreasing with rate given by the equation $f(x) = 0.024x^2 - 0.460$. Similarly by taking the assumption of GM (for trapezoidal) > GM (for rectangular), a section was obtained for trapezoidal footing with height 0.85 m and width 2.1 m.

For the present model test, a linear scaling factor was adopted as suggested by Harris and Sabnis in the second edition of 'Structural Modeling and Experimental Techniques' (CRC Press, Taylor and Francis Group, 2nd edition, 1999). Linear scaling of length, width and height for model was taken in the ratio of 0.067 of the prototype. Models were prepared with concrete and string rods as reinforcement for footings. A general outline of the footings is shown in Fig. 1. The outline of the cross section was obtained by making two transverse beams and one longitudinal beam passing through the columns. A combined footing with two columns was adopted for the study. Figure 2 shows the reinforcement cage made of string rods.

The spherical-shaped footing with internal void space is shown in Fig. 3. One additional concrete cover was placed on the top of the footing.

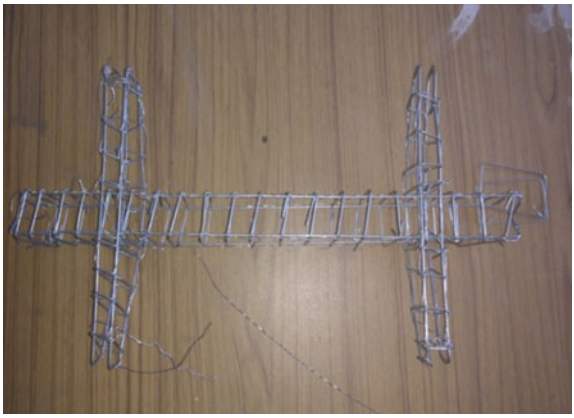

Fig. 2 Reinforcement cage

Fig. 3 Modified footing with voids inside

3 Experimental Set-up

A steel tank of dimension 1 × 1 × 1 m was filled up to 0.9 m with a required quantity of dry sand for achieving a relative density around 50%. Water was slowly poured in the tank so that the sand became fully saturated. The tank was connected with the shake table, and harmonic loading was imparted at a frequency of 0.5, 1 and 1.5 Hz. Footing was placed on the sand with zero depth of foundation. Four accelerometers were connected as shown in Fig. 4, two on the footing and two on the tank in vertical and horizontal directions to record the acceleration time history.

Figures 5, 6 and 7 show the peak vertical acceleration imposed on the footing against time at 0.5, 1.0 and 1.5 Hz frequency, respectively. In all the cases, it is observed that the peak vertical acceleration of the rectangular conventional footing is the highest and that of the spherical footing is the lowest. Figures 8, 9 and 10 show the peak horizontal acceleration imposed on the footing against time at 0.5, 1.0 and 1.5 Hz frequency, respectively. In all the cases, it is observed that the peak

Fig. 4 Accelerometers placed both vertically and horizontally at column face

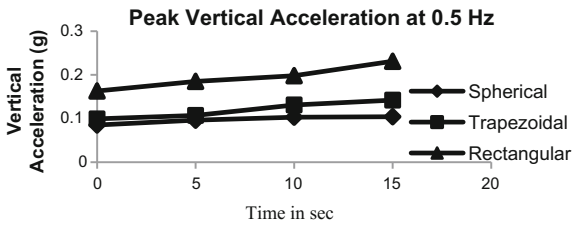

Fig. 5 Peak vertical acceleration versus time at 0.5 Hz

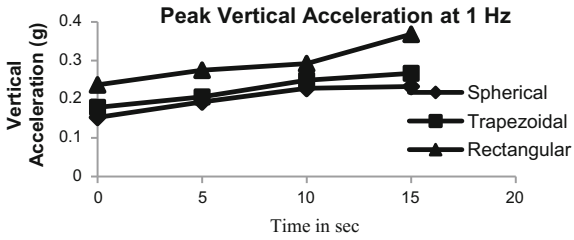

Fig. 6 Peak vertical acceleration versus time at 1.0 Hz

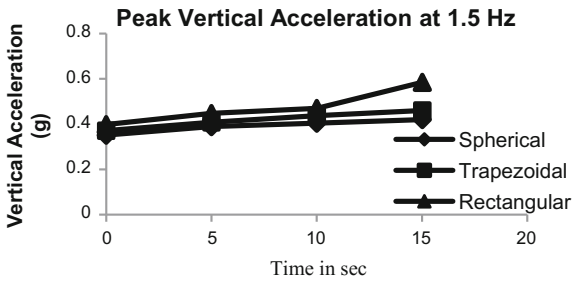

Fig. 7 Peak vertical acceleration versus time at 1.5 Hz

horizontal acceleration of the rectangular conventional footing is the least and that of the spherical footing is the highest. This acceleration response indicates that the spherical footing oscillates more along horizontal direction than the rectangular footing does. These oscillations make the spherical footing float more in the liquefied soil.

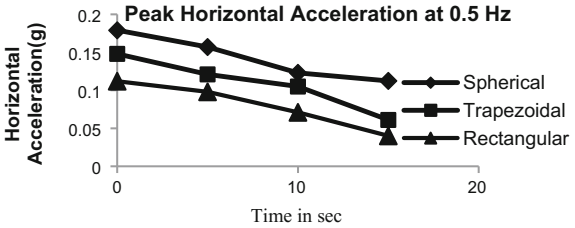

Fig. 8 Peak horizontal acceleration versus time at 0.5 Hz

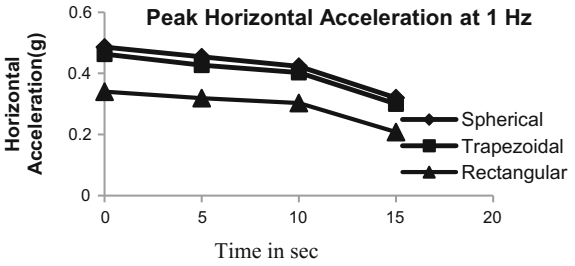

Fig. 9 Peak horizontal acceleration versus time at 1 Hz

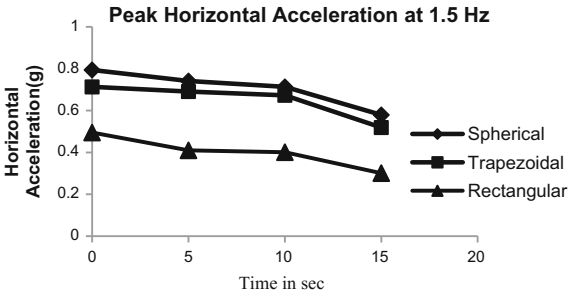

Fig. 10 Peak horizontal acceleration versus time at 1.5 Hz

In order to measure the deformation of the footing during vibration, a special arrangement was made after finding it difficult to use the LVDTs. One high-resolution camera was fixed on the tank, and on the other side, one graph sheet was fixed on a hardboard. The photographic image of the footing on the graph sheet was used to note the tilting and settlement of the footings. Thus during the dynamic tests, videography was taken from the start to the end of the test.

Tests were repeated with different dead loads placed over the footings. A comparison of vertical settlement of different footings carrying different dead weights under different frequencies like 0.5, 1.0 and 1.5 Hz is shown through Tables 1, 2 and 3. It is observed that the vertical settlement is more with increase in dead load. Moreover, the rectangular footing suffered the maximum settlement; spherical footing shows the lease settlement. Vertical settlement also increases with increase in frequency.

Table 1 Vertical settlement at 0.5 Hz

Vertical settlement (mm) at 0.5 Hz				
Shape of section	Without any vertical load	With 5 kg load	With 10 kg load	With 15 kg load
Spherical	15	22	28	35
Trapezoidal	20	28	35	42
Rectangular	30	40	47	55

Table 2 Vertical settlement at 1 Hz

Vertical settlement (mm) at 1.0 Hz				
Shape of section	Without any vertical load	With 5 kg load	With 10 kg load	With 15 kg load
Spherical	32	45	53	61
Trapezoidal	40	55	66	72
Rectangular	55	68	80	87

Table 3 Vertical settlement at 1.5 Hz

Vertical settlement (mm) at 1.5 Hz				
Shape of section	Without any vertical load	With 5 kg load	With 10 kg load	With 15 kg load
Spherical	50	67	82	93
Trapezoidal	65	84	102	114
Rectangular	77	101	115	128

The results obtained above show that the vertical settlement is greatly reduced in terms of spherical and trapezoidal section than conventional rectangular footing.

4 Analysis of Data Obtained from Static Load Tests

To check the suitability of the new designs in terms of load-carrying capacity, static load tests were performed on them and the load versus settlement curves were drawn. The test bed was made of the same foundation sand compacted at 50% relative density and saturated completely by water. Fig. 11 shows the load versus settlement curves obtained from the static load test on the footings. The ultimate load-bearing capacity was found by applying double tangent method in the figure and is shown in Table 4.

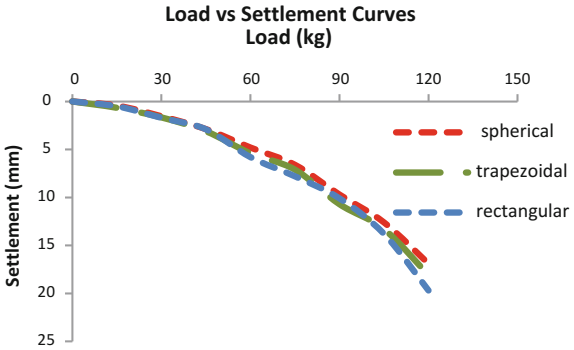

Fig. 11 Load versus settlement curves

Table 4 Ultimate load-carrying capacity of three footings under static vertical loadings

Shape of the footing	Ultimate load-bearing capacity (kg) experimental
Rectangular	97
Spherical	118
Trapezoidal	107

5 Tilting of Footing

To measure the tilting of footing, if any, a bamboo piece was attached with one of the columns and photographs were taken to observe the initial, during the test and final position of the footing. Figures 12 and 13 show the initial and final positions of spherical footing and rectangular footing with 15 kg surcharge load. It can be observed that the spherical footing did not tilt but the rectangular footing tilted after the shake table test. The amount of the tilt was so high that proper measurement could not be taken.

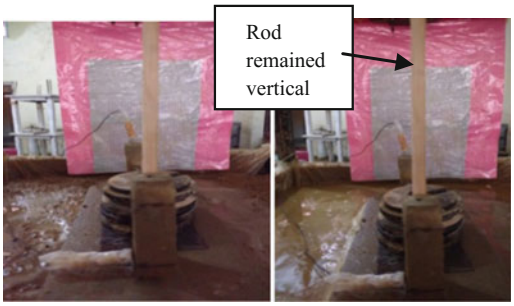

Fig. 12 Images of spherical footing before (left) and after (right) soil liquefaction

Sinking of footing without tilting

Fig. 13 Images of rectangular footing before (left) and after (right) soil liquefaction

6 Conclusions

The main conclusions derived from the experimental investigations of the conventional rectangular footing and the modified footings are that under static load; all the three footings behaved similarly with little difference in ultimate load-carrying capacity, whereas under dynamic loading, the spherical-shaped footing shows more stable behaviour than trapezoidal and rectangular footing. The spherical footing floats for a longer time during liquefaction and does not tilt, whereas the rectangular footing tilts very quickly.

References

Dungca, J. R., Kuwano, J., Takashashi, A., Saruwatari, T., & Tokimatsu, K. (2006). Shaking table tests on the lateral response of a pile buried in liquefied sand. *Soil Dynamics and Earthquake Engineering, 26*(2006), 287–295.

Knappett, J. A., Haigh, S. K., & Madabushi, S. P. J. (2004). Mechannism of shallow foundations under earthquake loading. *Soil Dynamics and Earthquake Engineering, 26*(2006), 91–102.

Liu, L., & Dobry, R. (1997). Seismic Response of Shallow Foundation on liquefiable sand. *Journal of Geotechnical Geoenvironmental Engineering, 123*(6), 557–567.

Shamoto Y., Zhang, J.-M., Gotosigera, & Tokimatsu, K. (1996). *A new approach to evaluate post-liquefaction permanent deformation in saturated sand*. Paper no. 1097, Eleventh WCEE.

Effect of Soil Heterogeneity on Soil–Structure Interaction

Ravi Kant Mittal and Sanket Rawat

Abstract Soil–structure interaction due to its significant effect on the response of the structure had already gained importance and therefore been incorporated in the Indian seismic code IS 1893-Part 4:2005. Since the advent of soil–structure interaction, continuous researches have been done on this topic and hence the concepts kept on modifying for more realistic results. The existing literature has already shown some of the critical parameters that are missing in Indian seismic code. Still, there is research gap in this area as some of the other important parameters too need to be included. Due to lack of proper geotechnical reports before the start of construction, thereby the misinterpretation of soil properties by the designer increases the susceptibility of the structure to failure in spite of including the code-specified effects such as soil–structure interaction. Critical situation occurs when the soft layer is underlying a hard stratum which the designers may misinterpret as the hard layer to the full depth due to improper geotechnical reports. Also, there is not any guideline in Indian seismic code to direct the designers to deal with the heterogeneous soil condition. In this research, a parametric study is carried out on a 150 m tall RCC chimney considering the effect on structural response of it by incorporating the effect of different conditions of layered soil mass. The results obtained show that soil heterogeneity patterns affect the design forces considerably and hence there is a critical need for inclusion of these factors in Indian seismic code. The paper subsequently concludes that, if appropriate provisions from some international literature are properly adopted, a substantial variation in the seismic response can be achieved and hence in many cases may result in structural-work cost saving. Overall with this study, the paper attempts to address the legitimate concern of design engineers regarding the potential variation in design values, especially for the sites when the soft soil underlies a hard stratum.

R. K. Mittal · S. Rawat (✉)
Department of Civil Engineering, Birla Institute of Technology and Science, 333031 Pilani, India
e-mail: sanketrawat@gmail.com

R. K. Mittal
e-mail: ravimittal@pilani.bits-pilani.ac.in

B. Adimoolam and S. Banerjee (eds.), *Soil Dynamics and Earthquake Geotechnical Engineering*, Lecture Notes in Civil Engineering 15,
https://doi.org/10.1007/978-981-13-0562-7_3

Keywords Heterogeneous soil · Soil–structure interaction · Indian seismic code Layered stratum

1 Introduction

Earthquake force contemplation in design has always been given prominence due to its unpredictable nature. Earlier soil characteristics were not considered to be of significant role in the behavior of structure due to ground motion. However, certain devastating collapses in the history (e.g., Kobe Earthquake, 1995) made it clear that soil characteristics have significant role in the behavior of structure as much as other factors corresponding to the earthquake, i.e., source mechanism and the geology of the seismic-wave path possess. Soil–structure interaction (SSI) due to its extensive impact on the design parameters has been included in Indian seismic code IS 1893 (Part 4):2005. This consideration during design makes a structure more flexible and hence increases the natural period of the structure (Chowdhury and Dasgupta 2008). Furthermore, SSI effect also intensifies the effective damping ratio of the system. This assumption of smooth idealization of design spectra leads to the consent that SSI can be conveniently neglected for conservative design of the structure though it is only valid for specific classes of structures and soil conditions, such as light structures in relatively stiff soil. However, the population rise and limitation of land have forced the user to construct a tall and stiff structure without concerning about the type of soil. Moreover, the increase in natural period of the structure due to consideration of SSI is not always advantageous as recommended by the simplified design spectrums. Soft soil sediments can considerably lengthen the period of seismic waves, and the increase in natural period of structure may lead to resonance with long period ground vibrations (Chowdhury and Dasgupta 2008). The existing literature (Mittal and Gajinkar 2014) has suggested that the formulae specified in IS 1893-Part 4 should be modified to take damping, effective shear modulus, and embedment effect into account for more realistic results. The major factor which still has not been addressed in the code and the related literature is the effect of non-homogenous strata. The stabilization of top soil generally tends to neglect the effect on othersoil strata present beneath the top soil. This neglection proves to be conservative in several cases; however, its effect may not be ignored completely. It has been observed that on radiation damping and energy dissipation are adversely affected by layering. Layer boundaries cause the outgoing waves to reflect back. These layers act as waveguides, entrapping, and reinforcing wave energy (Hadijan and Ellsion 1985). Thus, energy disperses more gradually than it would have been in an analogous homogeneous medium, and damping is effectively reduced. Results derived from several existing literature (Gazetas 1983; Hadijan and Ellsion 1985) have been taken as reference, and the above-mentioned factor has been incorporated in the calculation of effective horizontal seismic coefficient. The results obtained show the significant influence of the effect of the layered stratum on the response of the structure and hence highlight the necessity of

inclusion of this factor in the Indian seismic code for a better earthquake resistant and cost-effective design.

2 Existing Provisions in Indian Seismic Code

Soil–structure interaction criteria are specifically included in IS 1893-Part 4:2005, criteria for earthquake resistant design for structures such as industrial structures including stack-like structures. Different clauses are present in which formulae and methods are mentioned. Clause 14 of code mainly deals with the time period of vibration of stack-like structure. Furthermore, methods for calculating design base shear and bending moment have been specified in clause 17 of the code. Formulae to get horizontal and rocking stiffness have been mentioned in Table 12 of the code.

3 SSI Provisions in the Existing Literature

Various parameters such as effective damping ratio, embedment correction factor, and effective shear modulus obtained from the existing literature (Richart et al. 1970; Arya et al. 1984; Kramer 2004) and international codes (EN 1998-5:2004) have been suggested for inclusion in Indian seismic code (Mittal and Gajinkar 2014).

4 Modified Provisions for Present Study

The stiffness (both horizontal and rocking) is modified in the present study due to the presence of layered strata. The modified formulae and provisions have been adopted from Gazetas (1983), and Hadijan and Ellsion (1985).

4.1 Static Stiffness of Circular Foundations on a Stratum-Over-Half Space

Horizontal stiffness ($1 \leq \frac{H}{R} < 4$)

$$K_{\mathrm{H}} = \frac{8G_1R}{(2-\upsilon_1)}\left[\frac{1+\frac{R}{2H}}{1+\frac{RG_1}{2HG_2}}\right] \tag{1}$$

Rocking stiffness $\left(0.75 \leq \frac{H}{R} < 2\right)$

$$K_{\mathrm{R}} = \frac{8G_1R^3}{3(1-\upsilon_1)}\left[\frac{1+\frac{R}{6H}}{1+\frac{RG_1}{6HG_2}}\right] \tag{2}$$

4.2 Elastic Stratum on a Rigid Base

Horizontal stiffness $\left(\frac{H}{R} > 1\right)$

$$K_{\mathrm{H,surface}} = \frac{8GR}{2-\upsilon}\left(1+\frac{R}{2H}\right) \tag{3}$$

Rocking stiffness $\left(4 \geq \frac{H}{R} > 1\right)$

$$K_{\mathrm{R,surface}} = \frac{8GR^3}{3(1-\upsilon)}\left(1+\frac{R}{6H}\right) \tag{4}$$

4.3 Elastic Stratum on a Rigid Base, Embedded Circular Foundation $\left(\frac{D}{R} < 2\right)$

Horizontal stiffness

$$K_{\mathrm{H,embedded}} = \frac{8GR}{2-\upsilon}\left(1+\frac{R}{2H}\right)\left(1+\frac{2D}{3R}\right)\left(1+\frac{5D}{4H}\right) \tag{5}$$

Rocking stiffness

$$K_{\mathrm{R,embedded}} = \frac{8GR^3}{1-\upsilon}\left(1+\frac{R}{6H}\right)\left(1+\frac{2D}{R}\right)\left(1+\frac{0.7D}{H}\right) \tag{6}$$

Here, G_1 is the shear modulus of upper layer and G_2 is the shear modulus of lower stratum. H is the depth of the top stratum. Suffixes 1 and 2 represent the

corresponding property of top and bottom layers, respectively. R is equivalent radius of footing. D is the depth of embedment.

5 Problem Statement

To check for the response of RCC chimney subjected to earthquake force resting on two-layered soil strata, SSI with inclusion of modified stiffness has been included in the analysis.

The chimney height is taken as 150 m with raft diameter of 18 m and area of shell 8.5 m^2. The time period of vibration for the structure fixed at base and the flexible base period are computed separately. The damping ratio for the flexible base is also calculated, and the horizontal acceleration coefficient is calculated using the modified time period and damping ratio. The stiffness is first calculated on the basis of provisions available in code, and then for comparison, the modified stiffness is computed based on formulae as mentioned above. The equivalent lateral force static method (clause 17.1, IS 1893-Part 4) of analysis is used to compute the design base shear and design bending moment. The parametric problem data has been obtained from the text by Chowdhury and Dasgupta (2008). The properties of different types of soils that are used in study are mentioned in Table 1 which is extracted from the paper presented by Mehta and Gandhi (2008).

6 Results and Discussions

MS Excel spreadsheet is developed to analyze for response variation (shear at the base of chimney) using the code-specified equivalent static lateral force method for tall chimneys. The below-mentioned graphs describe the results of analysis for different responses and hence illustrate the importance of layered strata effect on seismic response of tall chimneys when it is struck by a long or a short duration earthquake.

Table 1 Properties of soil used in the study (Mehta and Gandhi 2008)

Velocity of shear waves (m/s)	Soil type	Unit weight, γ (kN/m^3)	Poisson's ratio ν	Shear modulus, G (kN/m^2)	Elastic modulus (kN/m^2)
150	Soft soil	16	0.49	36,700	14.95×10^4
300	Stiff soil	20	0.45	183,500	25.84×10^5
600	Dense soil	22.4	0.35	822,000	50.53×10^7
1200	Rock	25.6	0.30	3,758,900	30.42×10^7

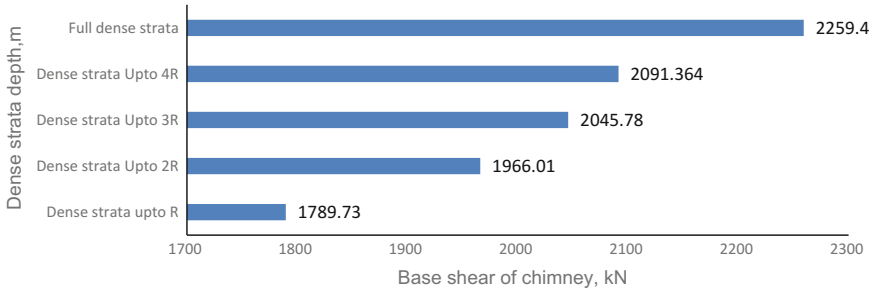

Fig. 1 Variation in base shear on increase in depth of top strata

Fig. 2 Percentage change in base shear at the base on increase in depth of top strata

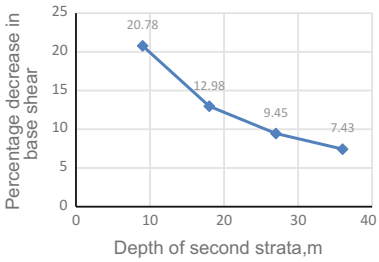

Figures 1 and 2 depict the variation in shear at the base of chimney in the two cases: The first one being in which the soil was assumed to be consisting of a dense stratum to the full depth or top layer was stabilized using natural or mechanical methods making it dense. In the second case, the less dense stratum is considered to be underlying the denser one. The depth of the top stratum is varied, and the results derived in the literature have been incorporated to make the analysis more realistic. In this study, soft stratum is considered below the dense stratum. However, the user can input the data of the soil type in the Excel sheet as per his requirements and consequently results can be obtained.

It can be clearly observed that if the structure is analyzed using the conventional process rather than following the realistic method, the percentage base shear variation in the two cases comes out to be 20.78% when the depth of top (dense) stratum is equal to the radius of circular foundation. Furthermore, this percentage difference decreases as the depth of the top dense stratum is increased. The results of the study are in compliance with the fact that the strata role becomes almost negligible after depth equal to two times the width of foundation.

7 Conclusions

The results of the present study primarily highlight the necessity of inclusion of the layered strata effect in soil–structure interaction analysis. Effect of two-layered soil strata is considered in the analysis along with the effect of increase in depth of the top stratum. To accentuate its significance, effect of the presence of soft stratum underneath dense soil is studied. Noteworthy decrease in shear at the base of chimney was observed when the effect of soil underneath the top layer is considered which further emphasized on the consideration of layered strata effect in Indian seismic code. The paper subsequently concludes that, if appropriate provisions related to the modification in stiffness in case of layered stratum, from some international literature, are properly implemented, a substantial variation in the seismic response can be achieved and hence in many cases may result in structural-work cost saving. On the whole, with this study, the paper attempts to address the genuine concern of design engineers regarding the potential variation in design values in both embedded foundation and foundation at surface, especially for the sites when the soft soil underlies a hard stratum.

References

Arya, S. C., O'Neill, M., & Pincus G. (1984). *Design of structures and foundations for vibrating machines*. Houston, Texas: Gulf Publishing Company.

Chowdhury, I., & Dasgupta, S. P. (2008). *Dynamics of structure and foundation—A unified approach*. Boca Raton: CRC Press.

EN, 1998-5. (2004). *Design of structures for earthquake Resistance-Part 5: Foundations, retaining structures and geotechnical aspects*. UK: British Standard.

Gazetas, G. (1983). Analysis of machine foundation vibrations: State of the art. *Soil Dynamics and Earthquake Engineering, 4*(4) (1985).

Hadjian, A. H., & Ellison, B. (1985). Equivalent properties for layered media. *Soil Dynamics and Earthquake Engineering, 2*(1) (1985).

Indian Standard Code. (2002). IS: 1893 (Part 4), *Criteria for earthquake resistant design of structures (Part 4) Industrial stack-like structures*. New Delhi: Bureau of Indian Standards, India

Kramer, S. L. (2004). *International series in civil engineering and engineering mechanics: Geotechnical earthquake engineering*. Upper Saddle River, New Jersey: Prentice Hall.

Mehta, D., & Gandhi, N. J. (2008). Time response study of tall chimneys, under the effect of Soil Structure Interaction and long period earthquake impulse. In *Proceedings of the 14th World Conference on Earthquake Engineering*, Beijing, China.

Mittal, R. K., & Gajinkar, V. (2014). Evaluation of soil-structure interaction guidelines in Indian seismic codes. *IJCIET, 5*(5), 97–104.

Richart, F. E., Jr., Hall, J. R., Jr., & Woods, R. D. (1970). *Vibrations of soils and foundations*. Englewood Cliffs, N.J.: Prentice Hall.

Nonlinear 1D Ground Response Analysis of Soil Profile Using Different Procedures

Devdeep Basu and Arindam Dey

Abstract Earthquakes are natural phenomena that have caused the loss of millions of lives and property across the globe, and they pose a severe threat to mankind. The earthquake-induced damage at any particular site will be governed by the response of the soil deposit present there. In this paper, ground response analysis (GRA) studies are done for a typical soil stratigraphic profile of IIT Guwahati region. Nonlinear 1D GRA is performed for the soil profile using six different procedures. Both total stress and effective stress analyses are done. The Sikkim earthquake motion recorded at IIT Guwahati with peak bedrock level acceleration (PBRA) of 0.02 g, and three of its scaled-up components with PBRA of 0.06, 0.18, and 0.36 g are used as input motions. Based on some of the computed response parameters, a comparison is made among these different analysis procedures. The suitability of each of these procedures under different circumstances is also scrutinized.

Keywords 1D · Nonlinear GRA · Masing · Non-masing · Ground response parameters

1 Introduction

Numerous moderate to large magnitude earthquakes have occurred in Northeast India in the past, and as a result, this entire region has been designated as zone *V* as per IS:1893 Part 1 (2002), which is the zone of highest seismicity in the country. Severe damages as a result of both structural failures as well as settlement and liquefaction-related failures have been reported during the occurrence of some of

D. Basu · A. Dey (✉)
Department of Civil Engineering, Indian Institute of Technology Guwahati, Guwahati 781039, India
e-mail: arindamdeyiitk@gmail.com

D. Basu
e-mail: basudevdeep@gmail.com

B. Adimoolam and S. Banerjee (eds.), *Soil Dynamics and Earthquake Geotechnical Engineering*, Lecture Notes in Civil Engineering 15,
https://doi.org/10.1007/978-981-13-0562-7_4

the most notable seismic events for this region, like the 1897 Shillong Plateau earthquake (M_w = 8.3), the 1950 Assam–Tibet earthquake (M_w = 8.6).

In this paper, a 1D GRA study for one typical soil profile of IIT Guwahati campus, situated on the banks of river Brahmaputra, has been presented. The various procedures of nonlinear 1D GRA have been compared based on some of the computed ground response parameters like peak horizontal acceleration (PHA), maximum shear strain, excess pore water pressure (PWP) ratio (which is the ratio of excess PWP to effective vertical stress). All the wave propagation problems presented herein have been solved with the aid of site response analysis code DEEPSOIL v6.0 (2015).

2 Fundamentals of Nonlinear 1D Ground Response Analysis

In nonlinear GRA, any soil profile is discretized into a number of layers using multiple degree of freedom lumped parameter model. Subsequently, the dynamic equation of motion is solved numerically in small time steps using Newmark β method.

Any nonlinear stress–strain model following Masing or non-masing rules can be used during the integration process. The stress–strain models developed by Kondner and Zelasko (1963), Hashash and Park (2001) are commonly used for performing nonlinear GRA incorporating Masing load/unload/reload criteria. The nonlinear stress–strain model developed by Phillips and Hashash (2009) is implemented in the site response code DEEPSOIL 6.0 (2015), for incorporating non-masing criteria. This model uses a hysteretic damping reduction factor (MRDF procedure) which modifies the Masing rules and thus incorporates the non-masing load/unload/reload criteria.

The different procedures of nonlinear GRA employed in DEEPSOIL 6.0 (2015) are listed in Table 1.

Table 1 Summary of different procedures of nonlinear ground response analysis

Abbreviated notation	Description of procedure
NLM1	Masing criteria, Total stress analysis (no PWP is considered)
NLM2	Masing criteria, Effective stress analysis with PWP dissipation
NLM3	Masing criteria, Effective stress analysis without PWP dissipation
NLNM1	Non-Masing criteria, Total stress analysis (no PWP is considered)
NLNM2	Non-Masing criteria, Effective stress analysis with PWP dissipation
NLNM3	Non-Masing criteria, Effective stress analysis without PWP dissipation

3 Methodology

3.1 Modeling of Soil Profile

The soil properties of different layers in the profile are taken from an existing borehole log report (Fig. 1). Shear wave velocities (V_s) of the soil layers are computed from the specified SPT-N values (measured at intervals of 1.5 m) using the correlation suggested by Imai and Tonouchi (1982). The modulus reduction and damping curves for the soil layers are obtained based on the formulations of Ishibashi and Zhang (1993), and they are subsequently fitted using MRDF procedure, which defines the parameters for the nonlinear stress–strain model. For all the analysis presented herein, elastic bedrock having a shear wave velocity of 5000 m/s is considered underlying the soil profile.

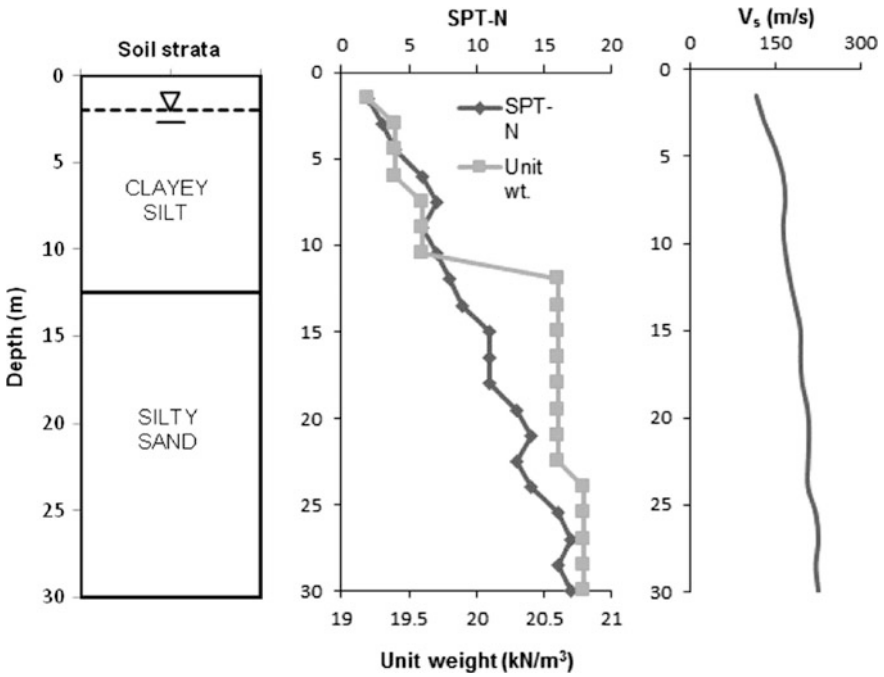

Fig. 1 Soil deposit of IIT Guwahati along with plots of SPT-N, unit weight, and V_s variation with depth

3.2 Description of Seismic Loading

The 2011 Sikkim earthquake motion recorded at IIT Guwahati with a peak bedrock level acceleration (PBRA) of 0.02 g (Fig. 2) and three of its scaled-up components having PBRAs of 0.06, 0.18, and 0.36 g are applied at the soil profile base for all the analyses.

4 Results and Discussions

4.1 Comparison Between NLM2 and NLM3/NLNM2 and NLNM3

No significant difference is observed between the peak horizontal acceleration (PHA) profiles (Fig. 3) and maximum strain profiles (Fig. 4) obtained using NLM2

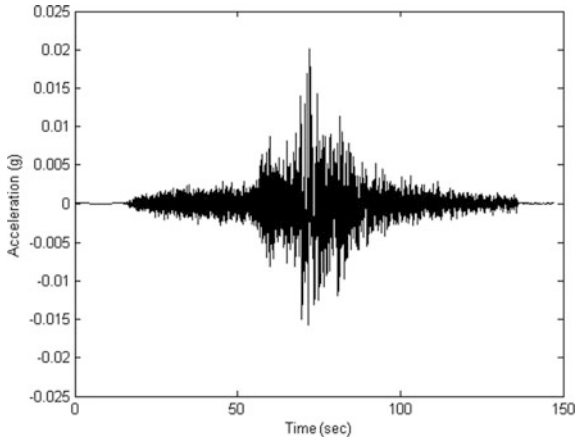

Fig. 2 Acceleration time history of the 2011 Sikkim earthquake motion recorded at IIT Guwahati

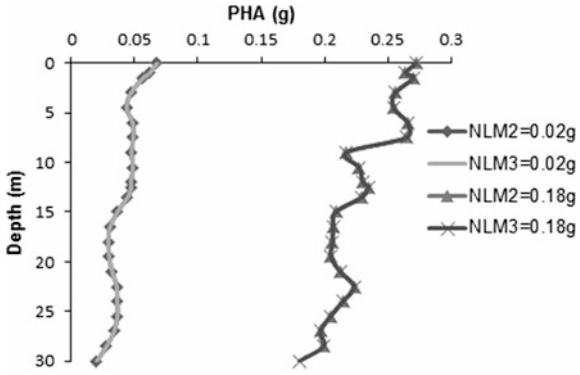

Fig. 3 PHA variation with depth for two motion components having PBRA of 0.02 and 0.18 g

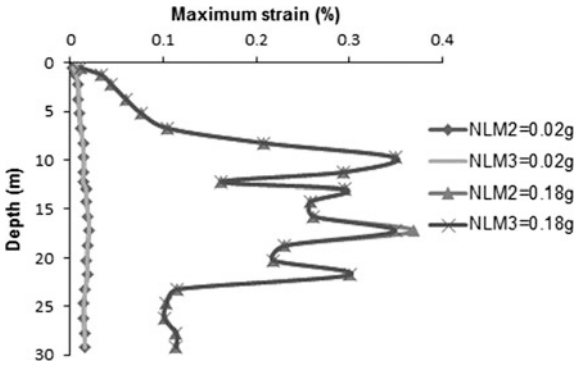

Fig. 4 Maximum strain versus depth for two motion components having PBRA of 0.02 and 0.18 g

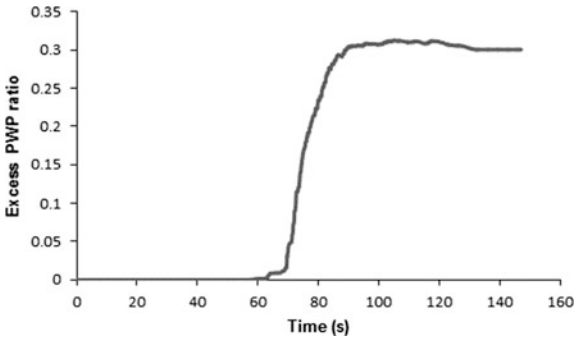

Fig. 5 Excess PWP dissipation with time for 0.18 g PBRA seismic motion in the silty sand soil strata (NLM2 procedure)

and NLM3 procedures of GRA. This implies that the excess PWP dissipation (Fig. 5) that occurs during the time span in which the seismic loading acts is negligible enough to have any role in altering the response parameters computed using these two procedures. The same logic holds good for NLNM2 and NLNM3 GRA procedures which shows similar observations (Figs. 6 and 7).

4.2 Comparison Between NLM2 and NLNM2

For the seismic motions with PBRA of 0.02 and 0.06 g, the obtained PHA profiles (Fig. 8) and maximum strain profiles (Fig. 9) are almost similar for both NLM2 and NLNM2 procedures. However, for seismic motions having higher PBRA (greater than 0.06 g), the difference in obtained PHA profiles (Fig. 10) and maximum strain profiles (Fig. 11) for these two procedures is more prominent.

The basic difference between Masing and non-masing procedures lies in the way in which the target modulus reduction and damping curves are fitted to obtain the

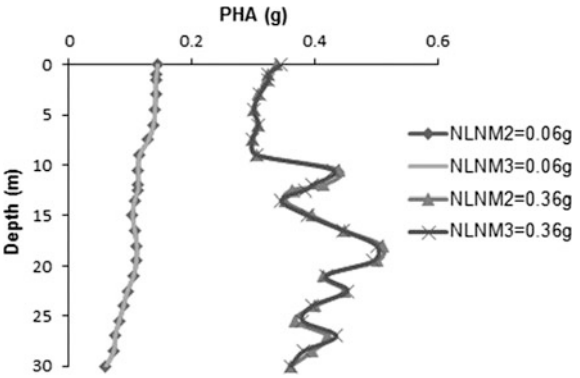

Fig. 6 PHA variation with depth variation for two motion components having PBRA of 0.06 and 0.36 g

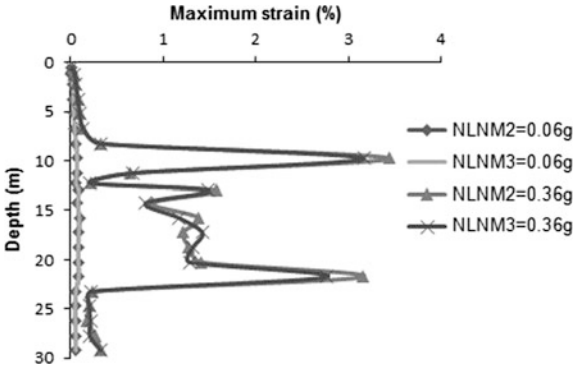

Fig. 7 Maximum strain versus depth for two motion components having PBRA of 0.06 and 0.36 g

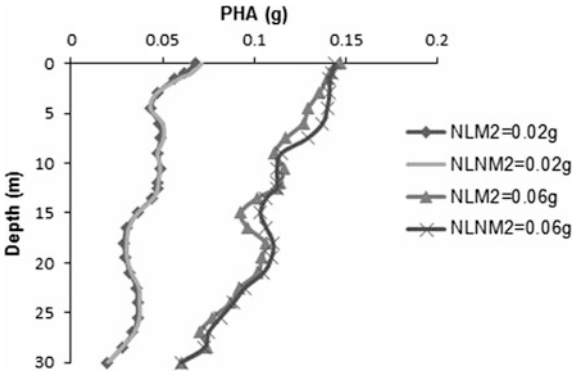

Fig. 8 PHA profiles for seismic motions having PBRA of 0.02 and 0.06 g

parameters of nonlinear stress–strain model. At low strains, Masing procedure gives a good fit with the target modulus reduction and damping curves, whereas at high strains, it overestimates the hysteretic damping significantly. In non-masing MRDF curve fitting procedure, even at high strains the target damping curve is fitted

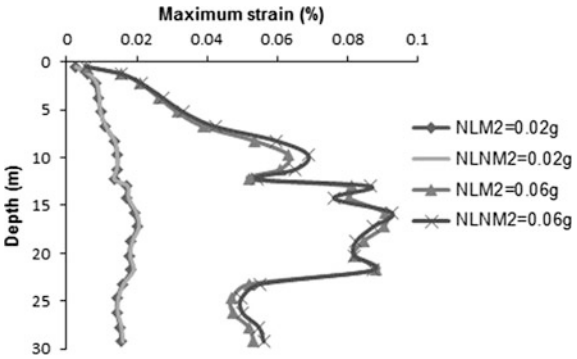

Fig. 9 Maximum strain profiles for seismic motions having PBRA of 0.02 and 0.06 g

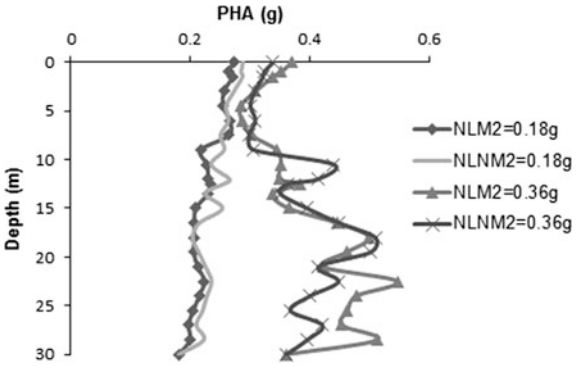

Fig. 10 PHA profiles for seismic motions having PBRA of 0.18 and 0.36 g

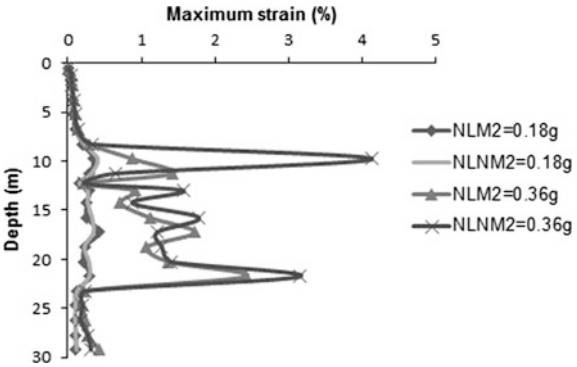

Fig. 11 Maximum strain profiles for seismic motions having PBRA of 0.18 and 0.36 g

accurately. For lower PBRA input motions, the maximum strains developed in the soil layers are less. Thus, at low strains, results obtained for both Masing and non-masing procedures are similar and accurate. However, at high strains, usually developed for motions with high PBRA values, the difference between Masing and non-masing procedures becomes significant.

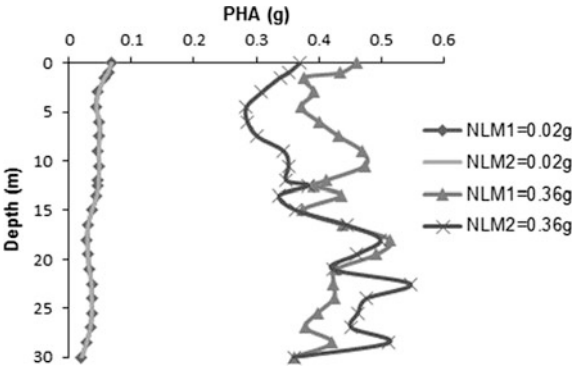

Fig. 12 PHA profiles obtained incorporating masing criteria for motions with PBRA of 0.02 and 0.36 g

4.3 Comparison Between NLM1 and NLM2/NLNM1 and NLNM2

It is observed that total stress analysis (NLM1 or NLNM1) without PWP generation produces higher values of peak ground acceleration (PGA, which is the peak horizontal acceleration at ground surface) than effective stress analysis. This is because of the fact that in effective stress analysis, the PGA values are calculated based on effective stresses developed in soil, whereas total stresses are used to compute the PGA in total stress analysis procedure. For larger amplitude motions with high PBRA values (greater than 0.06 g), significant PWP develops in a soil profile which brings down the effective stresses. As a result, a marked difference in results is observed between total stress and effective stress analysis procedures. For motions having low PBRA values, PWP developed in a soil profile is minimal (almost zero), and thus the two analysis procedures produce similar results. Figure 12 shows the PHA profiles developed for total stress and effective stress analyses incorporating Masing criteria. PHA profiles obtained using non-Masing criteria are shown in Fig. 13 for the two procedures.

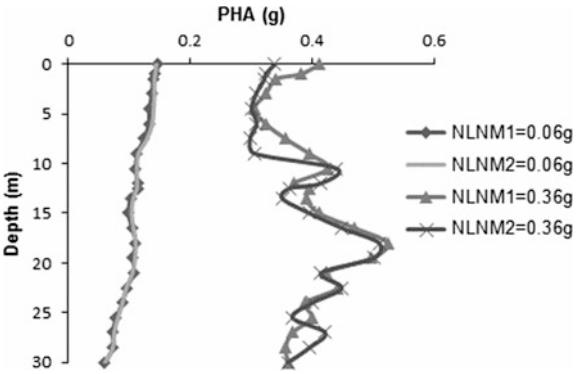

Fig. 13 PHA profiles obtained incorporating non-masing criteria for motions with PBRA of 0.06 and 0.36 g

However, NLM2 procedure produced higher PHA values than NLM1 procedure (for 0.36 g PBRA motion) at depths greater than 20 m. This is possibly on account of higher strains that might have developed in the soil profile for NLM2 procedure in the deeper layers. Higher strains induce greater hysteretic damping and, thus, lowers the stress developed and subsequently the PHA.

5 Conclusions

In this paper, a comparison among different procedures of nonlinear 1D GRA and their suitability under different circumstances has been presented. Results have been presented in terms of parameters like PHA, PGA, excess PWP ratio, and maximum shear strain. For both Masing and non-Masing analyses, the PHA and maximum strain profiles obtained when PWP dissipation is allowed have been observed to be similar to the profiles of the same when PWP dissipation is not allowed. A comparison has been made between Masing and non-Masing analysis procedures using motions having different PBRA values. It has been observed that for motions having high PBRA values (greater than 0.06 g), the difference between Masing and non-Masing analysis procedures becomes significant. Finally, total stress and effective stress analysis procedures (both Masing and non-Masing) have been compared. Higher PGA values are obtained for total stress analysis when seismic motions selected have high PBRA values (greater than 0.06 g). Thus, an idea about the seismic site response for IIT Guwahati region, quantified with respect to some response parameters, has been developed in this study.

References

Hashash, Y. M. A., Musgrove, M. I., Harmon, J. A., Groholski, D. R., Phillips, C. A., & Park, D. (2015). DEEPSOIL 6.0, User Manual, pp. 1–116.

Hashash, Y. M. A., & Park, D. (2001). Non-linear one-dimensional seismic ground motion propagation in the Mississippi embayment. *Engineering Geology, 62*(1–2), 185–206.

Imai, T., & Tonouchi, K. (1982). Correlation of N value with S-wave velocity and shear modulus. In *Proceedings of 2nd European Symposium on Penetration Testing,* Amsterdam, pp. 67–72.

IS: 1893 Part 1. (2002). *Criteria for earthquake resistant design of structures*. India: Bureau of Indian Standards.

Ishibashi, I., & Zhang, X. (1993). Unified dynamic shear moduli and damping ratios of sand and clay. *Soils and Foundations, 33*(1), 182–191.

Kondner, R. L., & Zelasko, J. S. (1963). A hyperbolic stress-strain formulation of sands. In *Proceedings of the 2nd Pan American Conference on Soil Mechanics and Foundation Engineering*, Sao Paulo, Brasil, pp. 289–324.

Phillips, C., & Hashash, Y. M. A. (2009). Damping formulation for non-linear 1D site response analyses. *Soil Dynamics and Earthquake Engineering, 29,* 1143–1158.

Fuzzy Probability Approach in Seismic Hazard Analysis

Prasad Hiremath, Mohammad Muzzaffar Khan and G. Kalyan Kumar

Abstract Seismic hazard assessment like many other problems in seismology is a complicated problem, owing to the variety of parameters affecting the occurrence of the earthquake. Assessment of seismic hazard based on the theory of probability becomes hard particularly under highly uncertain conditions, i.e., where neither the statistical data nor the physical knowledge required for a purely probabilistic risk analysis is sufficient. Insufficiency of information will afflict the calculated risk probabilities with imprecision and will to the underestimation of the risk. This uncertainty, which is a result of vagueness and incompleteness of the data, should be considered in a rationale way. Essentials of seismic hazard analysis are identified and the concept of fuzzy logic is applied to seismic hazard analysis, generalizing the conventional probabilistic seismic hazard analysis (PSHA) to fuzzy probabilistic seismic hazard analysis (FPSHA). The β and λ values which are the input parameters for the PSHA are evaluated using earthquake data for the Warangal region. The uncertainty associated with these values will be too high for a site with moderate earthquake activity, and the previous earthquake data is scarce. Fuzzy logic will help in containing these uncertainties by its property of considering the possibility of a certain event occurring. This study presents an approach for seismic hazard analysis based on fuzzy set theory. Seismic activity is based on the seismic activity rate, λ, which is equal to the number of events with magnitudes equal to or greater than a defined magnitude level, say M_0, during a specified time period, T; the parameter b or β ($\beta = b \ln 10$). The variables β and λ are first converted into Gaussian fuzzy sets using α-cut method. The ranges of β and λ are chosen based on previous studies. The fuzzified variables are used in seismic hazard analysis. The outputs are defuzzified using the center of area method, and fuzzy hazard curve is

P. Hiremath (✉) · M. M. Khan · G. K. Kumar
Department of Civil Engineering, National Institute of Technology Warangal, Warangal, India
e-mail: prasadbvbcet@gmail.com

M. M. Khan
e-mail: mmkmatrix@gmail.com

G. K. Kumar
e-mail: kalyanu.g@gmail.com

B. Adimoolam and S. Banerjee (eds.), *Soil Dynamics and Earthquake Geotechnical Engineering*, Lecture Notes in Civil Engineering 15,
https://doi.org/10.1007/978-981-13-0562-7_5

developed for the study region. The output is compared with PSHA results. The horizontal PGA expected in Warangal on stiff ground, with a 10% probability of exceedance in 50 years (which corresponds to a return period of 475 years) is 0.0836 g, whereas, that with a 2% probability of exceedance in 50 years (return period = 2475 years) is 0.153 g.

Keywords Fuzzy logic · PSHA · Gaussian fuzzy sets · Peak ground acceleration

1 Introduction

The study of earthquakes dates back many centuries. Written records of earthquakes in China date back as far as 3000 years. Still, compared with millions of years where earthquakes have been occurring, humankind's experience with earthquake is very brief. Today, hundreds of millions of people throughout the world live with a significant risk to their lives and property from earthquakes. The health of many local, regional, and even national economies is also at risk from earthquakes. It is impossible to prevent earthquakes from occurring, but it is possible to mitigate their adverse effects: to reduce life losses, injuries, and damage. In order to realize this, the starting point is being able to estimate the adverse outcomes of the earthquake by means of risk assessment methods in a reliable and realistic way.

Seismic hazard such as ground shaking, liquefaction, landslides, fault movement, which are associated with an earthquake, may produce adverse effects on human activities. Seismic hazard analyses involve the quantitative estimation of ground shaking hazards at a particular site. Seismic hazards may be analyzed deterministically, as when a particular earthquake scenario is assumed, or probabilistically, in which uncertainties in earthquake size, location, and time of occurrence are explicitly considered.

The accuracy of PSHA depends on the accuracy with which uncertainty in earthquake size, location, recurrence, and effects can be characterized. Therefore, it is quite sensible to employ a concept which can model different forms of uncertainty present in natural hazards. A reasonable option is complementing probability theory with an extra dimension of uncertainty provided by fuzzy set theory. This concept has received the generic name of fuzzy probability after Zadeh. However, this generic term has been interpreted and mathematically formalized in various ways. One of the most attractive interpretations of fuzzy probability is where probability of a crisp event, due to sparsity of data sample, is expressed in terms of a fuzzy number. It will be shown that this concept is especially appropriate for situations for which our physical knowledge and available statistical data are insufficient to characterize their likelihood of occurrence with a probability distribution.

The term fuzzy logic was first coined for the proposal of fuzzy set theory by Zadeh (1965). Brown and Yao (1983) in their pioneering research on the application of fuzzy set theory in structural engineering have tried to make use of fuzzy

set theory for two of the structural engineering-related problems. Initially, a justification for the theory is provided, and then, simple fuzzy operations are developed and contrasted with those of conventional set theory. Frangopol et al. (1987) proposed a model which is able to reproduce both the randomness and the imprecision in conjunction with earthquake occurrences. Elham et al. (2015) in their study presented a new model for probabilistic seismic hazard assessment based on fuzzy set theory.

In the current study, fuzzy sets have been developed which can be used in the probabilistic seismic hazard assessment of Warangal, Telangana. For this, all the variables to be used in seismic hazard assessment must be defined in terms of fuzzy sets. Then, using α-cut method, the seismic hazard equations are evaluated. The outputs will be in fuzzy sets which will be defuzzified using the center method. At last, the expected peak ground acceleration values from the seismic sources are calculated. The results obtained are compared with the results of PSHA.

2 Methodology

In the present study, four input parameters, i.e., distance (R), magnitude (M), λ, and β, are defined as fuzzy sets by the discrete membership functions $\mu(R)$, $\mu(M)$, $\mu(\lambda)$, and $\mu(\beta)$, respectively. The input parameters, λ and β, for single seismic zone were taken from the previous study of the Warangal region by Deviprasad (2014). Due to the uncertainty of the four mentioned parameters, maximum and minimum values were determined by a Gaussian membership function. It may be noted that λ and β are parts of G–R relationship and R and M are uncertain inputs of an attenuation relationship. These uncertain parameters used in G–R relation and attenuation relationship are assessed using fuzzy logic approach. The results obtained with these fuzzified inputs will be defuzzified using centroid method. The defuzzified values are used for the seismic hazard assessment by Cornell–McGuire approach.

2.1 Gutenberg–Richter Frequency–Magnitude Recurrence Relationship

Gutenberg–Richter parameters 'a' and 'b', which are the basic input for the seismic hazard analysis, have been carefully evaluated through regression analyses using the established catalogue. Table 1 presents the completeness intervals and exceedance rates computed by the CUVI method (Mulargia and Tinti 1985) and Stepp's (1972) method.

The prime input values for the probabilistic seismic hazard analysis, β and λ, will be further processed with the fuzzy approach. To minimize the vagueness, a suitable range for β value and λ value was chosen. For the chosen ranges, using

Table 1 Seismicity parameters from CUVI and Stepp's method

Single source zone	N	a	b	$M_{\min}$	$\lambda = 10^{(a-bM)}$	$\beta = 2.303b$
Stepp's method	248	3.43	0.80	3	10.69	1.85
CUVI method	248	3.33	0.78	3	9.75	1.80

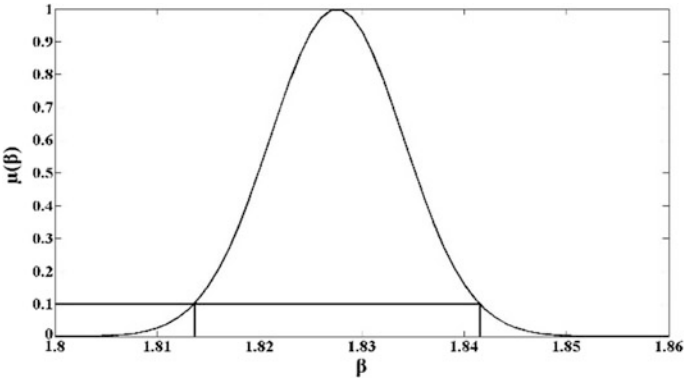

Fig. 1 Gaussian membership curve for β values

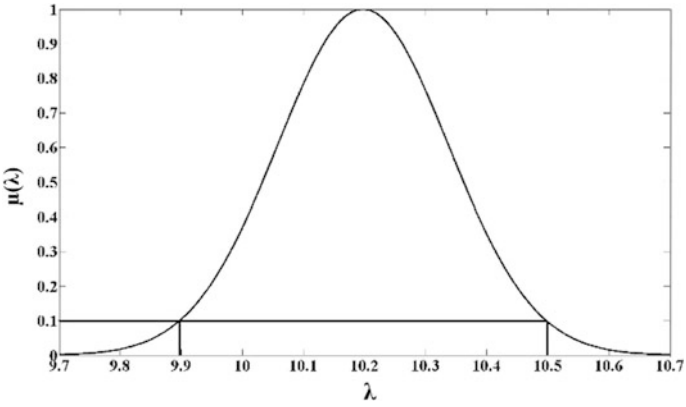

Fig. 2 Gaussian membership curve for λ values

their standard deviation and mean Gaussian membership curve was drawn as shown in Figs. 1 and 2.

As an example, in the first trial minimum value of β from the α-cut = 0.1 and minimum value of λ from the α-cut = 0.1 can be used as inputs. In the second trial, minimum value of β and maximum value of λ can be given as inputs. In that case, we will be having four possible combinations of β and λ values.

2.2 Fuzzy Attenuation Relation

Attenuation relationship given by Abrahamson and Silva has been used for calculating PGA values. Fuzzy logic approach is used for different ranges of magnitude (M) and distance (R). Gaussian curves were developed for both M and R as it was done in the case of G–R relations.

2.2.1 Fuzzification of the Magnitude

The magnitude range for a PSHA analysis that was done earlier was 3–6.5. The interval chosen was 0.4375. For each interval, using standard deviation and mean, Gaussian membership curves were drawn. α-cut of 0.1 was applied to get minimum and maximum values of magnitude. One interesting observation that can be made here is that the magnitude range is 6.2812–6.7187 which is greater than the highest value chosen in the conventional PSHA. 6.2812 is the median value of the last but one magnitude range. The fact that the magnitude value higher than the maximum magnitude value for the region being covered under the fuzzy universe makes this method more credible.

Gaussian membership curve for magnitude range 3–3.4375 is shown in Fig. 3. The thick horizontal line at $\mu(M) = 0.1$ cutting the Gaussian membership curve at two points is the α-cut at 0.1.

2.2.2 Fuzzification of Hypocentral Distance

The distance is also divided into ranges for the conventional PSHA. The least distance is 11.46 km, and 350 km is the maximum distance. As it is done in the

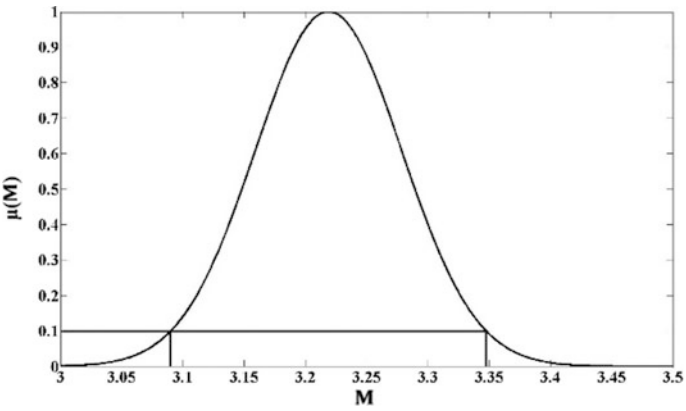

Fig. 3 Gaussian membership curve for magnitude range of 3–3.4375

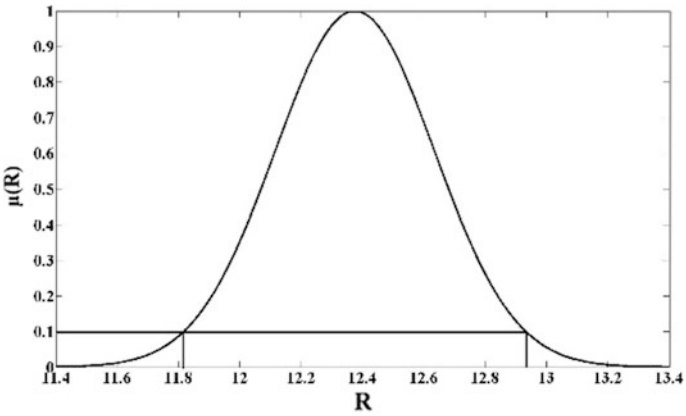

Fig. 4 Gaussian membership curve for the distance range 11.46–13.29

earlier cases of fuzzification, here also for each distance range, a Gaussian membership curve is drawn and from α-cut method. Minimum and maximum values of distance were noted for further calculations. Gaussian membership curve drawn for the distance of range 11.46–13.29 km is shown in Fig. 4.

Distance and magnitude are to be given as inputs in the attenuation relationship of Abrahamson and Silva (1997). We are having two values for magnitude and two values for distance. Similar to the case of *G–R* relationship, here also four combinations of magnitude and distance are possible. Spectral acceleration values are calculated for all these four combinations of *M* and *R*. As there are nine ranges of magnitude chosen, for each of these nine ranges four values of spectral acceleration are obtained. Out of these four values, minimum and maximum values are chosen.

2.3 Probabilistic Seismic Hazard Analysis

In the present study, Cornell–McGuire approach is used to estimate the seismic hazard. The computations needed in the PSHA are performed using the program CRISIS 2007 (Ordaz et al. 2007).

In the analysis, we have four possible combinations of λ and β values and two sets of spectral acceleration values, i.e., minimum and maximum spectral acceleration values sets. It makes a total of eight possible combinations. Hence, eight trials have been run in CRISIS 2007 software. One of the best ways to represent the values obtained using fuzzy logic is to present the results in the form of ranges. From the values obtained from all the eight trials, minimum and maximum values of annual rate of exceedance are extracted and are shown in Fig. 5.

2.3.1 Seismic Hazard Curves

The effect of all the earthquakes at different locations, sizes, sources with different probability of exceedance is integrated into one curve. It shows the probability of different ground motions at a site, exceeding during a specified period of time in the form of a range.

The expected value of the PGA ranges corresponding to a return period of typical engineering interest, e.g., for 475 years (10% probability of exceedance in 50 years exposure time), and the range of peak horizontal acceleration can be read from Fig. 5 as 0.038–0.064 g. Different return periods can also be selected for reporting PGA values depending on the type and importance of the structure. All the hazard curves are developed for the rock sites. For any particular site, the local soil profile (thickness of the layers and type of soil) will transform the predicted ground motions.

2.3.2 Uniform Hazard Spectrum

Uniform hazard spectrum (UHS) is the spectral amplitudes of acceleration which can be evaluated at all the natural periods for a constant probability of exceedance at a site. Such a response spectrum is commonly known as the UHS. Fig. 6 shows the UHS corresponding to the upper bounds of 10% probability of exceedance in 50 years (475 years return period).

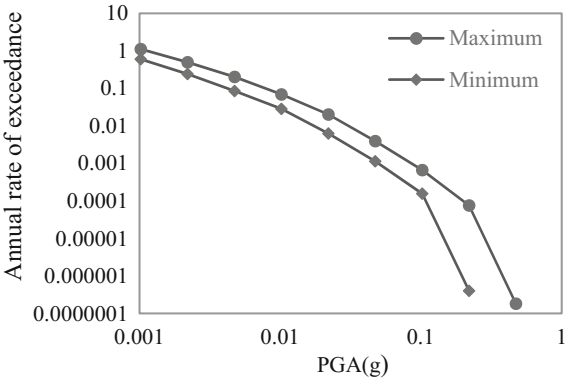

Fig. 5 Hazard curve for single seismic source zone

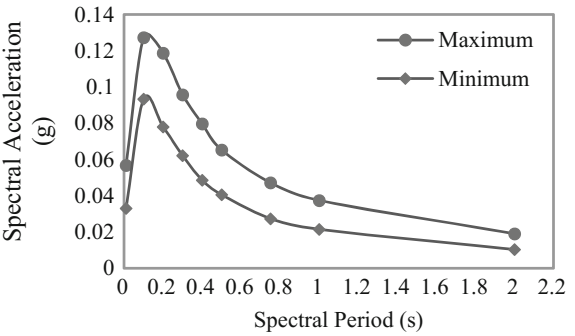

Fig. 6 UHS corresponding to 10% probability of exceedance in 50 years

3 Conclusion

In this study, a modular framework for seismic hazard assessment was presented. The quintessential strategy in developing the new framework is to improve and enhance each component of the conventional probabilistic seismic hazard analysis.

- The horizontal PGA expected in Warangal, with a 10% probability of exceedance in 50 years (which corresponds to a return period of 475 years), is varying from 0.038 to 0.064 g, whereas that with a 2% probability of exceedance in 50 years (return period = 2475 years) is in range of 0.08–0.113 g.
- The annual rates of exceedance and expected PGA calculated using PSHA method are observed to be lying in the ranges that are given by the FPSHA.
- The current study revealed that fuzzy sets could help to incorporate all the uncertainties in PSHA. However, a complete comparison could not be pulled off with previous studies, since not only the applied methods are different, as we have used fuzzy set theory, but also many of the input parameters and attenuation relationships are different.

References

Abrahamson, N. A., & Silva, W. J. (1997). Empirical response spectral attenuation relations for shallow crustal earthquakes. *Seismological Research Letters, 68,* 94–127.

Brown, C. B., & Yao, J. T. (1983). Fuzzy sets and structural engineering. *Journal of Structural Engineering, 109*(5), 1211–1225.

Deviprasad, B. S. (2014). *Probabilistic seismic hazard analysis of Warangal district*' (M. Tech dissertation thesis). NIT Warangal.

Elham, B., Tahernia, N., & Shafiee, A. (2015). Fuzzy—probabilistic seismic hazard assessment, casestudy: Tehran region, Iran. *Natural Hazards, 77*, 525–541.

Frangopol, D. M., Ikejima, K., & Hong, K. (1987). Seismic hazard prediction using a probabilistic-fuzzy approach. *Structural Safety, 5*(2), 109–117.

Mulargia, E., & Tinti, S. (1985). Seismic sample areas defined from incomplete catalogues: An application to the Italian territory. *Physics of the Earth and Planetary Interiors, 40,* 273–300.

Ordaz, M., Aguilar, A., & Arboleda, J. (2007). *CRISIS2007—Ver. 1.1: Program for computing seismic hazard*. UNAM, Mexico: Instituto de Ingenieria.

Stepp, J. C. (1972). Analysis of completeness in the earthquake sample in the puget sound area and its effect on statistical estimates of Earthquake Hazard. In *Proceedings of the International Conference on Microzonation*, Seattle, Washington.

Zadeh, L. A. (1965). Fuzzy probabilities. *Information Processing and Management, 8,* 363–372.

Effect of Saturation on Dynamic Properties of Solani Sand

Priyanka Sharma and B. K. Maheshwari

Abstract Degree of saturation influences significantly the properties of soil. Therefore, dynamic soil properties will also have effect of water content. Hence, it is important to evaluate these dynamic properties of soil, namely the shear modulus and the damping ratio for different degree of saturation. In the present study, a series of cyclic triaxial tests have been carried out on samples of Solani Sand (collected from the bed of Solani River near Roorkee) at three different degrees of saturation, i.e., (S_r = 0, 50, and 98%) at the same effective confining pressure of 100 kPa and at a frequency of 1 Hz in medium-to-large shear strain values (between 0.01 and 1%). The objective of the analysis is to examine the effect of degree of saturation on the behavior of dynamic properties of sands. Thus, results of dry, partially saturated, and fully saturated sand samples are presented and compared.

Keywords Shear modulus · Damping ratio · Degree of saturation
Solani sand · Cyclic triaxial test

1 Introduction

Earthquake damage distribution is highly influenced by the dynamic properties of the soil. For any geotechnical earthquake engineering problem such as ground response analysis, soil–structure interaction, and liquefaction, dynamic soil properties are very essential input parameters. The most important properties are the shear modulus and the damping ratio. The major factors that influence the dynamic properties of soil are the void ratio, effective confining pressure, and degree of saturation. Since 1980, many efforts have been reported on the study of the effects

P. Sharma (✉) · B. K. Maheshwari
Department of Earthquake Engineering, Indian Institute of Technology Roorkee, Roorkee 247667, India
e-mail: pri88.deq2015@iitr.ac.in

B. K. Maheshwari
e-mail: bkmahfeq@iitr.ac.in

B. Adimoolam and S. Banerjee (eds.), *Soil Dynamics and Earthquake Geotechnical Engineering*, Lecture Notes in Civil Engineering 15,
https://doi.org/10.1007/978-981-13-0562-7_6

of saturation on small strain stiffness of unsaturated soils obtained from resonant column (RC) or bender element (BE) testing. A series of resonant column tests were conducted in the torsional mode of vibration to assess the effect of saturation on damping of sands (Madhusudhan 2011). Strain-controlled cyclic triaxial element test has been carried out on dry and saturated soil samples in medium-to-large shear strain levels of Ahmedabad sands (RaviShankar et al. 2005). Very few researches are done to analyze the behavior of dynamic properties with the saturation at high strain. Moreover, the nonlinear dynamic responses of grounds caused by strong earthquake motions demand the evaluation of dynamic soil properties corresponding to large strain levels (Maheshwari et al. 2012).

Hence, in the present study, a series of cyclic triaxial tests have been carried out on sand samples of Solani sand (collected from the bed of Solani River near Roorkee) at three different degrees of saturation level (S_r = 0, 50, and 98%) at the same effective confining pressure in medium-to-large shear strain values. The objective of the analysis is to examine the behavior of dynamic properties of sands based on the degree of saturation of the sand samples such as dry, partially saturated, and fully saturated condition.

2 Testing Procedure Adopted

Cyclic triaxial test was carried out on Solani sand samples of 50 mm diameter and 100 mm height with 50% relative density and at confining pressure of 100 kPa, using a modern system (Wykeham 2008) as per ASTM standard D3999-91 (2003). For a particular test, harmonic excitation of a given frequency of 1 Hz was applied as a sine wave in axial direction (ASTM: D5311/D5311M 2013). The samples were tested at different shear strain values, i.e., at 0.03, 0.08, 0.32, 0.90, 1.005, 1.5, and 2.01%. When cyclic triaxial test is performed, a hysteresis loop is formed (Kramer 1996). The slope of the line connecting the extreme points on the hysteresis loop is the secant dynamic modulus E. The shear modulus G is given as,

$$G = E/2(1+\nu) \tag{1}$$

where ν is the Poisson ratio. The damping ratio is obtained as

$$D = \frac{1}{4\pi}\frac{\Delta W}{W} \tag{2}$$

where ΔW is the energy loss per cycle and W is the maximum elastic energy that can be stored in a unit volume of viscoelastic body.

3 Results and Discussions

In this paper, a comparative study of the dynamic properties of Solani sand for varying degree of saturation by testing samples under strain controlled on cyclic triaxial system is presented. Figure 1 presents the variation of shear modulus of dry sample (B = 0.01), partially saturated sample (B = 0.50), and fully saturated sample (B = 0.95) of Solani sand at relative density of 50% under an effective confining pressure of 100 kPa and at frequency of 1 Hz with the shear strain. It can be observed from Fig. 1 that the shear modulus decreases with the increase in shear strain, which was expected. Moreover, it is observed that the shear modulus of dry sand is greater than that of partially saturated sand and fully saturated sand. However, there is not much difference noticed in the shear modulus of partially saturated sand and that of fully saturated sand. When the shear strain is higher than 1%, the decrease in shear modulus almost reduces to a very low value for all the three states of soil. However, for dry sand, shear modulus is higher as compared to partially saturated and fully saturated sand. Similar trend for decrease in shear modulus for dry to fully saturated state was observed for Ahmedabad sands at high strain levels by RaviShankar et al. (2005).

In Fig. 2, the variation of the damping ratio with shear strain for different degrees of saturation is shown. As expected and observed, damping ratio increases with the increase in shear strain. However, as degree of saturation increases, an increase in the damping ratio is observed with the increase in strain. It can be observed from Fig. 2 that the damping ratio of saturated sands is greater than that of partially saturated and fully saturated sands at most of the strains. However, the difference in damping ratios of partially saturated and fully saturated sand is smaller. Madhusudan and Kumar (2013) conducted series of resonant column tests to study the effect of saturation on damping ratio and concluded that that minimum damping ratio is always associated with the dry state and reaches its maximum

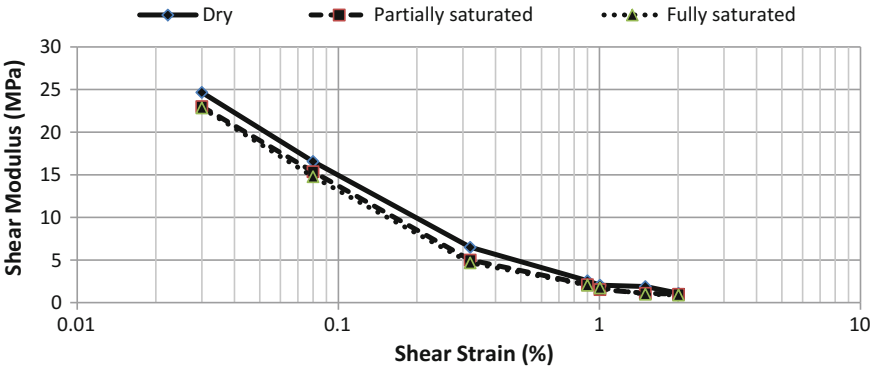

Fig. 1 Variation of shear modulus (G) with shear strain for different degrees of saturation

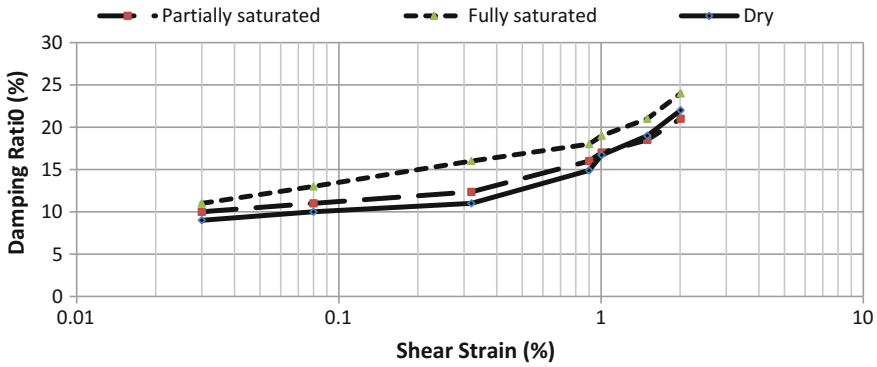

Fig. 2 Variation of damping ratio with shear strain for different degrees of saturation

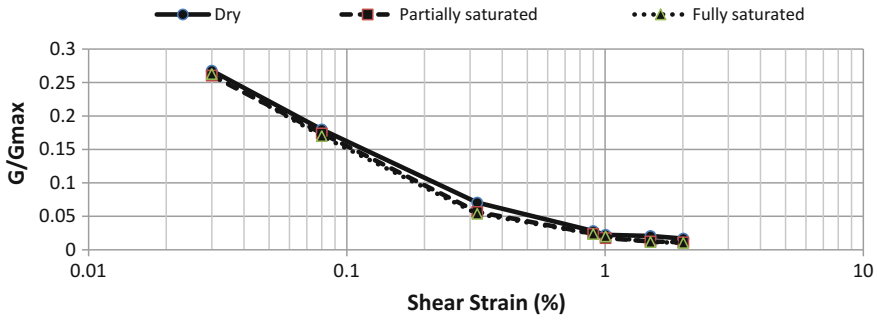

Fig. 3 Variation of normalized shear modulus (G/G_{max}) with shear strain for different degrees of saturation

value for fully saturated sands. Hence, the trend of results in the present study at high strain is similar to that observed by Madhusudan and Kumar (2013) at low strain.

In Fig. 3, the variation of the normalized shear modulus ratio with the increase in shear strain is shown for different degrees of saturation. It can be observed that as the soil is in unsaturated condition, the normalized shear modulus ratio is relatively higher than that of the saturated sand sample. However, smaller difference is noticed for partially saturated and fully saturated samples of Solani sand. Also comparing Figs. 3 with 1, it can be observed that these three curves are closer than before due to normalization with G_{max}.

4 Conclusion

The dynamic properties such as shear modulus and damping ratio on sand samples of Solani sand (collected from the bed of Solani River near Roorkee) have been examined at three different degrees of saturation (S_r = 0, 50, and 98%) using a series of cyclic triaxial tests, at the same effective confining pressure in large shear strain range. Based on the results presented, the following conclusions can be drawn:

(1) With the increase in shear strain, shear modulus decreases while damping ratio increases, as expected.
(2) It was observed that as degree of saturation decreases, the shear modulus increases with the increase in strain. The shear modulus is relatively higher for dry sands as compared to saturated sands but there is a slight difference noticed for partially and fully saturated sands.
(3) The damping ratio is greater for the saturated sand sample than that of the dry and partially saturated sands.
(4) Effect of saturation on normalized shear modulus (G/G_{max}) is smaller than that on shear modulus (G).

The above conclusions are based on the limited test data and to arrive on a quantitative outcome, a more number of samples need to be tested. Nonetheless, the research presented has very much practical significance, as not much study has been reported for this theme.

References

ASTM: D3999-91. (2003). Test method for the determination of the modulus and damping properties of soils using cyclic triaxial apparatus. Annual book of ASTM standards. West Conshohocken, PA: ASTM International.

ASTM: D5311/D5311M. (2013). Standard test method for load controlled cyclic triaxial strength of soil.

Kramer, S. L. (1996). *Geotechnical earthquake engineering*. New Delhi, India: Pearson Education.

Madhusudhan, B. N. (2011). Dynamic properties of dry to fully saturated states using resonant column and bender element tests, Ph.D. thesis, Indian Institute of Science, Bangalore, India.

Madhusudhan, B. N., & Kumar, J. (2013). Damping of sands for varying saturation. *Journal of Geotechnical and Geoenvironmental Engineering, 139*(9), 1625–1630.

Maheshwari, B. K., Kale, S. S., & Kaynia, A. M. (2012). Dynamic properties of Solani sand at large strains: a parametric study. *International Journal of Geotechnical Engineering, 6*(3), 353–358.

RaviShankar, B., Sitharam, T.G., & Govinda Raju, L. (2005). Dynamic Properties of Ahmedabad Sands at Large Strains. In *Proceedings of Indian Geotechnical Conference,* Ahmedabad, pp. 369–372.

Wykeham F. (2008). Manuals of automatic dynamic triaxial system. In *Soil Mechanics Division*. U.K.: Controls Testing Equipment.

Effects of Discontinuities on Rock Slope

Aniruddha Bhaduri and B. K. Maheshwari

Abstract Discontinuities possess a major role in the stability of a rock slope and also influence the behavior and failure patterns of it under different loading environments. In this paper, the effects of different joint patterns on the stability of a 260-m-high slope with a face angle (ψ_f) of 55° are examined under different loading environments. Under gravity loading, when the slope is having out-of-plane joints, it becomes more stable when the dip of the discontinuity (ψ) increases, although failure pattern changes. Plane and rotational failure patterns are observed when ψ becomes less than and greater than ψ_f, respectively. In case of joints dipping into the plane, the shear displacement becomes significantly less than the previous cases, which indicates a toppling failure. Similar observations can be made under rainfall condition and under seismic loading. In the seismic case, shear displacement and block rotations are obtained. The failure mechanisms of the slopes under different joint sets are investigated by obtaining displacements at different time intervals of the seismic loading. Universal distinct element code (UDEC 4.0) is used for all the simulations.

Keywords Discontinuity · Failure pattern · Plane · Rotational Toppling

1 Introduction

Rockslides are a common phenomenon in hilly areas. If the rock slope consists of discontinuities, then the fractured rock slope becomes vulnerable toward failure. The failure patterns of a rock slope depend on the alignments and the orientations of

A. Bhaduri (✉) · B. K. Maheshwari
Department of Earthquake Engineering, Indian Institute of Technology Roorkee, Roorkee 247 667, India
e-mail: aniruddha241991@gmail.com

B. K. Maheshwari
e-mail: bkmahfeq@iitr.ac.in

B. Adimoolam and S. Banerjee (eds.), *Soil Dynamics and Earthquake Geotechnical Engineering*, Lecture Notes in Civil Engineering 15,
https://doi.org/10.1007/978-981-13-0562-7_7

the discontinuities. The basic terminology which defines the orientation of the discontinuities is termed as dip or dip inclination (ψ). It is defined as the maximum inclination of the discontinuity measured from the horizontal. Different failure patterns can be observed depending upon the joint orientations (i.e., out-of-plane and into-the-plane joints) with respect to the dip of the slope face (ψ_f).

Many researchers have used different numerical techniques to get a proper view about the failure mechanism of a jointed rock slope, of which continuum (finite element) and discontinuum (distinct element) techniques are the most common. But continuum techniques have some major difficulties in analyzing a discontinuous medium consisting of several intersecting interfaces. On the other hand, discontinuum codes (like UDEC) are suitable in these cases due to some advantages like allowing finite displacements and rotations of discrete bodies and also recognizing new contact surfaces with progress. Thus, use of discontinuum codes is preferable over the continuum codes in case of discontinuous rock slopes. Bhasin and Kaynia (2004), Noorzad et al. (2008), Pal et al. (2012), Kainthola et al. (2012), and many other researchers have successfully applied the universal distinct element code UDEC (Itasca 2004) for analyzing discontinuous rock slopes.

This paper presents the effects of discontinuities on a 260-m-high jointed rock slope under different loading conditions like static gravity loading and seismic loading. The main objective of the study is to investigate the effects of joint orientations on the mode of failures like plane, rotational sliding, and toppling failures. Modeling and analysis of the slopes have been carried out by using distinct element code UDEC 4.0. Understanding the failure patterns and mechanisms will be helpful while implementing proper method for stabilizing a rock slope.

2 Failure Patterns

There are three common types of failure patterns observed in a rock slope: plane failure, rotational sliding failure, and toppling failure.

2.1 Plane Failure

This type of failure occurs when the sliding plane becomes parallel or sub-parallel to the slope face. Also here, ψ_f is greater than the dip of the sliding plane (ψ) and ψ is greater than the joint friction angle (ϕ or Jfric) of the discontinuity.

2.2 Rotational Sliding Failure

This type of failure occurs when the unstable rock mass slides down along a curved surface. Shear displacement can occur along a circular or non-circular path. When the rock mass becomes densely fractured and fragmented, then this type of failure occurs.

2.3 Toppling Failure

In this mode, the unstable blocks of rocks rotate with respect to a fixed base. When the center of gravity of the column slab of block lies outside the base of the column block, then the rotation takes place. In the jointed rock mass, the discontinuities should be dipping into the face and going away from the face. ψ should be steep, and joints should be closely spaced.

3 Problem Statement

Here, the stability of a 260-m-high rock slope has been simulated. The geometry of the slope is taken from Hammah et al. (2007) and also given by Duncan and Mah (2004). Figure 1 shows the basic geometry of the slope.

The material properties taken for the analysis are given in Table 1.

4 Results and Analysis

Mainly two types of analyses are done: gravity analysis and seismic analysis.

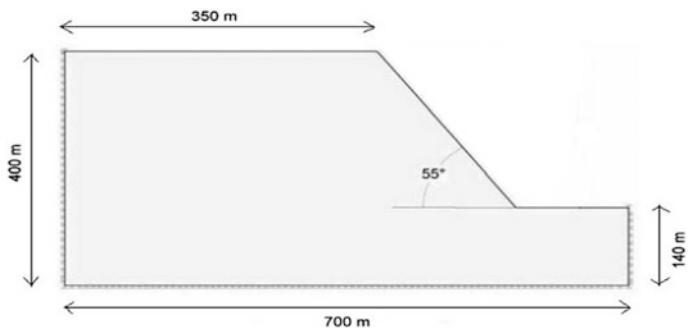

Fig. 1 Basic slope geometry

Table 1 Material properties

Rock mass	Discontinuities
Density = 2610 kg/m^3	Joint normal stiffness (Jk_n) = 100 GPa
Angle of internal friction = 43°	Joint shear stiffness (Jk_s) = 10 GPa
Poisson's ratio = 0.26	Cohesion = 0.1 MPa
Cohesion = 0.675 MPa	Joint friction angle (Jfric) = 40°
Bulk modulus = 9.072 GPa	Joint spacing = 20 m
Shear modulus = 5.184 GPa	–
Tensile strength = 0 MPa	–

4.1 Static Gravity Analysis

Under this analysis, four types of joint alignments are considered. Slope having one joint set with a (1) ψ of 35° out of the plane, (2) ψ of 60° out of the plane, (3) ψ of 75° out of the plane, and (4) ψ of 70° into the plane. Mohr–Coulomb plasticity model has been considered for the material. The factor of safety and the maximum shear displacement values are calculated for all the cases. The results of the analysis are shown in Table 2.

Figure 2 shows the failure patterns for different cases.

From Table 2, we can see that when ψ increases in the out-of-plane direction, the factor of safety also increases and the maximum shear displacement decreases. Thus, the slope becomes more stable with the increase in ψ. But if we compare Fig. 2a–c, we can see that the failure patterns are different. Plane, rotational sliding, and circular sliding failures are observed in the first, second, and third cases, respectively. Plane failure is observed in the first case because here ψ is less than ψ_f. As this postulate does not hold in the second and third cases, rotational sliding failure takes place. In the case when joints are dipping into the plane, we can see that the shear displacement is very small as compared to the other cases. This indicates that it is not a case of shear failure rather a toppling failure. Further parametric studies have been conducted in slopes having two joint orientations (in one case, ψ is 35° out of plane, and in another case ψ is 75° into the plane) by reducing the Jfric in a gradual manner which can correspond to rainfall condition. It has been observed in both the cases that as the joint friction angle reduces, the shear displacement increases and FOS decreases. But a comparative study between the two cases shows that the shear displacement in the case when ψ dips into the plane

Table 2 Results of gravity analysis

Joint alignment	Cases	Dip angle(°)	FOS	Shear displacement (cm)
Out of the plane	First case	35	1.32	5.636
	Second case	60	1.44	4.525
	Third case	75	1.56	3.848
Into the plane	–	70	1.35	0.036

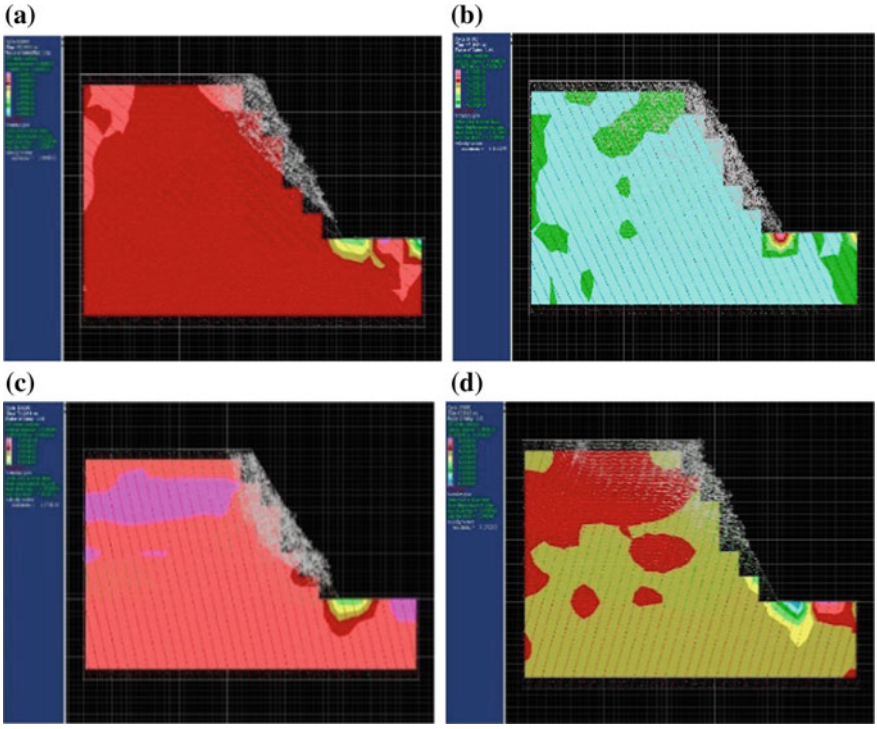

Fig. 2 **a** Plane, **b** rotational sliding, **c** circular sliding, and **d** toppling failure

is very less with respect to the other case when ψ dips out of plane. This observation shows that slope is prone to shear failure when it consists of joints dipping in the out-of-plane direction, while the slope is prone to toppling failure when joint set dips in the into-the-plane direction.

4.2 Slope Under Seismic Loading

Under this condition, again two types of joint alignments are considered. In the first case, the joint set is dipping 70° out of plane, and in the second case, the joint set is dipping 70° into the plane. Here, elastic, isotropic constitutive model has been taken for the material. The seismic loading has been applied as a sinusoidal stress history at the base of the model. The stress history represents the seismic loading of Uttarkashi Earthquake on October 20, 1991. The sinusoidal shear wave which has been applied at the base of the model has a frequency of 3 Hz for a period of 3 s and PGA of 0.3 g. When the sinusoidal loading is applied, the boundary condition has been changed to free field/viscous boundary at the base and in the sides of the model. The viscous boundary conditions are applied to absorb the incoming waves

Fig. 3 Input sinusoidal shear stress waveform at the base of the model

Table 3 Results of seismic analyses

Time duration (s)	Max. shear displacement (cm)		Block rotation (°)	
	First case	Second case	First case	Second case
0	2.10	2.20	0.305	0.580
1	2.38	2.55	0.365	0.756
3	3.51	2.68	0.780	1.315
5	6.87	3.68	1.105	1.902
7	10.26	6.71	1.396	2.133
9	14.09	10.35	1.678	2.340
11	16.70	14.94	1.997	2.585
13	–	18.86	–	2.789

hitting the boundaries. It prevents the reflection of the waves back into the model. The sinusoidal shear stress wave which is applied into the model is shown in Fig. 3.

In these analyses, the behavior of the slope has been observed during and after the earthquake event took place. Maximum shear displacement and the block rotations are observed at each time-step. The results of the analyses have been shown in Table 3.

From Table 3, it is observed that in the first case, the slope failed in shear after 11 s due to great contact overlap. In other observations, it can be seen that in the second case, the maximum shear displacement is lesser, while the block rotation is greater than the first case.

Figures 4 and 5 represent the comparison between two cases with respect to their shear displacements and block rotations, respectively. These observations indicate that when joint sets are dipping in the out-of-plane direction, it is prone to shear failure, while when joint sets are dipping into the plane, toppling failure occurs.

The failure mechanisms for both the first and second cases are shown in Figs. 6 and 7, respectively, at 3-s, 5-s, 9-s, and 11-s time interval.

In Figs. 6 and 7, the plots of velocity vectors along with the total displacements are shown. We can see from both the figures that the displacements are increasing

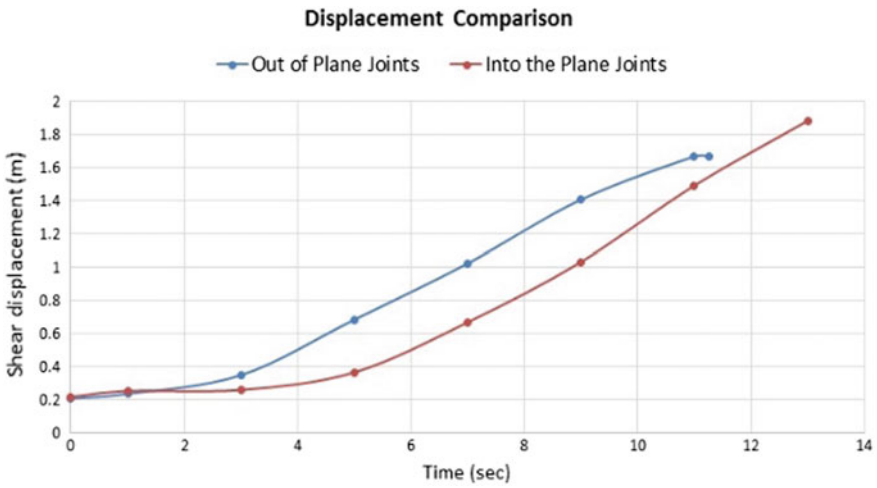

Fig. 4 Comparisons between displacements

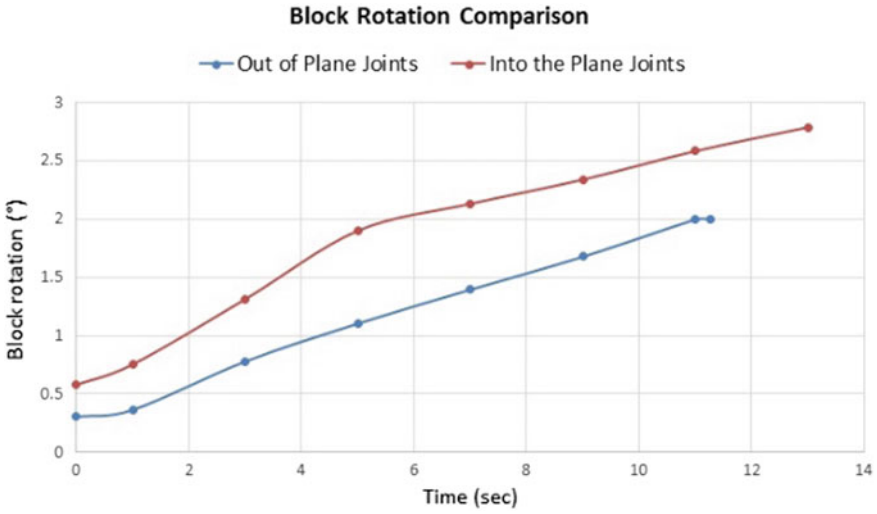

Fig. 5 Comparisons between block rotations

with time. But in Fig. 6, it can also be noted that the lateral and downward shear displacement is more with respect to Fig. 7, while in Fig. 7, in the left portion of slope, the slabs of the blocks are coming out. These observations along with the values obtained from Table 3 indicates that the slope in the first case is prone to shear failure, while in the second case, it is prone to toppling failure.

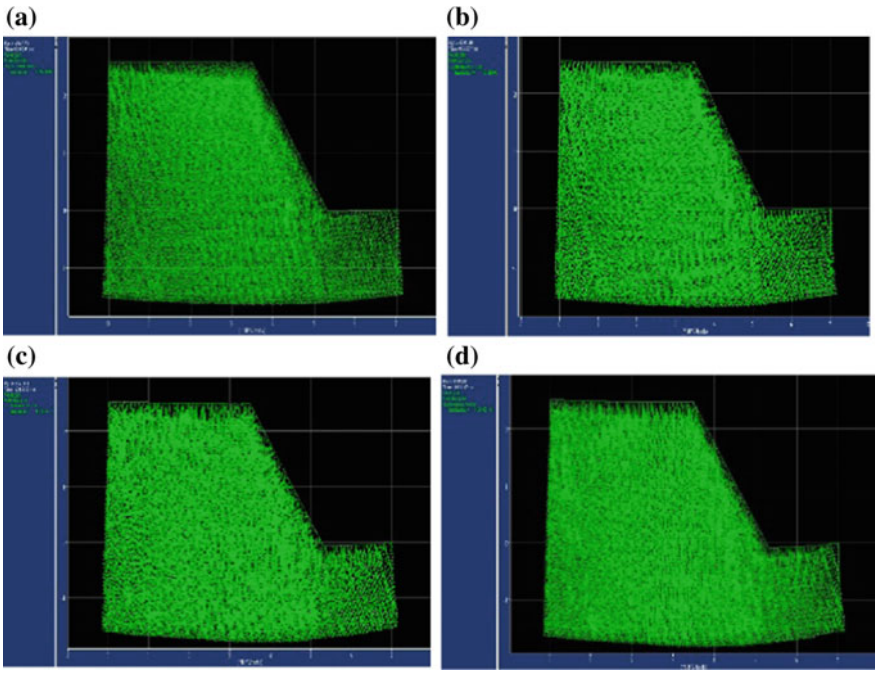

Fig. 6 Failure mechanisms of slopes having out-of-plane joints at **a** 3 s, **b** 5 s, **c** 9 s and **d** 11 s

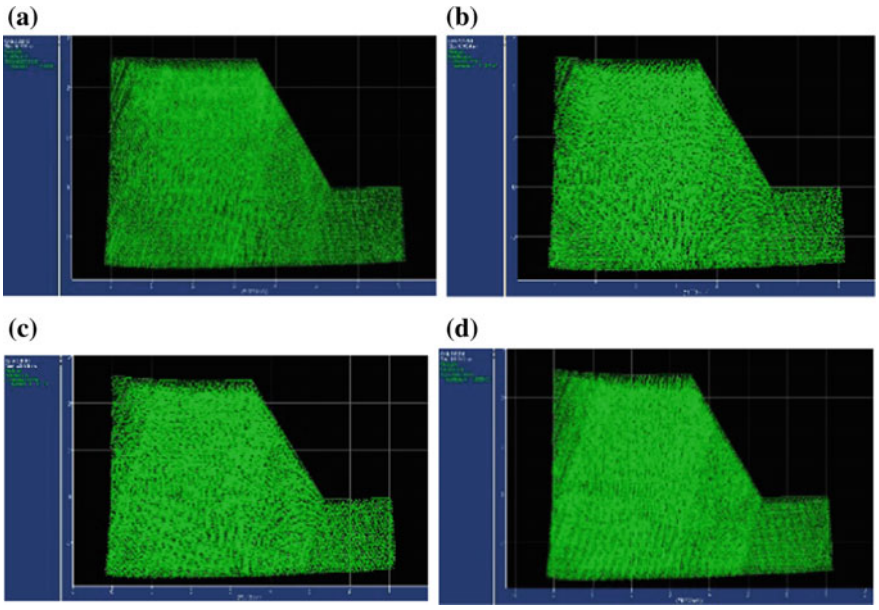

Fig. 7 Failure mechanisms of slopes having into-the-plane joints at **a** 3 s, **b** 5 s, **c** 9 s and **d** 11 s

5 Conclusions

Numerical analysis has been carried out for a 260-m-high rock slope to simulate the effects of joints and their orientations on their respective failure mechanisms. Two types of joint orientations are considered: out-of-plane and into-the-plane joints. The slope has been analyzed under different loading conditions. In the static gravity analysis, it has been observed that when the joint set dips in the out of the plane direction, plane and sliding failures occur. As the dip inclination of the joint set (ψ) gets stepper, the slope becomes more stable against sliding although failure pattern differs. Plane failure takes place when ψ is less than ψ_F, and rotational sliding occurs otherwise. When ψ dips into the plane, then sliding is not the failure pattern, whereas toppling failure occurs. Under rainfall condition, when joint sets dip into the plane, it is more stable against sliding failure in comparison with the case when joint set dips out of plane.

In the seismic analysis, sinusoidal shear stress wave has been applied into the model. Two cases have been investigated. It has been observed that the block rotation is more and the shear displacement is less in the case when slope is having joint sets dipping into the plane in comparison with the case where joint set dips out of the plane. This again indicates a toppling failure for into-the-plane joint alignments and shear failure for the out-of-plane joint sets. These understandings help in suggesting suitable remedial measures for stabilizing a rock slope under different circumstances.

References

Bhasin, R., & Kaynia, A. M. (2004). Static and dynamic simulation of a 700-m high rock slope in western Norway. *Journal of Engineering Geology, 71,* 213–226.

Duncan, C. W., & Mah, C. W. (2004). *Rock slope engineering* (pp. 129–213). Spoon Press.

Hammah, R. E., Yacoub, T. E., Corkum, B., Wibowo, F., & Curran, J. H. (2007). Analysis of blocky rock slopes with finite element shear strength reduction analysis. In *1st Canada–US Rock Mechanics Symposium* (pp. 329–334).

Itasca Consulting Group, Inc. (2004). UDEC theory and background, version 4.0.

Kainthola, A., Singh, P. K., Wasnik, A. B., & Singh, T. N. (2012). Distinct element modelling of Mahabaleshwar road cut hill slope. *Geomaterials, 2*(4), 105–113.

Noorzad, A., Aminpoor, M., & Salari, H. (2008). Seismic slope stability analysis of jointed rock masses on the northern abutment of Gotvand dam, Iran. In *14th World Conference on Earthquake Engineering (14WCEE)*, Bejing, China.

Pal, S., Kaynia, A. M., Bhasin, R. K., & Paul, D. K. (2012). Earthquake stability analysis of rock slopes: A case study. *Journal of Rock Mechanics and Rock Engineering, 45,* 205–215.

Indirect Estimation of Local Soil Response in Light of Past as well as Recent Earthquakes in the Shillong Plateau

Abhishek Kumar and Olympa Baro

Abstract The northeastern region of India is a seismically active zone. The Shillong Plateau (SP) located in the southwestern portion of northeast India surrounded by an intense network of active tectonic faults. The 1897 Assam earthquake (EQ) (M_W 8.1) and other major EQs ($M_W \geq 7.0$) had originated in the faults surrounding the SP, thus highlighting the SP as a zone of high seismicity. During these past major to great EQs, widespread damages in the form of destruction to buildings, excessive ground shaking, uneven settlements, occurrence of ground fissures, and sand vents were reported across the SP and its adjoining regions. Such large-scale catastrophes during an EQ are the combined effect of the ground motions generated during an EQ and its modification by the subsoil at a site. Presence of local soil influences the frequency content, duration, and amplitude of the ground motions generated during an EQ. To understand the ground motion amplification potential at a site due to local soil, recorded ground motions, dynamic soil properties, in situ subsoil characteristics, etc., are required to be known at the site of interest. For majority of location, however, regional dynamic soil properties and in situ subsoil properties are not readily available. In the absence of regional dynamic soil properties, site response studies considering available dynamic soil properties from other regions are followed worldwide. In the present study, response of local soil in the SP is assessed considering the observed ground motion scenario during different EQs at selected sites. Ground motion amplification during each EQ is determined considering the peak horizontal acceleration (PHA) at the bedrock level and the peak ground acceleration (PGA) at the ground surface level. The PHA during each EQ is estimated using regional ground motion prediction equations (GMPEs). The PGA on the other hand is derived based on felt intensities during various EQ at considered sites from isoseismal maps. Thus, the response of in situ soil over a wide range of ground motions is assessed based on actual scenario

A. Kumar (✉) · O. Baro
Department of Civil Engineering, Indian Institute of Technology Guwahati, Guwahati 781039, India
e-mail: abhiak@iitg.ernet.in

O. Baro
e-mail: olympa.baro@iitg.ac.in

B. Adimoolam and S. Banerjee (eds.), *Soil Dynamics and Earthquake Geotechnical Engineering*, Lecture Notes in Civil Engineering 15,
https://doi.org/10.1007/978-981-13-0562-7_8

developed at the surface. This work will be helpful to understand the response of soil during probable future EQs in the absence of regional dynamic soil properties for the SP.

Keywords Shillong Plateau · Local soil effects · Isoseismal maps Amplification factor

1 Introduction

The northeastern region of the Indian subcontinent consists of a number of tectonic faults. The intraplate tectonic movements along these faults have led to the origin of several earthquakes (EQs) in the past (Baro and Kumar 2015). Along with the occurrences of these EQs, the fault movements had also led to the formation of the Shillong Plateau (SP) within the region (Baro and Kumar 2015). The SP is thus surrounded by active faults which have evidenced numerous EQs in the past. The 1897 Assam EQ (M_W-8.1) is one of the great EQs of India which had originated on a fault lying toward the northern boundary of the SP. The tectonic activity of the faults surrounding the SP makes it essential to understand the seismic hazard potential of the plateau (Baro and Kumar 2016).

Seismic hazard analysis of a region involves the estimation of level of ground shaking that could occur at a site due to the presence of seismic sources surrounding the site. The level of ground shaking at a site is expressed in terms of ground motion parameters such as peak ground acceleration (PGA) or peak horizontal acceleration (PHA). To arrive at a particular ground motion parameter, ground motion prediction equations (GMPEs) are used. GMPEs express above ground motion parameters as functions of magnitude, epicentral or hypocentral distances, fault type, site class, etc. Further, GMPEs are developed by performing regression analysis of the recorded ground motions within a region and hence are best suited for that region. Instrumental recording of EQs is a recent phenomenon, especially in India which began only after 1986. In case of non-availability of recorded ground motion data, multiple GMPEs developed for other regions with similar tectonic characteristics are selected to estimate the ground motion parameter for a particular region. Nath and Thingbaijam (2011) emphasized that even though several GMPEs have been developed for India, however while performing seismic hazard analysis for Indian regions during past studies, due consideration was not given to the selection of GMPEs matching the tectonics of the region. Further, Nath and Thingbaijam (2011) based on the log-likelihood (LLH) method of Scherbaum et al. (2009) considered multiple GMPEs and ranked these GMPEs according to their suitability for the Himalayan, northeastern, and peninsular regions of India. For the northeastern region which is an intraplate region, Nath and Thingbaijam (2011) selected eight GMPEs which were developed for various intraplate regions of the world. Among eight GMPEs selected by Nath and Thingbaijam (2011), the top three are used in this study to estimate the PHA at bedrock level for the SP. These

include GMPEs given by Hwang and Huo (1997), Raghukanth and Iyengar (2007) and Nath et al. (2009). In addition, the GMPEs were given by NDMA (2010) and Anbazhagan et al. (2013) are also employed to estimate the PHA for the SP. The GMPE proposed by NDMA (2010) was developed for the entire country with separate set of coefficients for seven different regions within the country including northeast India. Anbazhagan et al. (2013) developed a GMPE for the Himalayan region considering both recorded and synthetically generated ground motion data. The synthetic EQ data was developed for past EQs with no ground motion records, which also included the 1897 Assam EQ originating on the northern edge of the SP. The GMPEs proposed by NDMA (2010) and Anbazhagan et al. (2013) are capable of estimating the PHA for EQs of $M_W \geq 8.0$.

Present work also tests the suitability of the GMPEs proposed by NDMA (2010) and Anbazhagan et al. (2013) for the SP by comparing with the three highly ranked GMPEs for northeast India as per Nath and Thingbaijam (2011).

2 Analysis

The five GMPEs mentioned above are used to estimate the PHA values at selected sites within the SP at the bedrock level. The PHA values thus estimated could be used for hazard estimation of the SP in the future. However, such seismic hazard analysis performed without taking into consideration the effects of the local soil is of limited use. The local soil has the characteristics to modify the EQ ground motion as it travels from the bedrock to the ground surface. Hence, it is essential to consider the local soil effects when estimating the hazard potential of a region. In this study, the effect of local soil is taken into consideration by estimating the ground motion parameter PGA at the surface level for the SP. Thus, the PGA values of some of the past major EQs originating in the faults around the SP are estimated in this study.

To estimate the PGA values, a correlation is developed between Modified Mercalli Intensity (MMI) and PGA in the absence of any correlation existing at present for the SP. Proposed correlation is developed taking into account MMI and PGA values obtained during the 2016 Myanmar EQ (M_W-6.9) and the 2016 Imphal EQ (M_W-6.7) as per United States Geological Survey (USGS) (https://www.usgs.gov/). Even though these two EQs had not occurred on the faults surrounding the SP, the shaking due to the EQs was felt within the plateau. Further, there are no recent major EQs in the vicinity of the SP to develop such correlation. Using the MMI and PGA values reported during the above-mentioned EQs a MMI versus PGA plot is developed as shown in Fig. 1. Figure 1 also shows the correlation developed between MMI and PGA for the SP.

The developed correlation shown in Fig. 1 is used to estimate PGA values during 1885 Bengal EQ (M_L-7.0), 1869 Cachar EQ (M_W-7.5), 1918 Srimangal EQ (M_S-7.6), and 1930 Dhubri EQ (M_S-7.1) based on reported MMI values. It has to be highlighted here that above-mentioned four EQs had originated on faults lying at a

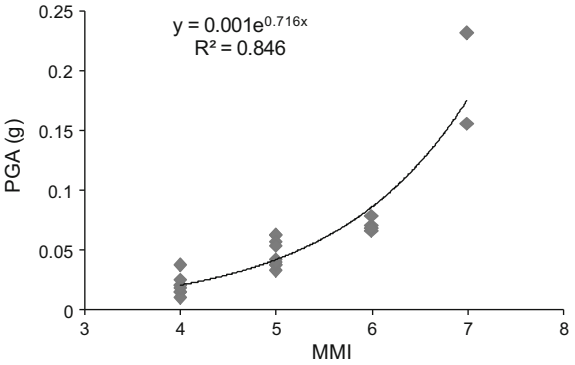

Fig. 1 Correlation between MMI and PGA for the SP

close vicinity of the SP and had caused damages in the SP. The MMI felt within the SP during the above-mentioned past EQs are collected from isoseismal maps. The isoseismal maps were developed by the Geological Survey of India. The Geological Survey of India developed the isoseismal maps for each of these EQs in different intensity scales. Sabri (2002) re-evaluated the intensities for each of the EQs and redrew the isoseismal maps using the European Macroseismic Scale (EMS). In this study, the isoseismal maps developed by Sabri (2002) are used and the EMS scale is converted to MMI scale as per Musson et al. (2010). It was observed from the isoseismal maps that during the various past EQs different sites across the SP experienced different shaking intensities. MMI of VI and V were felt across Shillong city during the 1869 Cachar EQ and 1918 Srimanagal EQ, respectively. Similarly, during the same 1918 Srimanagal EQ, MMI of VI was felt in Cherrapunji. Further, MMI of V and VI during the 1885 Bengal EQ and the 1930 Dhubri EQ, respectively, were reported in Cherrapunji. At Tura as well, MMI of V was reported during the 1885 Bengal EQ. It can be observed from Fig. 1 that the proposed correlation is valid only till a MMI value of 7. For this reason, the PGA value for the 1897 Assam EQ is not estimated using the proposed correlation since a MMI of X was reported due to this EQ within the SP. Thus, employing various MMI values from the isoseismal maps into the proposed correlation, PGA values at the surface level across the SP are estimated.

It has been mentioned earlier that five GMPEs proposed by Hwang and Huo (1997), Raghukanth and Iyengar (2007), Nath et al. (2009), NDMA (2010), and Anbazhagan et al. (2013) are selected in this study to estimate the PHA values at the bedrock level. Using these five GMPEs, PHA values within the SP are estimated as listed in Table 1. It has to be highlighted that soil response which is examined earlier from MMI values is a function of PHA as highlighted by Kumar et al. (2015). In addition, from Table 1 it can be observed that a wide range of PHA from 0.02 to 0.19g has been considered in the present work representing a wide range of ground motion scenario. Taking into account, PHA estimated using each of the five selected GMPEs and above-estimated PGA, amplification factor (AF) which is the

Table 1 PHA and AF values estimated for the past EQs in the SP

Site		Shillong city	Shillong city	Tura	Cherrapunji	Cherrapunji	Cherrapunji
GMPEs		EQ					
		1869 Cachar	1918 Srimangal	1885 Bengal	1885 Bengal	1918 Srimangal	1930 Dhubri
Hwang and Huo (1997)	PHA	0.14	0.13	0.07	0.04	0.20	0.06
	AF	0.51	0.28	0.54	1.00	0.37	1.26
Raghukanth and Iyengar (2007)	PHA	0.12	0.10	0.02	0.01	0.16	0.02
	AF	0.59	0.37	1.93	4.31	0.45	3.80
Nath et al. (2009)	PHA	0.19	0.17	0.11	0.06	0.12	0.10
	AF	0.38	0.21	0.34	0.56	0.64	0.72
NDMA (2010)	PHA	0.02	0.11	0.05	0.03	0.14	0.05
	AF	3.86	0.34	0.66	1.04	0.52	1.34
Anbazhagan et al. (2013)	PHA	0.07	0.06	0.03	0.02	0.09	0.03
	AF	1.08	0.56	1.30	2.11	0.78	2.61

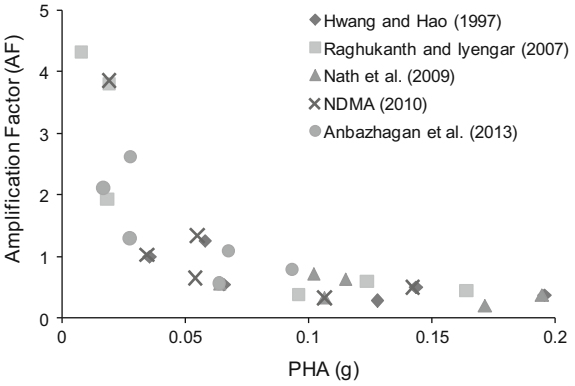

Fig. 2 PHA versus AF obtained from present work

ratio of the PGA to PHA are estimated. Table 1 lists PHA and AF values estimated at various sites within the SP during different EQs.

Kumar et al. (2016b) highlighted that overall soil response can be understood by analyzing collectively the response of soil during different bedrock scenario known as dynamic soil response curve (DSRC). In order to generate an overall understanding of the soil response, DSRC from this work is shown in Fig. 2.

It can be observed from Fig. 2 that for higher PHA values lower values of AF are obtained. This is in accordance to the findings of EPRI (2012), Romero and Rix (2005), and Kumar et al. (2016a, b) where it was found that higher values of PHA give lower values of AF. EPRI (2012) and Kumar et al. (2016a) reported that for PHA higher than $0.5g$ deamplification of AF occurs. From Fig. 2, it can be observed that in this study the deamplification of AF has started to occur at $0.05g$. It has to be highlighted here that most of the sites across the SP are of site classes of A

(firm or hard rocks) or B (soft to firm rocks) as per Mittal et al. (2012). The sites Shillong, Tura, and Cherrapunji chosen in this study are of site classes A, B, and A, respectively. Since the sites are mostly rocks the ground motion amplification is very less within the SP. Hence in Fig. 2, as the PHA value begins to increase the AF starts to decrease.

Another observation which can be made from Fig. 2 is that the GMPEs proposed by NDMA (2010) and Anbazhagan et al. (2013) are closely matching with the other three highly ranked GMPEs.

Nath and Thingbaijam (2011) did not consider GMPEs proposed by NDMA (2010) and Anbazhagan et al. (2013) for northeast India. However, collectively based on PHA observed from Table 1 as well as DSRC from Fig. 2 it can be concluded that the GMPEs proposed by NDMA (2010) and Anbazhagan et al. (2013) are also equally suitable for northeast India both in arriving at seismic hazard values as well as to understand soil response. Similar validation for PHA $> 0.2g$ has not been attempted here and can be attempted during future works.

3 Conclusion

The SP has experienced several damaging EQs in the past. To reduce the risk of damages from similar EQs in the future it is essential to understand the level of ground shaking which occurred within the SP during the past EQs. Hence, in this study an attempt is made to estimate the PHA values at the bedrock level with the help of GMPEs as well as the PGA at the ground surface from isoseismal maps of past EQs. A total of five GMPEs are used to estimate the PHA values. Three of the GMPEs are found to be suitable for northeast India by previous works. Suitability of the remaining two GMPEs for the SP however is tested in this study. Further in situ soil response is studied over a wide range of PHA which is in accordance with existing literature.

References

Anbazhagan, P., Abhishek Kumar, Sitharam, T.G. (2013) Ground motion prediction equation considering combined dataset of recorded and simulated ground motions. *Soil Dynamics and Earthquake Engineering* 53:92–108

Baro, O., & Kumar, A. (2015). A review on the tectonic setting and seismic activity of the Shillong plateau in the light of past studies. *Disaster Advances, 8,* 34–45.

Baro, O., & Kumar, A. (2016). Seismic source characterization for the Shillong plateau in northeast India. *Journal of Seismology* (Under Review).

EPRI. (2012). *Guidelines for determining design basis ground motion*. Palo Alto, CA: Electric Power Research Institute, 1, EPRI TR-102293.

Hwang, H., & Huo, J. R. (1997). Attenuation relations of ground motion for rock and soil sites in eastern United States. *Soil Dynamics and Earthquake Engineering, 16,* 363–372.

Kumar, A., Harinarayan, N. H., & Baro, O. (2015). High amplification factor for low amplitude ground motion: Assessment for Delhi. *Disaster Advances, 8*(12), 1–11.

Kumar, A., Baro, O., & Harinarayan, N. H. (2016a). Obtaining the surface PGA from site response analyses based on globally recorded ground motions and matching with the codal values. *Natural Hazards, 81,* 543–572.

Kumar, A., Harinarayan, N. H., & Baro, O. (2016b). Predicting the surface response spectrum for Nepal based on nonlinear soil response evidenced collectively during recent and past earthquakes. *Natural Hazards* (Under Review).

Mittal, H., Kumar, A., & Ramhmachhuani, R. (2012). Indian national strong motion instrumentation network and site characterization of its stations. *International Journal of Geosciences, 3,* 1151–1167.

Musson, R. M. W., Grünthal, G., & Stucchi, M. (2010). The comparison of macroseismic intensity scales. *Journal of Seismology, 14*(2), 413–428.

Nath, S. K., Raj, A., Thingbaijam, K. K. S., & Kumar, A. (2009). Ground motion synthesis and seismic scenario in Guwahati City–A stochastic approach. *Seismological Research Letters, 80,* 233–242.

Nath, S. K., & Thingbaijam, K. K. S. (2011). Peak ground motion predictions in India: An appraisal for rock sites. *Journal of Seismology, 15,* 295–315.

National Disaster Management Authority (NDMA). (2010). *Development of Probabilistic Seismic Hazard Map of India*. Government of India: National Disaster Management Authority.

Raghukanth, S. T. G., & Iyengar, R. N. (2007). Estimation of seismic spectral acceleration in Peninsular India. *Journal of Earth System Science, 16,* 199–214.

Romero, S. M., & Rix, G. J. (2005). *Ground motion amplification of soils in the upper Mississippi embayment*. Report No. GIT-CEE/GEO-01-1, National Science Foundation Mid America Earthquake Centre.

Sabri, M. S. A. (2002). *Earthquake intensity-attenuation relationship for Bangladesh and its surrounding region* (Master's thesis). Bangladesh University of Engineering and Technology, Dhaka, Bangladesh.

Scherbaum, F., Delavaud, E., & Riggelsen, C. (2009). Model selection in seismic hazard analysis: An information theoretic perspective. *Bulletin of Seismological Society of America, 99,* 3234–3247.

United States Geological Survey (USGS). https://www.usgs.gov/. Assessed July 28, 2016.

Development of Predictive Equation for Vibration Due to DMC Piling

V. Jaya, P. T. Prijil and K. Balan

Abstract Conventional casting of bored cast-in-situ pile which is also known as direct mud circulation (DMC) method was accepted as the most reliable piling system all over the world. Compared to precast pile driving, chiseling action in DMC piling produces low energy. This low energy can produce stress waves in the ground which may cause problems to the adjacent structures. This paper deals with the development of predictive equation for the peak particle velocity (PPV) for different types of soil due to ground vibrations caused during DMC method of piling. Ground vibration analyses were carried out for different soil profiles with different hammer energy impacts. The ground acceleration produced during DMC piling at different distances and depths from the source of vibration were measured on layered soft clay and lateritic soil mediums. The PPV depends on the soil constants k and n. These soil constants for different soil types, such as soft clay and lateritic clay, are compared in this paper. Developed soil constants of DMC piles are then compared with those of driven piles.

Keywords DMC piling · Peak particle velocity · Soil constants
Vibration prediction

V. Jaya
Department of Civil Engineering, Government Engineering College,
Barton Hill, Trivandrum 695035, India
e-mail: jayasraj@gmail.com

P. T. Prijil (✉) · K. Balan
Department of Civil Engineering, College of Engineering Trivandrum,
Trivandrum 695016, India
e-mail: pt.prijil@gmail.com

K. Balan
e-mail: drkbalan@gmail.com

B. Adimoolam and S. Banerjee (eds.), *Soil Dynamics and Earthquake Geotechnical Engineering*, Lecture Notes in Civil Engineering 15,
https://doi.org/10.1007/978-981-13-0562-7_9

1 Introduction

Piling methods are essential for the construction of buildings, transmission towers, and high-rise structures where adequate ground support is not directly available. Conventional bored cast-in-situ piling methods are widely used nowadays over impact-type piling methods. In contrast, vibrations originating from the piling instruments have serious adverse effects on adjacent structures and their foundations, as well as on vibration sensitive installation and occupants of buildings. Thus, the vibration assessment and prediction has become a topic of great interest. Due to the subjective nature, it is difficult to determine the accurate vibration level associated with the piling. In order to analyze the vibration-related problems, the combined effect of several factors such as site characteristics, layering of soil structure, propagation of body and surface waves in the particular soil type are to be considered. Accurate prediction of vibration levels are required to protect the construction companies from fraudulent claims.

Current practices for dealing with the ground vibration during piling operation mainly consider peak particle velocity (PPV) values determined by empirical relations which are easy to predict and compare. The literatures associated with the prediction of PPV values are originally established via empirical correlation determined from actual observation of low-rise residence structural damages (Siskind et al. 1980). Even though there are several empirical methods available for prediction of PPV, most important empirical relations are based on the pioneer generalized form by Wiss (1981). Majority of the studies in ground vibration prediction are related to blasting or mining operations, like predictor equation developed by Aloui et al. (2016). Standards for limiting the ground vibration based on PPV values for blasting and mining operations such as USBM standards, 50.8 mm/s criteria by Svinkin (2003, 2013), can be applied to piling vibrations.

2 Measurement of Ground Vibration

2.1 Site Description

Eight sites with different types of soil strata were selected for the study. Three sites were located at Ernakulam District, three at Alappuzha District, and two at Thiruvananthapuram District in Kerala State.

2.1.1 Type 1: Soft Clay Stratum

Kuttanad region in Alappuzha District is a low-lying area. The soil in this region is highly compressible soft clay overlain by either poorly graded sand or filled laterite

with water table near the ground. Typical borehole details of sites with soft clay are shown in Fig. 2 in Balan et al. (2015).

2.1.2 Type 2: Hard Lateritic Clay Stratum

Lateritic soil is present almost all over the state of Kerala except in coastal and hilly regions. Soil strata present in five sites located at Thiruvananthapuram and Ernakulam are generally laterite with high gravel content as top layer followed by hard lateritic clay with silt content with SPT N value in the range of 25–50 in shallow depths and >50 in deeper layers. Typical bore log details are shown in Fig. 3 in Balan et al. (2015).

2.2 Field Setup

Ground vibrations are induced as the piling operations progressed. Four auxiliary boreholes of diameter 10 cm and at a distance of 2, 4, 8, and 16 m were made at radially opposite directions of piling spot as shown in Fig. 1. Accelerometers placed over steel rods are themselves placed in these boreholes at different depths.

2.3 Peak Particle Velocity

Accelerometers were placed over steel rods which themselves were placed in boreholes at different depths. The ground vibration signals obtained by accelerometers were acceleration time histories, which had amplitude in *g*'s. These acceleration signals are, for engineering purposes, usually quantified in terms of peak particle velocity (PPV). Acceleration signals are processed by doing numerical integration to get corresponding PPV. Digital filter (IIR—infinite impulse response filter) was used to eliminate noise. Figures 2 and 3 represent a typical acceleration time history measured using an accelerometer and PPV time history after application of IIR filter, respectively.

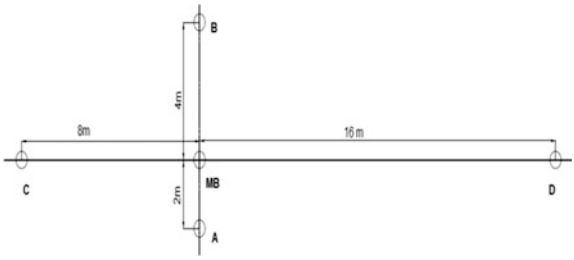

Fig. 1 Field layout showing the position of point of impact and accelerometers

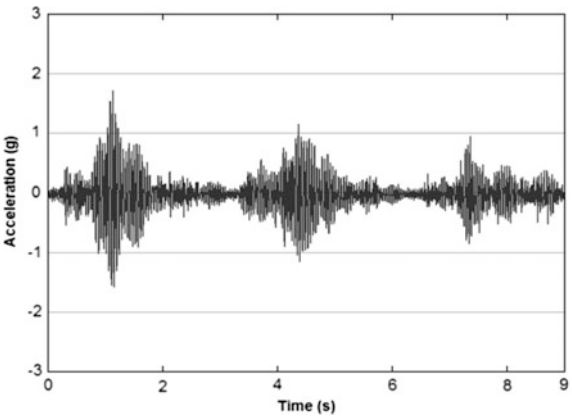

Fig. 2 Acceleration time history of pile driving vibrations

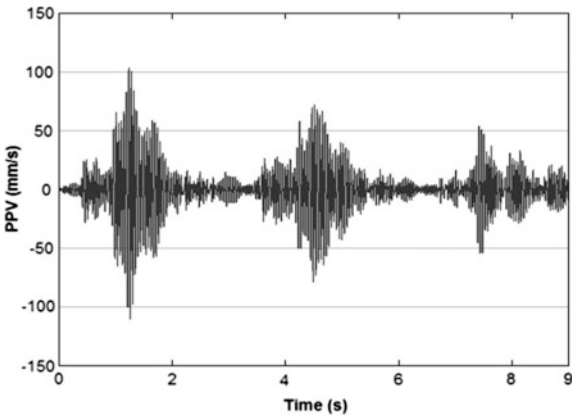

Fig. 3 PPV signal after application of IIR filter

3 Determination of Soil Constants

Vibration predictors generally have two constants such as k and n. These constants are entirely dependent on soil condition and impact source type. The PPV is related to chisel impact energy and distance from the impact by the prediction Eq. (1) (Wiss 1981).

$$V = k\left[\frac{\sqrt{E_n}}{D}\right]^n \tag{1}$$

where

E_n	hammer energy in joules
D	distance from the source in meters
k and n	soil constants and
$\frac{\sqrt{E_n}}{D}$	scaled distance.

Soil constants are determined for each mean depth of impacts and for each site. Table 1 shows the calculated soil constants for various depths and their average values for sites where stiff lateritic clay is present.

Magnitude of soil constant k shows a sudden decrease after a depth of three meters. With the increase in the depth of impact, the magnitude of the surface waves produced will be decreased. Average values are taken accordingly, viz. up to three meters and below three meters. Average values of n are also calculated in a similar manner.

Soil constants are determined for soft clay for four sites having soft clay stratum present below a depth of two meters, and the average values are shown in Table 2.

Similar to the previous case, average values of soil constants are taken up to four meters depth and below four meters depth.

Medium stiff lateritic clay was present in two out of eight study sites. Water table was present near the ground. Average values of soil constants are calculated for these sites, and the results are listed in Table 3. Average soil constants are determined for shallow depths and for depths more than three meters.

Table 1 Average soil constants for stiff lateritic clay

Depth (m)	k	n	Average	
			k	n
1	0.627	1.296	0.610	1.315
2	0.615	1.361		
3	0.589	1.287		
4	0.479	1.194	0.362	1.147
5	0.296	1.144		
7	0.310	1.102		

Table 2 Average values of soil constants for soft clay

Depth (m)	k	n	Average	
			k	n
2	0.621	0.809	0.521	0.898
3	0.432	1.051		
4	0.510	0.834		
5	0.494	0.804	0.411	0.808
7	0.328	0.812		

Table 3 Average soil constants for medium stiff lateritic clay

Depth (m)	k	n	Average	
			k	n
1	0.409	0.937	0.418	0.927
2	0.440	0.929		
3	0.406	0.915		
4	0.386	0.814	0.385	0.812
5	0.399	0.796		
7	0.371	0.826		

Table 4 Average values of soil constants for surface fills

Depth (m)	Sand		Gravelly Laterite	
	k	n	k	n
0	0.391	1.111	0.326	1.194
1	0.609	1.102	0.306	1.079
2	0.304	1.032	0.274	1.041
Average	0.435	1.082	0.302	1.105

Table 5 Predictor equation for different soil types

Soil type	Average soil constants		Predictor equation, (PPV)
	k	n	
Hard lateritic clay	0.610	1.315	$0.610 \times \left[\frac{\sqrt{E_n}}{D}\right]^{1.315}$
Soft clay under WT	0.521	0.898	$0.521 \times \left[\frac{\sqrt{E_n}}{D}\right]^{0.898}$
Medium stiff clay under WT	0.418	0.927	$0.418 \times \left[\frac{\sqrt{E_n}}{D}\right]^{0.927}$
Sand	0.435	1.082	$0.435 \times \left[\frac{\sqrt{E_n}}{D}\right]^{1.082}$
Gravelly laterite	0.302	1.105	$0.302 \times \left[\frac{\sqrt{E_n}}{D}\right]^{1.105}$

Surface fills in the study sites were either poorly graded sand or gravelly laterite. Depth of surface fills varied from 0.8 to 2 m. Table 4 shows calculated values of soil constants and their average values.

PPV predictors are developed using the average values of soil constants for the five different types of soil strata. Table 5 shows the developed predictors for different soil strata. Since magnitudes of soil constants at shallow depths are higher, it determines the maximum possible values of PPV; average values at shallow depths are selected for three cases, viz. hard lateritic clay, medium stiff lateritic clay, and soft clay.

Figure 4 shows variation of predicted PPV for different soil types with scaled distances for shallow depths. These variation will have more engineering significance since it will represent the surface waves, which will propagate more distance than the body waves with higher amplitudes.

Figure 5 represents variation of PPV with scaled distance of impact for different soil types using developed predictor equation for a depth of impact greater than three meters. Scaled distance decreased when either energy of the impact decreased or distance from the source increased. For a particular site where impact energy remains constant, distance from the source alone is the indication of scaled distance.

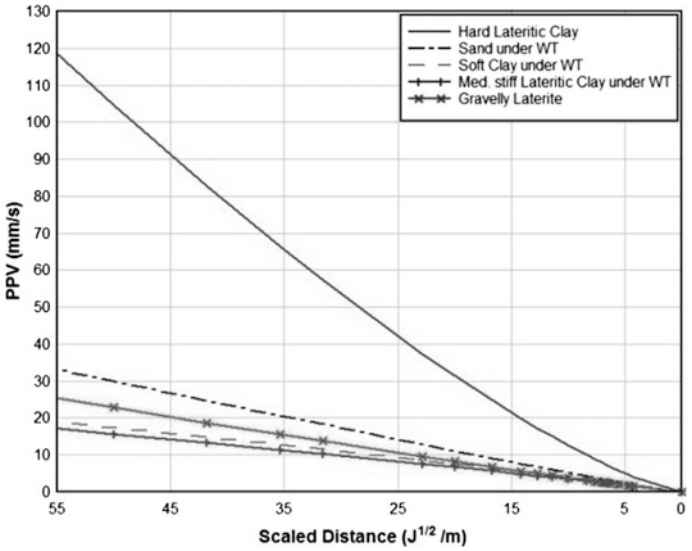

Fig. 4 Variation of predicted PPV values with scaled distances for shallow depths

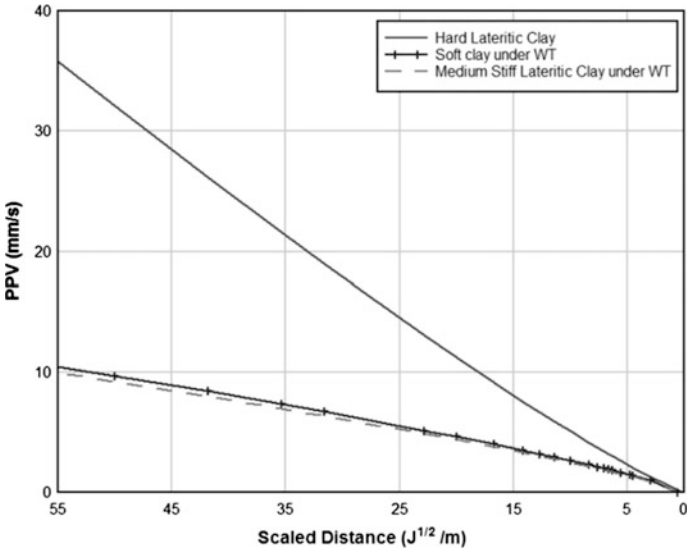

Fig. 5 Variation of predicted PPV values with scaled distances for depth greater than 3 m

Threshold values set by different country's standards by considering safety for low-rise buildings include 50.8 mm/s criteria (Svinkin 2003). A maximum PPV of 2 in./s or 50.8 mm/s is permissible for most of the modern structures if the frequency of excitation is higher.

4 Conclusions

Predictor equations for PPV are developed for each soil type. Efficiency of pile impact was not considered in the study. It is evident that presence of water table decreases the ground vibration amplitude. Medium stiff lateritic clay, highly compressible soft clay, poorly graded sand and gravelly laterite will propagate ground waves similar in terms of magnitude in immersed condition. Structures situated in these types of sites will be safe against damage during piling operations except for damage due to liquefaction of surface sand.

Sites where hard lateritic clay is present will show higher magnitudes of PPV and susceptibility for damage at shallow depths. Maximum possible PPV will exceed the permissible limit of 50.8 mm/s when the scaled distance is more than 30 $J^{1/2}$/m. Piling vibrations at depths more than three meters will induce only 1/3rd of that produced in shallow depths for higher scaled distances.

References

Aloui, M., Bleuzen, Y., Essefi, E., & Abbes, C. (2016). Ground vibrations and air blast effects induced by blasting in open pit mines: Case of Metlaoui Mining Basin, South western Tunisia. *Journal of Geology and Geophysics, 5*, 3.

Balan, K., Jaya, V., & Arun, C. (2015). Prediction of ground vibrations produced in DMC type of piling through soft and hard strata. *Indian Geotechnical Journal*.

Siskind, D. E., Stagg, M. S., Kopp, J. W., & Dowding, C. H. (1980). *Structure response and damage produced by ground vibration from surface mine blasting*. Report of Investigations 8507, Office of Surface Mines, US department of Interiors, USA.

Svinkin, M. R. (2003). *Drawbacks of blast vibration regulations*. www.vulcanhammer.net/svinkin/BLST-CRT.pdf.

Svinkin, M. R. (2013). Forensic engineering of construction vibrations. *Forensic Engineering, 166* (2), 81–93.

Wiss, J. F. (1981). Construction vibrations: State-of-the-art. *Journal of Geotechnical Engineering Division, 107*(No. GT2), 167–181.

Effect of Fines on Pore Pressure Development During Cyclic Loading

Muttana S. Balreddy, S. V. Dinesh and T. G. Sitharam

Abstract Earthquake is one of the natural calamities that occur on large geographical area. During earthquakes, liquefaction of saturated soil deposit is a major cause for failure of various infrastructure as well as lifeline facilities. The cause for liquefaction is the build-up of excess hydrostatic pressure due to the application of cyclic shear stresses induced during ground shaking. From the literature review, it is understood that the mechanism of pore pressure generation of sand and sand–fines mixtures is still not clear and requires further investigation/research. In this paper, a series of stress-controlled cyclic triaxial undrained shear tests were conducted on reconstituted sample of sand–fines mixtures for evaluating and understanding the pore pressure build-up in soils. Sand was procured from Cauvery river bed, Karnataka, and locally available low plasticity clay fines were used to prepare sand–fines mixtures. The results indicate that the presence of fines reduces the pore pressure build-up when compared to clean sand.

Keywords Pore pressure generation · Liquefaction · Sand–fines mixtures Relative density

M. S. Balreddy (✉) · S. V. Dinesh
Department of Civil Engineering, Siddaganga Institute of Technology, Tumakuru 5720103, Karnataka, India
e-mail: muttanab@gmail.com

S. V. Dinesh
e-mail: dineshsv2004@gmail.com

T. G. Sitharam
Department of Civil Engineering, Indian Institute of Science, Bangalore 560012, Karnataka, India
e-mail: sitharam@civil.iisc.ernet.in

B. Adimoolam and S. Banerjee (eds.), *Soil Dynamics and Earthquake Geotechnical Engineering*, Lecture Notes in Civil Engineering 15,
https://doi.org/10.1007/978-981-13-0562-7_10

1 Introduction

The liquefaction phenomenon has received intensive attention since the devastating earthquakes of Alaska and Niigata in Japan. The development of excess pore pressure under undrained loading condition is a hallmark of all liquefaction phenomena. Since then, many investigations have been carried out research in this area. For cyclic loading, two methods are used to study the rate and magnitude of pore pressure generation. The first method is stress-controlled cyclic tests, in which the generation of excess pore pressure is evaluated as a function of the number of loading cycles. The second method is strain-controlled cyclic tests with measurement of excess pore pressure with loading cycles for a given shear strain level. Lee and Albaisa (1974) found a continuous increase in excess pore pressure as the cyclic loading progressed. They suggested that the excess pore pressure falls within a narrowband for a given sand and is insensitive to the soil's initial density and consolidation stress. Dobry et al. (1982) examined pore pressure generation during strain-controlled, undrained cyclic loading as a function of the shear strain. They too observed that the measured excess pore pressure fell within a narrowband and found that it did not develop until a threshold shear strain is reached. Polito and Martin (2003) and Sitharam and Govindaraju (2007) studied the behaviour pore pressure generation, in which the parameters such as amount and the nature of the fines (plastic or non-plastic) play a critical role.

Hazirbaba and Rathje (2009) reported decrease in excess pore water pressure in silty sands and increase in threshold strain. They also reported that limited data are available wrt effect of plastic fines on pore pressure build-up.

Mohtar et al. (2013) examined the pore pressure generation in sand with bentonite. They concluded that the presence of bentonite fines reduces the mean pore pressure generated per loading cycle.

Bayat et al. (2014) showed that pore pressure build-up in sandy soil mixed with plastic fines is slower than pure sand.

Benghalia et al. (2015) conducted tests on Chelf sand with Chelf fines having PI = 13 (low plastic fines). They concluded that the pore pressure decreases up to 10% fines content and then rises again moderately.

Eswara Rao et al. (2015) studied the effect of plastic fines (PI = 33) content on pore pressure generation. They found that the pore pressure increases for 10% plastic fines but there is decrement with increase in fines content up to 15% for 20% fines and 40% for 40% fines.

Therefore in the present paper, an attempt is made to understand the pore pressure generation during cyclic loading in sand–fines mixtures. The mixtures are silty sand and low plasticity clayey sands.

2 Experimental Investigation

2.1 Index Properties of Sand, Fines and Sand–Fines Mixtures

The sand sample used in the present investigation was collected from the Cauvery river bed, Karnataka. In order to study the effect of fines in the sandy soil on pore pressure build-up, clayey sand with low plasticity was collected from local area. Figure 1 shows the grain size distribution curves of both soil samples used in the present investigation. Table 1 gives the summary of the index properties of these soils.

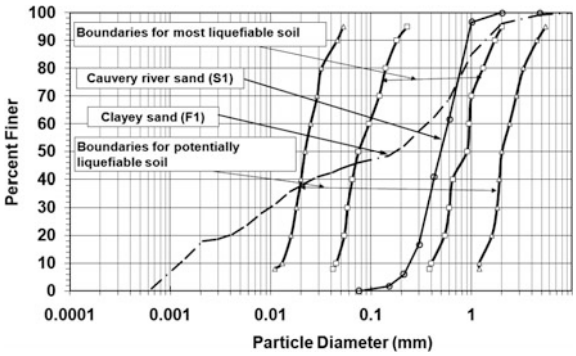

Fig. 1 Grain size distribution curves of sand, clayey sand and those susceptible to liquefaction proposed by Tsuchida (Iwasaki, 1986)

Table 1 Index properties of soils

Properties	Cauvery River sand (S1)	Clayey sand (F1)
Specific gravity (G)	2.62	2.65
Gravel (%)	–	1
Sand (%)	100	53
Silt (%)	–	28
Clay (%)		18
C_u	2.40	–
C_c	0.90	–
e_{max}	0.99	–
e_{min}	0.72	
LL (%)	0	46
PL (%)	0	27
PI	0	19
IS classification	SP	SC

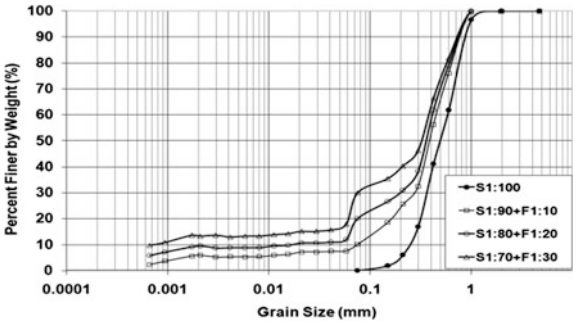

Fig. 2 Grain size distribution curves of soil mixture

Table 2 Index properties of sand and sand–fines mixtures

Soil mixtures	S1:90 + F1:10	S1:80 + F1:20	S1:70 + F1:30
Fines (%)	10	20	30
D_{10}	0.075	0.021	0.0008
e_{max}	0.98	1.06	1.31
e_{min}	0.60	0.61	0.72
LL	22	26	37
PI	0	6	17
IS classification	SW-SM	SC	SC

The fines <75 μm size used in the experimental program were obtained from the clayey sand. These fines were mixed with the clean Cauvery River sand in 90:10, 80:20 and 70:30 (i.e. S1:70 + F1:30) proportions. Figure 2 shows the grain size distribution curves of sand–fines mixtures used in the present investigation. Table 2 shows the index properties of sand–fines mixtures.

2.2 Sample Preparation

Triaxial cylindrical soil specimens of 50 mm diameter and height 100 mm were prepared by dry deposition method. The required mass of oven-dried Cauvery River sand (S1) and F1 fines corresponding to gross void ratio were weighed separately, and both mixtures were divided into ten equal parts. The sand and fines were mixed uniformly, and each part was gently poured into the mould by using a funnel having a 12-mm-diameter nozzle in dry state with zero fall height so that a loose soil sample is formed. The required relative density is achieved by giving uniform blows on all four sides of the mould by wooden mallet. In this way, the sample was prepared by filling the mould in ten layers of equal height. Then, the sample was subjected to small vacuum of 5 kPa and carbon dioxide gas was passed for one hour.

2.3 Saturation, Consolidation and Shearing

The specimens were drained by de-aired distilled water through soil sample at a very small head of 5 kPa. The specimens were saturated by applying a back pressure of 100 kPa, and saturation time was maintained till Skempton's pore pressure coefficient '*B*' value exceeds 0.95. Required cell pressure (100 kPa) was applied, and specimens were isotropically consolidated till the end of Casagrande's primary consolidation. After the consolidation process, the specimens were subjected to undrained shearing at constant confining pressure.

2.4 Stress-Controlled Test

The isotropically consolidated cylindrical specimens were subjected to undrained stress-controlled, constant amplitude cyclic loading tests at a frequency of 0.1 Hz. ASTM D 5311 (1996) code was followed for stress-controlled technique. The loading system consists of a submersible load cell of 5 kN capacity, and the deformation was measured by LVDT. Four transducers were used to record the lateral deformation, volume change, pore water pressure and cell pressures. The data was acquired by a computer-controlled data acquisition system (CCDAS). 128 data points were captured in each loading cycle. The cyclic stress, axial strain, pore water pressure and confining pressures are the test parameters and were recorded by CCDAS. Tests were continued till excess pore water pressure is equal to confining pressure or the double amplitude axial strain is in excess of 5%.

3 Results and Discussion

Figure 3 shows the plot of residual pore pressure ratio versus cycle ratio for sand–fines mixtures with 0–30% fines content at relative density 50%. The pore pressure ratio was computed based on residual pore water pressure at zero deviator stress at the end of each loading cycle. The term r_u is a function of the cycle ratio (N/N_L), which is the ratio of number of applied uniform cycles of loading (N) to the number of cycles required to cause liquefaction (N_L). It is observed that all the specimens failed by flow liquefaction. It is clearly observed from Figs. 3 and 4 that the pore pressure development in sand and silty sand with 10% fines shows the same trend.

Sand–fines mixtures containing 20% fines with PI = 6 and 30% fines with PI = 17 also fail by flow liquefaction. However, the rate of pore pressure generation is faster than compared to sand and sand–fines mixtures containing 10% fines. The results indicate that pore pressure generation is faster with increase in PI.

Figure 5 shows the plot of residual pore pressure ratio versus cycle ratio for sand–fines mixtures with 0–30% fines content at relative density 70%. It is

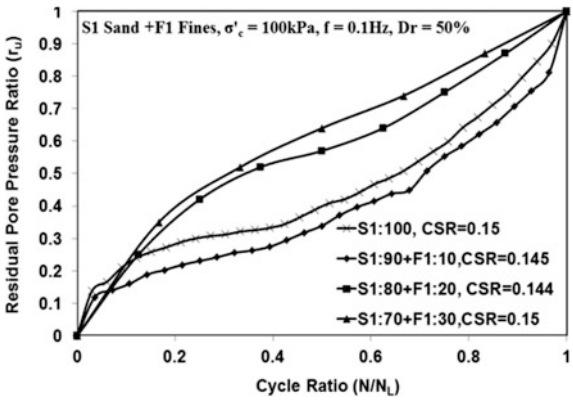

Fig. 3 Residual pore pressure ratio versus cycle ratio of sand–fines mixtures at Dr = 50%

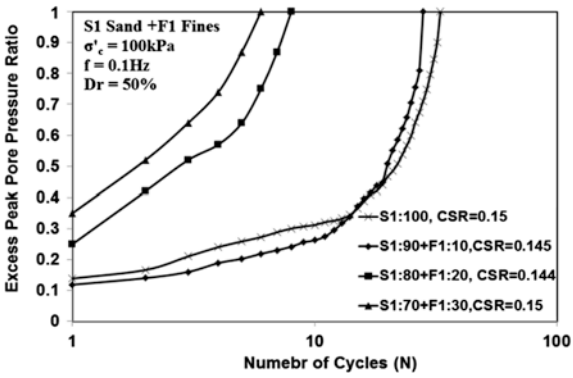

Fig. 4 Excess peak pore pressure generation at Dr = 50% for sand–fines mixtures

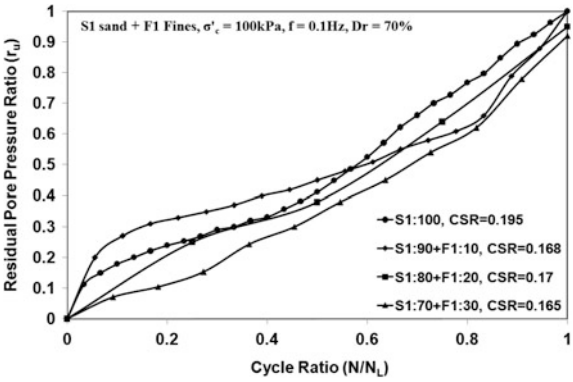

Fig. 5 Residual pore pressure ratio versus cycle ratio of sand–fines mixtures at Dr = 70%

observed that the specimens of sand–fines mixtures containing 20 and 30% fines fail by cyclic mobility due to residual pore pressure not reaching one and effective stress not becoming zero. The residual pore pressure values vary in a narrowband more or less uniformly for all the mixtures.

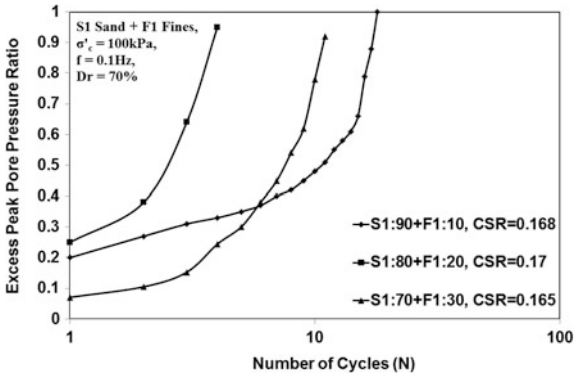

Fig. 6 Excess peak pore pressure generation at Dr = 70% for sand–fines mixtures

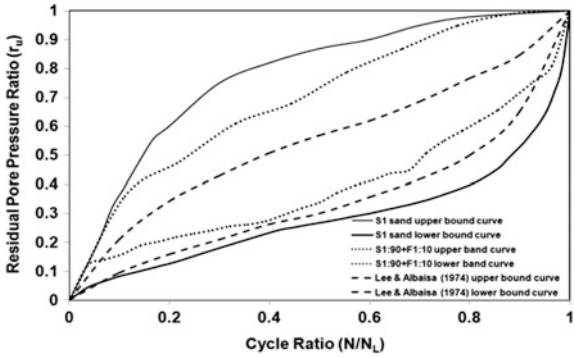

Fig. 7 Residual pore pressure ratio versus cycle ratio of present work with the work of Lee and Albaisa (1974)

Figure 6 shows that the specimens with 20 and 30% fines with PI = 6 and 17 compacted at Dr = 70% fail by cyclic mobility. The results also indicate that the pore pressure build-up is faster with 20% fines than specimen with 30% fines. This indicates that in dense samples the pore pressure build-up decreases with increase in PI > 6 and shows clay-like behaviour, and these results are in agreement with Bayat et al. (2014).

Figure 7 shows the plot of residual pore pressure ratio (r_u) versus cycle ratio (N/N_L) for S1 sand and sand–fines mixtures containing 10% fines at loose and dense state. In addition, the band of pore pressure ratio for sample is shown along with the data of Lee and Albaisa (1974). The Lee and Albaisa (1974) band is generated from large number of tests conducted at 30–100% relative density for Monterey sand. The shape of pore pressure ratio band of S1 sand and sand–fines mixtures is similar to that of Lee and Albaisa (1974). The upper band of present work clearly locates above that of Lee and Albaisa (1974) and lower band of S1 sand locates below that of Lee and Albaisa (1974) but the lower band of S1:90 + F1:10 locates above the lower band of S1 sand and Lee and Albaisa (1974). The pore pressure ratio is much wider at any cycle ratio for S1 sand compared to sand–fines mixtures.

4 Conclusions

The following conclusions are drawn from the experimental evidence.

1. The clean sand and sand–fines mixtures containing 10–30% fines attain pore pressure ratio of 1 and fails by flow liquefaction at Dr = 50%. However, sand–fines mixtures with 20 and 30% fines content at Dr = 70% will have $r_u < 1$ and fails by cyclic mobility.
2. The excess pore water pressure in dense sand–fines specimens (Dr = 70%) decreases with increase in PI (PI > 6).
3. The pore pressure build-up is faster with increase in PI in loosely compacted specimens (Dr = 50%) when compared to dense specimens (Dr = 70%).
4. The shape of pore pressure ratio curves of sand and sand–fines mixtures is similar to published Lee and Albaisa (1974). The S1 sand and sand–fines mixture band are broader than Lee and Albaisa (1974).

References

ASTM D 5311. (1996). *Standard test methods for load controlled cyclic triaxial strength of soil*. American Society for Testing and Materials, USA.

Bayat, M., Bayat, E., Aminpour, H., & Salarpour, A. (2014). Shear strength and pore-water pressure characteristics of sandy soil mixed with plastic fine. *Arabian Journal of Geosciences, 7*(3), 1049–1057.

Benghalia, Y., Bouafia, A., Canou, J., & Claude Dupla, J. (2015). Liquefaction susceptibility study of sandy soils: effect of low plastic fines. *Arabian Journal of Geosciences, 8,* 605–618.

Dobry, R., Ladd, R. S., Chang, R. M., & Powell, D. (1982). *NBS Building Science Series 138: Prediction of pore water pressure build up and liquefaction of sands during earthquakes by the cyclic strain method* (pp. 1–150). Washington DC.

Eswara Rao, S., Varghese, V., & Patel, S. (2015). An experimental study on effect of plastic fines content on liquefaction properties of sand. In *50th Indian Geotechnical Conference*, Pune, India.

Hazirbaba, K., & Rathje, E. M. (2009). Pore pressure of silty sands due to induced cyclic shear strains. *Journal of Geotechnical and Geoenvironmental Engineering, ASCE, 135*(12), 1892–1905.

Lee, K. L., & Albaisa, A. (1974). Earthquake induced settlements in saturated sands. *Journal of Geotechnical Engineering Division, ASCE, 100*(GT4), 387–406.

Mohtar, C. S., Bobet, A., Drnevich, V. P., Johnston, C. T., & Santagata, M. C. (2013). Pore pressure generation in sand with bentonite: from small strains to liquefaction. *Géotechnique, 64* (2), 108–117.

Polito, C. P., & Martin, J. R. (2003). A reconciliation of the effects of non-plastic fines on the liquefaction resistance of sands reported in the literature. *Earthquake Spectra, 19*(3), 635–651.

Sitharam, T. G., & Govindaraju, L. (2007). Pore pressure generation in silty sands during cyclic loading. *Geomechanics and Geoengineering: An International Journal, 2*(4), 295–306.

Comparative Study of Dynamic Response Analysis of Shallow Foundation on Layered Soils

M. V. Ravi Kishore Reddy, Supriya Mohanty and Pradeep Kumar Ramancharla

Abstract Dynamic response analysis of shallow foundation in time-varying motion is very much essential in the present days. As the seismic events are unpredictable, it draws the attention of researchers towards the response of the soil foundation system against dynamic loading. Hence, in the present study, an attempt has been made to investigate the dynamic response of a shallow foundation (continuous footing) resting on different layered soil deposits subjected to seismic loadings. The layered soil deposits considered for the analysis are weak clay underlain by stiff clay (case I) and loose sand underlain by stiff clay (case II). In addition, comparative studies have been made considering the parameters like layered soil types (case I and II), water table effects (dry and partially saturated) and seismic loadings (Bhuj earthquake: M_w—7.7 and Nepal earthquake: M_w—7.8) conditions. The modelling of the soil foundation system has been carried out using two-dimensional finite element software CyclicTP. The response of the dynamic analysis of shallow foundation on layered soils is presented in the form of peak acceleration; horizontal and vertical displacement; shear stress versus shear strain; and excess pore pressure variations at different locations. The results of the analysis indicate that the peak acceleration, horizontal and vertical displacements are more in both the cases (I and II) under the excitation of Nepal earthquake than the Bhuj earthquake motion. Also, it is observed that the response in terms of peak acceleration, horizontal and vertical displacement is more in partially saturated state than in dry state for both the earthquake motions.

Keywords Dynamic response · Seismic loading · Nonlinear analysis
Peak acceleration · Displacement history

M. V. Ravi Kishore Reddy · S. Mohanty (✉) · P. K. Ramancharla
Earthquake Engineering Research Centre, International Institute of Information Technology, Hyderabad 500032, Telangana, India
e-mail: supriya.mohanty@iiit.ac.in

M. V. Ravi Kishore Reddy
e-mail: meegada.reddy@research.iiit.ac.in

P. K. Ramancharla
e-mail: ramancharla@iiit.ac.in

B. Adimoolam and S. Banerjee (eds.), *Soil Dynamics and Earthquake Geotechnical Engineering*, Lecture Notes in Civil Engineering 15,
https://doi.org/10.1007/978-981-13-0562-7_11

1 Introduction

The response analysis of a system to any dynamic load such as blasting, explosions, earthquake is very much essential in the present days. As the earthquake events are unpredictable, it draws the attention of researchers towards the response analysis of soil foundation system against earthquake loading. The response of the soil foundation system depends on the nature of the soil, type of loading and the type of foundation. The response of the soil foundation system during seismic events is of great importance, and it may be directly related to the damage and loss of life and property. Many researchers have performed numerical analysis on the seismic response and settlement of foundation and structures resting on different soils (Asgari et al. 2014; Liu and Dobry 1997; Ragheb 1994; Stokoe et al. 2013; Yoshimi and Tokimatsu 1977). Study on liquefaction of soil, its effects on footings and buildings have been investigated by many researchers (Elgamal et al. 2005; Ishihara et al. 1993; Kishida 1966; Seed and Idriss 1967). Also, studies have been done on dynamic behaviour and liquefaction evaluation of Indian pond ash samples (Mohanty and Patra 2012; Mohanty and Patra 2014; Mohanty and Patra 2016a, b).

As the determination of the response of a soil foundation system is demanding in a layered soil deposit than in homogeneous soil deposit, it is attempted to investigate the dynamic response of a shallow foundation (continuous footing) resting on different layered soil deposits (case I: weak clay underlain by stiff clay, and case II: loose sand underlain by stiff clay) subjected to seismic loadings. Also, comparative studies have been made considering the parameters like layered soil types (case I and II), water table effects (dry and partially saturated) and seismic loadings (Bhuj: M_w—7.7 and Nepal: M_w—7.8 earthquakes) conditions. The results of the analysis were presented in terms of acceleration, displacement and pore pressure time history, shear stress variation with shear strain at different locations.

2 Input Data

The following parameters are considered for the dynamic response analysis of shallow foundation resting on layered soil deposit.

2.1 Foundation Parameters

Foundation width (B): 1.5 m, height above ground surface: 0.4 m, depth below ground surface: 1 m, Young's modulus of concrete: 25E+6 kPa, Poisson's ratio: 0.3, mass density: 2300 kg/m^3.

2.2 Soil Parameters

The soil domain has a width of 15 m and a depth of 15 m, and the water table is considered at a depth of 2 m below the ground surface. Hard rock has been considered at a depth of 15 m below the ground surface. Table 1 represents the details of soil parameters considered in the present study.

2.3 Input Motions

Input motions considered for the analysis are Bhuj earthquake (M_w = 7.7, 2001) and Nepal earthquake (M_w = 7.8, 2015). Peak acceleration values noticed for Bhuj and Nepal earthquake are 0.106 g at 46.94 s and 0.1639 g at 49.31 s, respectively. Typical diagram of input motion of Bhuj and Nepal earthquake used in the present analysis is shown in Fig. 1.

Table 1 Details of soil parameters considered

Case	Layer no.	Thick (m)	Soil type (V_s in m/s)
I	1	2.5	Cohesive soft (V_s = 100)
	2	3	Cohesive stiff (V_s = 300)
	3	3	Cohesive stiff (V_s = 300)
	4	6.5	Cohesive stiff (V_s = 300)
II	1	2.5	Cohesionless loose (V_s = 185)
	2	3	Cohesive stiff (V_s = 300)
	3	3	Cohesive stiff (V_s = 300)
	4	6.5	Cohesive stiff (V_s = 300)

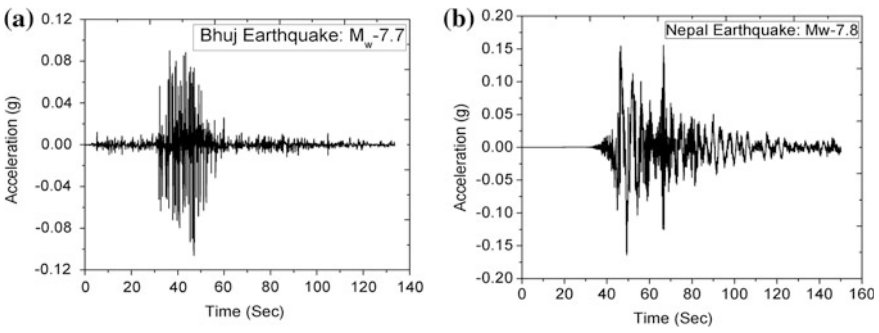

Fig. 1 Acceleration time history of **a** Bhuj and **b** Nepal earthquake

3 Numerical Modelling

The modelling of the soil foundation system has been carried out using two-dimensional finite element software CyclicTP. Cyclic TP is a PC-based graphical pre-processor and post-processor (user-interface) for two-dimensional finite element analysis of shallow foundations subjected to seismic excitations. Both linear analysis (with viscous damping) and nonlinear analysis (plasticity-based nonlinear soil compatibility) can be performed by this program. 9 (solid phase)–4 (fluid phase)-noded quadratic element has been employed for modelling the soil domain. The soil domain has a total number of 1246 elements. A typical representation of generated finite element mesh of the soil domain (case I) is shown in Fig. 2. The boundary conditions considered in the finite element modelling of the foundation soil system are: (i) at any given depth, displacement degrees of freedom of the left and right boundaries were tied together both horizontally and vertically, (ii) the soil surface was traction free, with zero prescribed pore pressure, and (iii) the base and lateral boundaries were impervious.

4 Results and Discussions

Here, the results of 2D dynamic response analysis of shallow foundation are presented in terms of acceleration, displacement, stress–strain and excess pore pressure responses. The results are discussed in the following sections.

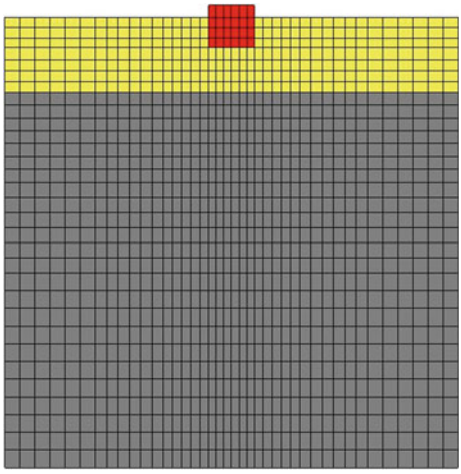

Fig. 2 Generated finite element mesh of the soil domain (case I)

4.1 Acceleration Responses

The acceleration responses have been recorded at different depths of the soil domain. Typical diagrams of acceleration time history and PGA variation with depth for partially saturated soil of case I under the excitation of Bhuj earthquake are presented in Figs. 3 and 4, respectively. The peak ground acceleration (PGA) value of 1.7745 m/s^2 is observed at 47.07 s for case I partially saturated soil under Nepal earthquake as input motion.

It is observed that PGA value is more in case I than in case II soil (Table 2). Also, PGA values are found to be more in partially saturated condition than in dry condition for both the cases under the considered input motions.

4.2 Displacement Responses

The displacement responses have been recorded at different depths of the soil domain. Typical diagram of horizontal displacement variation with depth for partially saturated soil of case I under the excitation of Bhuj earthquake is presented in

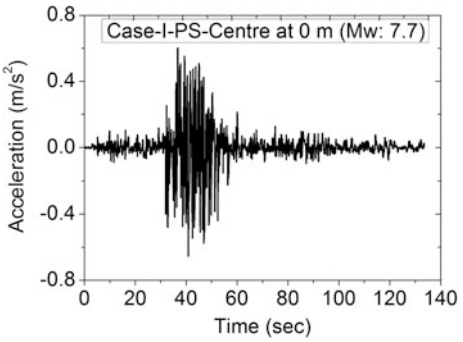

Fig. 3 Acceleration time history for partially saturated soil of case I at 0 m from the centre of footing (M_w: 7.7)

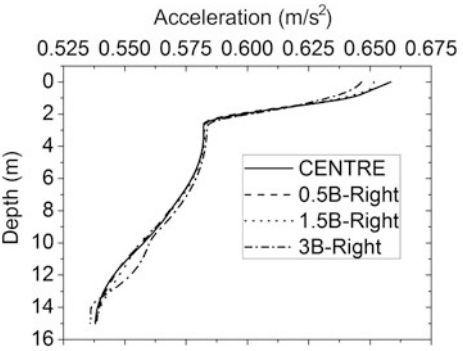

Fig. 4 Variation of acceleration with depth for partially saturated soil of case I (M_w: 7.7)

Table 2 Variation of peak ground acceleration (PGA) at different locations

Case	Condition	M_w	PGA (m/s^2)			
Distance from footing centre →			Centre	0.5B (R)	1.5B (R)	3B (R)
I	Dry	7.7	0.6510	0.6510	0.6429	0.6417
		7.8	1.7688	1.7688	1.7689	1.7684
	Partially saturated (PS)	7.7	0.6585	0.6585	0.6515	0.6466
		7.8	1.7740	1.7740	1.7744	1.7745
II	Dry	7.7	0.5938	0.5938	0.5922	0.5953
		7.8	1.7405	1.7405	1.7412	1.7415
	Partially saturated (PS)	7.7	0.597	0.597	0.596	0.599
		7.8	1.7439	1.7439	1.7447	1.744

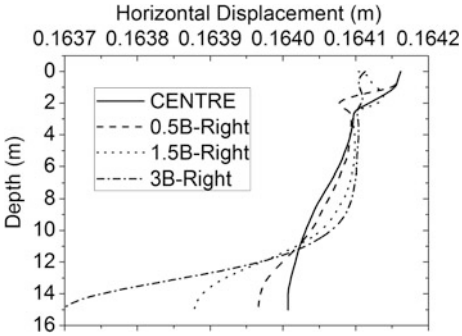

Fig. 5 Variation of horizontal displacement with depth for partially saturated soil of case I (M_w: 7.7)

Table 3 Variation of horizontal displacement at different locations

Case	Condition	M_w	Horizontal displacement (m)			
Distance from footing centre →			Centre	0.5B (R)	1.5B (R)	3B (R)
I	Dry	7.7	0.161	0.161	0.161	0.161
		7.8	1.2495	1.2495	1.2492	1.2493
	Partially saturated (PS)	7.7	0.16416	0.16416	0.16414	0.16411
		7.8	1.3083	1.3083	1.3081	1.3081
II	Dry	7.7	0.1648	0.1648	0.1648	0.1648
		7.8	1.3042	1.3042	1.304	1.3041
	Partially saturated (PS)	7.7	0.1674	0.1674	0.1673	0.1673
		7.8	1.3805	1.3805	1.3803	1.3804

Fig. 5. The peak horizontal and vertical displacements are found to be 1.3805 and 0.0138 m, respectively, under Nepal input motion (Tables 3 and 4). The horizontal displacement is observed to be more at the centre location. The vertical displacement values are found to be very less as compared to horizontal displacement.

Table 4 Variation of vertical displacement at different locations

Case	Condition	M_w	Vertical displacement (m)			
Distance from footing centre →			Centre	0.5B (R)	1.5B (R)	3B (R)
I	Dry	7.7	6e−5	8e−5	0.0001	6e−5
		7.8	0.0135	0.0135	0.0131	0.0137
	Partially saturated (PS)	7.7	0.0002	0.0002	6e-5	0.0002
		7.8	0.0136	0.0136	0.0133	0.0138
II	Dry	7.7	0.0002	0.0002	0.0003	0.0002
		7.8	0.0131	0.0132	0.0132	0.0135
	Partially saturated (PS)	7.7	8e−5	9e−5	9e−5	7e−5
		7.8	0.0132	0.0132	0.0133	0.0135

Hence, the possibility of lateral spreading is more in partially saturated soils under the considered input motions.

4.3 Stress–Strain Responses

Shear stress versus shear strain responses was obtained at different depths and also at different locations from the centre of the footing. Typical shear stress versus shear strain variation recorded at a distance of 3B away from the centre of the footing (right) and at a depth of 11.38 m for dry soil of case II under the excitation of Bhuj earthquake is presented in Fig. 6. From the results, it can be noticed that the shear stress value decreases with the increase in duration of input motions at all the locations. However, the peak value of shear stress increases with increase in depth from the ground surface and distance away from the centre of the footing. The maximum value of shear stress was found to be 85.67 kPa for dry soil of case II under Nepal earthquake at distance of 3B away from the centre of the footing (right).

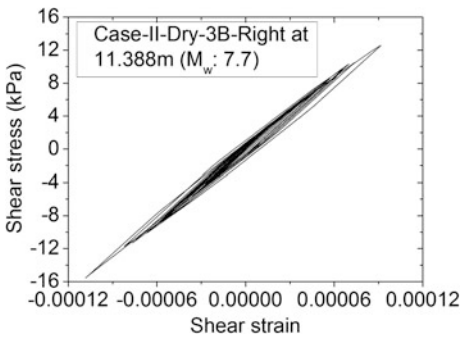

Fig. 6 Variation of shear stress with shear strain at a distance of 3B away from the centre of the footing and at a depth of 11.38 m for dry soil of case II (M_w: 7.7)

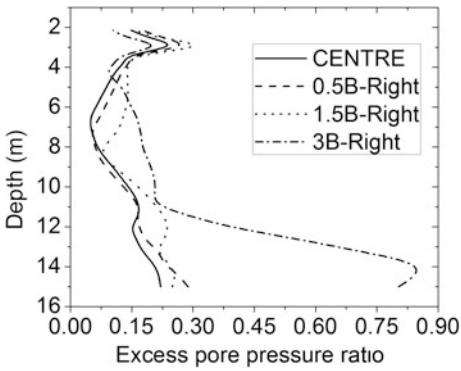

Fig. 7 Variation of excess pore pressure ratio with depth for partially saturated soil of case II (M_w: 7.8)

4.4 Excess Pore Pressure Responses

Excess pore pressure time histories were obtained at different depths and different locations from the centre of the footing. It is observed that excess pore pressure increases with increase in depth. The maximum value of excess pore pressure was found to be 114.8 kPa for partially saturated soil of case II under Nepal input motion. The excess pore pressure is observed to be more at distance away from the centre of the footing (3B). The maximum value of excess pore pressure ratio was observed to be 0.85 for partially saturated soil of case II under Nepal input motion. As the excess pore pressure ratio is found to be less than one, the foundation is safe against liquefaction. Typical diagram of excess pore pressure ratio variation with depth for partially saturated soil of case II under the excitation of Nepal earthquake is presented in Fig. 7.

5 Conclusion

In this paper, comparative study of dynamic response of a shallow foundation resting on different layered soil deposits subjected to seismic loadings has been investigated. It can be observed that peak response of acceleration, displacement and excess pore pressure values are found to be more for partially saturated soil under the excitation of Nepal earthquake. This may be due to the more PGA value of Nepal earthquake (0.1639 g) than that of Bhuj earthquake motion (0.106 g). The maximum PGA value (1.7745 m/s^2) was noticed for partially saturated soil of case I under Nepal earthquake. The horizontal displacement (1.3805 m) values are observed to be more as compared to vertical displacement (0.0138 m). Here, the peak excess pore pressure ratio (0.85) is less than one but in extreme saturated situations, the excess pore pressure ratio may exceed one, which may cause foundation failure due to liquefaction. Hence, it is always advisable to perform

dynamic response analysis of foundation resting on layered soil deposits subjected to seismic loadings.

References

Asgari, A., Golshani, A., & Bagheri, M. (2014). Numerical evaluation of seismic response of shallow foundation on loose silt and silty sand. *Journal of Earth System Science, 123*(2), 365–379.

Elgamal, A., Lu, J., & Yang, Z. (2005). Liquefaction induced settlement of shallow foundations and remediation: 3D numerical simulation. *Journal of Earthquake Engineering, 9*(1), 17–45.

Ishihara, K., Acacio, A. A., & Towhata, I. (1993). Liquefaction induced ground damage in Dagupan in the July 16, 1990 Luzon earthquake. *Soils and Foundations, 33*(1), 133–154.

Kishida, H. (1966). Damage to reinforced concrete buildings on Nigata city with special reference to foundation engineering. *Soils and Foundations, 6*(1), 71–88.

Liu, L., & Dobry, R. (1997). Seismic response of shallow foundation on liquefiable sand. *Journal of Geotechnical and Geoenvironmental Engineering, ASCE, 123*(6), 557–567.

Mohanty, S., & Patra, N. R. (2012). Assessment of liquefaction potential of pond ash at Panipat in India using SHAKE2000. In *Proceedings of GeoCongress-2012, State of the Art and Practice in Geotechnical Engineering*, GSP: 225 (pp. 1829–1838). California: ASCE.

Mohanty, S., & Patra, N. R. (2014). Cyclic behaviour and liquefaction potential of Indian pond ash located in seismic zone III and IV. *Journal of Materials in Civil Engineering ASCE, 26*(7), 06014012.

Mohanty, S., & Patra, N. R. (2016a). Liquefaction and earthquake response analysis of Panipat pond ash embankment in India. *Journal of Earthquake & Tsunami*. https://doi.org/10.1142/s1793431116500093.

Mohanty, S., & Patra, N. R. (2016b). Dynamic response analysis of Talcher pond ash embankment in India. *Soil Dynamics and Earthquake Engineering, 84,* 238–250.

Ragheb, A. M. (1994). *Numerical analysis of seismically induced deformations in saturated granular soil strata*. Ph.D. thesis, Department of Civil Engineering, Rensselaer Polytechnic Institute, Troy, NY.

Seed, H. B., & Idriss, I. M. (1967). Analysis of soil liquefaction: Niigata earthquake. *Journal of the Soil Mechanics and Foundations Division, ASCE, 93*(3), 83–108.

Stokoe, K. H., Kacar, O., & Van Pelt, J. (2013). Predicting settlements of shallow footings on granular soil using nonlinear dynamic soil properties. In *Proceedings of 18th International Conference on Soil Mechanics and Geotechnical Engineering* (pp. 3467–3470). Paris.

Yoshimi, Y., & Tokimatsu, K. (1977). Settlement of buildings on saturated sand during earthquakes. *Soils and Foundations, 17*(1), 23–38.

Shake Table Studies on Embankments on Liquefiable Soil

G. Unni Kartha, K. S. Beena and C. P. Mohamed Thahir

Abstract Experimental studies using shaking table test on liquefaction have been widely conducted in the countries like Japan, where a number of earthquakes occur every year. Kerala, one of the coastal states, having large area of sand deposit is included in earthquake zone III. Hence, the liquefaction studies are of prime importance as many developmental projects like the coastal highway, high-speed railway tracks are on the anvil. The objective of the present study was to conduct model tests on embankments over liquefiable soil using one-dimensional shaking table. The system behaviour during shaking, effects of liquefaction on the embankment, effect of providing geotextile reinforcement to soil, pore water pressure build-up, failure mode also comes under the scope of the study. The experiments were conducted using an ingeniously developed shake table and data acquisition system. The model behaviour of embankment with and without geotextile reinforcements under shaking was conducted. The acceleration and frequency of shaking were kept as 0.2 g and 1 Hz, respectively. It was observed that geotextile reinforcement layer below the embankment can improve the liquefaction resistance of the soil. Additional reinforcement inside the soil bed further reduced the liquefaction, and the pore water pressure reduced considerably.

Keywords Liquefaction · Shake table · Embankment

G. Unni Kartha (✉) · K. S. Beena · C. P. Mohamed Thahir
Division of Civil Engineering, School of Engineering, Cochin University of Science and Technology, Kochi 682022, India
e-mail: unnikartha@gmail.com

K. S. Beena
e-mail: beenavg@gmail.com

C. P. Mohamed Thahir
e-mail: cpthahir@gmail.com

B. Adimoolam and S. Banerjee (eds.), *Soil Dynamics and Earthquake Geotechnical Engineering*, Lecture Notes in Civil Engineering 15,
https://doi.org/10.1007/978-981-13-0562-7_12

1 Introduction

Earthquakes are the most devastating natural phenomena which results in loss of life and damage of building structures such as residential and industrial buildings, dams, roads and railway embankments. "Liquefaction" denotes a condition in which soil undergoes continued deformation at constant low residual stress or with low residual resistance, due to the build-up and maintenance of high pore water pressures that reduce the effective confining pressure to a very low value (Seed 1968).

Experimental studies using shaking table test on liquefaction are widely conducted in the countries like Japan, where a number of earthquakes occur every year. But in countries like India, these types of studies are limited. Earthquake geotechnical engineering in India had received tremendous boost after the Gujarat earthquake of 2001. Earthquakes are not uncommon, but the damage suffered during earthquakes is on the rise because of the population growth, overcrowding of civil engineering facilities in urban areas and improper understanding of ground behaviour among many. Recent earthquakes in Gujarat (2001), Chamoli (1999), Jabalpur (1997), Latur (1993) and Uttarkashi (1991) in India have increased the research activities in the country in the field of earthquake engineering. Kerala, one of the coastal states, having large area of sand deposit, is included in earthquake zone III. The liquefaction studies are of prime importance in Kerala as many developmental projects like the coastal highway are about to start in the state.

This paper presents the results conducted on models of embankments over liquefiable soil using one-dimensional shaking table. The system behaviour during shaking, effects of liquefaction on the embankment, effect of providing geotextile reinforcement to soil, pore water pressure build-up, failure mode also comes under the scope of the study.

2 Previous Studies

Since the understanding of ground behaviour during shaking is still incomplete, different approaches like element tests, model tests, analytical/numerical model tests and field tests are required to understand the phenomenon. Unfortunately in India, lack of facilities for laboratory studies and non-availability of instrumentation in the field can be attributed as the main reasons for lesser number of studies. At the same time, it should be noted that uniaxial shake table tests are sufficient to understand the response and failure mechanism of earth structures like embankment, retaining wall (Prasad et al. 2004). Many researchers have used small-scale shake table with lengths in the range 2.0–1.5 m, width 0.5–1.0 m and depths 0.3–1.0 m and acceleration in the range 0.1–0.5 g and frequency 1–3 Hz (Prasad et al. 2004; Maheshwari et al. 2012; Varghese and Latha 2013; Orense et al. 2003; Ramakrishnan et al. 1998; Beena and Unni Kartha 2014).

The type of soil most susceptible to liquefaction is one in which the resistance to deformation is mobilized by friction between particles. If other factors such as grain shape, uniformity coefficient and relative density are equal, the frictional resistance of cohesion less soil decreases as the grain size of soils becomes smaller. Tsuchida (1970) summarized the results of sieve analyses performed on a number of alluvial and diluvial soils that were known to have liquefied or not to have liquefied during earthquakes. He proposed ranges of grain size curves separating liquefiable and non-liquefiable soils.

The shake table tests conducted by Koga and Matsuo (1990) on reduced scale embankment models founded on saturated sandy ground indicate that the ground beneath the embankment is not prone to liquefaction and it slumps and cracks as a result of softening of underlying ground. They also point that the extent of damage is more extensive with longer duration and lower frequency earthquake input motion. Studies by Prasad et al. (2004) have demonstrated densification as an effective technique for liquefaction countermeasure. Numerical studies have shown that techniques like sheet pile and stone column are effective methods in reducing liquefaction in soil under embankments (Bhatnagar et al. 2003). Reinforcement of soil with geogrid can be used in many field applications. This technique is found to be useful and cost-effective in the construction of roads, embankments, dams, and low-rise residential buildings. Recent researches have proved that inclusion of geogrids as reinforcement in layers of soil is potential solution for reducing liquefaction (Maheshwari et al. 2012).

In this study, the effect of geotextile reinforcement when it is placed as a separator and also within the supporting soil is studied and compared.

3 Properties of Materials Used in the Study

Figure 1 represents the particle size distribution of Aluva River sand, in comparison with the boundaries defined by Tsuchida. It is found that the particle size distribution of the sand lies within the boundaries of potentially liquefiable soil. Table 1 shows the properties of Aluva River sand.

The tests are conducted keeping the density of sand layer as 14.1 kN/m^3. The details of embankment model and soil are as shown in Table 2. Figure 2 shows the schematic diagram of the embankment over the soil bed. The properties of geotextile used as reinforcement are shown in Table 3.

4 Experimental Set-up

The experiments are conducted using an ingeniously developed shake table and data acquisition system. The shake table consists of a rigid box of size 1500 mm × 500 mm × 600 mm (L × B × H) made of Perspex and Steel. It is

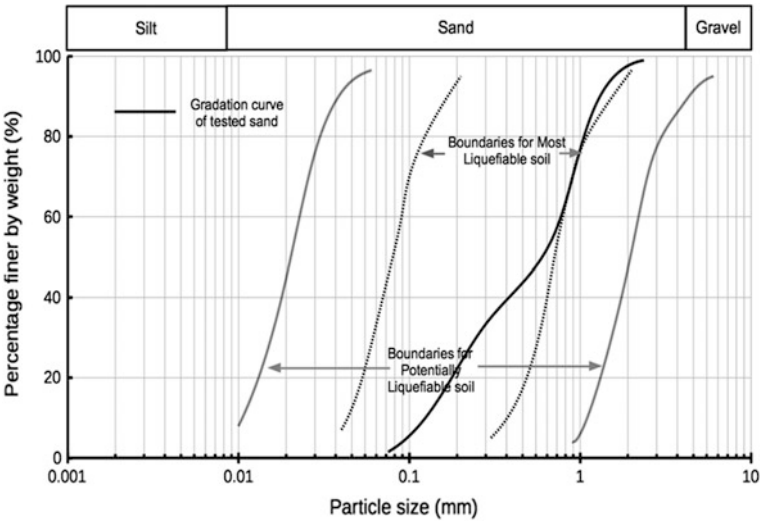

Fig. 1 Particle size range proposed by Tsuchida

Table 1 Properties of Aluva river sand

1.	% Silt size	1.37
2.	% Sand size	98.63
3.	% Gravel	0
4.	D_{10} (mm)	0.18
5.	D_{30} (mm)	0.35
6.	D_{60} (mm)	0.71
7.	Uniformity coefficient (C_u)	3.94
8.	Coefficient of curvature (C_c)	0.96
9.	Specific gravity	2.65
10.	Maximum void ratio (e_{max})	0.88
11.	Minimum void ratio (e_{min})	0.63

Table 2 Properties of embankment model

1.	Soil type	Moist red earth
2.	Height of embankment (mm)	200
3.	Slope of embankment	1 in 1.5
4.	Total weight of embankment (kN)	0.73
5.	Density (kN/m^3)	14.60

mounted on a platform connected to a pulley system that runs by a 5 HP three-phase electric motor. The ratio of pulleys is so designed to create a frequency of 1 Hz. The amplitude of shake is selected to keep the peak acceleration at 0.2 g. The data acquisition system consists of accelerometers and pore water pressure

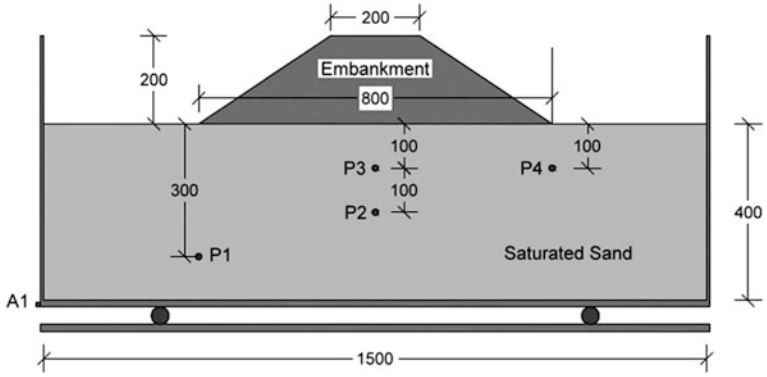

Fig. 2 Schematic diagram of test set-up

Table 3 Properties of geotextiles used

1.	Thickness (mm)	0.31
2.	Opening size (mm)	0.075
3.	Specific gravity	0.880
4.	Tensile strength (breaking strength at 200 mm wide and 100 mm length) Lengthwise (kN)	3.6
5.	Tensile strength (breaking strength at 200 mm wide and 100 mm length) Widthwise (kN)	2.0

sensors. The location of the sensors is shown in Fig. 2. The container box has baffle walls at it bottom to allow water uniformly to saturate in the sand bed.

Four experiments were conducted as part of the study.

(1) Soil without embankment;
(2) Soil with embankment;
(3) Soil with embankment and geotextile as separator at its base;
(4) Soil with embankment and geotextile reinforcement at its base and 100 mm within the soil.

The dry sand bed is formed first at the required density, and the embankment is created on top of it. After forming the model, it is saturated from the bottom very slowly without disturbing the layers. The saturation process took 4 h on an average.

All experiments are conducted in a controlled manner keeping density and input motions as constant. The sensor locations are shown in Fig. 2.

5 Results and Discussions

The excess pore water pressure that builds up during shaking is measured using the sensors kept at various locations. Figure 3 shows the variation of pore water pressure developed in the sensor P2 kept 200 mm below the embankment for all the cases studied. It is observed that the pore water pressure build-up is more when the embankment is present in the model. The maximum value observed is 3 kPa. When geotextile reinforcement is provided at the base, the pore water pressure builds up to

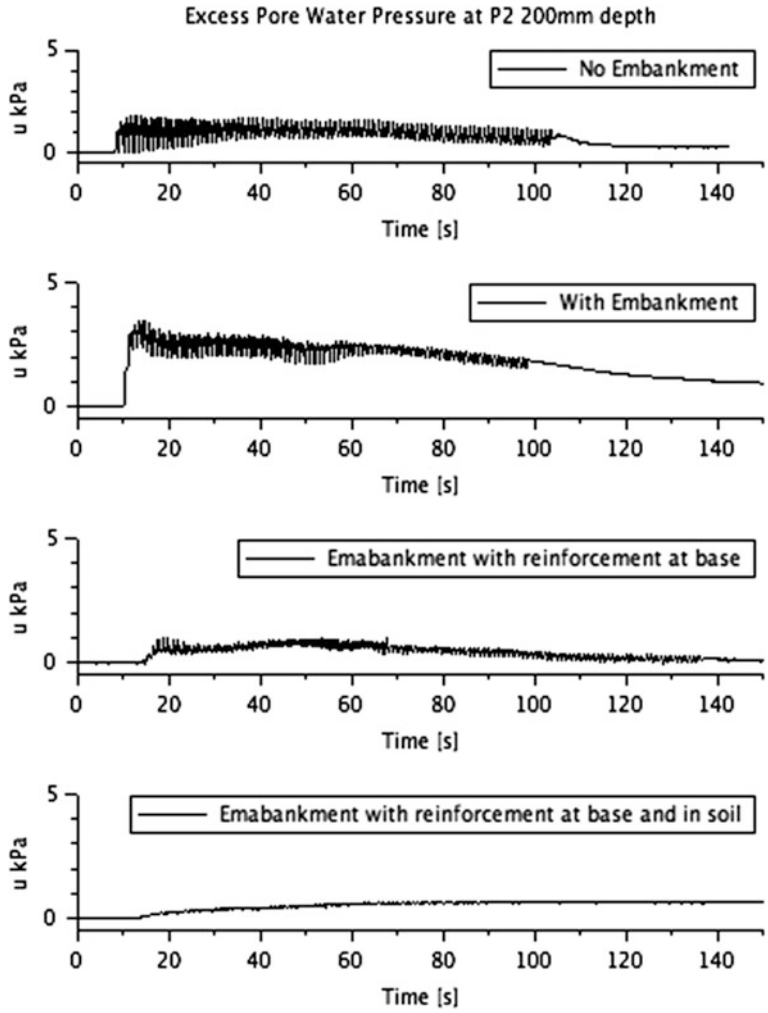

Fig. 3 Excess pore water pressure at P2, 200 mm below the embankment

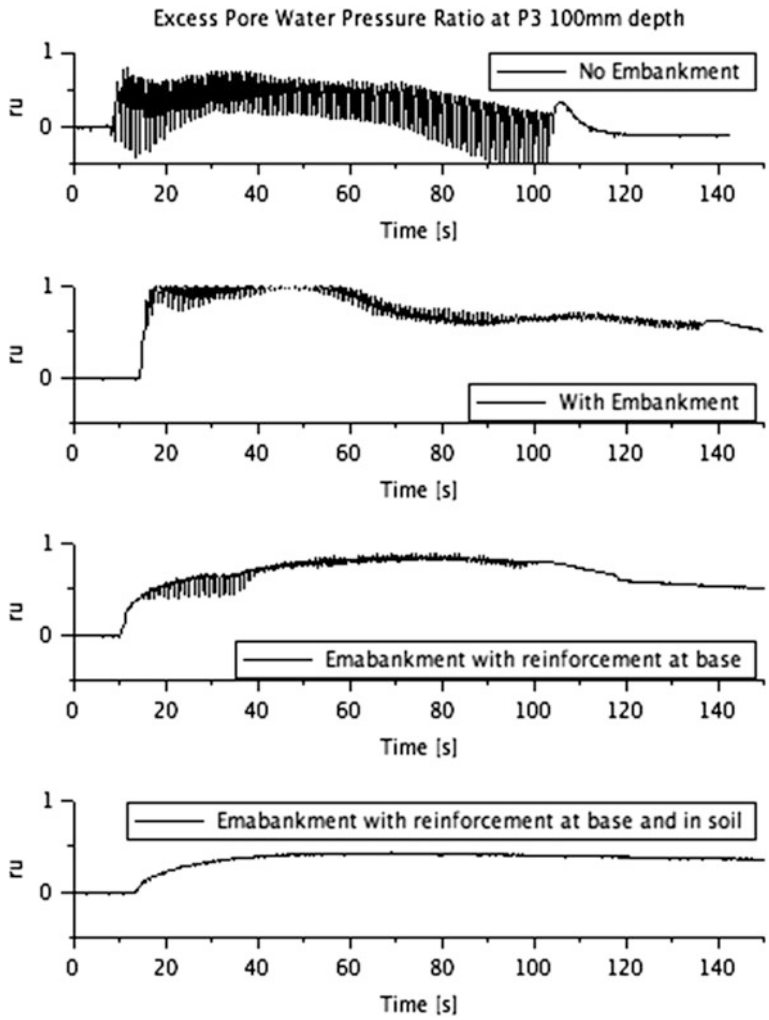

Fig. 4 Excess pore water pressure ratio at P3, 200 mm below the embankment

a lesser value of 1.0 kPa. The pressure build-up is minimum in the case where an additional reinforcement is provided at a depth of 100 mm in the sand layer.

Figure 4 shows the plot of excess pore water pressure ratio r_u, which is the ratio of excess pore water pressure to effective stress, at P3, 200 mm below the ground level. The ground nearly liquefied when the embankment was present, indicated by a value of 1.0 of pore water pressure ratio (r_u). The failure of the embankments is

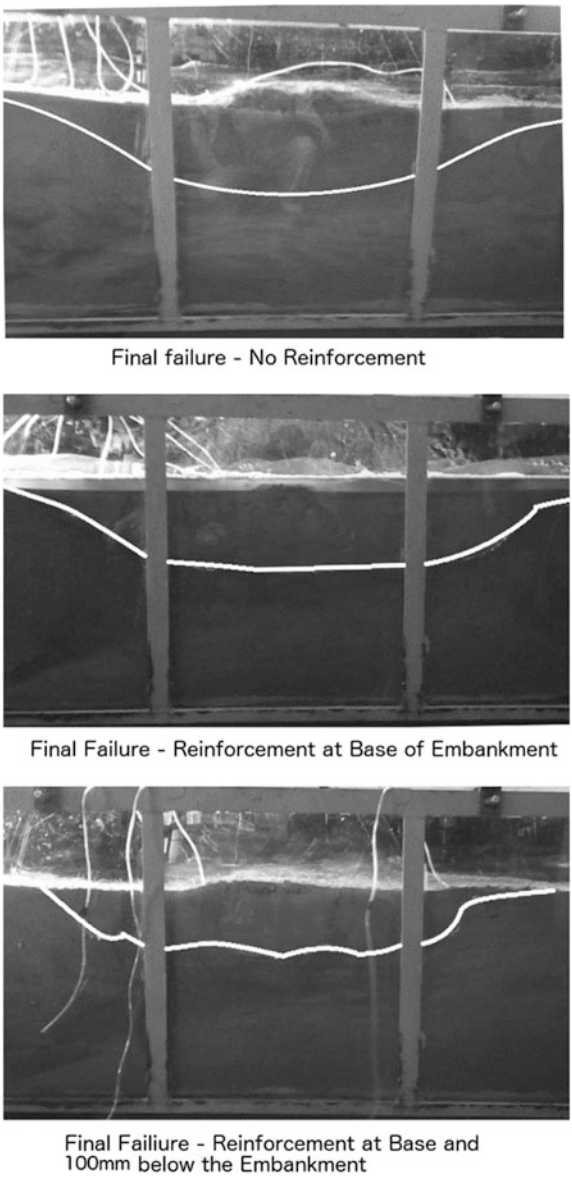

Fig. 5 Failure modes of test cases

shown in Fig. 5. Intense deformation of embankment due to soil liquefaction in foundation ground was observed, which can be classified as type 3 failure (Sasaki and Tamura 2007). This type of failure is induced by the deformation of the subsoil layer during shaking.

6 Conclusion

The experimental investigation provided a better understanding of the response of embankments on liquefiable deposits, the results interpreted qualitatively. The results from the experiments show that the pore pressure build-up will be more in the presence of embankment. This behaviour is due to the fact that the embankment will prevent the dissipation of excess pressure developed through the top surface. Providing the geotextile reinforcement at the base reduces the pore water pressure build-up. Providing an additional layer of geotextile reinforcement also leads to a reduction the pore water pressure build-up. It may be concluded that providing geotextile reinforcements can mitigate the effects of liquefaction.

References

Beena, K. S., & Unni Kartha, G. (2014). Stone columns for liquefaction mitigation: An experimental investigation. In *6th International Geotechnical Symposium on Disaster Mitigation in Special Geoenvironmental Conditions* (pp. 169–172). IIT Chennai.

Bhatnagar, S., Kumari, S., & Sawant, V. A. (2003). Numerical analysis of earth embankment resting on liquefiable soil and remedial measures. *International Journal of Geomechanics,* 1–13.

Koga, Y., & Matsuo, O. (1990). Shaking table tests of embankment resting on liquefiable sandy ground. *Soils and Foundations, 30*(4).

Maheshwari, B. K., Singh, H. P., & Saran, S. (2012). Effects of reinforcement on liquefaction resistance of Solani sand. *Journal of Geotechnical and Geoenvironmental Engineering, 138*(7), 831–840.

Orense, R. P., Morimoto, I., Yamamoto, Y., Yumiyama, T., Yamamoto, H., & Sugawara, K. (2003). Study on wall-type gravel drains as liquefaction countermeasure for underground structures. *Soil Dynamics Earthquake Engineering, 23,* 19–39.

Prasad, S. K., Towhata, I., Chandradhara, G. P., & Nanjundaswamy, P. (2004). Shaking table tests in earthquake geotechnical engineering. *Current Science, 87*(10).

Ramakrishnan, S., Budhu, M., & Britto, A. (1998). Laboratory seismic tests on geotextile wrap-faced and geotextile-reinforced segmental retaining walls. *Geosynthetics Internationals, 5*(1–2).

Sasaki, Y., & Tamura, K. I. (2007). Failure mode of embankments due to recent earthquakes in Japan. In *4th International Conference on Earthquake Geotechnical Engineering* (No. 1479).

Seed, H. B. (1968). Landslides during earthquakes due to soil liquefaction. *Journal of Soil Mechanics and Foundations, Division, 94*(5), 1055–1123.

Tsuchida, H. (1970). Prediction and countermeasure against the liquefaction in sand deposits. *Abstract of the Seminar in the Port and Harbor Research Institute*.

Varghese, R. M., & Latha, G. M. (2013). Initiation of liquefaction in sand under different surcharge and overburden stresses. In *Proceedings of Indian Geotechnical Conference*, Roorkee.

Development of Design Charts for the Dynamic Active Thrust from c–ϕ Soil Backfills

Ashish Gupta, Vinay Kumar Chandaluri, Vishwas A. Sawant and Sanjay Kumar Shukla

Abstract This paper presents design charts to calculate dynamic active thrust on retaining walls resulting from c–ϕ soil backfills. Shukla (J Geotech Geoenviron Eng ASCE 135:690–696, 2015) derived an explicit generalized analytical expression to calculate dynamic active thrust using the pseudo-static approach. This approach evaluates the dynamic active thrust accounting for all possible and the influencing factors. Using the explicit generalized analytical expression, the influence of various key factors such as backfill inclination, dimensionless cohesion, and angle of shearing resistance, horizontal and vertical seismic coefficients are studied. The design charts are presented in non-dimensional form. These charts are straightforward and can be adopted for the design of retaining walls in seismic zone. The active earth pressure coefficient and the critical value of inclination of the failure plane, obtained from the present study, are validated with studies reported in the literature.

Keywords Retaining walls · c–ϕ soil backfills · Seismic loads Surcharge · Dimensionless cohesion · Dynamic active thrust · Active earth pressure coefficient

A. Gupta (✉) · V. K. Chandaluri · V. A. Sawant
Department of Civil Engineering, Indian Institute of Technology, Roorkee, Roorkee 247667, Uttarakhand, India
e-mail: shi_g2000@rediffmail.com

V. K. Chandaluri
e-mail: vinay2744@gmail.com

V. A. Sawant
e-mail: sawntfce@iitr.ac.in

S. K. Shukla
SOE, Faculty of Health, Engineering and Science, Edith Cowan University, Joondalup, Australia
e-mail: s.shukla@ecu.edu.au

B. Adimoolam and S. Banerjee (eds.), *Soil Dynamics and Earthquake Geotechnical Engineering*, Lecture Notes in Civil Engineering 15,
https://doi.org/10.1007/978-981-13-0562-7_13

1 Introduction

In practical situations, the dynamic active thrust on retaining walls is calculated using explicit analytical expressions. Mononobe-Okabe expression is typically used for calculating the dynamic active thrust for the cohesionless soils. But this expression cannot be used for analyzing the real field situations where c–ϕ soil backfills are present.

Shukla et al. (2009) gave a simple expression for calculating the dynamic active thrust from the c–ϕ soil backfills. The wall friction and the adhesion between soil backfill and retaining wall face are ignored in this study. The back face of the wall is assumed to be vertical.

Kim et al. (2010) obtained an expression for calculating the total dynamic active thrust in terms of the inclination of the failure plane. But the calculation of inclination of the failure plane was based on the trial and error procedure. Thus, this expression has limited applications in real design practices.

Shukla (2011) studied the effects of tension cracks, wall–backfill adhesion, and surcharge loading on dynamic active thrust. The effect of wall friction and other factors on dynamic active thrust was presented by Shukla and Bathurst (2012). Shukla (2013) presented an expression to calculate the dynamic active thrust for sloping soil backfill.

Shukla (2015) developed a generalized analytical expression for the dynamic active thrust on retaining wall supporting a c–ϕ soil sloping backfill. Effect of wall geometry, different properties of backfill and wall–backfill interface, tension cracks, surcharge, horizontal and the vertical ground acceleration were examined. The expression for the critical value of inclination of the failure plane is also developed in this study.

In the present study, design charts have been developed for dynamic active thrust by using the explicit generalized analytical expression proposed by Shukla (2015). These charts can be adoptable for the design of retaining walls for the seismic stability.

2 Analytical Derivation

Figure 1 shows a retaining wall supporting a c–ϕ soil backfill of height H with an active trial failure wedge $A_1A_2A_3$ of weight W. The backfill face of wall A_1A_2 is inclined at an angle β with the horizontal. Sloping backfill A_1A_3 is inclined at an angle i with the horizontal. The failure plane is assumed along A_2A_3 and passes through the bottom of the wall. A_2A_3 is inclined at an angle α to the horizontal. k_hW and k_vW are the horizontal and vertical seismic inertial forces, where k_h and k_v are the horizontal and the vertical seismic coefficients. A surcharge q per unit surface area is placed at the top of the sloping backfill. k_hqB and k_vqB are the surcharge loads along with the horizontal and vertical seismic inertial forces, where B is the length of sloping backfill A_1A_3.

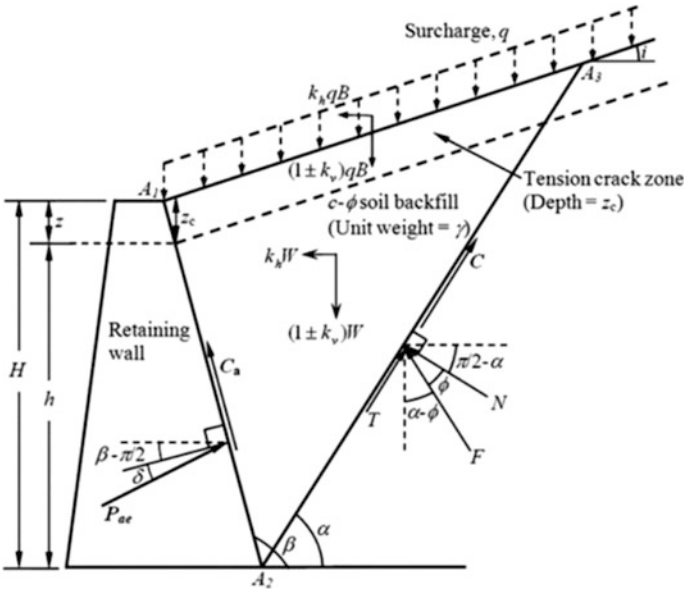

Fig. 1 Forces shown in a trial failure wedge supporting a c–ϕ soil backfill in active state (after Shukla 2015)

z_c is the depth of tension crack from backfill surface. To simplify, the wall height H is taken as the sum of z and h. The force F is the resultant of frictional force T and normal force N acting on the failure plane A_2A_3. C is the total cohesive force on the failure plane. C_a is the total adhesive force mobilized along the wall–backfill interface, and a_f is the adhesion factor. P_{ae} is the dynamic active thrust, inclined at an angle δ.

Taking equilibrium of forces in the vertical and horizontal direction, respectively,

$$P_{ae}\cos(\beta+\delta) + (1 \pm k_v)(W + qB) - F\cos(\alpha - \phi) - \frac{\bar{c}H\sin(\beta - i)\sin\alpha}{\sin\beta\sin(\alpha - i)} - a_f\bar{c}H = 0 \quad (1)$$

$$P_{ae}\sin(\beta+\delta) - k_h(W + qB) - F\sin(\alpha - \phi) + \frac{\bar{c}H\sin(\beta - i)\cos\alpha}{\sin\beta\sin(\alpha - i)} - a_f\bar{c}H\cot\beta = 0 \quad (2)$$

Eliminating F from Eqs. (1) and (2) and further simplifying, P_{ae} can be expressed as,

$$P_{ae} = \frac{1}{2}\left(\frac{a_1 \tan^2 \alpha - b_1 \tan \alpha + c_1}{a_2 \tan^2 \alpha - b_2 \tan \alpha + c_2}\right)\gamma H^2 \tag{3}$$

In which,

$$\theta = \tan^{-1}\left[\frac{k_h}{1 \pm k_v}\right] \tag{4}$$

$$a_f = \frac{c_a}{c} \tag{5}$$

where c_a is the adhesion between the wall back face and the soil backfill.

$$m_1 = \left(\frac{1 \pm k_v}{\cos \theta}\right)\left[\frac{2q}{\gamma H} + \frac{\sin(\beta - i)}{\sin \beta}\right]\text{cosec}\beta \tag{6}$$

$$m_2 = a_f\left(\frac{2c}{\gamma H}\right)\left(1 - \frac{z_c}{2H}\right)\text{cosec}\beta \tag{7}$$

$$m_3 = \left(\frac{2c}{\gamma H}\right)\left(1 - \frac{z_c}{2H}\right)\sin(\beta - i)\cos\phi\text{cosec}\beta \tag{8}$$

$$a_1 = m_1 \cos\beta\cos(\theta - \phi) + m_2 \cos i \ \sin(\beta + \phi) + m_3 \tag{9}$$

$$b_1 = m_1 \sin(\beta - \theta + \phi) - m_2 \cos(i + \beta + \phi) \tag{10}$$

$$c_1 = m_3 - m_1 \sin\beta\sin(\theta - \phi) - m_2 \sin i\cos(\beta + \phi) \tag{11}$$

$$a_2 = \cos i \ \cos(\beta + \delta + \phi) \tag{12}$$

$$b_2 = \sin(\beta + \delta + \phi + i) \tag{13}$$

$$c_2 = \sin i \ \sin(\beta + \delta + \phi) \tag{14}$$

a_1, b_1, c_1 and a_2, b_2, c_2 are the non-dimensional constants.
In Eqs. (7) and (8),

$$z_c = \frac{2c}{\gamma}\tan\left(\frac{\pi}{4} + \frac{\emptyset}{2}\right) \tag{15}$$

For optimizing the value of dynamic active thrust P_{ae}, the following condition should be satisfied.

$$\frac{\partial P_{ae}}{\partial(\tan \alpha)} = 0 \tag{16}$$

Or,

$$(a_2b_1 - a_1b_2)\tan^2\alpha - 2(a_2c_1 - a_1c_2)\tan\alpha + (b_2c_1 - b_1c_2) = 0 \tag{17}$$

Above quadratic equation (15) is solved for tanα, to get the critical value of inclination of the failure plane, $\alpha = \alpha_c$ as,

$$\alpha_c = \tan^{-1}\left[\frac{(a_2c_1 - a_1c_2) \pm \sqrt{(a_2c_1 - a_1c_2)^2 - (a_2b_1 - a_1b_2)(b_2c_1 - b_1c_2)}}{(a_2b_1 - a_1b_2)}\right] \tag{18}$$

Substituting $\alpha = \alpha_c$ into Eq. (3), P_{ae} is obtained as by Shukla (2015),

$$P_{ae} = \frac{1}{2}\left(\frac{a_1\tan^2\alpha_c - b_1\tan\alpha_c + c_1}{a_2\tan^2\alpha_c - b_2\tan\alpha_c + c_2}\right)\gamma H^2 \tag{19}$$

Or,

$$K_{ae} = P^*_{ae} = \frac{P_{ae}}{0.5\gamma H^2} = \left(\frac{a_1\tan^2\alpha_c - b_1\tan\alpha_c + c_1}{a_2\tan^2\alpha_c - b_2\tan\alpha_c + c_2}\right) \tag{20}$$

where K_{ae} is the active earth pressure coefficient.

3 Results and Discussions

Based on the generalized expression derived (Eq. 20), design charts are presented for calculating the total active thrust on retaining wall for different values of k_h, k_v, and c^* with and without q^*, where c^* and q^* are non-dimensional cohesion and non-dimensional surcharge defined in Eqs. (21) and (22), respectively.

$$c* = c/\gamma H \tag{21}$$

$$q* = q/\gamma H \tag{22}$$

The charts are presented for a vertical wall ($\beta = 90^o$). In the presented charts, k_h ranges from 0.0 to 0.5 and three different values of $k_v = 0.0$, 0.25 k_h and 0.5 k_h are considered. The vertical inertial force is considered as positive in upward direction. Design charts obtained from the present study are shown in Figs. 2a–e and 3a–e. Figure 2a–e are design charts for calculating the total active thrust from c–ϕ soil backfill without surcharge loading ($q^* = 0.0$). In Fig. 3a–e, the effect of surcharge on the active earth pressure coefficient is additionally considered. The non-dimensional surcharge is taken as 0.1 ($q^* = 0.1$).

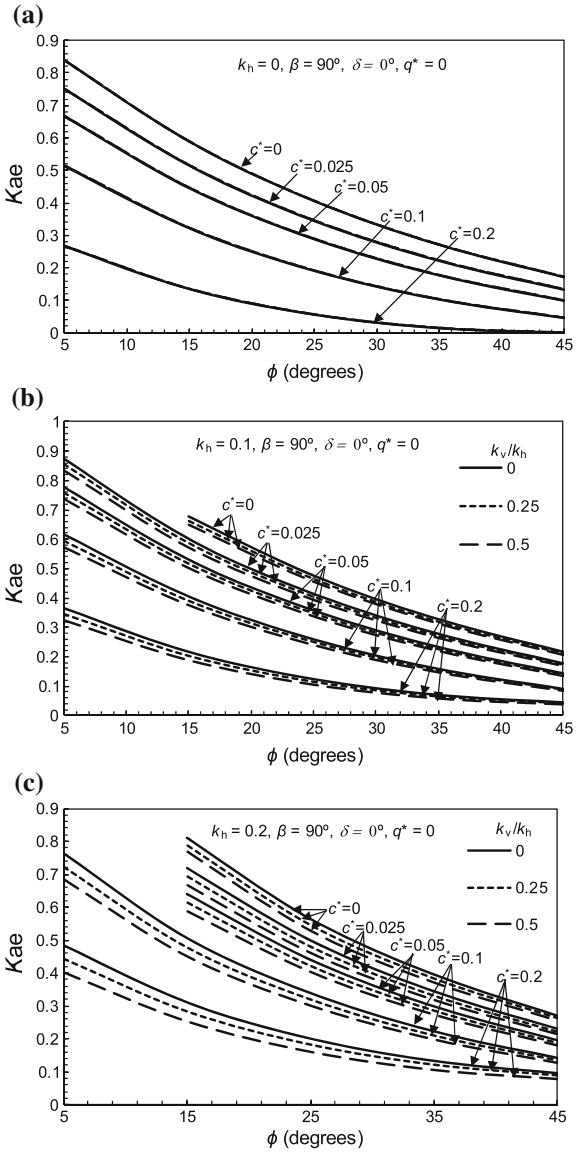

Fig. 2 **a–e** Design charts for calculating total active thrust from c–ϕ soil backfill for different values of k_h, k_v, and c^* without backfill surcharge loading

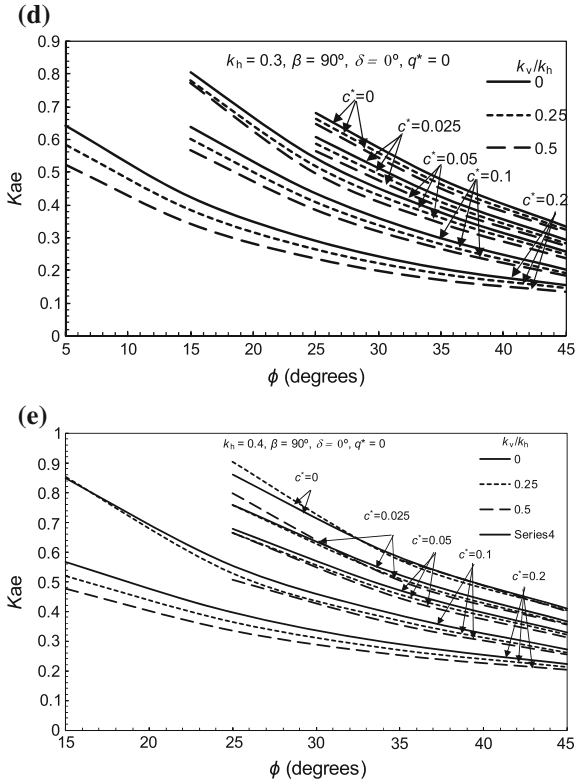

Fig. 2 (continued)

From Figs. 2 and 3, it can be clearly observed that the value of K_{ae} decreases with increase in cohesion as well as increase in angle of shearing resistance of soil. For $\phi = 15°$, $c^* = 0.1$, when q^* increases from 0.0 to 0.1, the value of K_{ae} increases about 30–36%. However, the percentage increase is decreasing with increase in the value of k_h.

For $\phi = 15°$, $c^* = 0.1$, the value of K_{ae} increases by about 25.8, 57.1 and 98.1%, when k_h value increases from 0.0 to 0.1, 0.2, and 0.3, respectively.

The value of α_c and K_{ae} obtained from the present study for different values of k_h and ϕ has been compared with studies reported in the literature as shown in

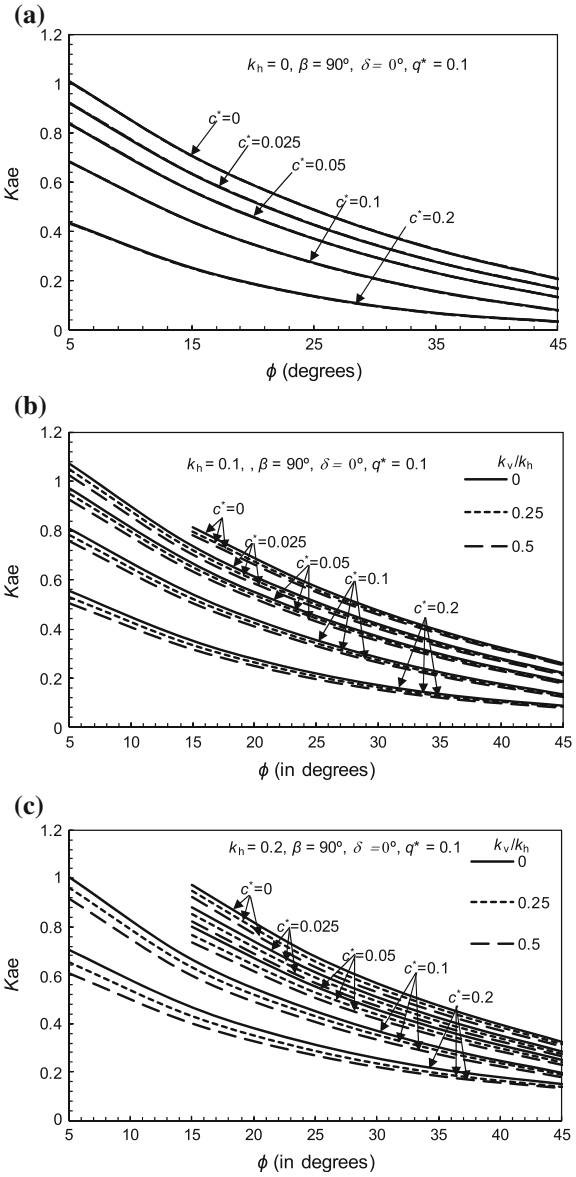

Fig. 3 **a–e** Design charts for calculating total active thrust from c–ϕ soil backfill for different values of k_h, k_v, and c^* with $q^* = 0.1$

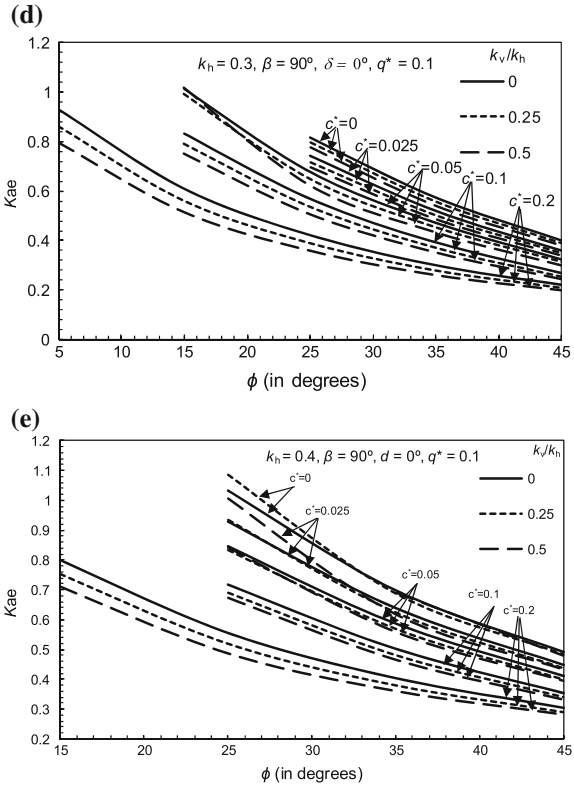

Fig. 3 (continued)

Tables 1 and 2, respectively. From Tables 1 and 2, it can be noted that all the results are in good agreement.

4 Conclusions

The present study provides the design charts for calculating total active thrust from c–ϕ soil backfills on retaining wall considering both the horizontal and vertical seismic coefficients and non-dimensional cohesion with and without non-dimensional surcharge. Based on the design charts from the present study, the following conclusions can be summarized:

1. The value of active earth pressure coefficient decreases with increase in non-dimensional cohesion as well as increase in angle of shearing resistance of soil backfills irrespective of the backfill non-dimensional surcharge loading.

Table 1 Comparison of results for calculation of critical value of inclination of failure plane ($i = 0°$, $k_v = 0$, $c = 0$, $\delta = (2/3)\phi$, and $\beta = 90°$)

ϕ	$k_h = 0.0$					$k_h = 0.05$					$k_h = 0.1$					$k_h = 0.2$				
	LEM	HSM	M-O	Chang	Present analysis	LEM	HSM	M-O	Chang	Present analysis	LEM	HSM	M-O	Chang	Present analysis	LEM	HSM	M-O	Chang	Present analysis
20°	50	49.9	50	50	50.01	47	47.1	46.6	47	46.65	43	43.9	42.8	43	42.83	33	36.3	33.4	33	33.37
25°	53	52.9	53	53	53.01	50	50.5	50.1	50	50.1	47	47.8	46.9	47	46.89	39	41.7	39.4	39	39.38
30°	55	55.9	56	56	55.98	53	53.7	53.4	53	53.37	51	50.6	50.5	51	50.53	44	46.1	44.1	44	44.11

LEM: Ghanbari and Ahmadabadi (2010) (Based on Limit Equilibrium)
HSM: Ghanbari and Ahmadabadi (2010) (Based on Horizontal Slice Method)
M-O: Mononobe and Matsuo (1929)

Table 2 Comparison of results for calculation of active earth pressure coefficient ($i = 0°$, $k_v = 0$, $c = 0$, $\delta = (2/3)\phi$, and $\beta = 90°$)

ϕ	$k_h = 0.0$					$k_h = 0.05$					$k_h = 0.1$					$k_h = 0.2$				
	LEM	HSM	M-O	Chang	Present analysis	LEM	HSM	M-O	Chang	Present analysis	LEM	HSM	M-O	Chang	Present analysis	LEM	HSM	M-O	Chang	Present analysis
20°	0.438	0.440	0.438	0.426	0.438	0.478	0.479	0.479	0.656	0.478	0.526	0.526	0.525	0.511	0.525	0.647	0.645	0.647	0.629	0.647
25°	0.361	0.362	0.361	0.346	0.361	0.397	0.398	0.397	0.380	0.397	0.438	0.438	0.438	0.419	0.438	0.539	0.539	0.539	0.516	0.539
30°	0.297	0.299	0.297	0.279	0.297	0.330	0.330	0.330	0.310	0.330	0.366	0.366	0.366	0.344	0.366	0.454	0.453	0.454	0.426	0.454

LEM: Ghanbari and Ahmadabadi (2010) (Based on Limit Equilibrium)
HSM: Ghanbari and Ahmadabadi (2010) (Based on Horizontal Slice Method)
M-O: Mononobe and Matsuo (1929)

2. The active earth pressure coefficient increases with increase in the value of horizontal seismic coefficient. However, the percentage increase is marginally decreasing with the increase in horizontal seismic coefficient value.
3. The critical value of inclination of the failure plane and the active earth pressure coefficient obtained from the present study for different values of horizontal seismic coefficient and angle of shearing resistance has been compared with studies reported in the literature, and the results found are in good agreement.

References

Ghanbari, A., & Ahmadabadi, M. (2010). Active earth pressure on inclined retaining walls in static and pseudo-static conditions. *International Journal of Civil Engineering, 8*(2), 159–173.

Kim, W. C., Park, D., & Kim, B. (2010). Development of a generalised formula for dynamic active earth thrust. *Geotechnique, 60*(9), 721–727.

Mononobe, N., & Matsuo, H. (1929). On the determination of earth pressure during earthquake. In *Proceedings of the World Engineering Congress* (pp. 177–185), Tokyo, Japan.

Shukla, S. K. (2011). Dynamic active thrust from c-ϕ soil backfills. *Soil Dynamics and Earthquake Engineering, 31*(3), 526–529.

Shukla, S. K. (2013). Seismic active earth pressure from the sloping c-ϕ soil backfills. *Indian Geotechnical Journal, 43*(3), 274–279.

Shukla, S. K. (2015). Generalized analytical expression for dynamic active thrust from c-ϕ soil backfills. *International Journal of Geotechnical Engineering, 9*(4), 416–421.

Shukla, S. K., & Bathurst, R. J. (2012). An analytical expression for the dynamic active thrust from c-ϕ soil backfills on retaining wall with wall friction and adhesion. *Geomechanics and Engineering, 4*(3), 209–218.

Shukla, S. K., Gupta, S. K., & Sivakugan, N. (2009). Active earth pressure on retaining all for c-ϕ soil backfill under seismic loading condition. *Journal of Geotechnical and Geoenvironmental Engineering, ASCE, 135*(5), 690–696.

Pseudo-static Stability Analysis of MSW Landfills in Goa

Tanvi Mardolkar and Purnanand Savoikar

Abstract In the conventional method for determining the seismic stability of geotechnical structures using pseudo-static or pseudo-dynamic analysis, the horizontal seismic acceleration coefficient is assumed arbitrarily or based upon past experience, neglecting effect of seismic wave velocities, seismic displacements, time period, spectral acceleration, faulting pattern, etc. In the present study, pseudo-static limit equilibrium slope stability analysis of landfill (proposed in Goa) is performed by considering the effects of the above parameters using conventional and rational method of selection of horizontal seismic coefficient considering the effect of vertical seismic acceleration. The effect of water table and leachate buildup is also considered. It is observed that due to the loss of shear strength as a result of pore pressure buildup in case of wet condition, there is decrease in F.O.S. up to 30%.

Keywords MSW landfills · Pseudo-static · Leachate buildup

1 Introduction

There is an immense increase in waste generation with rapid increase in industrialization. The unscientific disposal of municipal solid waste (MSW) in the past several years has led to the contamination of environment and natural resources in and around such dumpsites thereby posing serious risk to human and animal health. MSW has therefore emerged as a growing challenge for various states and municipal authorities in the country. MSW is heterogeneous mixtures of wastes consisting of residential and commercial origin. Municipal solid waste landfills are

T. Mardolkar · P. Savoikar (✉)
Department of Civil Engineering, Goa College of Engineering,
Farmagudi 403401, Goa, India
e-mail: psavoikar@gmail.com

T. Mardolkar
e-mail: sweettanu045@gmail.com

B. Adimoolam and S. Banerjee (eds.), *Soil Dynamics and Earthquake Geotechnical Engineering*, Lecture Notes in Civil Engineering 15,
https://doi.org/10.1007/978-981-13-0562-7_14

huge geotechnical structures, and their heights may be as small as 10 m to as high as 100 m or even more. The aim of engineered landfills is to avoid any leachate released into subsurface environment and controls the exposure of the environment and humans to the detrimental effect.

The stability of landfills against these seismic forces can be evaluated by computing factor of safety for different modes of failure, and the permanent safety can also be evaluated by permanent displacement to check the serviceability of landfills after earthquake. Most of the landfill failures occur due to the excessive leachate buildup in the waste mass. Proper management of leachate is very important for any landfill construction.

2 Literature Review

Behavior of MSW landfills during earthquakes, along with the recordings of the past events containing static and dynamic properties of landfills, helps in analyzing the seismic behavior of landfills.

Various researchers such as Kandolkar et al. (2010), Bray and Travassarou (2009), Savoikar and Aldonkar (2011) carried out pseudo-static limit equilibrium slope stability analysis of hill type embankment by considering rational method for selecting horizontal seismic acceleration coefficient. By varying the angle of failure surface, F.O.S. was evaluated. Design charts were developed for F.O.S. for different values of various parameters such as width-to-height ratio, failure plane inclination. The papers clearly illustrated the importance of rational method for selecting horizontal seismic acceleration coefficient. However, the effect of water table or leachate buildup is ignored. Qian (2006) developed calculation method of limit equilibrium analysis for translational failure. Four leachate buildup conditions were considered during development of calculation method for analyzing translational failure to represent various conditions in landfills. Excessive leachate buildup is a triggering mechanism for translational failure. It was concluded that as the leachate level increases the F.O.S. decreases.

In this paper, the effect of water table/leachate buildup is considered for landfill analysis using rational method for selecting the horizontal seismic coefficient suggested by Bray and Travassarou (2009).

2.1 Landfills in India

Unfortunately, even today MSW is continued to be disposed of as uncontrolled dump in developing countries such as India. Increasing prices of land and in the amount of waste forces engineers to create higher and steeper dumps and landfills to

Fig. 1 Landfill construction at Saligao

accommodate more waste. In its 2009–10 annual report, the Ministry of New and Renewable Energy (MNRE) estimated that approximately 55 million tons of MSW are generated in urban areas of India annually. Among the four geographical regions in India, Northern India generates the highest amount of MSW.

As per MSW Rules 2000, Government of Goa has taken an initiative to establish a Centralized Municipal Solid Waste Management Facilities at an existing MSW dumpsite located at Calangute/Saligao Villages in North Goa district (Fig. 1). Major portion of the MSW generated in the North Goa district is dumped haphazardly and unscientifically at this site by nearby panchayats for last 20 years. Unscientific dumping of MSW at this site resulted in contamination of environment. Major focus of the project is on the issues pertaining to odor and leachate generation and their scientific management to minimize the same. Plant operation shall be carried out using the electricity produced in-house from the organic fraction of the MSW.

Efforts are also taken for providing an in-house auditorium/resource center for displaying the recycling and waste treatment process, gardens, public conveniences, and café for encouraging public tours. The facility shall not only serve as a tourist attraction, but also as learning center to create awareness about the positive environmental impact of the solid waste treatment facility in the State of Goa. This would also facilitate image building of the state government with respect to environmental restoration.

3 Methodology

A hill type landfill model is used for the present analysis with height H, top width B, side slope of θ (tan − 1(1/S)). Biplanar failure surface makes an angle β with horizontal. Limit equilibrium method is used to analyze the pseudo-static stability of the landfill with and without considering the effect of leachate buildup. Four ideal seepage cases are considered during the development of calculation methods for analyzing translational failures with seepage as shown in Fig. 2.

Case—1 is parallel-to-subgrade and back slope seepage buildup. In this case, the seepage flows parallel to the subgrade. Such type of leachate buildup normally occurs when landfill is in normal operating condition.
Case—2 is parallel-to-subgrade seepage buildup. The seepage flow is parallel to the landfill bottom slope, and the leachate depth exceeds the limited depth of 300 mm.
Case—3 is horizontal seepage buildup with seepage parallel to back slope. Such situation may occur when there is breakage of leachate collection pump or has lost power in an active landfill with a temporary or partial final cover. The incoming liquid can cause a rapid rise of the leachate level in the waste mass.
Case—4 is horizontal seepage buildup. In fourth case, horizontal seepage builds up and either ends at the liner system or extends deeply into the waste mass. Such type of buildup of seepage buildup might occur in partially or fully closed landfills during power shutdown, when pump shutdown problems cause high liquid accumulation in the lower part of the landfill.

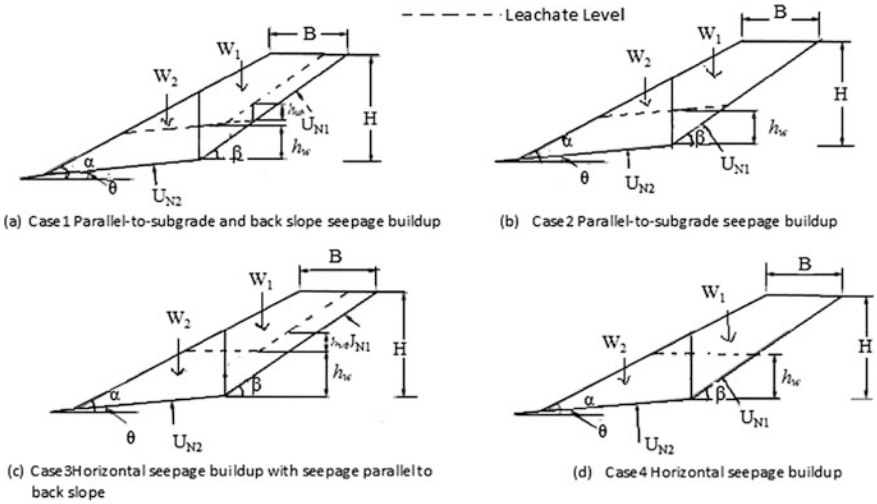

Fig. 2 Different cases of leachate buildup

The equation derived for factor of safety without considering the effect of water table is given below:

$$\mathrm{FS} = \frac{\begin{array}{l}(1 \mp k_{\mathrm{v}})\left\{W_1.\cos^2\theta + W_2.\cos^2\beta\right\}\tan\phi \\ - k_{\mathrm{h}}.\tan\phi\{W_1.\sin\theta.\cos\theta + W_2.\sin\beta.\cos\beta\} \\ + c(L_1.\cos\theta + L_2.\cos\beta)\end{array}}{\begin{array}{l}(1 - k_{\mathrm{v}})\{W_1.\cos\theta.\sin\theta + W_2.\cos\beta.\sin\beta\} \\ + k_{\mathrm{h}}\left(W_1 + W_2 - W_1.\sin^2\theta - W_2.\sin^2\beta\right)\end{array}}$$

The destabilizing forces due to pore pressure generated as the result of leachate buildup acts at the bottom of active and passive wedges. They are defined as U_{N1}, U_{N2} in Fig. 3.

The pressures caused by pore water due to leachate buildup either in active or closed condition can be evaluated using the equations recommended by Qian (2008).

The equation derived for factor of safety considering the effect of water table is given below:

$$\mathrm{F.O.S.} = \frac{\begin{array}{l}(1 \mp k_{\mathrm{v}})\{W_1.\cos^2\theta + W_2.\cos^2\beta\}\tan\phi \\ - k_{\mathrm{h}}.\tan\phi\{W_1.\sin\theta.\cos\theta + W_2.\sin\beta.\sin\beta\} + (U_{\mathrm{N1}}\cos\theta + U_{\mathrm{N2}}\cos\beta)\tan\phi \\ + c(L_1.\cos\theta + L_2.\cos\beta)\end{array}}{\begin{array}{l}(1 - k_{\mathrm{v}})\{W_1.\cos\theta.\sin\theta + W_2.\cos\beta.\sin\beta\} + (U_{\mathrm{N1}}\sin\theta + U_{\mathrm{N2}}\sin\beta) \\ + k_{\mathrm{h}}(W_1 + W_2 - W_1.\sin^2\theta - W_2.\sin^2\beta)\end{array}}$$

where W_1 and W_2 are the weight of the active and passive wedges, respectively, and U_{N1} and U_{N2} are the forces due to pore water pressure. k_{h} and k_{v} are horizontal and vertical seismic coefficients, respectively. The vertical seismic coefficient k_{v} is taken as $0.5k_{\mathrm{h}}$. The forces due to pore pressure are found for active and closed conditions. Active condition is when waste is being dumped and the front slope of the fill is not assumed to be covered by the final cover. In a closed condition, the filling is assumed to be complete and the front slope is assumed to be covered with an impermeable or very low permeable.

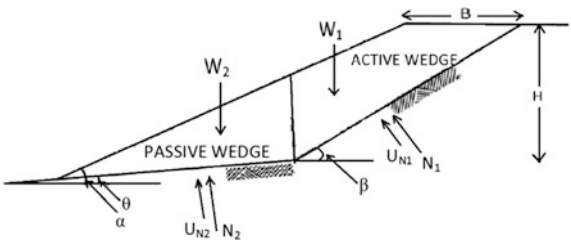

Fig. 3 Leachate buildup condition

4 Results and Discussions

A parametric study is done to analyze the effect of various parameters such as landfill side slope (1:S), failure angle, magnitude, acceleration coefficient on the factor of safety. To obtain the values of k_h (horizontal seismic coefficient), both rational as well as conventional methods are used. The mathematical model suggested by Bray and Travasarou (2009) is used in the analysis. The attenuation relationship suggested by Idriss (2002) is used to obtain spectral acceleration (S_a).

The analyses are performed for both cases, i.e., with or without considering the effect of leachate buildup, and the values are compared. The following parameters are assumed as per the literature survey and considered for the analysis: the unit weight of solid waste, γ_{sw}, of 10.5 kN/m^3 (Qian 2008); a saturated unit weight of solid waste, $(\gamma_{sw})_{sat}$, of 13 kN/m^3 (Qian 2008), Gs, of 1.60; a porosity, n, of 0.50. The height is 20 m, and top width taken into account is 15 m (Kandolkar et al. 2010). The shear strength parameters of solid waste are taken as: c = 15 kPa and ϕ = 20 (Kandolkar et al. 2010). The leachate level is assumed to be present at the depth of 1.5 m, and side slope taken into account is 1:1. The failure angle is of 0.667θ, i.e., 30° (approximately). It must be noted that assumption of $h_{wb} = 0.5h_w$ (Qian 2008) for Case 1 and Case 3 is used in the following analysis, where h_w is the vertical leachate depth in landfill measured from the toe of back slope, and h_{wb} is the vertical leachate depth in landfill measured along back slope for Case 1 and Case 3. Constant earthquake magnitude of 5 is considered. For parametric variation, three different types of earthquakes with moment magnitude M_w = 5, 6.5, and 7.0 are used. The value of failure angle β varies from 0.35 to 0.85 θ.

4.1 Effect of Failure Plane Angle, β

Failure angle β is varied as mentioned above for various values of embankment side slopes such as 1:1, 1:2, 1:2.5 (Fig. 4). It can be seen that as failure slope angle becomes steeper, factor of safety increases for both the cases. In case of dry condition, the F.O.S. remains almost constant and then increases slightly, whereas in case of pore pressure buildup conditions, the F.O.S. decreases gradually with increase in failure angle. This behavior is observed in wet condition since shear strength is reduced.

4.2 Effect of Earthquake Magnitude

Figure 5 depicts variation of factor of safety with failure plane angle β for various values of moment magnitude and horizontal seismic coefficient. As the value of moment magnitude increases, the value of horizontal seismic coefficient also

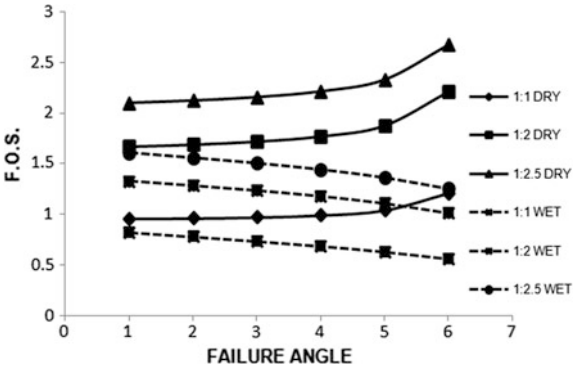

Fig. 4 Effect of side slope in dry and wet conditions

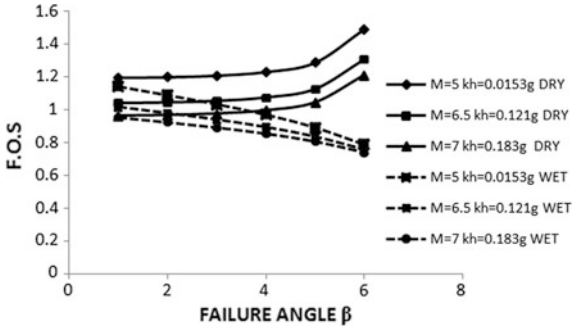

Fig. 5 Effect of magnitude with and without considering leachate buildup condition

increases, and hence, the driving force increases which in turn lowers the factor of safety. The trend of variation of factor of safety in this case (Fig. 5) is similar to that of side slope variation as in the previous case (Fig. 4). The relation between the moment magnitude and k_h is given below:

$$k_h = e^{\frac{-a+\sqrt{b}}{0.665}}$$

where

$$a = 2.83 - 0.55\ln(S_a)$$
$$b = (a^2 - 1.33(\ln(D_a) + 1.1 - 3.04\ln(S_a) + 0.224(\ln(S_a))^2 - 1.5T_s - 0.278(M_w - 7) - \varepsilon)$$
$$T_s = 4H/V_s$$

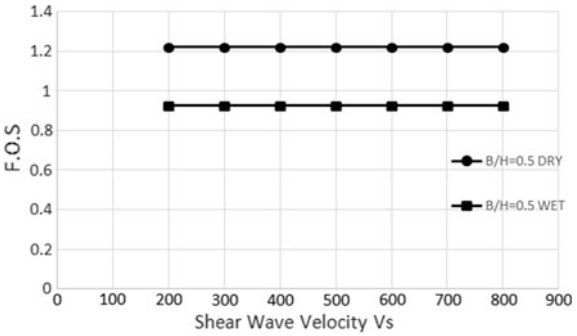

Fig. 6 Effect of stiffness with and without considering leachate buildup condition

4.3 *Effect of Stiffness of Landfill*

Effect of stiffness of the landfill (i.e., shear wave velocity, V_s) is observed in Fig. 6. The velocity is varied from 200 to 800 m/s. There is no effect on the F.O.S. values in both dry as well as wet cases.

4.4 *Effect of Leachate Buildup for All Four Cases*

Figure 7 shows the variation of F.O.S. with leachate buildup depths in all the four typical cases for both active and closed conditions.

The graph (Fig. 7) clearly shows a downward fall with increasing leachate buildup level. Case 1 and Case 2 conditions are on a safer side, whereas Case 3 and Case 4 conditions of F.O.S are unsafe. The fall in the factor of safety is steeper for Case 1 and Case 2, whereas in Case 3 and Case 4 the factor of safety is almost constant.

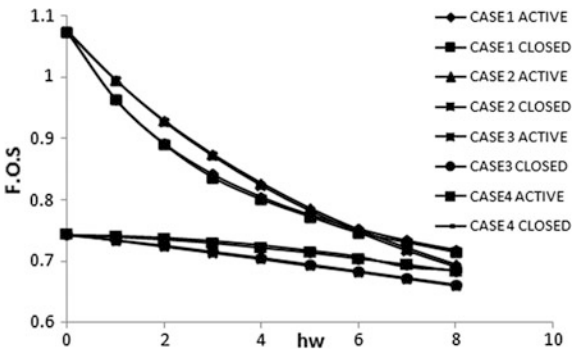

Fig. 7 Relationship between h_w and FS in various leachate buildup cases for active and closed conditions

5 Conclusions

The F.O.S. increases as the slope becomes steeper for both dry and wet conditions. The F.O.S. increases as the failure angle increases in case of dry condition. Due to the loss of shear strength as a result of pore pressure buildup in case of wet condition, there is decrease in F.O.S. up to 30%. The similar trend is followed also when the moment magnitude values are changed. This also illustrates the importance of k_h value by rational method where moment magnitude is one of the factor on which k_h value depends upon. There is no effect of shear wave velocity on F.O.S. Such similar trend is observed by Kandolkar et al. (2010). For all the four cases in active and closed conditions, overall there is decrease in F.O.S. with increase in leachate level. But there is higher fall in the value for Case 1 and Case 2, whereas the values tend to be constant in Case 3 and Case 4. The design charts developed can be helpful in the preliminary design of landfills.

References

Bray, J., & Travasarou, T. (2009). Pseudostatic coefficient for use in simplified seismic slope stability evaluation. *Journal of Geotechnical and Geoenvironmental Engineering, 135*(9), 1336–1340.

Idriss, I. (2002). Attenuation relationship derived by I. M. Idriss in 2002. *Interim Report Issued for USGS Review*. PEER Centre, University of California, Berkeley.

Kandolkar, S., Aldonkar, S., & Savoikar, P. (2010). Rational pseudo-static stability analysis of embankment. In *Indian Geotechnical Conference–2010, GEOtrendz*, December 16–18, 2010.

Qian, X. (2006). Translational failure of geosynthetic lined landfills under different leachate buildup condition. In *Advances in unsaturated soil, seepage and environmental geotechnics, GSP148*.

Qian, X. (2008 March). Limit equilibrium analysis of translational failure of landfills under different leachate buildup conditions. *Water Science and Engineering, 1*(1), 44–62.

Savoikar, P., & Aldonkar, S. S. (2011). Rational pseudo-static seismic stability analysis of MSW landfills. In *International Congress on Geo-Environmental Engineering 2011*, Takamatsu, Japan.

Study of Local Site Effects for Strong Motion Recording Stations of Delhi

Bhavesh Pandey, Ravi S. Jakka and Ashok Kumar

Abstract Effects of local site conditions on strong ground motion characteristics are a well-known phenomenon studied by many researchers. Similar studies were also carried out in past for Delhi to understand the amplification of ground motion in various locations using different methods. In this study, an attempt is made to study the amplifications in eight locations of Delhi where strong motion recording stations are located. For this study, shear wave velocity profiles were used for performing ground response analysis using equivalent linear approach. For input motion, response spectra compatible motion was used, compatible to response spectra for Rock sites as per IS 1893:2002. Transfer functions from available earthquake records and ambient vibration records were also calculated for comparison. The results obtained were presented in the form of response spectra and amplification functions for all the sites. The results suggest an amplification of the order of 2–3 with respect to actual motion at sites coming under site class D of NEHRP. No amplification was found at IMD site which suggest that it can be used as a reference site for Delhi. Other two sites with NEHRP site class C found to have amplification of the order of 1–2. Similarly, output response spectra, at surface, for all the sites except IMD and Kalkaji were found to be amplified with respect to the corresponding response spectra of IS 1893:2002.

Keywords Site amplification · Local site effects · Response spectra
Reference site · HVSR · Strong ground motion

B. Pandey · R. S. Jakka (✉) · A. Kumar
Indian Institute of Technology Roorkee, Rorkee 247667, India
e-mail: rsjakka@gmail.com

B. Pandey
e-mail: bhawesh.pandey@gmail.com

A. Kumar
e-mail: ashokeq@gmail.com

B. Adimoolam and S. Banerjee (eds.), *Soil Dynamics and Earthquake Geotechnical Engineering*, Lecture Notes in Civil Engineering 15,
https://doi.org/10.1007/978-981-13-0562-7_15

1 Introduction

It is a well-known fact that earthquakes pose a real threat to northern and north-eastern parts of the country. Most of the areas of northeast region, northern Bihar, northern Uttarakhand, Himachal Pradesh, Jammu and Kashmir, and some parts of Kutch are mapped in seismic Zone V as per IS 1893-2002. Similarly most of the regions adjacent to Zone V, such as entire Gangetic plains, southern region of Uttarakhand, and some parts of Rajasthan, are in seismic Zone IV (IS 1893-2002).

Himalayan region being one of the most seismically active regions of the world has experienced several earthquake disasters in past. Indian peninsula has experienced several earthquakes more than magnitude 8.0, such as, Kutch Gujarat, 1819; Assam earthquake, 1897; Kangra earthquake, 1905; Bihar–Nepal earthquake, 1934; Assam earthquake, 1950 in last 200 years. Also, very recent Nepal earthquake of 7.9 M in Nepal on April 25, 2015 cannot be overlooked. This earthquake was followed by more than 100 aftershocks with the largest being the one with a magnitude of 7.3 (as per Indian Meteorological Department website www.imd.gov.in) on May 12, 2015. These earthquakes continuously remind us to improve our preparedness for future earthquakes so that a large number of valuable lives can be saved.

Learning from past earthquakes, Indian agencies are continuously working on the methods and technologies to improve our preparedness for any large earthquake in future.

Delhi, the national capital of India, confronts a high seismic threat, as it is very close to the seismically active regions of Himalayas. Along with that there are other tectonic features close to Delhi which may be a cause of medium-intensity earthquakes in Delhi region. Delhi sits in the Seismic Zone IV as per IS-1893:2002. Delhi's high population density and proximity to various tectonic features warrant us to be more proactive in our preparedness for any future seismic event.

Thickness of the alluvium is variable in Delhi, and seeing such varieties is critical in evaluating site amplification. Various studies had been carried out in Delhi region related to site amplification. These studies are based on (a) micro-tremors (e.g. Mukhopadhyay et al. 2002), (b) earthquakes (Singh et al. 2002; Nath et al. 2003; Mittal et al. 2013a, b), (c) standard penetration test (Iyengar and Ghosh 2004), and (d) numerical modeling of wave propagation (e.g., Parvez et al. 2006).

Mukhopadhyay et al. (2002) worked on estimation of fundamental frequency and corresponding amplification factors at various locations of Delhi using micro-tremor data. Singh et al. (2002) and Mittal et al. (2013a, b) used standard spectral ratio (SSR) method for estimation of amplification. They reported high amplifications at different sites in Delhi which were of the order of 10–20. Iyengar and Ghosh (2004) evaluated amplification at 17 sites in Delhi by using standard penetration test (SPT) to obtain shear wave velocity profiles which were further used to obtain local site effects. They reported amplification of the order of 2–3 at the natural frequency of the sites. Singh et al. (2010) studied implications of Delhi

Table 1 V_{s30} and NEHRP site class

S. No.	Site name	V_{s30} (m/s)	NEHRP site class
1.	GEC Jaffarpur	338	D
2.	Jamia	346	D
3.	Kalkaji	564	C
4.	Shivaji College Raja Garden	346	D
5.	Vikaspuri	360	D
6.	IMD Ridge	543	C
7.	NPTI, Badarpur	322	D
8.	JNU	565	C

earthquake of November 25, 2007, on seismic hazard and concluded that the recorded PGA values at different locations were poorly explained by the estimates provided by previous studies.

It can be seen clearly that none of the study comes to a consensus; hence, an attempt is made in this study to estimate site amplification factors for eight locations of Delhi. Five locations, viz. Shivaji College, NPTI, Vikaspuri, Jamia Millia Islamia University, and GEC Jaffarpur, are situated on over deep alluvium and are in site class D of NEHRP (Pandey et al. 2016). Another set of sites were IMD, Kalkaji, and JNU which are shown as site class D of NEHRP as per the site characterization study conducted by Pandey et al. (2016). Site class and respective V_{s30} values, calculated as per site characterization study of Pandey et al. (2016), for these sites were shown in Table 1.

2 Methodology

There are various methods which can be used for estimation of site amplification. There are methods which use earthquake records or ambient vibration records from the sites of interest such as standard spectral ratio technique and horizontal-to-vertical spectral ratio technique. Other than this, there are theoretical methods such theoretical ground response analysis. For this study, theoretical ground response analysis (GRA) using equivalent linear approach has been used. For conducting GRA, a software STRATA (Kottke et al. 2013) has been used in this study.

For GRA, two kinds of input are required; one is information regarding soil strata and another is input motion. All the sites chosen for this study are having strong motion recording stations (Mittal et al. 2012), and the site characterization report for these sites is available (Pandey et al. 2016). This gives us the benefit of having details of underlying soil strata of the location and availability of earthquake records at the same location. The available records from these sites were used for comparison of transfer functions from GRA and HVSR (Nakamura 1989). Along

Fig. 1 Locations of eight strong motion recording stations considered in this study

with this, response spectra obtained from GRA and response spectra from recorded motion were also compared with response spectra in IS 1893:2002. For input ground motion, response spectra compatible motion was generated compatible with response spectra for rock sites. As IS 1893:2002 provides response spectra for outcrop/surface motion, the response spectra compatible motion was corrected for free surface effect and then was applied at top of the layer having shear wave velocity more than 750 m/s. The location of sites is shown in Fig. 1.

3 Results

Results of this study were compiled in two forms; one is transfer function comparison and another is response spectra comparison. For ease of comparison, the results were divided into two groups as per their NEHRP site class.

For transfer function comparison (Figs. 2 and 3), four kinds of transfer functions were generated—(a) transfer function between surface and half space (top of the layer having velocity greater than 750 m/s) from GRA, (b) transfer function between surface and bedrock outcrop (top of the layer having velocity greater than 750 m/s), (c) transfer function obtained from HVSR of earthquake records available from these stations, and (d) transfer function from HVSR using ambient vibration records.

For response spectra comparison (Figs. 4 and 5), normalized response spectrum obtained at surface from GRA and normalized response spectrum obtained from earthquake records were compared with response spectrum as per IS 1893:2002.

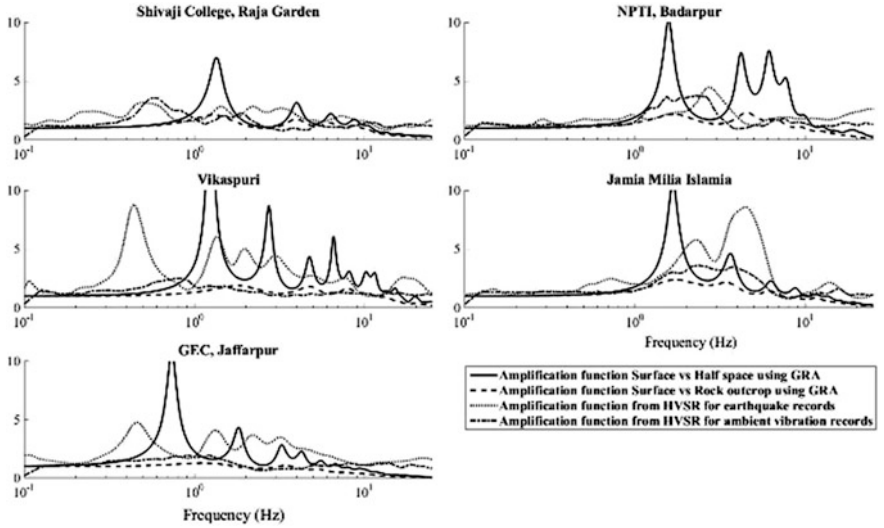

Fig. 2 Comparison of transfer functions for sites in class D of NEHRP

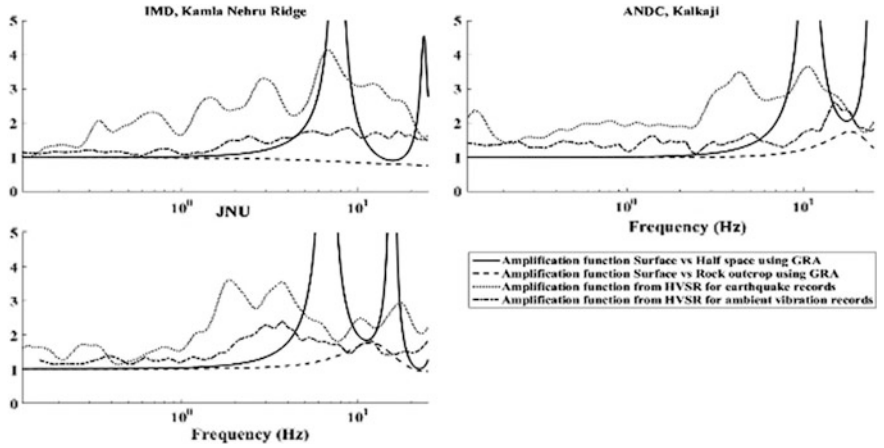

Fig. 3 Comparison of transfer functions of sites belonging to NEHRP site class C

For sites of site class D (Fig. 1), it can be clearly seen that all the four kinds of transfer functions are very close to each other in respect to frequency. Also amplification function between surface/half space and surface/outcrop is similar in terms of frequency although amplitude is very low for surface/outcrop amplification function which is of the order of 2–3.

Similarly, for site class C sites (Fig. 2), amplification functions match very well with each other in terms of frequency. Here also remarkable difference can be seen

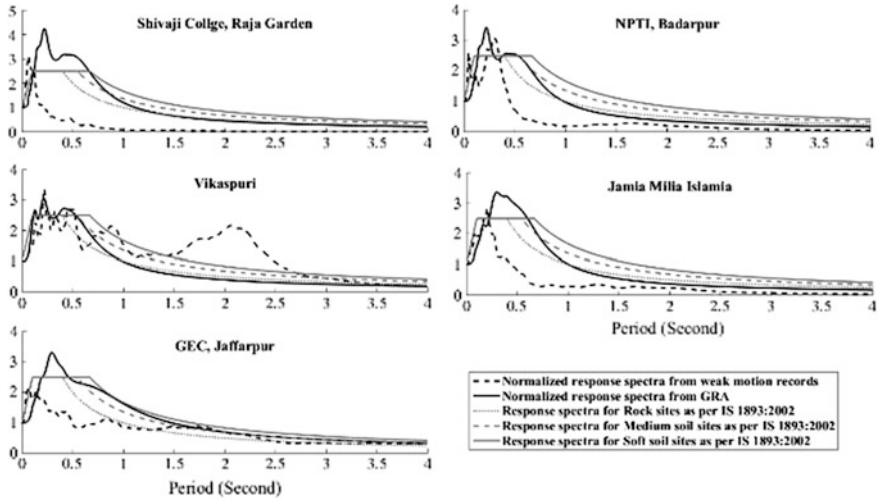

Fig. 4 Response spectra comparison for sites of NEHRP site class D

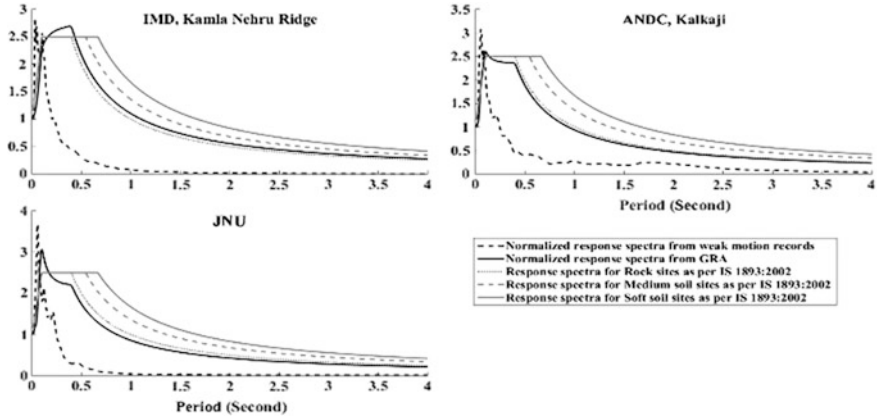

Fig. 5 Response spectra comparison for sites belonging to NEHRP site class C

between surface/half space function and surface/outcrop function. Another interesting observation which can be easily made from Fig. 2 is surface/outcrop transfer function for IMD is almost flat with value 1, which means there is no amplification between surface motion obtained after GRA and original response spectra compatible motion. The same thing is also evident from response spectra comparison in Fig. 5 where response spectra obtained for surface motion after GRA are almost matching with response spectra from IS 1893:2002 for rock sites. It will be interesting to note that almost similar results were obtained for Kalkaji site (Figs. 3 and 5) except at higher frequency (or lower period) where some amplification of 1.7 was

found. For third site in class C group, i.e., JNU, amplification of 1.8 is found in surface/outcrop transfer function at 10 Hz frequency. The similar kind of amplification is also evident in response spectra plotted for JNU. These results clearly shows that IMD can comfortably be used as a reference site for earthquake engineering studies but Kalkaji can only be used for such studies at lower frequencies. Another inference which can be made from this analysis is even though a site looks like a rock outcrop, as is the case with JNU, and have high V_{s30} value, still care should be taken in considering any site as reference site.

Comparing the response spectra of all the sites shows that all the response spectra are amplified. Hence, by observing amplification of response spectra it can be clearly said that expected acceleration would be much higher than response spectra proposed in IS 1893:2002 for the maximum considered earthquake. Also the mismatch between response spectra obtained from earthquake records and GRA is due to the huge difference between intensity of recorded motion and input motion for GRA as the recorded motion has very low PGA values.

4 Conclusion and Discussion

Lots of variations were found in amplification ratios of different transfer function for each site. Hence, it can be concluded from this study that amplification ratios must be chosen with care whenever any analysis for seismic hazard assessment is to be. However, not much difference is observed in fundamental frequency estimated by different transfer functions. Also the amplification function obtained from surface/outcrop seems to be more realistic for engineering purposes as normally we tend to compare to amplification of a site with reference to other site location. Surface/half space transfer function can be very useful for studies related to attenuation studies as bedrock motion is very important for such studies.

Another inference from this study is that sites which look like rock outcrop may not be an actual rock outcrop as it was shown from the result of amplification function and response spectra of JNU in Figs. 3 and 5. Also it can be concluded that IMD can be used as a reference rock outcrop site for motion with PGA of order of 0.24 g. Kalkaji can also be used as reference outcrop if study deals with low frequency range. Using IMD as a reference site, it can be suggested that an amplification of the order of 2–3 can be expected at sites having site class D with respect to ground motion at IMD for a ground motion of intensity as used in this study.

Comparison of response spectra also conforms the amplifications observed through transfer functions. This study also suggests higher acceleration values for soil sites at almost all the periods. Hence, provision must be made in response spectra provided in IS 1893:2002 for amplification as well. Currently, the difference in response spectra provided in IS 1893:2002 for rock sites and soil sites is just in frequency bandwidth, and it does not provide any provision for amplification.

References

IS-1893:2002 (Part-1). *Indian Standard criteria for earthquake resistant design of structures, Part 1 —General provisions and buildings (Fifth Edition).* Bureau of Indian Standards, New Delhi, 42.

Iyengar, R. N., & Ghosh, S. (2004). Microzonation of earthquake hazard in greater Delhi area. *Current Science, 87,* 1193–1202.

Kottke, A. R., Wang, X., & Rathje, E. M. (2013). *Technical manual of strata*. Geotechnical Engineering Center, Department of Civil, Architectural and Environmental Engineering, University of Texas.

Mittal, H., Kumar, A., & Rebecca, R. (2012). Indian strong motion instrumentation network and its site characterization. *International Journal of Geosciences, 3*(6), 1151–1167.

Mittal, H., Kumar, A., & Kumar, A. (2013a). Site effects estimation in Delhi from the Indian strong motion instrumentation network. *Seismological Research Letters, 84*(1), 33–41.

Mittal, H., Kumar, A., & Singh, S. K. (2013b). Estimation of site effects in Delhi using standard spectral ratio. *Soil Dynamics and Earthquake Engineering, 50,* 53–61.

Mukhopadhyay, S., Pandey, Y., Dharmaraju, R., Chauhan, P. K. S., Singh, P., & Dev, A. (2002). Seismic microzonation of Delhi for ground–shaking site effects. *Current Science, 87,* 877–881.

Nakamura, Y. (1989). Method for dynamic characteristics estimation of subsurface using microtremor on the ground surface. *Quarterly Report of Railway Technical Research Institute (Japan), 30*(1), 25–33.

Nath, S. K., Sengupta, P., Srivastav, S. K., Bhattacharya, S. N., Dattatrayam, R. S., Prakash, R., et al. (2003). Estimation of S–wave site response in and around Delhi region from weak motion data. *Proceedings of the Indian Academy of Sciences (Journal of Earth System Science), 112,* 441–463.

Pandey, B., Jakka, R. S., Kumar, A., & Mittal, H. (2016). Site characterization of strong-motion recording stations of Delhi using joint inversion of phase velocity dispersion and H/V curve. *Bulletin of the Seismological Society of America, 106*(3), 1254–1266. https://doi.org/10.1785/0120150135.

Parvez, I., Vaccari, F., & Panza, G. F. (2006). Influence of source distance on site–effect in Delhi city. *Current Science, 91,* 827–835.

Singh, S. K., Mohanty, W. K., Bansal, B. K., & Roonwal, G. (2002). Ground motion in Delhi from future large/great earthquakes in the central seismic gap of the Himalayan arc. *Bulletin of the Seismological Society of America, 92,* 555–569.

Singh, S. K., Kumar, A., Suresh, G., Ordaz, M., Pacheco, J. F., Sharma, M. L., et al. (2010). Delhi earthquake of 25 November 2007 (Mw 4.1): Implications for seismic hazard. *Current Science, 99*(7), 939–947.

Mitigation of Dynamic Loading Effects on Retaining Walls Using Recycled Tire Chips

S. Bali Reddy and A. Murali Krishna

Abstract This paper presents the results of shaking table tests on retaining wall models using recycled tire chips as compressible inclusions. Scrap tire derived tire chips of 10 × 10 mm size and about 20 mm length have been used in the study. The 600-mm-height model wall is constructed in a Perspex container and instrumented with pressure sensors and LVDTs at different locations. Sinusoidal dynamic excitations were applied on the model walls. The dynamic response of the retaining walls with the variation in the acceleration and frequency of base shaking has been monitored and discussed. It is observed from these tests results that the horizontal displacement and incremental lateral earth pressures are significantly reduced by the inclusion of tire chips as cushion in between the wall and backfill. Reduction of the lateral earth pressure and displacement implies a lower design requirement which implies lesser dimensions of the retaining wall with reduced material cost.

Keywords Retaining wall · Recycled tire chips · Compressible inclusion
Reduction earth pressures · Wall displacements

1 Introduction

Earth retaining structures such as retaining walls, bridge abutments, bulk heads, braced excavations, and mechanically stabilized walls play a very important role in public life (Reddy and Krishna 2015). These structures are frequently representing the main elements of transportation system, port, harbors, and other infrastructure systems. Sometimes these civil engineering structures are often being affected by dynamic loading, like earthquakes. With frequent occurrences of natural disasters in

S. B. Reddy (✉) · A. M. Krishna
Department of Civil Engineering, Indian Institute of Technology Guwahati, Guwahati 781039, India
e-mail: sodom@iitg.ernet.in

A. M. Krishna
e-mail: amurali@iitg.ernet.in

B. Adimoolam and S. Banerjee (eds.), *Soil Dynamics and Earthquake Geotechnical Engineering*, Lecture Notes in Civil Engineering 15,
https://doi.org/10.1007/978-981-13-0562-7_16

India (Bhuj 2001, Sikkim 2011, and other earthquakes) and the associated sustainable implications, earthquake mitigation techniques are becoming matters of interest. Performances of retaining wall under static and seismic loading conditions depend upon the type of backfill soil, generally clean granular cohesion less backfill material is preferred. However, new lightweight fills' materials like shredded tire chips, EPS geofoam, fly ash are being explored as alternative backfill materials nowadays (Bathurst et al. 2007; Lal and Mandal 2012; Reddy and Krishna 2013, 2015). These materials are beneficial in reducing earth pressures and lateral displacements of the retaining walls.

Use of scrap tire derived geomaterials (tire shreds, tire chips, and tire crumbs) has been found increasing in various geotechnical engineering applications (Humphrey 1993; Cecich et al. 1996; Tweedie et al. 1998; Lee and Roh 2006; Hazarika and Yasuhara 2007; Anbazhagan et al. 2011; Sheikh et al. 2013; Dammala et al. 2015; Boominathan et al. 2015; Reddy and Krishna 2015). Different researchers (Inglis et al. 1996; Ertugrul and Trandafir 2011; Reddy and Krishna 2013) were studied on reduction of lateral earth pressures on retaining wall using EPS geofoam as compressible inclusion. In this paper, recycled tire chips are used as compressible inclusions just behind the retaining wall to mitigate the dynamic loading effects. Shaking table tests on retaining wall models using recycled tire chips as compressible inclusions were conducted in this study.

2 Equipment and Materials Used

A computer-controlled servo-hydraulic shaking table facility with a single degree of freedom (horizontal) was used to simulate the horizontal shaking action, associated with seismic and other vibration conditions. The shaking table can be operated for frequency up to 10 Hz with the amplitude of ±250 mm. Models of retaining walls have been built in a Perspex container fitted with compressible foam as back boundary to reduce the boundary effect. Retaining wall model of 600 mm height was constructed in a model container of 1200 mm × 600 mm in plan and 1000 mm height (Fig. 1). The model container was made of Perspex sheets of 10 mm thickness and braced by a steel frame made of steel angle sections that also facilitates for easy lifting and handling.

Locally available dry sand having specific gravity of 2.62 has been used as the backfill material. The sand has maximum unit weight of 16.1 kN/m^3 and minimum unit weight of 13.26 kN/m^3. The values of e_{max} and e_{min} are 0.94 and 0.64, respectively. The sand is classified as poorly graded sand with letter symbols SP as per the Unified Soil Classification System. Scrap tire derived tire chips of 10 × 10 mm size and about 20 mm length have been used as compressible inclusion for the study. Specific gravity and unit weight of the tire chips were determined as 1.08 and 6.45 kN/m^3, respectively.

Fig. 1 Retaining wall model container mounted on shake table

3 Model Preparation and Testing Procedure

The model wall of 600 mm high and 580 mm length was made with eight hollow rectangular steel sections, each of 25 mm wide and 75 mm height and 580 mm length, which were joined together using steel rods of 12 mm diameter. These steel rods were further connected to a bottom plywood base forming a rigid connection.

Two types of test cases were considered as shown in Fig. 2. In Case A, a retaining wall model with a conventional sandy backfill was used (control case); in Case B, behind the model wall, two different thickness of tire chips were placed vertically as compressible inclusions. The thickness chosen here was (t/H = 0.15 and 0.30) 0.15, 0.3 times of the wall height. Here, t = thickness of tire chips and H = height of the wall. The compressible inclusion was made by recycled tire chips. Backfilling was done by stagewise by free-falling technique (pacing the calculated amount of sand based on layer thickness and target density) and compacting manually to achieve the target density. For Case B, the compressible inclusion layer was prepared by filling the recycled tire chips inside a selected size

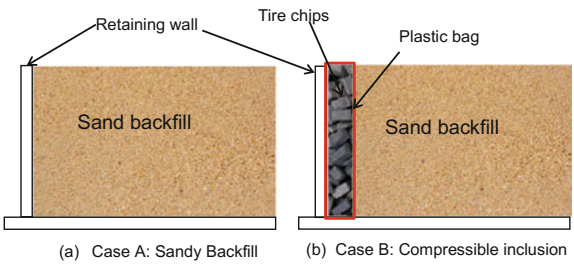

Fig. 2 Test case

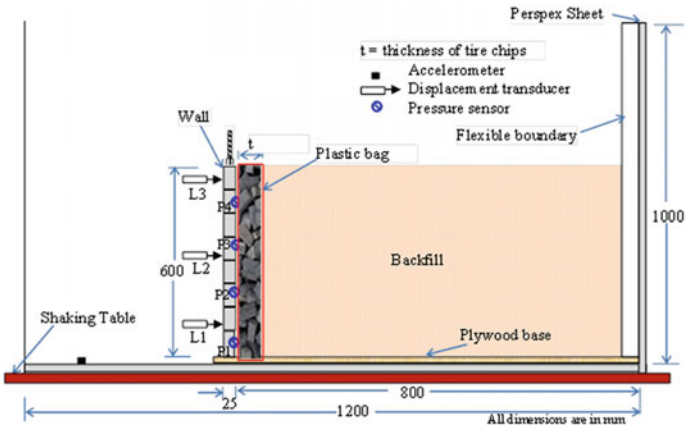

Fig. 3 Schematic diagram of retaining wall model

bag made of plastic sheet. The bag is required to wrap the tire chips so that they do not mix with the surrounding soils. Such confinement also makes the execution of backfilling easier. The average dry unit weight of tire chips achieved after filling and tamping was 6.345 kN/m^3.

For all tests, four pressure sensors (each of 50 kPa capacity), P1, P2, P3, and P4, were placed inside the wall, in contact with the facing at different elevations 487, 337, 187, and 37 mm, respectively. Three LVDTs L1, L2, and L3 were positioned at elevations 125, 380, and 580 mm, respectively, along the facing. Figure 3 shows the schematic diagram of retaining wall model. After completing the model preparation with external support to the facing, model was placed on shaking table. Then external support of facing was removed, and shaking table has been operated. Each model wall was subjected to 20 cycles of sinusoidal shaking at specified frequency and acceleration. The parameters varied in different model tests are given in Table 1. The dynamic response of each model wall, in terms of incremental lateral earth pressure and the displacement responses at different elevations at facing, is monitored using a data-acquisition system.

4 Results

Variation of horizontal displacements at different elevations of the wall with increasing number of dynamic loading cycles is shown in Fig. 4, for the test T1. The figure shows the nonlinearly increasing trend of displacements with increase in number of cycles. Further, higher displacements at higher elevations are noticed. Wall displacements of 0.61, 0.38, and 0.12 mm are seen from the figure, at 580, 380, and 125 mm elevation, respectively.

Table 1 Test parameters for different test

Test No.	*t*/*H*	Base acceleration, g	Frequency, Hz
T1	0.00	0.1	3
T2	0.15	0.1	3
T3	0.30	0.1	3
T4	0.0	0.3	5
T5	0.15	0.3	5
T6	0.30	0.3	5

t thickness of tire chips, *H* height of wall

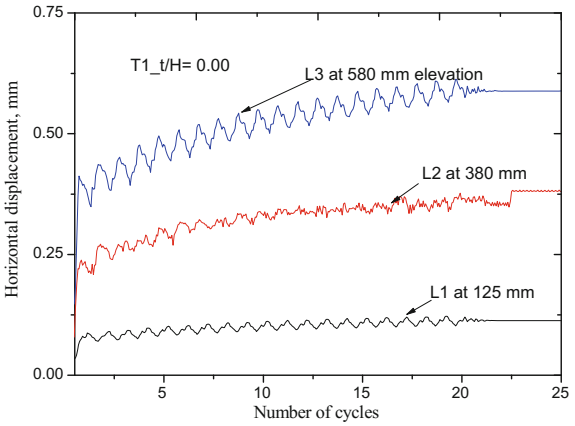

Fig. 4 Typical variation of displacement with number of cycles for the test T1

Figure 5a shows the displacement profiles, at the end of 20 cycles of dynamic motion (0.1 g acceleration and 3 Hz frequency), revealing the influence of compressible inclusion on the horizontal displacement response. Here the elevation (z) is represented in non-dimensional form after normalizing by the full wall height (*H*). It is observed, from the figure, that the displacements are significantly reduced with the inclusion of the compressible inclusion just behind the retaining wall. The maximum top displacement of 0.61 mm in the case of control model wall (T1) is reduced to 0.20 mm in the case of compressible compression model wall test (T3).

Incremental lateral earth pressures are observed during the dynamic excitation along the height of the wall in different tests. Figure 5b shows the measured incremental lateral earth pressures along the height of the wall for T1, T2, and T3 tests. It is observed, from the figure, that incremental lateral earth pressures are depicting the diminishing trend with increase in inclusion of compressible inclusion thickness. Maximum earth pressures are observed at bottom of the wall.

The measured top displacements and calculated percentage reduction are reported in Table 2, which shows around 68% reduction in top displacement. Maximum earth pressure values and calculated percentage reduction from earth pressures are reported in Table 2. Incremental earth pressures are reduced around 68% compared to test T1. This type of behavior can be observed when vertical compressible inclusion placed behind the retaining wall.

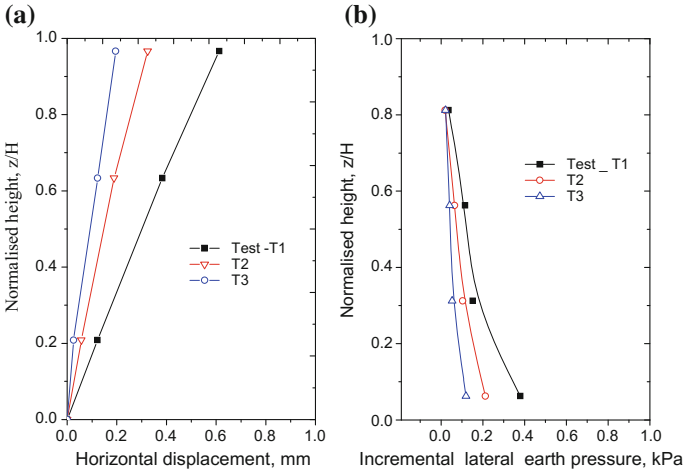

Fig. 5 Comparison of mode response for T1, T2, and T3 tests; **a** displacement profile, **b** earth pressure profile

Table 2 Displacement, earth pressure, and percent reduction for tests T1, T2, and T3

Parameter	Compressible inclusion, *t*/*H*		
	0.00	0.15	0.30
Top displacements, mm	0.613	0.324	0.195
% reduction of displacement	–	47.14	68.19
Maximum incremental earth pressure, kPa	0.379	0.211	0.119
% reduction of earth pressure	–	44.33	68.60

Further, the base acceleration of 0.3 g and 5 Hz frequency has been applied on different model walls to observe the effect of tire chips as compressible inclusion material. The response of the model wall is measured in terms of horizontal displacement and lateral earth pressures on model wall with different configurations and shown in Fig. 6. Wall top displacements of 3.05, 1.64, and 0.73 mm are seen from the figure, for T4, T5, and T6, respectively. From the laboratory model tests, large reductions in lateral earth pressures were achieved when $t/H = 0.30$ thickness tire chips were used as the vertical compressible inclusion.

Reduction of the lateral earth pressure and displacement implies a lower design requirement which implies lesser dimensions of the retaining wall with reduced material cost. However, the cushion thickness may vary depending upon many parameters such as wall rigidity, height of wall, stiffness of tire chips, and ground motion effect. However, model test results cannot be directly extrapolate to the response of field walls because of gravity and scaling effects, and the results obtained from this study will help in understanding the relative performance of retaining walls subjected to base shaking with compressible inclusions.

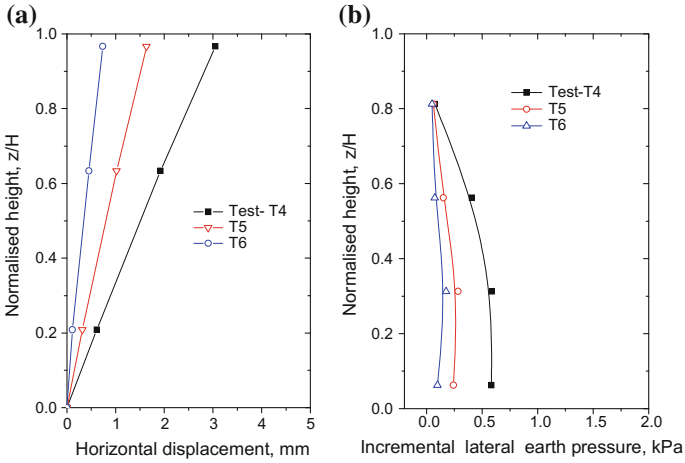

Fig. 6 Comparison of mode response for T4, T5, and T6 tests; **a** displacement profile, **b** earth pressure profile

5 Conclusions

A series of model tests were conducted using shaking table to examine the performance of retaining walls with recycled tire chips as compressible inclusion for mitigation of dynamic loading effects. Inclusion of recycled tire chips as vertical compressible inclusion just behind the retaining wall resulted in drastic reduction of the wall displacements, lateral earth pressures. The maximum horizontal displacement of model wall with compressible inclusions (recycled tire chips) is reduced by around 65% compared to the control test wall. Incremental earth pressure is reduced by around 75% compared to the control tests. This implies the dynamic performance of retaining wall improves with the use of recycled tire chips as cushion material.

References

Ahn Il-S., Cheng, L. (2014) Tire derived aggregate for retaining wall backfill under earthquake loading. *Construction and Building Materials* 57:105–116

Anbazhagan, P., Mamatha, M., Soumyashree, P., Sushyam, N., Bharatha, T. P., & Vivekan, R. W. (2011). Laboratory characterization of tire crumbs soil mixture for developing low cost damping materials. *International Journal of Earth Sciences and Engineering, 4*(6), 63–66.

Bathurst, R. J., Zarnani, S., & Gaskin, A. (2007). Shaking table testing of Geofoam seismic buffers. *Soil Dynamics and Earthquake Engineering, 27,* 324–332.

Boominathan, A., Banerjee, S., & Dhanya, J. S. (2015). Performance of soil-rubber tyre scrap mixture as seismic base isolators for foundations. In *6th International Conference on Earthquake Geotechnical Engineering,* Christchurch, New Zealand.

Cecich, V., Gonzales, L., Hoisaeter, A., Williams, J., & Reddy, K. (1996). Use of shredded tires as lightweight backfill material for retaining structures. *Waste Management and Research, 14,* 433–451.

Dammala, P., Reddy, S. B., & Krishna, A. M. (2015). Experimental investigation of applicability of sand tire chip mixtures as retaining wall backfill. In *IFCEE, ASCE Geotechnical special publication* (pp. 1420–1429). https://doi.org/10.1061/9780784479087.128.

Ertugrul, O., & Trandafir, A. (2011). Reduction of lateral earth forces acting on rigid nonyielding retaining walls by EPS Geofoam inclusions. *Journal of Materials in Civil Engineering, 23*(12), 1711–1718.

Hazarika, H., & Yasuhara, K. (2007), *Scrap tire derived geo materials—Opportunities challenges*. Taylor and Francis, UK.

Humphrey, D. N., Sandford, T. C., Cribbs, M. M., & Manion, W. P. (1993). Shear strength and compressibility of the tyre chips for use as retaining wall backfill. *Transportation Research Record, 1422,* 29–35.

Inglis, D., Macleod, G., Naesgaard, E., & Zergoun, M. (1996). Basement wall with seismic earth pressures and novel expanded polystyrene foam buffer layer. In *Proceedings of the 10th Annual Symposium of the Vancouver Geotechnical Society*, Vancouver and B.C.

Lal, R. R. B., & Mandal, J. N. (2012). Feasibility study on fly ash as backfill material in cellular reinforced walls. *EJGE, 17,* 1437–1458.

Lee, H. J., & Roh, H. S. (2006). The use of recycled tire chips to minimize dynamic earth pressure during compaction of backfill. *Construction Building Materials, 21*(5), 1016–1026.

Reddy, S. B., & Krishna, A. M. (2013). Numerical simulations of earth-retaining structures using EPS geofoam inclusions. In *Indian Geotechnical Conference,* IITRoorkee.

Reddy, S. B., & Krishna, A. M. (2015). Recycled tire chips mixed with sand as lightweight backfill material in retaining wall applications: An experimental investigation. *International Journal of Geosynthetics and Ground Engineering*. https://doi.org/10.1007/s40891-015-0036-0.

Sheikh, M. N., Mashiri, M. S., Vinod, J. S., & Tsang, H. H. (2013). Shear and compressibility behavior of sand-tire crumb mixtures. *Journal of Materials in Civil Engineering, ASCE, 25*(10), 1366–1374.

Tweedie, J. J., Humphrey, D. N., & Sandford, T. C. (1998). Tire shreds as retaining wall backfill, active conditions. *Journal of Geotechnical and Geoenvironmental Engineering, ASCE, 124* (11), 1061–1070.

[TH-05] An Experimental Study on Seismic Soil-Pile Foundation-Structure Interaction in Soft Clay

Rajib Saha, Animesh Pandey and Richi Prasad Sharma

Abstract Dynamic soil structure interaction (DSSI) is an important seismic design consideration for sustainable design of structures. Further, such interaction has been reported to be detrimental consequences superseding seismic codes in structure situated mainly in soft clay and liquefiable deposit as observed during past earthquakes, such as, 1964 Niigata earthquake, 1985 Mexico city earthquake, and 1995 Kobe earthquake. In practice, design is made based on assumption of fixed base condition with a perception of beneficial effect on the response of system based on few seismic codal guidelines and to avoid complexity in SSI modeling. In this context, present study is a humble effort to investigate the influence of DSSI in pile foundation-supported structure through scaled model study in very soft clay using shake table tests. This limited study indicates that lengthening of period is insignificant for stiff period of structure in soft clay which is in-general counter-intuitive. The reason may be foundation stiffness is considerably higher than superstructure. Further, it is observed from the acceleration signals that elastic forces may be significantly high in column as compared to pile head in particularly stiff period structures supported by pile foundation in soft clay, while an opposite trend is observed in moderately longer period of structure supported by similar foundation.

Keywords Fundamental period · Kaolin · Shake table

R. Saha (✉) · A. Pandey · R. P. Sharma
Civil Engineering Department, National Institute of Technolgy Agartala, Agartala 799046, Tripura, India
e-mail: rajib.iitbbsr@gmail.com

A. Pandey
e-mail: animeshxperia@gmail.com

R. P. Sharma
e-mail: richisharma.sharma@gmail.com

B. Adimoolam and S. Banerjee (eds.), *Soil Dynamics and Earthquake Geotechnical Engineering*, Lecture Notes in Civil Engineering 15,
https://doi.org/10.1007/978-981-13-0562-7_17

1 Introduction

Complexity involved with seismic soil-pile-structure interaction (SSPSI) problem and unavailability of standard and validated analysis techniques routinely results in ignoring or simplifying the presence of pile foundations for the structural design. In fact, non-incorporation or simplification of SSPSI may not warrant actual prediction of behavior of the whole structural system under seismic loading as highlighted in many studies (e.g., Jeremic et al. 2004; Boulanger et al. 1999; Tokimatsu et al. 2005). Further, these studies also highlighted the importance of SSPSI in estimation of design forces in pile foundation-supported structural system. However, post-analysis of failure of pile foundation-supported structure during past earthquakes such as 1965 Niigata earthquake, 1985 Mexico city earthquake, 1989 Loma Prieta earthquake, 1995 Kobe earthquake indicated the detrimental effect of dynamic soil structure interaction (DSSI) (Meymand 1998). Interestingly, it is observed in these case studies that DSSI has led to detrimental response in pile-supported structure during an earthquake event, mainly in liquefied and soft clayey-type soil deposit (Bhattacharya et al. 2014; Meymand 1998). This acted as prime motivation behind present study. In fact, few investigators have already mentioned the significance of experimental study since different phenomenon related to DSSI could not be predicted while studied through prototype structure attributing numerical analysis (e.g., Meymand 1998). Limited studies based on shake table tests pointed out design implications resulting from such interaction in non-liquefied (Tokimatsu et al. 2005) as well as liquefied soil (Lombardi and Bhattacharya 2013). Further, a number of experimental studies were also found in this direction which verifies the theoretically developed modeling issues and the effect of complex SSPSI (e.g., Meymand 1998; Boulanger et al. 1999; Tokimatsu et al. 2005; Boominathan and Ayothiraman 2005; Chau et al. 2009; Lombardi and Bhattacharya 2013). However, a recent shake table study by the first author along with other co-authors (Saha et al. 2015) reported increase in shear force at pile head considering dynamic soil-piled raft-structure interaction.

From the above view point, present study is an attempt to investigate the effect of SSPSI on dynamic characteristics and seismic force distribution in a model pile foundation-supported structural system embedded in soft clay by carrying out shake table experiment considering steady-state harmonic motion. Percentage lengthening of period and an approximate lateral shear force distribution are calculated based on experimental observation for a 3×3 flexible pile group-supported structural system. Hence, the outcome of present study may give insight into the problem in order to modify the existing design guidelines for a pile foundation-supported structural system.

2 Experimental Program

2.1 Structural Model

Simplistically, the superstructure is modeled as a SDOF structure in the present study which is supported by a model 3 × 3 flexible pile group in soft clay. Two different periods of vibration in fixed base condition, i.e., T_{fixed} = 0.3 and 0.7 s representative of shorter to moderately longer range period of structure is considered herein. The model column is prepared by two steel scales welded together and fixed with a base plate which carries lumped weights made of circular MS plates bolted at the top of the scale. The theoretically calculated weights are accordingly adjusted in order to simulate 0.30 s (m_1 = 230) and 0.70 s (m_2 = 1000) period of structure which is further verified by free and forced vibration tests. Hollow piles made of steel alloy rigidly connected with pile cap made of 30-mm-thick MS plate are used to support the superstructure load. A 3 × 3 frictional long pile group is designed to support the maximum load of superstructure (i.e., m_2 = 1000 g) and pile cap with a factor of safety of 2.0 considering very soft clay bed. Length to diameter of pile is kept as 33.33 which may be considered as long pile as per IS2911-Part 1 (2010). However, the detailed specification of superstructure, cap, and piles are presented in Table 1. Figure 1 presents the whole structural model.

The objective of the scale modeling procedure for DSSI experiments is to achieve "dynamic similarity," where model and prototype experience homologous forces. Meymand (1998) presented a detailed review on similitude rule and

Table 1 Detailed specification of superstructure, pile cap, and pile

Specification/parameters	Values
Length of steel column	300 mm
Width of column	20 mm
Thickness of column	2.0 mm
Buckling load of column	2.08 kg
Lateral stiffness of column	83 N/m
Young's modulus of steel column	5.64×10^4 N/mm^2
Mass of single pile	120 gm
Length of pile	400 mm
Outer diameter of pile	12 mm
Inner diameter of pile	10 mm
Thickness of pile	2 mm
Young's modulus of pile	2×10^5 N/mm^2
Moment of inertia of hollow pile	527×10^{-12} m^4
Buckling load of pile	10.34 kN
Size of pile cap	100 mm × 100 mm
Thickness of pile cap	30 mm
Mass of pile cap	1350 gm

Fig. 1 Model structural system

suggested a rational scaling law which is followed in the present study. Accordingly, a 3 × 3 frictional pile group is designed as per IS 2911 (2010) considering maximum superstructure load exhibited by 0.7 s SDOF along with pile cap. The thickness of pile cap is provided as per IS 2911 (2010).

2.2 *Model Container and Soil Preparation*

A lightweight cylindrical container made of alloy of tin attached with commercially available foam at periphery as a boundary-absorbing material (Lombardi and Bhattacharya 2013) is used to prepare the consolidated soft clay bed for carrying out the shake table experiment. The container is strengthened by mild steel jacket in order to withstand maximum vertical consolidation pressure of 1 kN/m^2. The dimension of the container is considered as 500 mm (diameter) × 700 mm (height) based on the maximum payload capacity of shake table as 100 kg and to ensure minimum distance of one and half times of length of rigid pile cap from the edge of boundary. The consolidation unit is fabricated by different shapes of mild steel sections with an attachment of inverted hydraulic jack of capacity of 10 ton which may generate desired level of consolidating pressure. One-dimensional consolidation is carried out in the present study by keeping drainage arrangements at the bottom of the chamber. A 30-mm-thick wooden plunk grooved into four perpendicular channels having 20 mm depth is placed at the base of the container which is further attached with four drainage valves at the outside of the chamber. At the top of the plank, a cotton cloth is placed to separate the 30-mm-thick filter material placed at the top of plank. Graded coarse sand pertaining to following filter characteristics, i.e., D_{60} filter/D_{10} filter = 5, D_{15} filter/D_{85} soil = 3, is used in this study.

Further, a filter paper is provided at the boundary of very soft kaolin layer and graded coarse sand. Commercially available kaolin having moderate plastic property is used for preparation of soil bed in the present study.

Total 90 kg of kaolin was mixed at 1.2 times L.L, i.e., 63 kg of water to form a kaolin slurry using a rotary cement mixer. A dispersing agent solution made of 45 g sodium hexametaphosphate mixed with 1000 ml of distilled water, known as "Calgon solution," is added with each batch of kaolin-water mix in a proportion of 10% of the total weight of water. Calgon solution is used to avoid flocculation and to produce a uniform consistency of kaolin paste. The whole mixing is performed in three batches to fill up the container. A model clay sample of total height of 550 mm is prepared. An initial consolidation pressure of 10 kPa was given for 7 days, and further it was increased to 40 kPa for next 7 days. Total settlement of 100 mm is observed after 15 days which comprises of 1D consolidation settlement and expulsion of air voids. After the preparation of kaolin sample, it was covered with a layer of 30 mm of wax so that the moisture content of soil is retained and it can be stored for further experiments. Further, the average water content, average vane shear strength, and shear wave velocity measured on the top of the prepared sample are obtained as 68.56% (before consolidation) and 61.54 (after consolidation), 1.1 kPa (before) and 2.37 kPa (after) and 27 m/sec (before) and 30 m/sec (after), respectively.

2.3 Shake Table, Instrumentation, and Input Motion

A simplified motor operated crank-shaft mechanism based shake table with payload capacity of 9800 N (size: 1.0 m × 1.0 m) developed in the laboratory of NIT Agartala is used to carry out the seismic experiments. This shake table is capable to generate only sine and swept sine signals with maximum displacement of ±25 mm. A tachometer is used to generate the different frequencies of swept sinusoidal motion with a range of 1–10 Hz and amplitude of 0.02 g in the present study. Accelerometer sensors are used to measure the dynamic response of structure and soil. Figure 2 presents the schematic view of whole experimental setup in shake table.

3 Results and Discussion

3.1 Lengthening of Fundamental Period Due to SSI

Figure 3i, ii presents the acceleration response in frequency domain for T_{fixed} of 0.3 and 0.7 s supported by a 3 × 3 pile group foundation embedded in soft clay. Real-time acceleration response recorded at superstructure mass under both SSI and fixed base condition, pile cap, and pile head are presented herein. It is observed

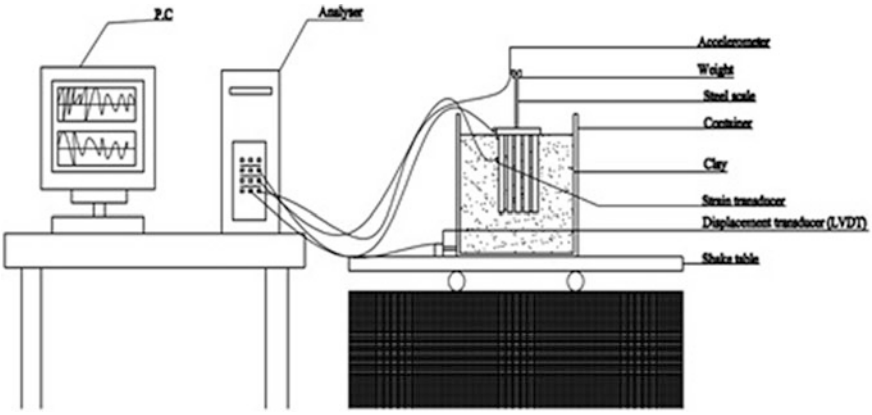

Fig. 2 Schematic view of the experimental setup

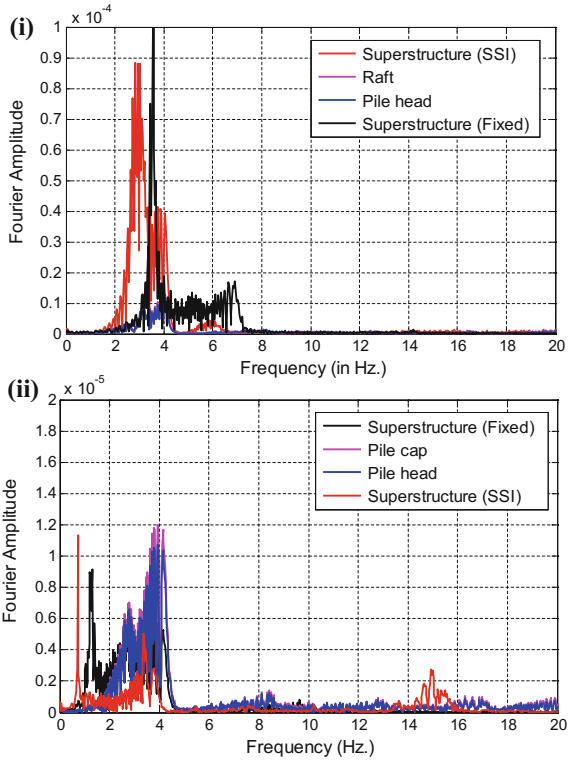

Fig. 3 Acceleration signals in frequency domain for **i** T_{fixed} = 0.3 s and **ii** 0.7 s with 3 × 3 pile group

from the figures that the percentage lengthening of superstructure having T_{fixed} = 0.3 and 0.7 s is calculated in order of 10 and 25% (approx.), respectively, which is marginal. The reason for marginal lengthening may be due to higher lateral

stiffness of in order of 35,480 N/m attributed by the model 3 × 3 pile group used in present study as compared to column stiffness of 83 N/m. In fact, a significant increase in period for stiffer period of structure in general was reported in many studies by the author along with other co-researchers. However, the present study indicates an opposite trend in case of T_{fixed} = 0.3 s. The relative stiffness of column to pile foundation in this case is found to be lesser which seems to be an important parameter may govern the SSI effect on dynamic response of structure supported by pile foundation even in very soft to soft clayey layer. This issue may be further investigated in detail which may help in resolving design issues related to SSI problem.

3.2 *Dynamic Response in Model Soil-Pile Foundation-Structure System*

Acceleration response recorded at different level of structure having T_{fixed} = 0.3 and 0.7 s for both SSI and fixed base condition is presented in Fig. 4i, ii, respectively.

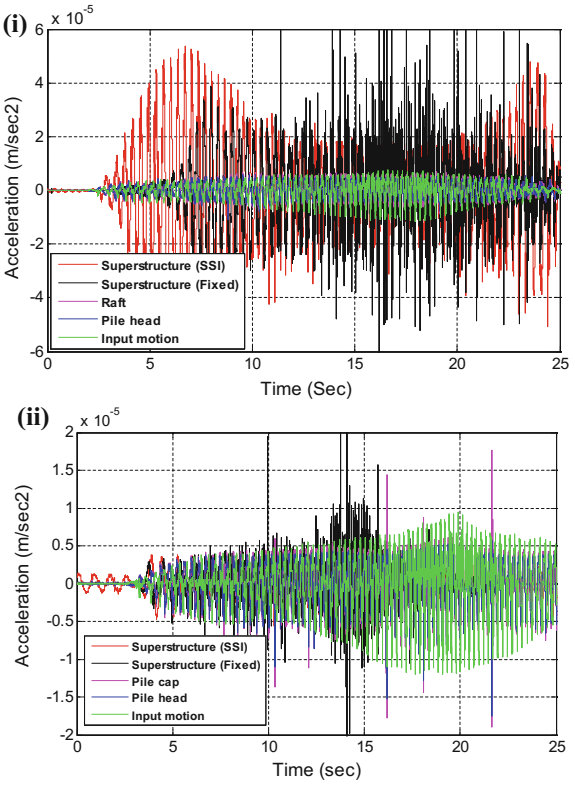

Fig. 4 Real-time acceleration for **i** T_{fixed} = 0.3 s and **ii** 0.7 s with 3 × 3 pile group

Acceleration response gives an approximate idea of elastic force transmitted to different elements of structure. It is observed in Fig. 4i that acceleration response is amplified significantly in superstructure having $T_{\text{fixed}} = 0.3$ s for both SSI and fixed base condition, while the response in pile cap and head are found to be subdued. On the other hand, a subdued response is observed in superstructure having relatively longer period, i.e., $T_{\text{fixed}} = 0.7$ s, which may be due to the beneficial effect of SSI. However, in case of $T_{\text{fixed}} = 0.7$ s structure, the response in pile cap and head is found to be considerably higher than superstructure response as observed in Fig. 4i, ii. Hence, this limited study indicates that the longer period structure supported by pile foundation may attract higher shear force at pile head due to such complex soil-pile foundation-structure interaction which needed to be confirmed by a detailed study. This may be due to higher mode effect.

4 Conclusions

Summarily, the present study is a limited effort to assess the effect of dynamic interaction of soil-pile foundation-structure on seismic response of structure. It may be concluded from this limited study that rigid pile group exhibiting higher foundation stiffness or lower ratio of lateral stiffness of superstructure and pile foundation may significantly reduce period lengthening of the stiffer structure embedded in very soft clayey layer which may be equivalent to fixed base condition. This implies that structure supported by conservatively designed pile group in soft soil may be designed as fixed base condition under seismic loading rather neglecting SPSI. Further, this limited study indicates that transfer of shear force at pile head may be a function of ratio of period of superstructure and pile group which may be studied in detail for the different soil conditions and frequency of motion.

References

Bhattacharya, S., Tokimatsu, K., Goda, K., Sarkar, R., Shadlou, M., & Rouholamin, M. (2014). Collapse of Showa Bridge during 1964 Niigata earthquake: A quantitative reappraisal on the failure mechanisms. *Soil Dynamics and Earthquake Engineering, 65,* 55–71.

Boominathan, A., & Ayothiraman, R., (2005). Dynamic behaviour of laterally loaded model piles in clay. *ICE*, GE-4, 207–215.

Boulanger, R. W., Curras, C. J., Kutter, B. L., Wilson, D. W., & Abghari, A. (1999). Seismic soil-pile-structure interaction experiments and analyses. *Journal of Geotechnical and Geoenvironmental Engineering, 125*(9), 750–759.

Chau, K. T., Shen, C. Y., & Guo, X. (2009). Nonlinear seismic soil–pile–structure interactions: shaking table tests and FEM analyses. *Soil Dynamics and Earthquake Engineering, 29*(2), 300–310.

IS: 2911 (Part 1/Sec 4). (2010). *Indian standard code of practice for design and construction of pile foundation: Part 1: Concrete piles, section 4 bored precast concrete piles*. Bureau of Indian Standards, New Delhi, India.

Jeremic, B., Kunnath, S., & Xiong, F. (2004). Influence of soil-foundation-structure interaction on seismic response of the I-880 viaduct. *Engineering Structure, 26*(3), 391–402.

Lombardi, D., & Bhattacharya, S. (2013). Modal analysis of pile-supported structures during seismic liquefaction. *Earthquake Engineering and Structural Dynamics*. https://doi.org/10.1002/eqe.2336.

Meymand, P. J. (1998). *Shaking table scale model tests of nonlinear soil-pile-superstructure interaction in soft clay* (Doctoral dissertation, University of California, Berkeley).

Saha, R., Dutta, S. C., & Haldar, S. (2015). Influence of dynamic soil-pile raft-structure interaction: An experimental approach. *Earthquake Engineering and Engineering Vibration, 14*(4), 625–645.

Tokimatsu, K., Suzuki, K., & Sato, M. (2005). Effects of inertial and kinematic interaction on seismic behaviour of pile with embedded foundation. *Soil Dynamics and Earthquake Engineering, 25,* 753–762.

Part II
Analytical and Numerical Modeling in Geomechanics

Numerical Modelling of Mechanised Tunnelling in Clay

K. Vineetha, A. Boominathan and Subhadeep Banerjee

Abstract Mechanised tunnelling method using Tunnel Boring Machine (TBM) is widely used in urban settings due to the lesser construction duration and minimal surface disruption. However, field-monitoring studies report ground movements and damages to the buildings under which the TBM ploughed through. Hence, it is important to attain a detailed understanding of the TBM–ground interaction before the initiation of any new tunnel construction activity so as to predict the variation in the in situ ground conditions, avoid any damage to the structures adjacent to the tunnel alignment and optimise the TBM performance. This paper comprises a brief review of various studies on the simulation of tunnelling in soft soils followed by the numerical back-analysis of a typical field-monitoring study involving underground tunnelling in clay using the general purpose finite element suite, ABAQUS. A circular tunnel with 8.16 m diameter, running straight and embedded in clay with 19.0 m overburden is considered. The deformation and pore pressure response is monitored along the ground surface and near the tunnel crown, respectively, for each excavation stage of 1.5 m. The numerical model clearly demonstrated the progressive changes in these parameters as the excavation advances.

Keywords Mechanised tunnelling · TBM · Finite element · ABAQUS
Ground movement

K. Vineetha (✉) · A. Boominathan · S. Banerjee
Department of Civil Engineering, Indian Institute
of Technology Madras, Chennai 600036, India
e-mail: vineetha.kombiyil22@gmail.com

A. Boominathan
e-mail: boomi@iitm.ac.in

S. Banerjee
e-mail: subhadeep@iitm.ac.in

B. Adimoolam and S. Banerjee (eds.), *Soil Dynamics and Earthquake Geotechnical Engineering*, Lecture Notes in Civil Engineering 15,
https://doi.org/10.1007/978-981-13-0562-7_18

1 Introduction and Background

The increasing demand for transportation facilities in the urban set-ups has urged the need for extensive underground networks. Mechanised tunnelling techniques involving Tunnel Boring Machine (TBM) are widely used for building up these networks due to the lesser construction duration and minimal surface disruption. Conversely, several field-monitoring studies (Chen et al. 2011; Standing and Selemetas 2013; Houhou et al. 2016) report ground disturbance and structural damage induced by the mechanised tunnelling methods. Hence, it is important to understand the ground–TBM interaction in order to predict the variation in the in situ ground conditions, avoid structural damage and control the TBM operational parameters to minimise the ground disturbances.

Majority of the researches on underground tunnelling in soft grounds are more focused on the conventional open-face tunnelling concept (Mair et al. 1993; Addenbrooke and Potts 2001; Ng and Lee 2005; Marshall et al. 2012; Pinto and Whittle 2014). Kasper and Meschke (2004), Lambrughi et al. (2012), Comodromos et al. (2014), Do et al. (2014) and Zheng et al. (2015) are a few studies discussing the ground deformation and stress transfer mechanism during closed-face tunnelling, which is the most commonly used tunnelling concept nowadays. It was noted that these studies involve essentially numerical techniques like finite difference and finite element methods due to their flexibility in accommodating the TBM as well as ground variables compared to the experimental and analytical approaches. However, attempts of rigorous modelling by incorporating the different TBM components like cutter-head torque, face pressure and grout pressure are still evolving. This research paper describes the numerical modelling procedure for mechanised tunnelling through stiff clay by appropriately accounting for all the TBM components. The results are then compared with an actual field-monitoring data in order to demonstrate the efficiency of the numerical model to predict the ground responses as the tunnel advances.

2 Development of the Computational Domain

In order to investigate the tunnelling-induced ground responses, a full three-dimensional model with circular twin-tunnel configuration was developed using the general purpose finite element suite, ABAQUS. Details of tunnelling and site conditions were referred from Standing and Selemetas (2013). The tunnels are of 8.16 m diameter, running straight with 16.0 m centre-to-centre distance and embedded in clay at a depth of 19.0 m. Figure 1 shows the cross section of the twin-tunnel alignment and the site stratigraphy up to a depth of 35.0 m below the ground surface.

The dimensions of the computational domain were chosen to be $H + 12\ D$ along the X-axis (across the direction of tunnelling), $H + 15\ D$ along the Y-axis (along the

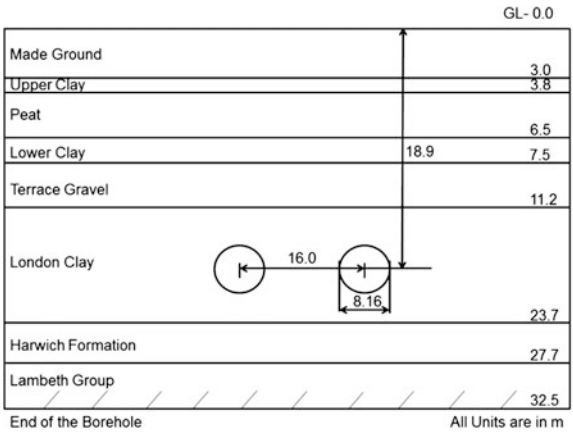

Fig. 1 Cross section of the twin-tunnel alignment

direction of tunnelling) and $H + 6\ D$ along the Z-axis, where H is the height of the overburden with respect to the tunnel axis and D is the tunnel diameter.

2.1 Finite Element Mesh

Figure 2 shows the 3D finite element mesh for the underground tunnel model considered in this study.

It consists of a heterogeneous soil section with eight distinct layers, TBM shield, lining and grout components. C3D8RP (eight-noded linear brick element with trilinear displacement, pore pressure and reduced integration scheme) was used to discretise soil and grout sections, whereas S4R (four-noded conventional stress/

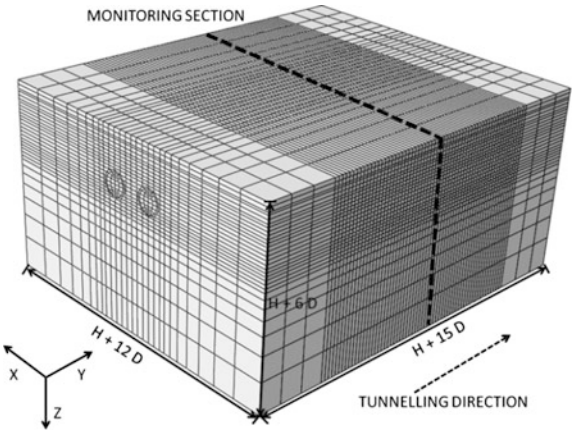

Fig. 2 Three-dimensional finite element mesh for the underground tunnel model considered in this study

displacement shell element with reduced integration scheme) was used for the TBM shield and tunnel lining.

Translations in *X*- and *Y*-directions were constrained along the vertical boundaries of the soil domain in *YZ*-plane and *XZ*-plane, respectively. Translations in all directions were constrained along the bottom boundary of the model. All the three rotational degrees of freedom were constrained for the TBM shield and lining.

2.2 Materials and Constitutive Relations

Soil properties used in the analysis are shown in Table 1. Groundwater table is assumed at the ground level. TBM shield, grout and tunnel lining material parameters used in the analysis are presented in Table 2.

Drucker–Prager constitutive relation with a cap is used to model the undrained behaviour of clay deposits. The addition of a cap yield surface helps to control volume dilatancy when the material yields in shear. Drucker–Prager constitutive relation without a cap is used to model the terrace gravel. The friction angle is 39° for the terrace gravel layer. Shield, lining and grout are modelled as simple linear elastic materials with an assumption that elastic strains developed in the material are less than 5%.

Table 1 Soil parameters

Material	Depth (m)	γ (kN/m^3)	E_u (MPa)	v	e_0	c_u (kPa)
Made ground	0–3.0	18	3	0.49	1.08	20
Upper clay	3.0–3.8	15	0.9	0.49	8.1	20
Peat	3.8–6.5	15	0.45	0.49	9	20
Lower clay	6.5–7.5	15	0.9	0.49	1.62	20
Terrace gravel	7.5–11.2	20	24	0.2	0.79	–
London clay	11.2–23.7	19	54	0.49	0.68	60 + 3z^a
Harwich formation	23.7–27.7	20	60	0.49	0.68	97.5 + 3z^a
Lambeth group	27.7–32.5	21	70	0.49	0.68	109.5 + 3z^a

[a]z = depth below top of London clay

Table 2 TBM shield, grout and tunnel lining material parameters

Material	Outer diameter (m)	Thickness (m)	γ (kN/m^3)	E (GPa)	v
Shield	8.12	0.1	80	1500	0.13
Grout	8.12	0.155	20	0.5	0.4
Lining	7.81	0.35	25	26.3	0.2

Table 3 Loads considered in the mechanised tunnelling simulation procedure

Load type	Magnitude[a]	Region of application
Cutter-head torque	1.12 MN m	Excavation face at every 1.5 m interval
Face pressure	2.0 bar	Excavation face at every 1.5 m interval
Traction from shield skin	5.54 MN	Excavated soil surface in contact with the shield
Tail grout pressure	1.6 bar	Excavated soil surface after shield removal

[a]Magnitudes are taken from Standing and Selemetas (2013)

3 Modelling Procedure for Mechanised Tunnelling

The in situ stress conditions were initially established with the introduction of gravity load in the soil domain. To eliminate boundary effects, initially tunnel is excavated 25.0 m away from the front boundary in the *X*–*Z* plane. Loads/pressures are applied as summarised in Table 3. Tunnel is excavated for a length of 1.5 m, equivalent to one lining ring width. The step time period is 3.9 h which is equivalent to the rate of advance of the TBM (0.375 m/h). A coupled pore fluid diffusion and stress analysis offered by ABAQUS/Standard (ABAQUS 2012) was carried out. Accordingly, the porous medium is modelled as a multiphase material considering the presence of two fluids, i.e. wetting liquid and gas. The finite element mesh is attached to the solid phase allowing the fluid flow through this mesh. An effective stress principle is used to describe the porous medium behaviour.

4 Results and Discussion

Ground response discussed in this section includes vertical displacement and pore pressure variation at selected locations, monitored for each excavation stage of 1.5 m during the excavation of the left tunnel. Results from the finite element study are compared with the field-monitoring data reported in Standing and Selemetas (2013). Figure 3 shows the vertical displacement profile on the ground surface along the monitoring section against the distance of the TBM face from the monitoring section as the tunnel advances. The coordinates $(x, y, z) = (0, 0, 0)$ correspond to the location on the ground surface above the centreline of the left tunnel lying in the monitoring section. Both the field data and finite element analysis results show an initial heave (<1 mm) as the TBM approaches the monitoring section with the distance of face at about $y = -20.0$ m. This is followed by a progressive settlement of about 3 mm in the field study and about 6 mm in the numerical study.

Figure 4 shows the peak pore pressure responses obtained from the finite element study, during the withdrawal of tail grout pressure and installation of the tunnel lining. Excess pore water pressures close to 100 kPa was recorded in both the field as well as finite element study as the TBM face approaches the monitoring

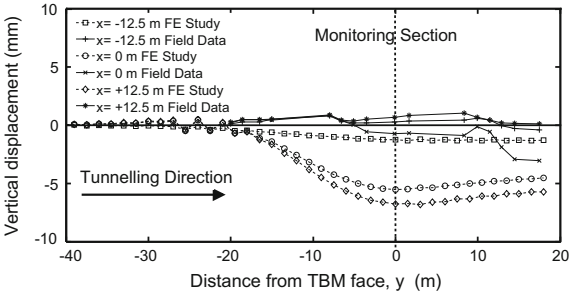

Fig. 3 Vertical displacement at selected locations during the tunnel advancement plotted against the distance of the TBM face from the monitoring section

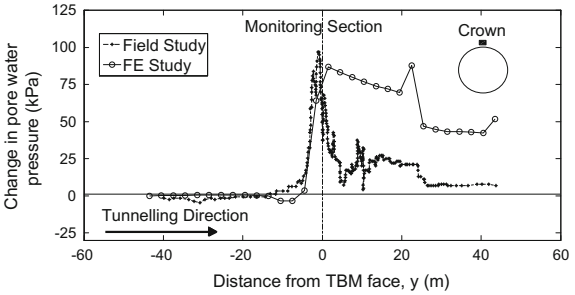

Fig. 4 Pore water pressure variation near the tunnel crown during the tunnel advancement plotted against the distance of the TBM face from the monitoring section

section. This can be attributed to the sudden settlement of soil above the tunnel crown due to the withdrawal of shield and installation of lining together with the fresh grout. As the tunnel advances beyond the monitoring section, it was observed that the pore pressure reduce gradually which can be attributed to the stress release above the tunnel due to grout hardening and transfer of overburden effectively to the tunnel lining.

The finite element study overestimates the pore water pressure variation beyond the monitoring section which might be due to the undrained analysis type. The adoption of tail grout pressure values gauged directly from the pump would have also influenced the pore pressure response. The values gauged from the pump will not be actually exerted in the field due to the different losses which include the grouting pipe and outlet friction resistance. However, the dissipation pattern of pore water pressure beyond the monitoring section in the finite element study is similar to the field study.

5 Conclusion

A three-dimensional finite element model is developed for simulating the mechanised shield tunnelling procedure in soft ground incorporating all the relevant components like torque, face pressure, shield skin friction, tail grout pressure, lining

installation, backup trailer weight, grout hardening and excavation. Profiles were plotted demonstrating the ground responses in terms of deformation and pore pressure variation as the tunnelling progresses. The results were found to be in good agreement with the actual field data. The pore pressure variation from the developed model highlights the significance of properly accounting for the relevant TBM components which are usually ignored in the numerical simulation of mechanised tunnel construction problems. Modelling methodology proposed in this study is relevant in the estimation of ground behaviour for situations with similar ground conditions and excavation procedure.

References

ABAQUS. (2012). Inc. ABAQUS user's manual, Version 6.12. Pawtucket, R.I.

Addenbrooke, T. I., & Potts, D. M. (2001). Twin tunnel interaction: Surface and subsurface effects. *The International Journal of Geomechanics*, *1*(2), 249–271.

Chen, R. P., Zhu, J., Liu, W., & Tang, X. W. (2011). Ground movement induced by parallel EPB tunnels in silty soils. *Tunnelling and Underground Space Technology, 26*(1), 163–171.

Comodromos, E. M., Papadopoulou, M. C., & Konstantinidis, G. K. (2014). Numerical assessment of subsidence and adjacent building movements induced by TBM-EPB tunneling. *Journal of Geotechnical and Geoenvironmental Engineering (ASCE)*, *140*(11), 0401406-1-12.

Do, N., Dias, D., Oreste, P., & Djeran-Maigre, I. (2014). Three-dimensional numerical simulation of a mechanized twin tunnels in soft ground. *Tunnelling and Underground Space Technology, 42,* 40–51.

Houhou, M. N., Emeriault, F., & Vanoudheusden, E. (2016). Three-dimensional back-analysis of an instrumented shallow tunnel excavated by a conventional method. *Geotechnical and Geological Engineering, 34*, 1101–1117.

Kasper, T., & Meschke, G. (2004). A 3D finite element simulation model for TBM tunnelling in soft ground. *International Journal for Numerical and Analytical Methods in Geomechanics, 28*, 1441–1460.

Lambrughi, A., Rodriguez, L. M., & Castellanza, R. (2012). Development and validation of a 3D numerical model for TBM–EPB mechanised excavations. *Computers and Geotechnics, 40*, 97–113.

Mair, R. J., Taylor, R. N., & Bracegirdle, A. (1993). Subsurface settlement profiles above tunnels in clays. *Geotechnique, 43*(2), 315–320.

Marshall, A. M., Farrell, R., Klar, A., & Mair, R. (2012). Tunnels in sands: the effect of size, depth and volume loss on greenfield displacements. *Geotechnique, 62*(5), 385–399.

Ng, C. W. W., & Lee, G. (2005). Three-dimensional ground settlements and stress-transfer mechanisms due to open-face tunnelling. *Canadian Geotechnical Journal, 42*, 1015–1029.

Pinto, F., & Whittle, A. J. (2014). Ground movements due to shallow tunnels in soft ground. I: Analytical solutions. *Journal of Geotechnical and Geoenvironmental Engineering (ASCE), 140*(4), 04013040-1-17.

Standing, J. R., & Selemetas, D. (2013). Greenfield ground response to EPBM tunnelling in London clay. *Geotechnique, 63*(12), 989–1007.

Zheng, G., Lu, P., & Diao, Y. (2015). Advance speed-based parametric study of greenfield deformation induced by EPBM tunnelling in soft ground. *Computers and Geotechnics, 65*, 220–232.

Numerical Analysis of Stone Columns in Soft Clay with Geotextile Encasement and Lime Stabilization

K. S. Amith and V. Ramana Murthy

Abstract Stone columns have been widely accepted as a method of foundation to support large area loads over soft clay beds. Laboratory studies were carried out in test tanks to study the behavior of stone columns in soft clay with different initial consistencies. The study was conducted without and with geotextile encasement, and also the influence of pretreatment of soft clay with lime on the behavior of stone columns was investigated. This paper presents the numerical analysis of the above stone column systems for load-settlement behavior and compares with laboratory test results. This analysis revealed that the numerical analysis using PLAXIS 3D software is useful to predict the behavior of stone columns under different field conditions.

Keywords Stone columns · Soft clay · Geotextile encasement
Lime stabilization · PLAXIS 3D

1 Introduction

Soft clays are present in several world nations, and these deposits are characterized by high natural water content, low shear strength and high compressibility (Murugesan and Rajagopal 2010). Construction of infrastructure facilities in such deposits is a challenge to civil engineers. Deep foundations have been widely used in such deposits despite heavy investment (Priebe 1995; Wood et al. 2000). Several ground improvement techniques such as preloading with vertical drains, electro-osmotic drainage, and stone columns were promulgated to improve these soil deposits. Several project sites are immensely benefitted by these techniques; especially to support area loads such as embankments and even to support building

K. S. Amith (✉) · V. Ramana Murthy
NIT-Warangal, Warangal, India
e-mail: amith.kadaba@gmail.com

V. Ramana Murthy
e-mail: vrm_nitw@yahoo.com

B. Adimoolam and S. Banerjee (eds.), *Soil Dynamics and Earthquake Geotechnical Engineering*, Lecture Notes in Civil Engineering 15,
https://doi.org/10.1007/978-981-13-0562-7_19

foundations (Ambily and Gandhi 2007). Stone columns not only improve the load carrying capacity of ground but also promote consolidation. However, in case of very low strength (C_u < 25 kPa) soils, difficulty in installation of stone columns was reported (Chummar 2000). The load-settlement behavior of stone columns was studied previously in the test tanks without and with geotextile encasement. Also, the influence of pretreatment of soft clay with lime on stone column behavior was studied. The present study is an effort to model the above systems in PLAXIS 3D software to predict the load-settlement behavior in relation to the laboratory test results.

2 Materials and Methodology

Analysis was carried out using PLAXIS 3D software to compare the load-settlement behavior of stone columns with different test conditions considering Mohr–Coulomb model. The dimensions of tanks used were 300 mm diameter and 300 mm height for installing single stone column and 500 mm × 500 mm × 500 mm for group of stone columns. The initial consistencies of clay bed adopted were 25, 40, and 55%. A stone column of 50 mm diameter and 280 mm height was made at the center of the clay bed with the help of a PVC pipe at a density of 1.6 g/cc corresponding to 70% relative density, and at the top of it, a leveling course of 20-mm-thick sand is placed and loaded with a plate having diameter twice the diameter of stone column. The tensile strength of geotextile (PD381) is 18 kN/m, which is used in the study. The clay properties are as follows: gravel = 4%, sand = 26%, fines = 70%, liquid limit = 56%, and plastic limit = 18%. Pressure-settlement plots were drawn, and the ultimate capacity is obtained by drawing the tangents to the initial and final straight line portions. For the formation of group three-stone columns in the test tank, three-stone columns were placed at the spacing of two times the diameter of the stone column and the remaining process is similar to that for single stone column. The input parameters for modeling the stone columns in soft clay are given in Tables 1 and 2. The bulging patterns of stone columns are shown in Figs. 1 and 2 without and with encasement.

Table 1 Input parameters for modeling stone columns in soft clay

Materials	Test consistencies (%)	W (%)	E (kPa)	Poissons ratio μ	C_u (kPa)	Φ (°)	Ψ (°)	Υ_{dry} (kN/m^3)	Υ_{sat} (kN/m^3)
Clay	25	46.5	1400	0.47	2.8			11.54	16.87
	40	38	2750	0.45	5.5			12.37	17.42
	55	35.1	4000	0.43	8			13.33	18.01
Stone aggregate			55,000	0.3		38	10	16.62	
Sand			20,000	0.3		30	4	15.6	

Table 2 Input parameters for modeling stone columns in lime stabilized soft clay

Materials	Test consistencies (%)	W (%)	E (kPa)	Poissons ratio μ	C_u (kPa)	Φ (°)	Ψ (deg)	Υ_{dry} (kN/m^3)	Υ_{sat} (kN/m^3)
Clay	25	28	90,000	0.3	180			14.7	18.85
	40	26	100,000	0.3	200			15.18	19.15
	55	23.8	140,000	0.3	280			15.7	20.68
Stone aggregate			55,000	0.3		38	10	16.62	
Sand			20,000	0.3		30	4	15.6	

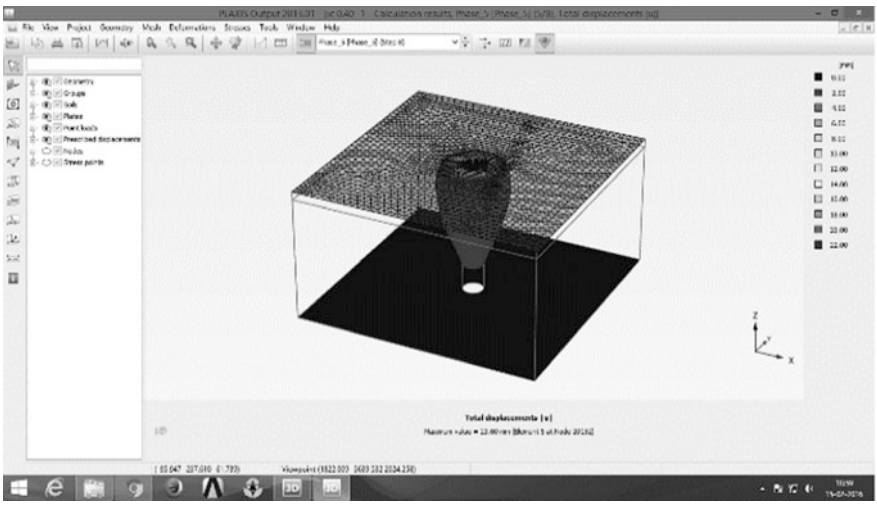

Fig. 1 Stone column in soft clay without geotextile encasement

3 Results and Discussions

3.1 Pressure-Settlement Behavior of Individual Stone Columns at Different Consistencies of Clay

Figure 3 shows the load-settlement plot for single stone column without encasement. It can be inferred from this figure that at I_c = 0.25, the ultimate load capacity is 20 kPa with the corresponding settlement of 7 mm. Similarly at I_c = 0.40, the ultimate load capacity is 28 kPa with corresponding settlement of 6 mm. At I_c = 0.55, the load carrying capacity is 55 kPa with corresponding settlement of 4 mm. These patterns indicate that the load capacity of stone columns increases with increasing consistency of clay bed. The relative variation of the

Fig. 2 Stone column in soft clay with geotextile encasement

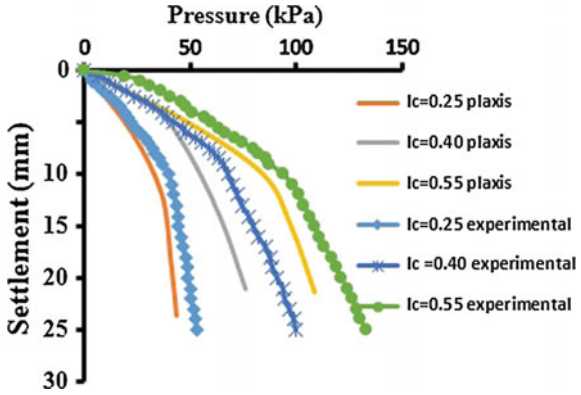

Fig. 3 Pressure-settlement plots of individual stone column at different consistencies of clay

load-settlement plots at different initial consistencies is also shown in Fig. 3 for ready comparison of numerical analysis and laboratory test results.

The load-settlement plots for individual encased stone column obtained through numerical analysis are presented in Fig. 4. It can be observed from this figure that the ultimate load carrying capacity of encased stone column is about 60 kPa at I_c = 0.25 with the corresponding settlement of 6 mm. At I_c = 0.40, the ultimate load carrying capacity is 75 kPa with corresponding settlement of 4 mm. However, at I_c = 0.55 the ultimate load capacity is 102 kPa with corresponding settlement of 3 mm. This can be attributed to the fact that as confinement increases, the load carrying capacity also increases. The relative variation of the load-settlement plots

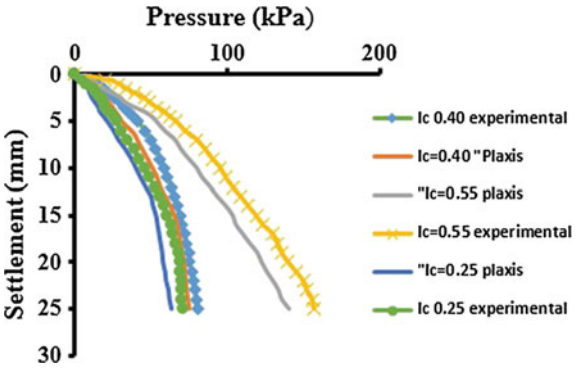

Fig. 4 Pressure-settlement plots of individual encased stone column at different consistencies of clay

at different consistencies is also shown in Fig. 4 for ready comparison of numerical analysis and laboratory test results.

3.2 *Pressure-Settlement Behavior of Three Group of Stone Columns at Different Consistencies of Clay*

Figures 5 and 6 show the pressure-settlement behavior of group of stone columns without and with encasement, respectively. From Fig. 5, it can be observed that at I_c = 0.25, the ultimate load is 36 kPa; at I_c = 0.40, the ultimate load carrying capacity is 55 kPa, and at I_c = 0.55, the ultimate load capacity is increased to 92 kPa. In all these cases, the settlement varied from 4 to 7 mm. Similarly, for encased stone column groups, the ultimate capacity is in the range of 85–175 kPa with the corresponding settlements of 6–8 mm. From these observations, it is revealed that the group capacity is altogether different from the mere multiplication of single column capacity with the number of columns in a group. This behavior could be attributed to the mutual confining effect in groups compared to single stone column.

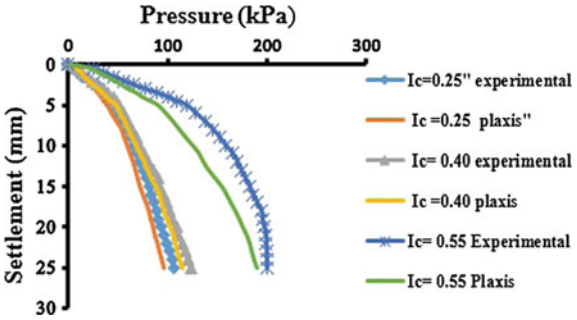

Fig. 5 Pressure-settlement plots of three-stone column groups at different consistencies of clay

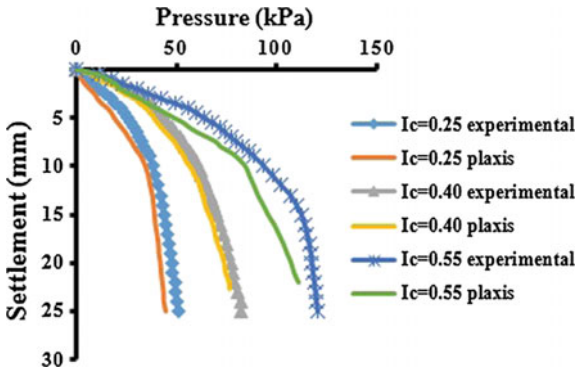

Fig. 6 Pressure-settlement plots for group of encased stone column at different consistencies of clay

3.3 *Pressure-Settlement Behavior of Stone Column Groups in Lime Stabilized Soft Clay at Different Initial Consistencies*

Figures 7, 8, and 9 show the load-settlement behavior of group of three-stone columns installed in 3% lime stabilized soft clay. It can be observed that at I_c = 0.25, the ultimate load carrying capacity obtained from numerical analysis is about 1400 kPa, whereas the laboratory value is 1500 kPa. At I_c = 0.40, numerical analysis showed that the ultimate load carrying capacity is 1000 kPa and the laboratory value is about 1200 kPa. Also at I_c = 0.55, the ultimate load carrying capacity obtained from numerical analysis is around 700 kPa, whereas the value is 750 kPa from laboratory testing. For all these cases, the settlement corresponding to ultimate loads varied from 5 to 9 mm. In lime stabilized clay, similar trends are observed for individual stone column also. The decrease in degree of improvement in lime stabilized clay with increasing consistency could be attributed to transition of failure from bulging to vertical displacement of stone column in lime stabilized

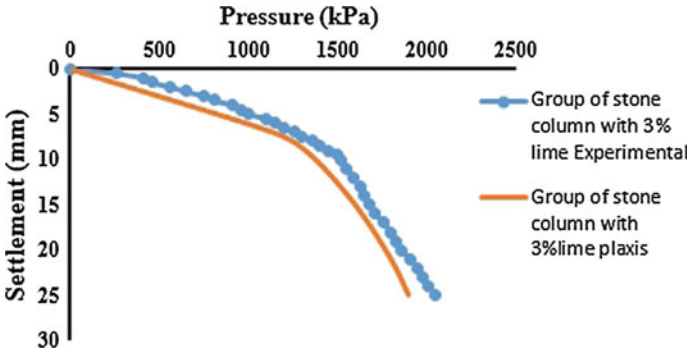

Fig. 7 Pressure-settlement plot for three-stone column group in soft clay stabilized with 3% lime at I_c = 0.25

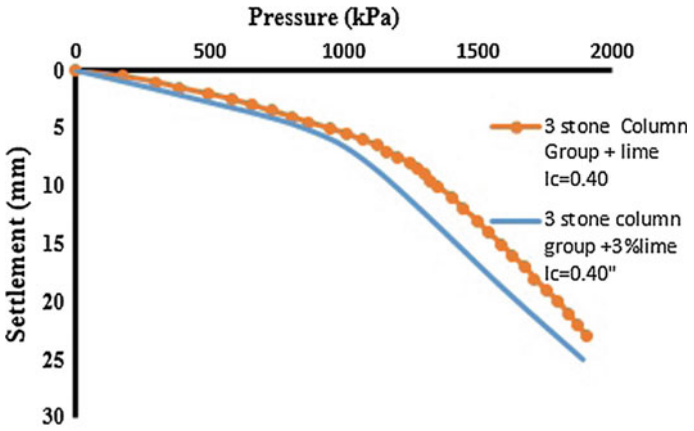

Fig. 8 Pressure-settlement plot for three-stone column group in soft clay stabilized with 3% lime at I_c = 0.40

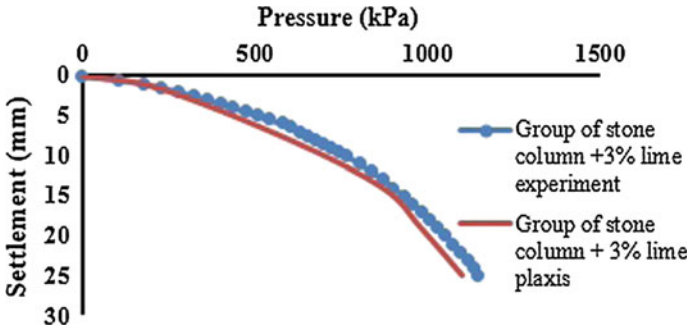

Fig. 9 Pressure-settlement plot for three-stone column group in soft clay stabilized with 3% lime at I_c = 0.55

clay bed. From the above observations, it is understood that the behavior of stone columns under different field conditions can be predicted using PLAXIS 3D software.

4 Conclusions

The following conclusions are drawn based on numerical investigations carried out on stone columns installed in soft clay without and with lime stabilization and geotextile encasement.

The ultimate load capacity of stone columns is increased with increasing undrained strength Cu of soft clay.

The load carrying capacity of geotextile-encased stone column is enhanced by almost 3 times that without encasement. The group capacity is not the multiplicative value of a single stone column capacity at any consistency with or without geotextile encasement.

The bulging of stone columns is reduced both with geotextile encasement and lime stabilization.

The degree of improvement in load carrying capacity of stone columns with lime stabilization is lesser in case of clay with high initial stiffness.

From PLAXIS 3D analysis, it is found that the load carrying capacity of stone columns is significantly increasing with increasing Young's modulus. This is true with increasing consistency of clay.

The load-settlement plots obtained from laboratory testing compared well with numerical method of finite element analysis for ordinary stone columns, geotextile-encased stone columns, and stone column in lime stabilized clay, indicating the potential use of PLAXIS 3D software to predict the behavior of stone columns in the field.

References

Ambily, A. P., & Gandhi, S. R. (2007). Behavior of stone columns based on experimental and FEM analysis. *Journal of Geotechnical and Geo Environmental Engineering, ASCE, 133*(4), 405–415.

Chummar, A. V. (2000). Ground improvement using stone columns: Problems encountered. In *Proceedings of GeoEng 2000* (pp. 19–24), Australia.

Murugesan, S., & Rajagopal, K. (2010). *Journal of Geotechnical and Geoenvironmental Engineering, 136*(1), 129–139.

Brinkgreve, R. B. J., Engin, E., & Swolfs, W. M. (2013). PLAXIS 3D 2013 user manual. Plaxis bv, Delft.

Priebe, H. J. (1995). The design of vibro replacement. *Ground Engineering, 28*(10), 31–37.

Wood, D. M., Hu, W., & Nash, F. T. (2000). Group effects in stone column foundations: Model tests. *Geotechnique, 50*(6), 689–698.

Stability Analysis of a Typical Sunderban Embankment During Diurnal Tidal Cycle

Kaustuv Bhattacharya, Gupinath Bhandari and Sibapriya Mukerjee

Abstract Earth embankments are utilized as protective structures along river, coastal banks and maybe thus exposed to steady or transient seepage induced by tides. In the Indian part of Sunderban region, the tidal head variation is 4–6 m in cycle time of 12 h. A model has been developed in FEM-based software, GeoStudio, to study the effect of transient seepage in such an embankment. The response to tidal head was found to be limited to a certain zone within the embankment. The cyclic pore water pressure distribution was seen to differ in various regions in this zone. Also, even though the cyclic FOS against stability was adequate, serviceability check indicates chances of failure near toe region.

Keywords Transient seepage · Unsaturated permeability · Sunderban embankment · Finite element method · Tidal cycle

1 Introduction

Earth embankments are used as efficient and economic forms of protective structures along rivers and coasts. These are exposed to hydrostatic and hydrodynamic forces as per location, topography, weather conditions, etc. The common hydrostatic element affecting the design life of such structure is seepage, which may be steady and/or transient in nature. Water retaining structures along rivers and coasts are exposed to tidal heads which may induce transient seepage, characterized by river water head which is a function of tidal cycle time. A single tidal cycle usually

K. Bhattacharya (✉) · G. Bhandari · S. Mukerjee
Department of Civil Engineering, Jadavpur University, Kolkata 700032, West Bengal, India
e-mail: kaustuv_poirot@yahoo.com

G. Bhandari
e-mail: g.bhandari.ju@gmail.com

S. Mukerjee
e-mail: sibapriya.mukherjee@gmail.com

B. Adimoolam and S. Banerjee (eds.), *Soil Dynamics and Earthquake Geotechnical Engineering*, Lecture Notes in Civil Engineering 15,
https://doi.org/10.1007/978-981-13-0562-7_20

consists of the phenomenon of rise-up, or ascent of river water from Low Tide Level (LTL) to High Tide Level (HTL), and further drawdown, or descent of the same from High Tide Level back to the Low Tide Level. The time period of rise-up and drawdown half cycles are termed as rise-up half cycle time and drawdown half cycle time, respectively.

2 Study Area

The Sunderban delta is formed at the confluence of the rivers Ganga, Brahmaputra and their distributaries. This region is shared by South 24 Pgs, West Bengal (India) and Khulna division (Bangladesh) with the latter having a share of about 60%. Network of creeks and channels divides the entire area into several small and large islands. The ground level of most of the islands is above the Low Tide Level (LTL) but below the High Tide Level (HTL); hence, there is requirement of embankments in order to protect the islands from tidal water inundation. The construction of these embankments (shown in Fig. 1) dates back to the eighteenth century, when human settlement started to flourish here, and is said to have been done mainly using locally available topsoil, which is predominantly silty clay/clayey silt. This study is based on the Indian part of Sunderban where the total length of existing earth embankments is approximately 3520 km. The water head difference due to diurnal tidal cycle is about 4–6 m, across various sites of the Sunderban. The time period for a single cycle is about 12 h, comprising 6 h of rise-up and drawdown half cycle time, respectively. Table 1 shows the soil properties from a bore-log in Patharpratima site.

Fig. 1 Typical Sunderban embankment at Sonakhali

Table 1 Soil properties from Patharpratima, West Bengal

Soil description and type	Grey clayey silt, CI
Volume compressibility, m_V (per kPa)	0.048
Bulk density (kN/m^3)	18.2
Saturated porosity (m^3/m^3)	0.465
D_{60} (mm)	0.034
Percentage of sand (%)	10
Percentage of silt (%)	62
Percentage of clay (%)	28
Liquid limit (%)	47
Saturated conductivity (K_{sat}) (m/s)	10^{-8}
Residual water content	0.18
Effective cohesion, c' (kN/m^2)	5
Effective angle of internal friction, Φ' (°)	25
Modulus of elasticity (with v = 0.3) (kPa)	2083

3 Numerical Analysis

A model was developed in the popular finite element-based software, GeoStudio. The soil properties were taken as per Table 1. The volumetric water content (VWC) function, shown in Fig. 2, has been developed as per Aubertin et al. (2003) using grain size distribution, liquid limit, porosity, coefficient of volume compressibility. The hydraulic conductivity function, shown in Fig. 3, has been estimated from the volumetric water content function using the Van Genuchten methodology (1980), with saturated permeability and residual water content as the input. The air entrant value and residual water content have been obtained from the volumetric water content curve. The landside groundwater table was taken at the existing ground level. The steady-state condition was established between the groundwater table and the Low Tide Level on the riverside. The tidal effect was simulated on the basis of hydraulic boundary conditions as a function of tidal cycle time. The difference between Low Tide Level and High Tide Level was taken as 4 m, and the full cycle time was taken as 12 h, consisting of 6 h each of rise-up and drawdown, respectively.

The finite element model with 489 nodes and 473 elements has been shown in Fig. 4. The shape of mesh was triangles and quadrilaterals with unstructured origin and individual element size of 0.5 m in the embankment and 1 m in other parts. A linear time stepping was applied for the transient stage analysis.

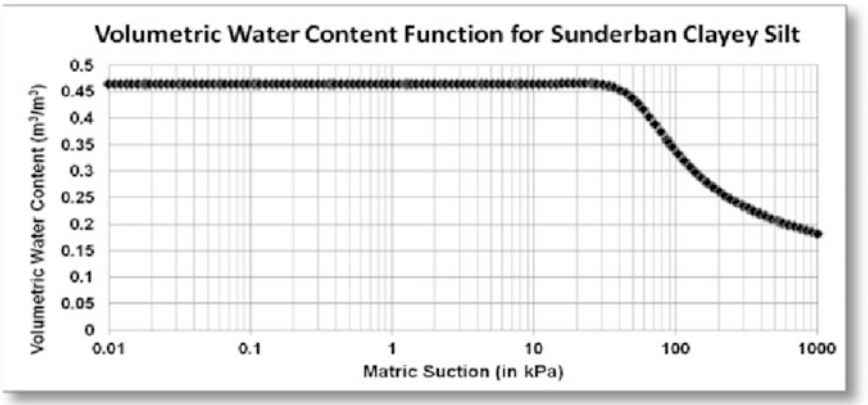

Fig. 2 VWC function for Sunderban clayey silt

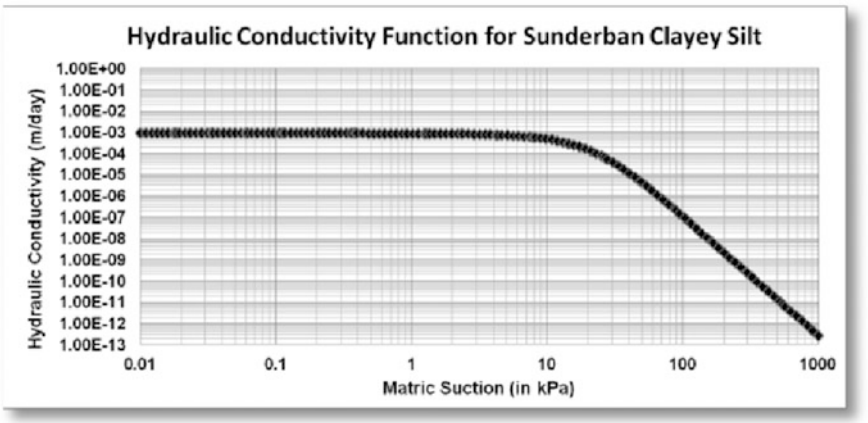

Fig. 3 Conductivity function for Sunderban clayey silt

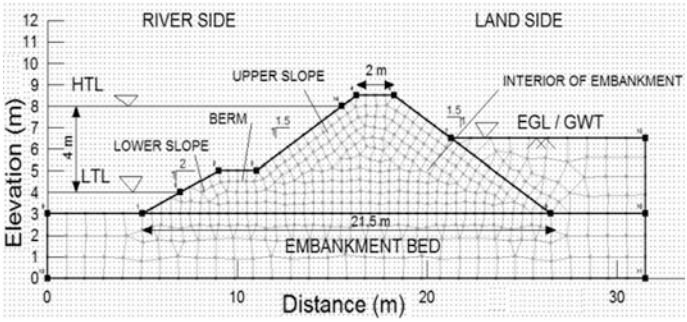

Fig. 4 FEM model of Embankment in GeoStudio

4 Results and Discussions

4.1 Dynamics of the Phreatic Surface

The dynamics of the phreatic surface during rise-up and drawdown of single tidal cycle has been shown in Figs. 5 and 6, respectively. It was observed that during rise-up (t = 1–6 h), the phreatic surface slowly developed along the lower slope, berm and upper slope, till High Tide Level at t = 6 h. The developed phreatic surface started to recede during drawdown phase (t = 6–12 h). However, at the end of a single tidal cycle, a cumulative effect in phreatic surface was seen as can be seen from Fig. 6, where the phreatic surface has moved up slightly encompassing more area above the berm region, compared to initial condition at t = 0 h.

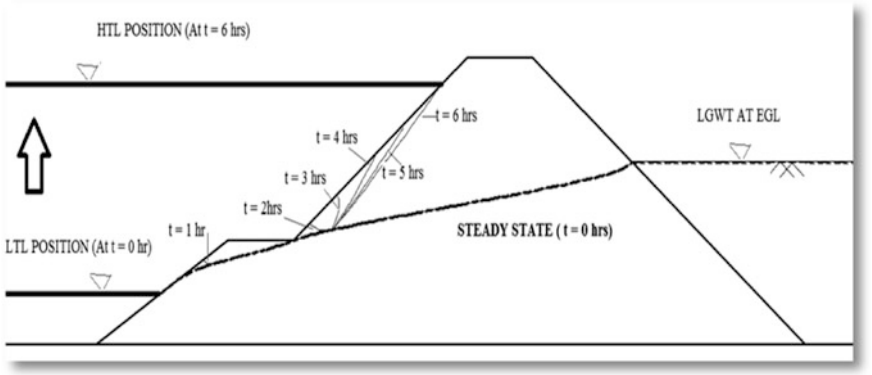

Fig. 5 Phreatic surface dynamics during rise-up

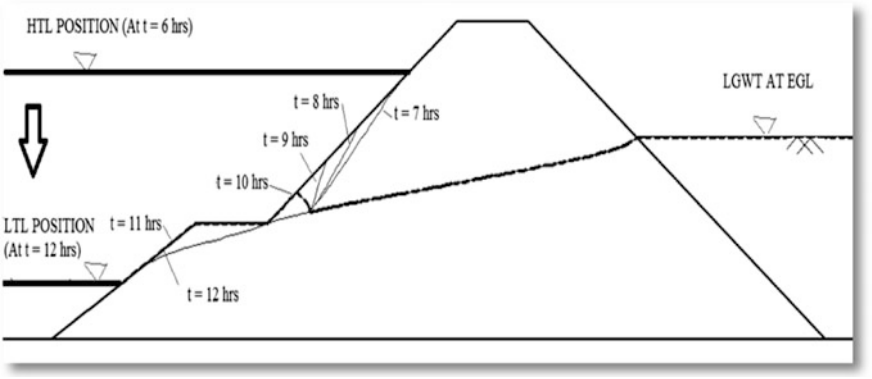

Fig. 6 Phreatic surface dynamics during drawdown

4.2 Distribution of Equipotential Contour

The equipotential total head contour due to transient seepage during a single tidal cycle has been shown in Figs. 7, 8, 9, 10 and 11. A zone is seen to develop along the river–embankment interface, through the rise-up stage. The equipotential total head is observed to slowly increase in this zone with rise-up half cycle time. This zone is termed as "Zone of Influence of Rise-up" (ZIR). During drawdown, this zone dissipates slowly till the end of a single tide cycle. However, cumulative effect is observed at the end of a single cycle (t = 12 h). It is seen that the zone has dissipated along lower slope; berm portion yet still persists in parts of the upper slope, as the river water prepares for the next tidal cycle. This indicates that during a single tidal cycle, the excess head induced due to transient seepage during rise-up does not fully dissipate at the end of drawdown stage, for certain regions within this zone. No change in total head induced during tidal cycle is observed in the interior part of the embankment which are regions outside the Zone of Influence of Rise-up.

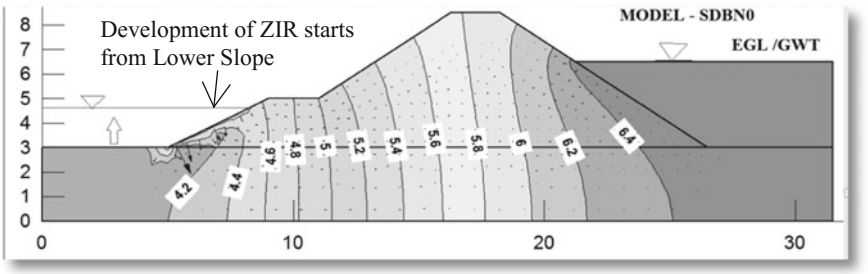

Fig. 7 Total head contour during rise-up, t = 1 h

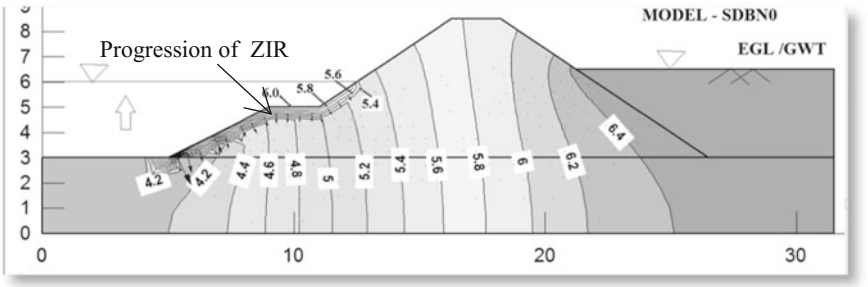

Fig. 8 Total head contour during rise-up, t = 3 h

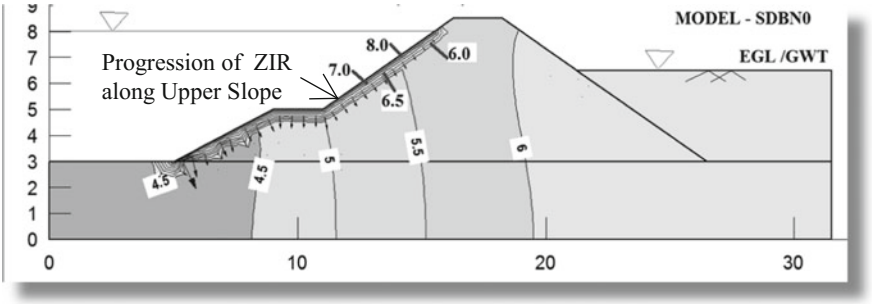

Fig. 9 Total head contour at HTL, t = 6 h

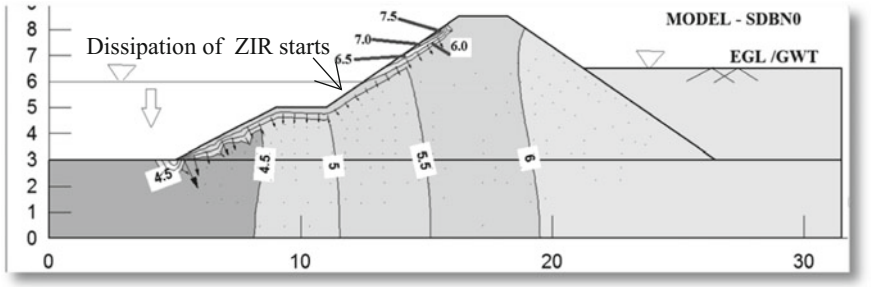

Fig. 10 Total head contour during drawdown, t = 9 h

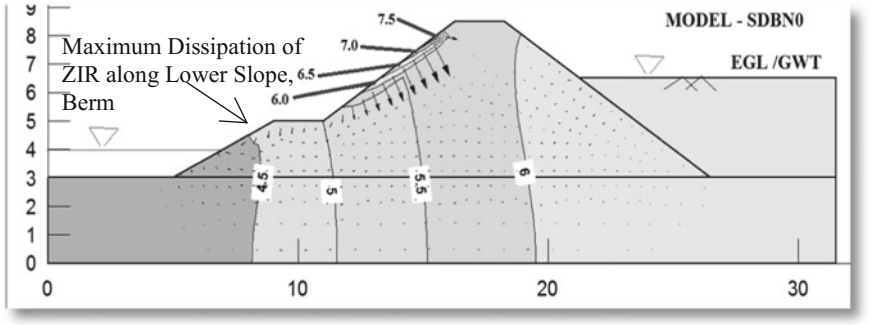

Fig. 11 Total head contour at end of one cycle, t = 12 h

4.3 *Pore Water Pressure Distribution for Various Zones Within the Embankment*

The excess pore water pressure (PWP) distribution in lower slope, berm, upper slope (shown in Fig. 4) for five tidal cycles has been shown in Figs. 12, 13 and 14, respectively. The parts of these regions that lie within the Zone of Influence of Rise-up have shown changes in PWP due to cyclic tidal behaviour. It is seen that there is gradual build-up of excess PWP during rise-up half cycle, followed by release of the same during drawdown half cycle. Similar pattern is observed for

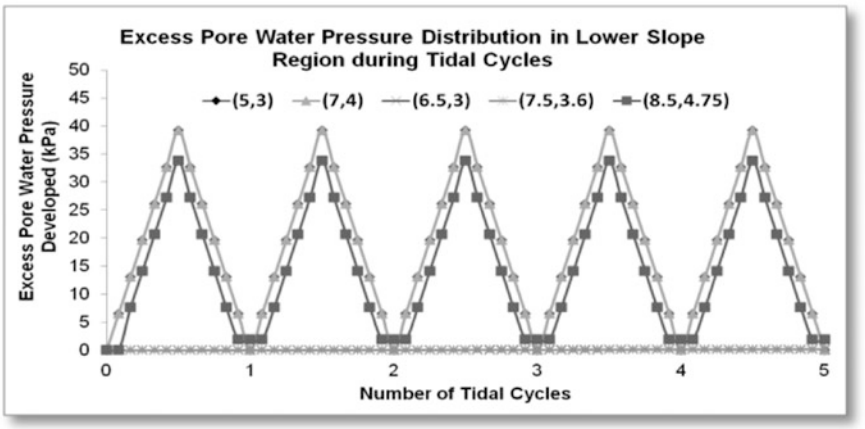

Fig. 12 Excess PWP distribution in lower slope region

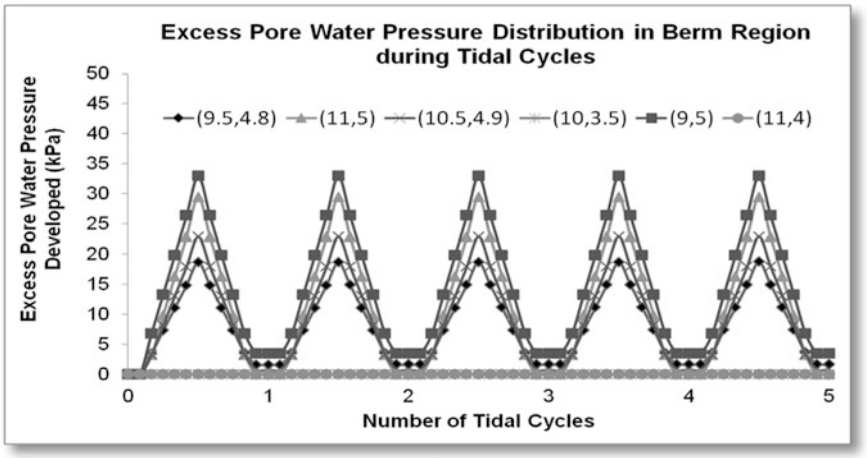

Fig. 13 Excess PWP distribution in berm region

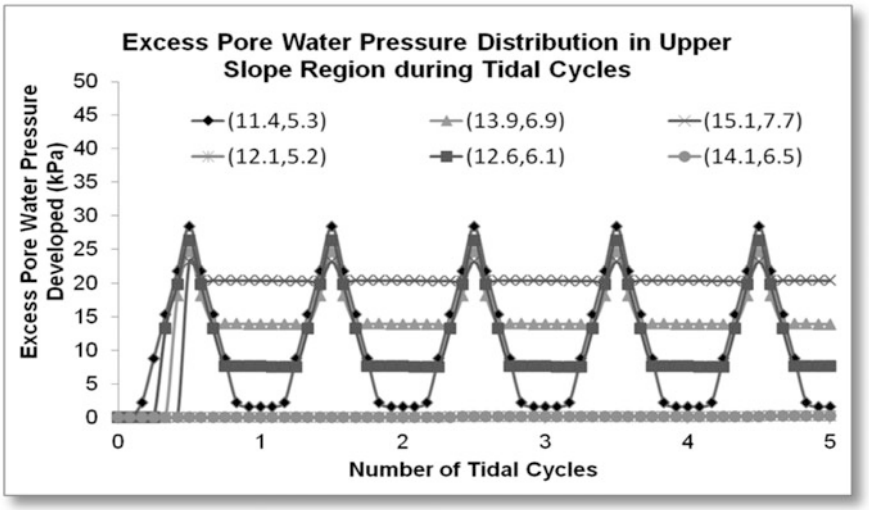

Fig. 14 Excess PWP distribution in upper slope region

multiple cycles, however, with a cumulative effect. It is seen that the maximum variation in excess PWP is observed for the lower slope followed by berm and upper slope region. The pattern varies as per region and is dependant on area of unsaturation, difference in level between HTL and LTL and tidal cycle time. Negligible variation in PWP was observed for points lying in the interior of the embankment as they lie outside the Zone of Influence of Rise-up.

4.4 Stability Factor

A slope stability analysis using Spencer methodology was performed using SLOPE/W. The minimum factor of safety plotted against number of tidal cycles is shown in Fig. 15. The Cyclic Factor of Safety Ratio (CFOS) is the ratio of the transient FOS (during tidal cycle) to the initial FOS, i.e. during steady state. The same was seen to increase during rise-up half cycle time and decrease during drawdown half cycle time. It was observed that the FOS remained constant more or less at the end of each cycle compared to initial conditions.

4.5 Serviceability

Additionally, a deformation analysis was performed using SIGMA/W. It was observed that even though the stability factor of safety is adequate for the typical

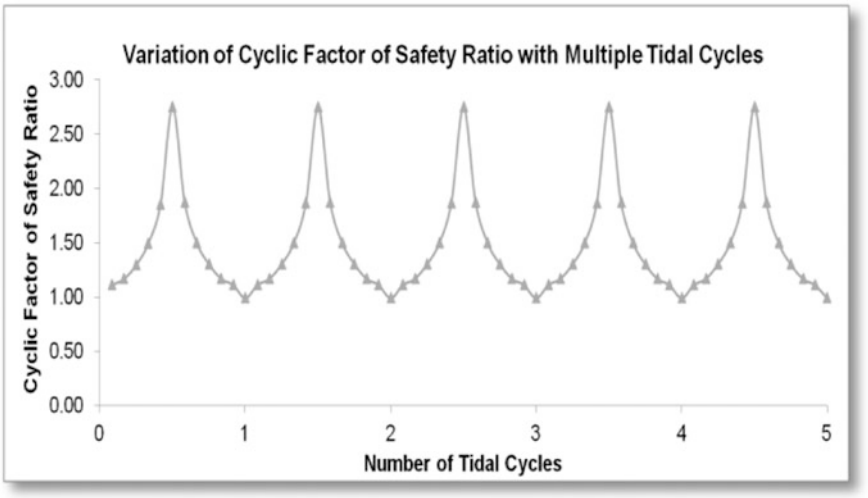

Fig. 15 Variation of CFOS with multiple tidal cycles

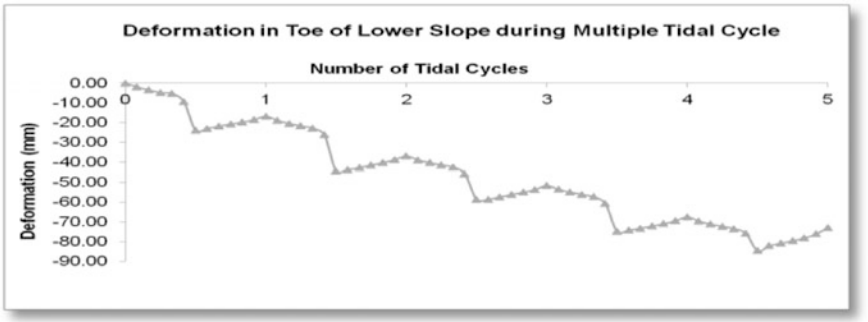

Fig. 16 Deformation pattern in toe of lower slope

Sunderban embankment during tidal cycles, the deformation of the toe region of the lower slope showed significant vertical settlement during rise-up and elastic rebound during drawdown, with a cumulative effect over multiple cycles. This has been shown in Fig. 16. This may be attributed to the highly plastic nature of the soil used in construction of the embankment. This may lead to deformation-based failure, instances of which have been reported from sites like Patharpratima, Gosaba, Sonakhali and other sites of Sunderban region. A typical lower slope failure in Sunderban embankment is shown in Fig. 1.

4.6 Comparison with Other Studies

The result patterns observed were in good agreement with similar type of study carried out by Desrosiers et al. (2013) for a tidal front embankment in Boston, UK.

5 Conclusions

(i) Changes in location of phreatic surface and variation in pore water pressure due to transient seepage induced by tidal behaviour are observed within the Zone of Influence of Rise-up only. The variations are influenced by the initial conditions, tidal head difference between LTL and HTL, tidal cycle time. Regions lying outside the ZIR show negligible response to the tide-induced transient seepage.

(ii) The excess pore water pressure variation pattern is different across regions within the ZIR, as observed for a typical Sunderban embankment with maximum variation in lower slope region during full tidal cycle.

(iii) Even though the stability factor of safety may be adequate for an embankment exposed to tidal behaviour, it is important to check for deformation at critical areas. For the Sunderban embankment, the toe region appears to be most susceptible to serviceability failure.

References

Aubertin, M., Mbonimpa, M., Bussière, B., & Chapuis, R. P. (2003). A model to predict the water retention curve from basic geotechnical properties. *Canadian Geotechnical Journal, 40*(6), 1104–1122.

Desrosiers, T., Bennett, V., Abdoun, T., & Simm, J. (2013) Comprehensive real-time field monitoring at active embankment subjected to tidal loading. *ASCE Geo-Congress*, pp. 1556–1565.

Van Genuchten, M. T. (1980). A closed-form equation for predicting the hydraulic conductivity of unsaturated soils (Masters' thesis). *Soil Science Society of America Journal, 44*, 892–898.

Rock Mass Slope Stability Analysis Under Static and Dynamic Conditions in Mumbai, India

Ahmed Shaz, Endalu Tadele Chala and K. Seshagiri Rao

Abstract The rock slope stability has gained much importance in the recent years owing to the development of infrastructure in/on rock slopes areas in the form of high-rise building, roads, railways, dams, and other rock engineering projects. Rock slope stability is generally affected by the property of rock material along with the discontinuities in the rock mass. It is also dependent on slope angle, slope height, surcharge, groundwater conditions, rainfall, and dynamic forces like earthquake. If these factors, coupled with deep weathering of the rock mass, complicate the entire behavior of the rock slope and makes the analysis of rock slopes challenging task. For the present work, fieldwork was carried out for joint mapping on differentially weathered volcanic rock of selected slope sections at Mumbai in Deccan trap regions. Block and core samples were collected from each category of the rocks and their respective geotechnical properties measured experimentally and presented her in. The rock slope stability analysis was done using numerical modeling techniques, finite element method (FEM)-based two-dimensional analyses (RS2), or Phase2 9.0 software from Rocscience. The rock slope having four different quality of rock mass was analyzed under static and pseudo-static conditions. Finally, the optimum support measures were provided to the slope for stabilizing it and the corresponding analysis was also done.

Keywords Rock slope stability · Rock mass properties · Numerical modeling RS2 · Stabilization

A. Shaz (✉)
Larsen & Toubro Ltd., Chennai 600089, India
e-mail: syedahmadshaz@gmail.com

E. T. Chala · K. Seshagiri Rao
Department of Civil Engineering, Indian Institute of Technology Delhi, New Delhi, India
e-mail: endu2020@gmail.com

K. Seshagiri Rao
e-mail: raoks@civil.iitd.ac.in

B. Adimoolam and S. Banerjee (eds.), *Soil Dynamics and Earthquake Geotechnical Engineering*, Lecture Notes in Civil Engineering 15,
https://doi.org/10.1007/978-981-13-0562-7_21

1 Introduction

Rock slope stability among many factors generally depends on the strength of the rock materials and characteristics of discontinuities (e.g., roughness, wall strength, aperture, fill material, and persistence). In tropical climate, weathering of rock material and discontinuity walls also affects the rock slope stability and significantly influences the response of rock masses to loadings and unloading of excavations.

In recent years, numerical methods such as finite element method (FEM), finite difference method (FDM), and discrete element method (DEM) are being more commonly applied to slope stability problems. Hudson and Feng (2007) provided a flowchart for numerical modeling of rock engineering. It is a common practice to model the behavior of discontinuities by a linear Coulomb relation using the parameters c and ϕ. However, the researchers in the field of rock mechanics and rock engineering well recognized that the shear strength parameters are not truly constant, and it depends upon the normal stress and scale (Bhasin and Kaynia 2004).

Hoek et al. (2002) has given c and ϕ in terms of Hoek parameters particularly to solve rock slope stability problems. For the present analyses and design of rock slopes, different degree of weathered blocks and core samples were collected from the rock slope of Deccan trap region, India. Specimens were prepared as per ISRM standards and tested for tensile, compression, and triaxial strengths. The average UCS and material constant of each weathered rock material was determined from experimental results. The GSI value of each of weathered rock mass was used for the estimation of rock mass properties (i.e., equivalent rock mass properties) for the analysis and design of slopes.

2 Geological Description and Specimen Prepared

The rock slope is located at the eastern scarp of Cumballa Hill in Tardeo, Mumbai. Regionally, the rocks in Maharashtra and around Mumbai are of volcanic origin known as Deccan trap. The Deccan trap is composed of very hard, tough, and compact rocks. The rocks are susceptible to weathering which begins on the exposed surface and along joints, cracks, and fissures. With time, it penetrates deep into the rock masses and resulting in complete loss of original skeleton structure of the rock mass. Chala et al. (2016) studied the strength properties of different degree of weathered basaltic rocks of some locations in Deccan trap and observed that weathering has drastically reduced the strength of rocks. They found the strength of slightly weathered basalt to be 50% less than the fresh basalt strength (Figs. 1 and 2).

For the present rock slope stability analysis, efforts were made to incorporate the effect of chemical weathering and discontinuity characteristics on rock mass through detail fieldwork such as joint mapping and laboratory investigations. Summary of the geotechnical properties of rocks is presented in Tables 1 and 2.

Fig. 1 Present rock slope appearance on out crops from eastern to western corner of the slope **a** dominant joint sets, discoloration, and staining of rock material due to weathering clearly visible **b** already stabilized portion of the rock slope

Fig. 2 Specimen prepared for testing under tensile, uniaxial, and triaxial loading

Table 1 Basalt intact rock properties and equivalent rock mass properties of fine breccia, coarse breccia, and tuff

Properties	Fine breccia	Coarse breccia	Tuff	Basalt
GSI	20	40	40	Intact
γ dry (kN/m^3)	21.79	21.50	20.56	27.91
γ sat (kN/m^3)	22.39	22.740	22.40	28.21
σt (MPa)	0.005	0.007	0.01	19.670
E (MPa)	517.14	514.0	892.1	34,937
c peak (MPa)	0.812	1.152	1.62	5.365
c residual (MPa)	0.0812	0.1152	0.016	0.5365
$\varphi^{(\circ)}$ peak	23.92°	41.51°	38.3°	65.7°
$\varphi^{(\circ)}$ residual	12°	20°	19°	32.53°

Table 2 Joint property of basalt

Joint property	Value
c (saw cut) (MPa)	0.0397
$\varphi^{(\circ)}$ (saw cut)	36.479°
Normal stiffness (MPa/m)	29,700
Shear stiffness (MPa/m)	12,270

3 Making Sections from Fence Diagram

Five sections of the hill slope were plotted for chainage 15, 35, 65, 90, and 110 m. After studying, the core samples were obtained from already drilled borehole (22.5–50 m deep) below existing ground level (EGL). From the borehole data, the rock present at various depths of the slope in a borehole of a particular section is marked and joined with the same rock in another borehole of the same section, to get the inclination of various rock strata beneath the EGL of the hill slope.

From the borehole study, it was found that basalt forms the top strata of the hill slope, as was observed on the site. Below the basalt layer is the layer of fine volcanic breccia (FVB) which forms the lower portion of the hill slope, it is followed by a layer of coarse volcanic breccia (CVB) and then welded tuff (Fig. 3).

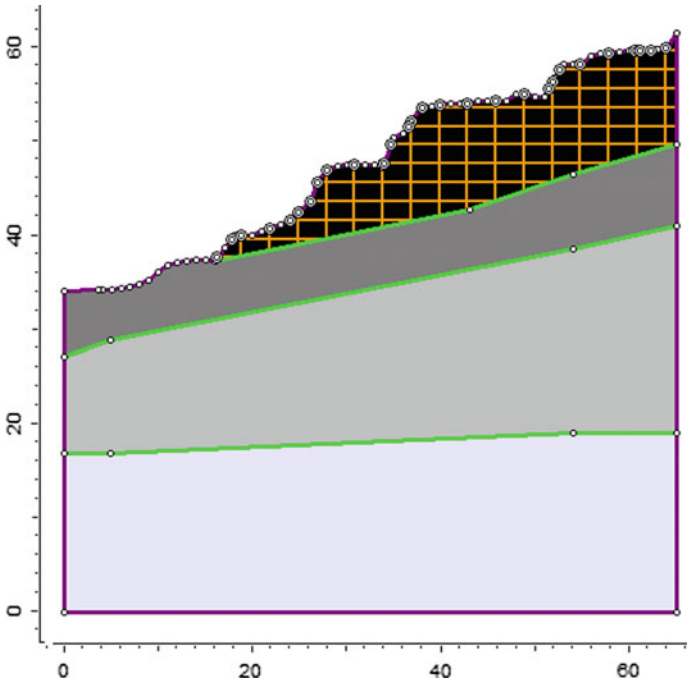

Fig. 3 Geometry and formation of the four rock masses at 65 m chainage

The angle of the slope varies throughout the slope section, and the average angle of the slope was found to be 30°.

4 Determining Rock Mass Properties

Rock material properties were obtained from laboratory testing including index properties tests, uniaxial, triaxial, Brazilian, and point load test. The joint properties were calculated using direct shear test.

For the top basalt layer, rock material property (σ_c = 68.85 MPa and E = 34.937 GPa) and joint property had been calculated in the laboratory and used in the analysis given (Tables 1 and 2). Normal stiffness and shear stiffness were taken from Kainthola et al. (2014).

Since none of the underlaying strata was exposed for the joint mapping, the equivalent rock mass properties were calculated based upon GSI Index chart (Marinos and Hoek 2000).

The structure of the rock mass (intact, blocky, very blocky, disturbed, disintegrated, and laminated) was studied along with the surface condition of the rock mass. Finally, GSI was quantified accordingly for fine volcanic breccia (FVB), coarse volcanic breccia (CVB), and welded tuff (Tuff) as 20, 40, and 40, respectively.

Rock data 5.0 software from Rocscience was used to determine the equivalent rock mass properties. The triaxial test data was given as an input to the software along with GSI value and uniaxial compressive test results (σ_c = 26.1, 33.3, 32.4 MPa and E = 11.32, 3.22 and 5.58 GPa) for FVB, CVB, and Tuff, respectively.

Also, the residual values of cohesion and friction angle were taken as 10 and 50% of the peak values, respectively, for the slope stability analysis. The intact and equivalent rock mass properties are provided in Tables 1 and 2.

5 Slope Stability Analysis

The geometry was made for different slope sections at respective chainage and each rock strata in every slope section was assigned with corresponding rock mass and joint properties accordingly in the Phase2 model. Then the boundary conditions were assigned to the model (Fig. 4).

The ground surface of the slope was made free in both X- and Y-direction. The vertical boundaries of the section were free to move in Y-direction only and restrained in X-direction. The base of the section of slope was fixed and was restricted to move in both X- and Y-direction. A uniform mesh was used in the FEM model for the analysis of all the five slope sections.

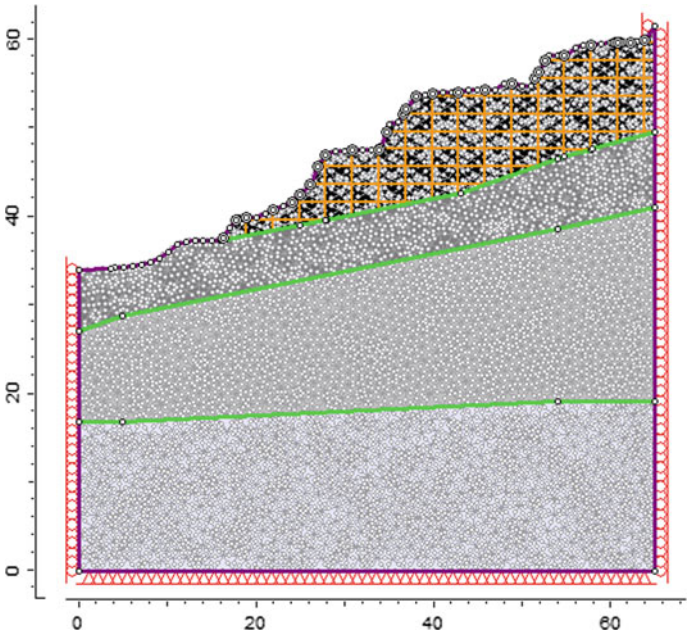

Fig. 4 Discretized Phase2 model of slope section at 65 m chainage

5.1 Static Analysis

Model of the slope sections was loaded with field stresses by taking gravitational load from actual ground surface. All the analyses were done using Mohr–Coulomb failure criterion (Table 3).

The critical SRF for the slope section at 65 m chainage was found to be 1.75 from the normal static gravitational analysis without any seismic conditions (Fig. 5).

Table 3 Results of the static analysis

Chainage of the slope section (m)	Factor of safety	Max. total displacement (m)
15	2.65	0.0073
35	1.89	0.0027
65	1.75	0.0019
90	2.85	0.0079
110	2.34	0.0024

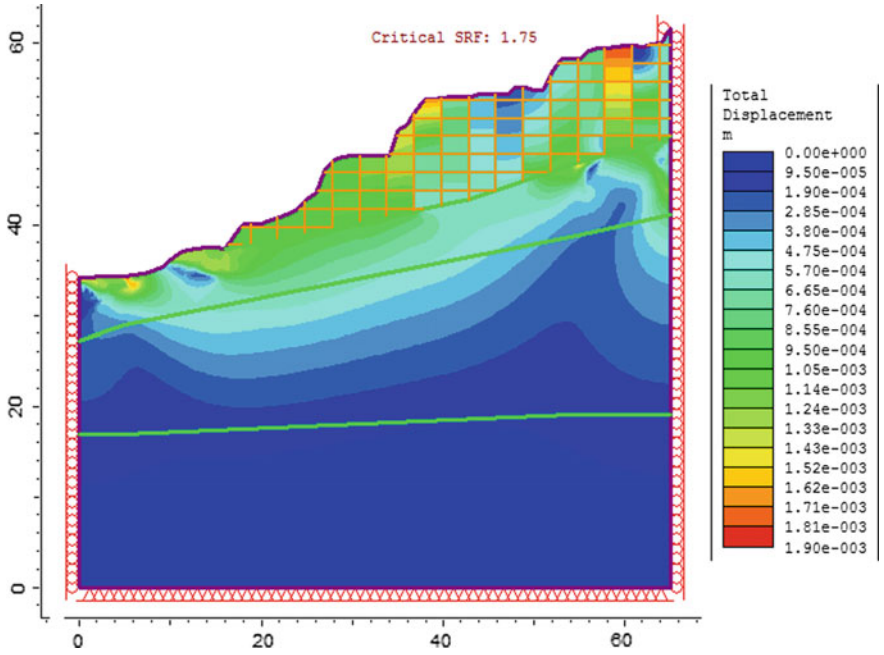

Fig. 5 Total displacement contour plot at critical SRF of section at 65 m chainage

5.2 *Dynamic Analysis*

The present rock slope is located at Mumbai which falls under seismic zone 3 for which the horizontal seismic coefficient value (K_h) is prescribed as 0.16 for moderate seismic intensity (I.S.1893.1.2002). Numerical analysis was done under pseudo-static loading using the horizontal seismic coefficient to model their stability under any seismic event. From static analysis, it has been concluded that the slope section at chainage 65 m has the minimum factor of safety. In this section, this slope section at 65 m chainage has been analyzed under different pseudo-static loading conditions along with the gravitational forces using FEM-based Phase2 software (Fig. 6).

The pseudo-static analysis was carried out for four cases with different seismic loading conditions along with the gravitational load, for the stability analysis of the hill slope at 65 m chainage. The result of the analysis is provided in Table 4.

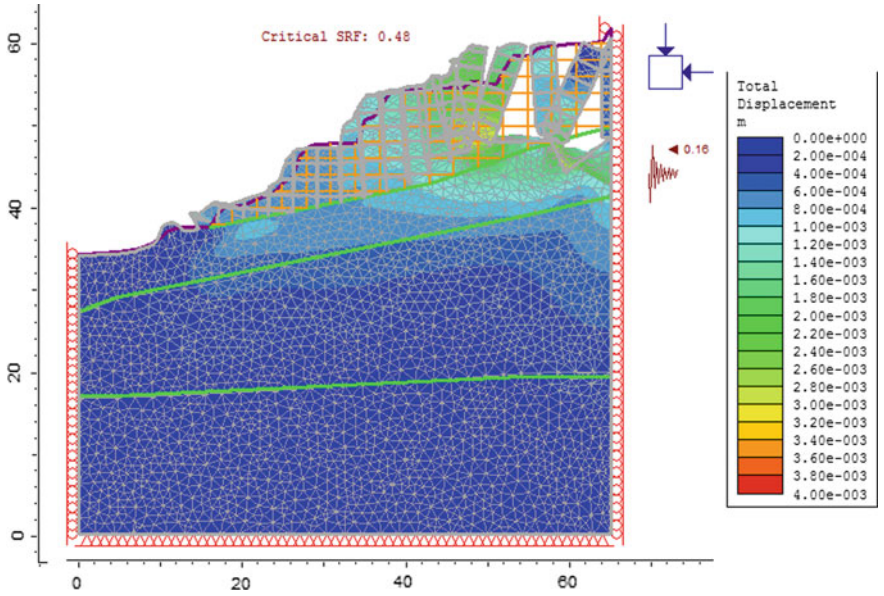

Fig. 6 Maximum deformed shear strain plot of 65 m chainage section with $K_h = 0.16$

Table 4 Factor of safety of the slope section with corresponding K_h value

Horizontal seismic coefficient (K_h)	Factor of safety
0 (static condition)	1.75
0.03	1.54
0.08	0.99
0.1	0.94
0.16	0.48

6 Stabilization of the Slopes

From the above analysis, it is clear that the slope is failing at $K_h = 0.16$ as prescribed by I.S.1893.1.2002 for seismic zone 3 areas. Hence, there was a need to provide optimum support system in order to stabilize the slope. The hill slope at 65 m chainage was therefore stabilized with shotcrete and fully bonded bolts so that the factor of safety can be reached greater than one in dynamic condition. Various trials had been done with different reinforcement to stabilize the slope at the corresponding loading condition.

The optimum support measures were provided using shotcrete ($f_{ck} = 35$ MPa and 100 mm thickness) and fully bonded bolts (32 mm Diameter, 10 m length with 3×3 m spacing) due to which the factor of safety of the most critical section(at 65 m chainage) was raised from 0.48 to 1.2 at pseudo-static and gravitational

loading conditions. The same support was provided to all the sections and the corresponding FOS was 1.82, 1.61, 1.2, 2.5, and 2.44 for slope sections at chainage 15, 35, 65, 90, and 110 m, respectively.

7 Conclusion

The fieldwork was carried out at the hilly site of Cumballa Hill in Tardeo, Mumbai, to get the joint mapping and other site parameters. Four different types of borehole rock samples were collected from various already drilled boreholes drilled 22.5–50 m below the existing ground level (EGL).

The laboratory testing was carried out to get the physical and strength parameters of the rock material. The summary of geotechnical properties is given in Tables 1 and 2. Then the borehole data was studied, and the slope sections were prepared at chainage 15, 35, 65, 90, and 110 m. Since the joint pattern in the bottom three rock layers was not exposed, the rock mass property was estimated from the structure and surface condition of the rock mass using GSI Index chart.

From the numerical modeling done using RS2 software on all the prepared sections for gravitational loading in dry condition, it was found that the slopes are in stable condition. The slope section at chainage 65 m was found to have the lowest factor of safety = 1.75. This slope section was further analyzed under pseudo-static loading along with gravitational load. It was found that the slope comes in critical condition at horizontal seismic coefficient (K_h) = 0.08. Since the site is located at Mumbai which comes under seismic zone 3 area, hence the slope was analyzed for K_h = 0.16 as recommended by I.S.1893.1.2002. The slope was found to be failing with factor of safety = 0.48. Hence, there was a need of providing support measures for slope stabilization. The optimum support measures were provided using shotcrete (f_{ck} = 35 MPa and 100 mm thickness) and fully bonded bolts (32 mm diameter, 10 m length with 3 × 3 m spacing) due to which the factor of safety for the most critical section (at 65 m chainage) was raised from 0.48 to 1.2 at the dynamic loading conditions. The same support was provided to all the slope sections and all the corresponding factor of safety was found to be 1.82, 1.61, 1.2, 2.5, and 2.44 at chainage 15, 35, 65, 90, and 110 m, respectively.

References

Bhasin, R., & Kaynia, A. M. (2004). Static and dynamic simulation of a 700-m high rock slope in western Norway. *Engineering Geology, 71*, 213–226.

Chala, E. T., Seshagiri Rao, K., & Malik, A. (2016). Estimating engineering properties of weathered rocks from Deccan trap. In *Indorock 2016 Proceedings, 6th Rock conference,* IIT Bombay, June 17–18.

Hoek, E., Carranza-Torres, C., & Corkum, B. (2002). Hoek-Brown failure criterion-2002 edition. In *Proceedings of NARMS-Tac* (Vol. 1, pp. 267–273).

Hudson, J. A., & Feng, X. T. (2007). Updated flowcharts for rock mechanics modelling and rock engineering design. *International Journal of Rock Mechanics and Mining Sciences, 44*, 174–195.

Kainthola, A., Singh, P. K., & Singh, T. N. (2014). Stability investigation of road cut slope in basaltic rock mass, Mahabaleshwar, India. *Geoscience Frontiers, 6*(6), 837–845.

Marinos, P., & Hoek, E. (2000, November). GSI: A geologically friendly tool for rock mass strength estimation. In *ISRM International Symposium*.

Numerical Analysis of MSE Wall Using Finite Element and Limit Equilibrium Methods

S. S. Konnur, A. M. Hulagabali, C. H. Solanki and G. R. Dodagoudar

Abstract Mechanically stabilized earth (MSE) retaining walls are the most suitable design alternatives to the conventional retaining walls due to their simple, rapid, and cost-effective construction, reduced right-of-way acquisition, etc.; hence, the MSE walls are used in many central, state, and private sector projects. But the design and analysis is a challenging task for geotechnical engineers. This paper deals with the study of stability and wall movement of a existing MSE wall constructed on a major state highway in central Texas, using a finite element (FE) analysis and limit equilibrium (LE) slope stability analysis program GEO5 2016. The detailed analyses for both internal and external stabilities were obtained from the finite element and limit equilibrium analysis, with a critical failure surfaces and the wall movement of a MSE wall. The factors of safety obtained from both analyses were compared. The study shows that the factors of safety obtained from finite element and the limit equilibrium analysis, for a given problem, match in an acceptable range with a different critical failure surfaces. Also, this paper deals with the effect of backfill soil and reinforcements on stability and excessive movements of MSE wall.

Keywords MSE retaining wall · Reinforcements · Finite element (FE) analysis Limit equilibrium (LE) analysis · Wall movement

S. S. Konnur (✉) · A. M. Hulagabali
Department of Civil Engineering, Basaveshwar Engineering College, Bagalkot, Karnataka, India
e-mail: konnursangamesh1991@gmail.com

A. M. Hulagabali
e-mail: anandmhulagabali@gmail.com

C. H. Solanki
Applied Mechanics Department, SVNIT Surat, Surat, Gujarat, India
e-mail: chs@amd.svnit.ac.in

G. R. Dodagoudar
Department of Civil Engineering, IIT Madras, Chennai, Tamilnadu, India
e-mail: goudar@iitm.ac.in

B. Adimoolam and S. Banerjee (eds.), *Soil Dynamics and Earthquake Geotechnical Engineering*, Lecture Notes in Civil Engineering 15,
https://doi.org/10.1007/978-981-13-0562-7_22

1 Introduction

Soil is an most widely used construction material, which is strong in compression and very weak in tension, and similarly, the steel is widely used as reinforcing material in almost of all civil engineering infrastructure projects which is very strong in tensile strength. Hence, the combination of both these soil and reinforcement will give very good engineering properties than properties of individual materials. Basically, reinforced soil has two components which are soil and reinforcement with different properties but basic concept is that the embedded reinforcement in soil provides tensile strength to the soil it is because of higher stiffness of the reinforcement. The basic mechanism of MSE is that while reinforcement is in the soil system the friction is formed between them and due to this friction soil movement is hold on the surface of reinforcement and then the shear stress is developed which produces tension in reinforcement this leads to confinement to the soil and results in decrease in soil deformation and increase in shear strength of the soil.

The complete design analysis of a mechanically stabilized earth (MSE) retaining wall includes evaluation of internal, external, and global stabilities as well as horizontal and vertical wall displacements (Abdelouhab et al. 2011). In these three parameters, the internal stability of MSE wall by means of pullout resistance and tensile strength of the reinforcement mainly depends on the type of reinforcement, spacing and length of the reinforcement, and the external stabilities by means of failure modes such as sliding, overturning, wall bearing, and global stability failure. Hence, these both internal and external failure modes are considered as slope failure through sliding surfaces, and the overall stability of an MSE wall can be evaluated using slope stability analysis (Payeur et al. 2015).

The two common and general methods of stability analysis are limit equilibrium and numerical methods in which limit equilibrium method considers the soil as a perfectly plastic and rigid material. The safety factor of limit equilibrium technique is calculated by Spencer method, Fellenius method, Morgenstern method, Janbu method, Bishop Method, etc. As we know that numerical modeling involves the calculation of stresses/displacements by method of discretization of continua and then assembling properties of each element and nodes by imposing boundary conditions to those elements and finally stresses/displacements are calculated by solving governing or system equations. But it is not possible to get exact safety factor by numerical method, but it can be determined by shear strength reduction technique (SSR).

In this paper, the stability analysis of an existed MSE wall project using both limit equilibrium and numerical method is presented. The slope stability analysis and stress/deformation analysis programs, GEO5 MSE (for LE) and GEO5 FEM (for numerical) are used in the present study. The calculated results from limit equilibrium method and numerical method are compared with each other.

2 Limit Equilibrium and Numerical Analysis Programs

GEO-5 fine is a powerfull program for solving geotechnical problems based on traditional and FE method. It is mainly designed to solve most geotechnical tasks, from the basic one to highly specialized programs. It works basically on the technique that initially the structure is designed analytically and then it is transferred analytical model into FEM program where the structure is verified by the FE method. GEO-5 fine contains two options, one for analysis internal and external stabilities, slope stability using a variety of popular limit equilibrium methods including the Bishops method, Spencer method, the Morgenstern-Price method, Janbu method and another one for analysis of stresses, displacements/deformations of wall. GEO-5 fine also provides explicit options for reinforcing elements including piers/piles, tiebacks (anchors), soil nails. In this study, the Spencer method is used in the analysis due its wide acceptance and the fact that it satisfies both force and moment equilibrium.

3 Mechanically Stabilized Earth Wall Project

The MSE wall project selected in this study was constructed on a major state highway in central Texas. The wall was required to support a new bridge abutment for an overpass on a new roadway passing over an existing roadway. The project contained numerous walls of varying heights. The wall analyzed in this study was the tallest wall with the steepest back slope and was the most critical case. A minimum FS of 1.3 was required in the design. The retained fill was placed simultaneously with the reinforcement (Abdelouhab et al. 2011).

The proposed geometry of the MSE wall and the soil profile are presented in Fig. 1. Soil properties used in the limit equilibrium and numerical analyses are listed in Table 1. The reinforcement consisted of galvanized metal ribbed straps

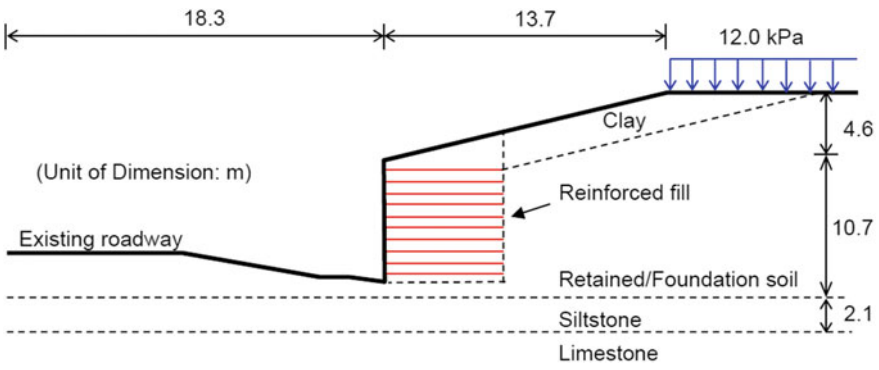

Fig. 1 Soil profile and slope geometry (Abdelouhab et al. 2011)

Table 1 Soil properties (Abdelouhab et al. 2011)

Soil description	Moist unit weight (kN/m^3)	Saturated unit weight (kN/m^3)	Cohesion (kPa)	Friction angle (°)
Siltstone	20.4	20.4	0	28
Limestone	21.7	21.7	56	30
Reinforced fill	19.6	20.1	0.05	34
Retained/ foundation soil	19.6	20.1	4.8	28
Clay	19.6	20.1	4.1	26

with a nominal width of 50 mm and a nominal thickness of 4 mm. The straps were 5.7 m in length with both horizontal and vertical spacing of 0.76 m. The allowable tendon strength of each metal strap was 89.6 kN. The allowable pullout strength of each metal strap was determined according to the FHWA design standard. A surcharge load of 12 kPa was considered at the back of the wall (as shown in Fig. 1) to account for the traffic load (Abdelouhab et al. 2011).

4 Stability Analysis

As mentioned earlier, the Spencer method was used in the limit equilibrium method in the GEO-5 MSE software. In the limit equilibrium analysis, trial failure surfaces were assumed to pass through the toe of the wall, since it is considered the most critical failure surface. A total of 232 circular failure surfaces were evaluated for the MSE wall, and the factor of safety for each failure surface was calculated. The most critical failure surface with a factor of safety of 1.5 is illustrated by the yellow line in Fig. 2 (Table 2).

The numerical analysis of the MSE wall was performed using the finite element program, GEO5 FEM. The numerical model was built with the same dimensions of that shown in Fig. 1. Horizontal displacement was fixed at the side boundaries, and the vertical displacement was fixed at the bottom boundary. In this study, the facing material of the wall was not physically modeled thus exclusion zone was set so that no failure surface passes through the facing of the wall.

Compared to the limit equilibrium method, the numerical analysis does not need a presumed failure surface. More information (stress, strain, displacement, etc.) can be extracted from a numerical model rather than a single factor of safety output. For example, the contour plot of shear strain increment is a good indicator of the critical failure surface of the MSE wall, as shown in Fig. 4. For comparison purposes, the critical failure surface determined by the GEO5 MSE software was also plotted. It is shown that in the numerical analysis the failure surface is similar to an active earth pressure failure case. The failure surface passed through the back toe of the reinforced zone, and the reinforced zone behaves as a coherent mass. The factor of

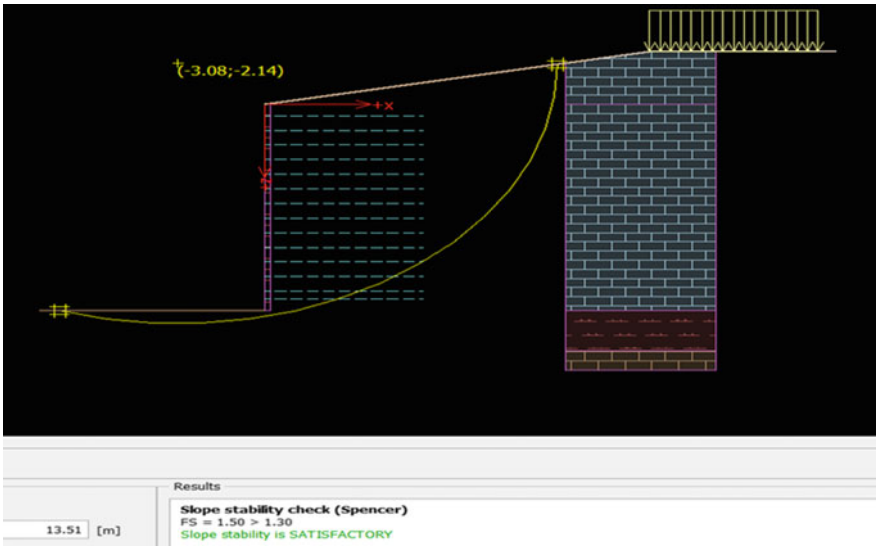

Fig. 2 Critical failure surfaces and the factor of safeties

Table 2 FOS for each trial critical failure surfaces

Critical failure surfaces	1	2	3	4	5	6	7	8	9	10
Factor of safety	1.5	1.5	9.6	1.5	7.2	1.5	1.5	1.5	1.5	1.5

safety determined by the shear strength reduction method is 1.56, which is close to that determined by the limit equilibrium method.

Figure 3 shows the discretized MSE wall with 3209 nodes and 1956 elements (1090 regions, 219 beams, 657 interfaces) in the numerical model and the Fig. 4 (displacement plot) indicated that entire reinforced zone is rotating around the front toe of wall, which confirmed that failure model of the wall is an active earth pressure failure. Figure 5 shows the comparison between the numerical solution and the limit equilibrium solutions, in which the factor of safety from numerical solution is 1.56 and factor of safety from limit equilibrium method is 1.5. The different predicted critical failure surfaces predicted from the two programs are due to the different underlying assumptions associated with the two different types of analyses.

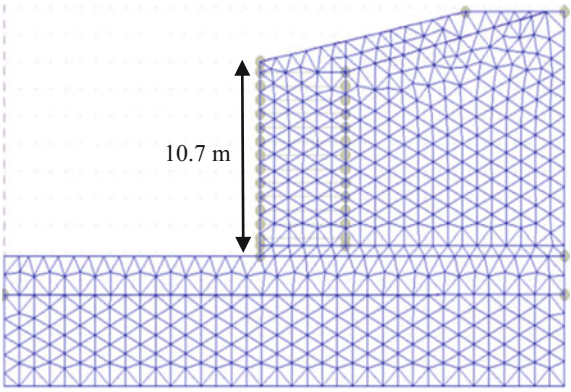

Fig. 3 Discretized MSE wall (Meshing)

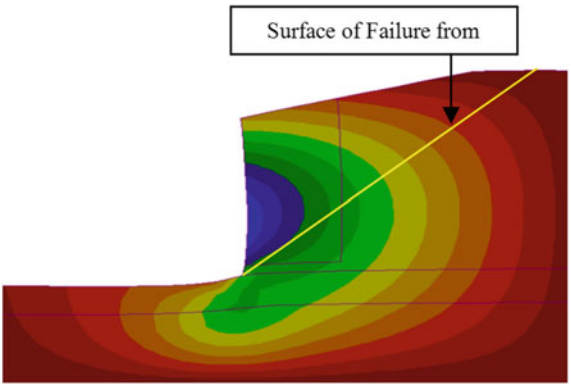

Fig. 4 Failure surface predicted by the numerical method

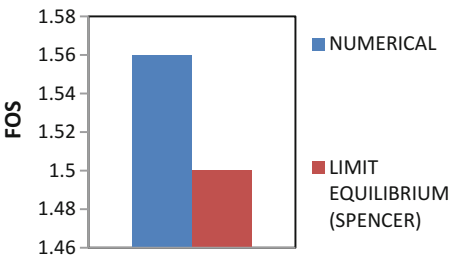

Fig. 5 FS of numerical and limit equilibrium (Spencer)

5 Conclusion

In this study, the stability of an MSE wall is analyzed using both limit equilibrium and numerical methods. It was found that the two analysis programs give different factor of safety for the retaining wall. This type of difference in factor of safety is due to the different underlying assumptions made with the two different analysis

methods. From FEM and limit equilibrium methods, FEM gives little higher factor of safety than LE method. This is because of discretization of single structure into number of nodes, element, and regions. So it gives more convenient results than other methods. Analyzed values from both methods are in well acceptable ranges and are in good agreement. For the difficulties of many real-world projects, it is suggested that two or more different analysis methods should be considered in order to get a better analysis of the MSE retaining wall projects.

References

Abdelouhab, A., Dias, D., & Freitag, N. (2011). Numerical analysis of the behaviour of mechanically stabilized earth walls reinforced with different types of strips. *Geotextiles and Geomembranes, 29*, 116–129.

Payeur, J. B., Corfdir, A., & Bourgeois, E. (2015). Dynamic behaviour of a MSEW under harmonic loading: Experimental characterization and 3D FE model. *Computers and Geotechnics, 65*, 199–211.

Field and Numerical Investigation on Time-Dependent Behavior of Jute Geotextile (JGT) Reinforced Rural Road

Souvik Patra and Ashis Kumar Bera

Abstract A rural road section reinforced with Jute Geotextiles (JGT) sandwiched between thin sand layers has been constructed to study the strength improvement of subgrade soil. In this present investigation, an attempt also has been made to develop a three-dimensional (3D) finite element (FE) model of the JGT reinforced and unreinforced rural road sections using general purpose FE software ABAQUS. Numerical simulation of time-dependent behavior for JGT reinforced rural road has been carried out using the data obtained from field investigation at regular time interval. In this present investigation, subgrade soil has been modeled using Mohr–Coulomb plasticity model, whereas JGT has been assumed as membrane type of material. From FE analysis, pavement responses under traffic loading such as rut depth, maximum tensile strain developed at JGT, and vertical compressive strain developed at the top of subgrade soil has been evaluated. From the field investigation, it has been found that the subgrade California bearing ratio (CBR) value is increased with increase in time under study. It has been found that the reinforced rural road sections are performing well in terms of rut depth than the unreinforced section.

Keywords Rural road · Jute geotextile · 3D-FE analysis · ABAQUS Subgrade

S. Patra (✉) · A. K. Bera
Department of Civil Engineering, Indian Institute of Engineering Science and Technology, Shibpur, Howrah 711103, India
e-mail: souvik4rmjgec@gmail.com

A. K. Bera
e-mail: ashis@civil.iiests.ac.in

B. Adimoolam and S. Banerjee (eds.), *Soil Dynamics and Earthquake Geotechnical Engineering*, Lecture Notes in Civil Engineering 15,
https://doi.org/10.1007/978-981-13-0562-7_23

1 Introduction

1.1 Background of Present Study

Construction of rural road subgrade with poor local soil is causing an excessive deformation to the subgrade soil and results in the failure of rural roads. In recent days, strengthening of the road subgrade with the help of natural fibers such as jute and coir is in practice. The problem of use of fabric made of natural fibers in civil engineering field is that loss of its tensile strength in a short time. From the previous literature (Ramaswamy and Aziz 1989; Basu et al. 2009), it has been found that the JGT may be efficiently used to strengthen the rural road subgrade. Field study on JGT reinforced road section by Rao (2003) indicated that the subgrade soil gain sufficient strength with time. In this present investigation, an attempt has been made to study the behavior of the JGT reinforced rural road section under traffic loading by using FE-based software "ABAQUS" based on field measured data.

1.2 Description of the Field Rural Road Section

In March 2013, a rural road section reinforced with JGT has been constructed from Kanksa to Bati (KB) at Murshidabad District in West Bengal, India. In this JGT reinforced rural road section, JGT has been placed in between granular subbase (GSB) and subgrade soil with the presence of sand layers on each side of it. Detail dimensions of the JGT reinforced rural road section have been shown in Fig. 1. A monitoring schedule has been followed at regular interval of six month for two years. Soil parameters of the subgrade such as CBR value, dry density, cohesion, and angle of internal friction have been determined for each monitoring. These field-measured parameters are used in FE analysis to define the conditions of the subgrade soil at initial condition (after laying of JGT), 12-month, 18-month, and at 24-month.

1.3 Plan for Numerical Analysis

In this present investigation, two series (series A and series B) of model have been considered. In the series A, unreinforced rural road sections have been considered with varying time. JGT reinforced rural road sections have been taken under series B. For both the series of models (series A and series B), the rural road subgrade CBR values have been taken from the field investigation. Based on the study

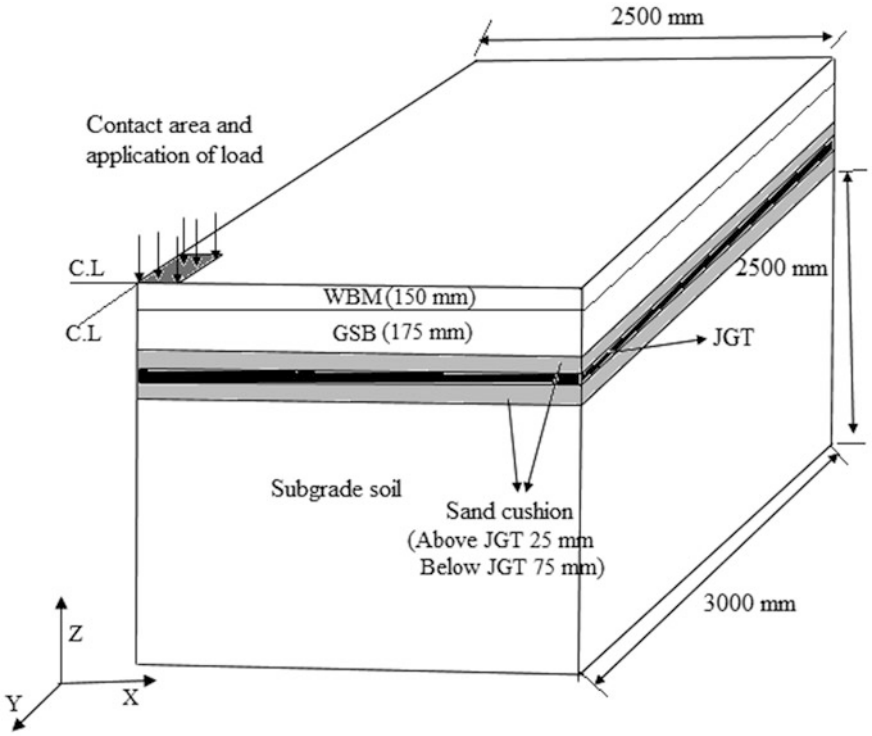

Fig. 1 Schematic diagram of reinforced section at initial condition

Table 1 Plan for numerical study

FE model series	Model name	Time from installation of JGT	Subgrade CBR value
Series A (unreinforced)	UR0	0	2.8
	UR12	12	3.8
	UR18	18	4.35
	UR24	24	5.57
Series B (reinforced)	R0	0	2.8
	R12	12	3.8
	R18	18	4.35
	R24	24	5.57

conducted by Bera and Roy (2012) and Saha et al. (2012), half-life of JGT has been considered as 12 month and full degradation time of JGT has been taken as 18 month. Details' plan and corresponding models' name for the FE analysis have been presented in Table 1.

2 FE Modeling Methodology

2.1 Idealization of Geometry

In this numerical study, geometry of the model has been idealized as a 3D model. Here only one-fourth of the model has been taken for computational purpose (Saad et al. 2006). On the basis of the previous literature (Gupta et al. 2014), the depth of the subgrade soil has been taken as 2.5 m in the present investigation.

2.2 Material Constitutive Behavior

In the present paper, subgrade soil has been considered as an elasto-plastic material. Plastic behavior of the subgrade soil has been defined by Mohr–Coulomb plasticity model, and parameters have been obtained from field investigation data. Resilient modulus of the subgrade soil and top granular layers (water-bound macadam, WBM and granular subbase, GSB) has been determined as per IRC 37:2012. In the present work, JGT has been considered as a membrane type material. In this investigation, JGT having a tensile strength of 20 kN has been used and elastic modulus of JGT has been determined at 2% strain from laboratory-wide width tensile strength test. It has been assumed that the elastic modulus of JGT at half-life will be half of the initial elastic modulus of 61.22 MPa. Poisson's ratio of JGT has been assumed as 0.25. It has been also assumed that the sand used in the present study is medium dense sand.

2.3 Load and Boundary Condition

In this work, traffic load has been simulated by triangular wave with a duration of 0.1 s based on the previous literature (Saad et al. 2006; Al-Khateeb et al. 2011). Peak wheel load has been assumed as 40 kN, and a tire contact pressure of 0.55 MPa has been applied on rectangular contact area. In the present paper, the length and breadth of the rectangular contact area have been calculated and the corresponding values are 406.5 and 177.6 mm, respectively. In this present, FE analysis bottom of the model has been considered as fixed support. Vertical walls adjacent to the loading area have been assumed as plane of symmetry along the direction of axis. Similar boundary condition has been used successfully by Perkins and Edens (2002). Horizontal displacements have been restricted, and only vertical displacements have been allowed on vertical faces away from loading area.

2.4 Meshing Criteria and Interaction Properties

Finest mesh has been created near the loaded area to capture the step stress and strain gradient more precisely in these areas. Discretization method used in this study has been shown in Fig. 2. In the present FE analysis, implicit direct integration method has been adopted. Here interaction between pavement layers has been defined by tie constraints. Interaction between JGT and sand layer has been simulated by coefficient of friction. In this study, JGT has been discretized by using M3D4R (a four-node quadrilateral membrane element with reduced integration). An eight-node linear brick element (C3D8R) has been used to mesh the other pavement layers.

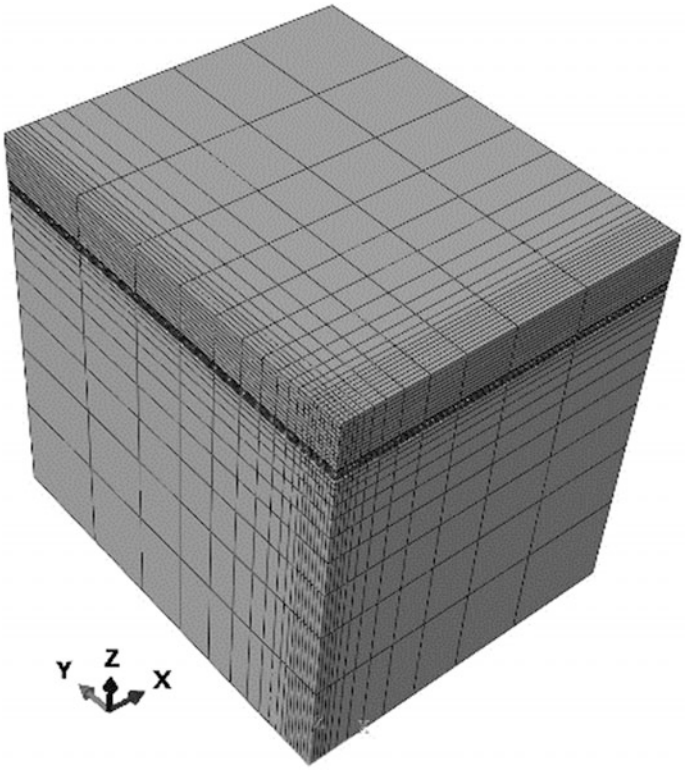

Fig. 2 Meshing technique adopted in the present investigation

3 Results and Discussion

3.1 Verification of the Model

The 3D finite element model has been qualitatively verified in two aspects: (i) vertical stress distribution and (ii) vertical compressive strain distribution along depth under the center line of the loading area. For this purpose, unreinforced rural road (UR0) has been idealized as a one-layer pavement system. Results obtained from ABAQUS analysis and vertical stress and strain computed from theoretical solution available in Ahlvin and Ulery (1962) have been presented in Fig. 3.

3.2 Study on Strength Increment of Subgrade Soil

Results obtained from regular field investigation indicate that the subgrade CBR value has been increased with time (Table 1). From Table 1, it has been seen that in 24 months the CBR value of subgrade soil increased about 1.98 times than the initial CBR value. Dry unit weight obtained from field monitoring with time is presented in Fig. 4. From Fig. 4, it has been also found that with time the values of

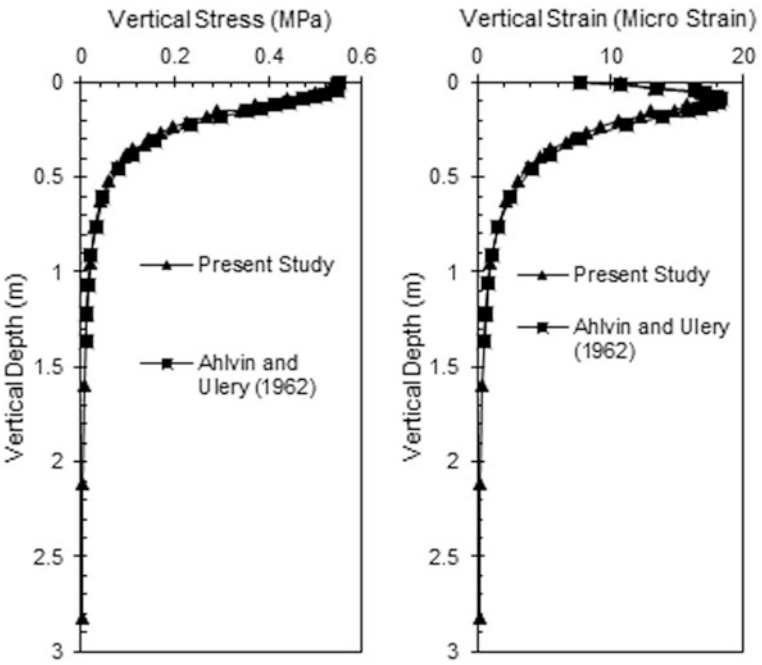

Fig. 3 Comparison between results obtain from FE analysis and theoretical solution

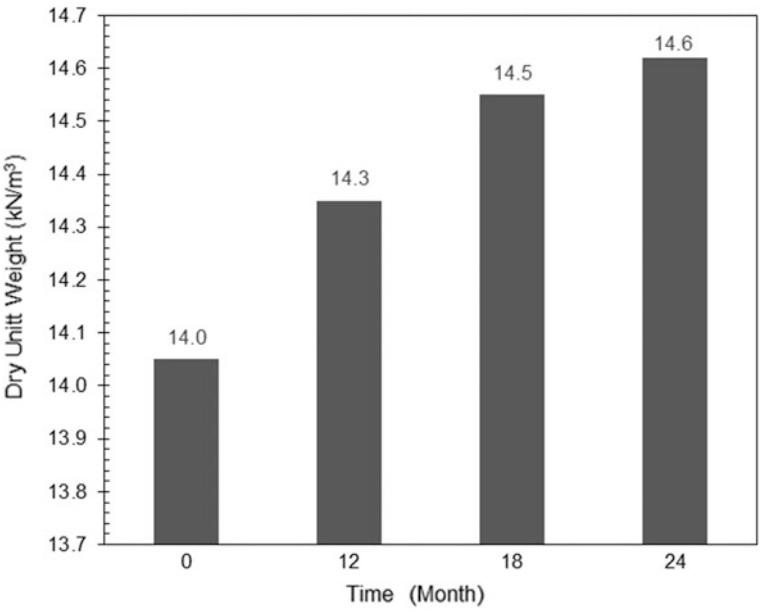

Fig. 4 Dry unit weight versus time curve for field JGT reinforced rural road section

dry unit weight of the subgrade soil is increases. Taskiran (2010) identified dry unit weight as the prime parameter influencing the CBR value of subgrade soil. Figure 4 also indicates that the dry unit weight has been increased about 1.04 time of its initial dry unit weight. Authors suggested that the increase in dry unit weight and subgrade CBR value may be happen due to consolidation process and compaction of the subgrade soil under traffic loading.

3.3 Utilization of JGT Strength Under Traffic Loading

In this present paper, reinforced section R0 and reinforced section R12 have been taken to study the utilization of JGT tensile strength under traffic loading. Maximum tensile stress and strain developed in JGT beneath the loading area has been taken from ABAQUS analysis. Utilization of JGT strength under traffic loading has been presented in Fig. 5. From Fig. 5, it has been seen that only a small fraction of tensile strength of JGT has been mobilized. In case of JGT, reinforced section at initial condition only 0.6% of tensile strength of JGT has been mobilized. It has been also observed that only 0.58% of tensile strength has been mobilized after 12 month of laying of JGT. Tensile strain has been developed around 0.1% in both the reinforced section R0 and reinforced section R12. Hufenus et al. (2006) reported that permanent strain in reinforcement under trafficking was usually below

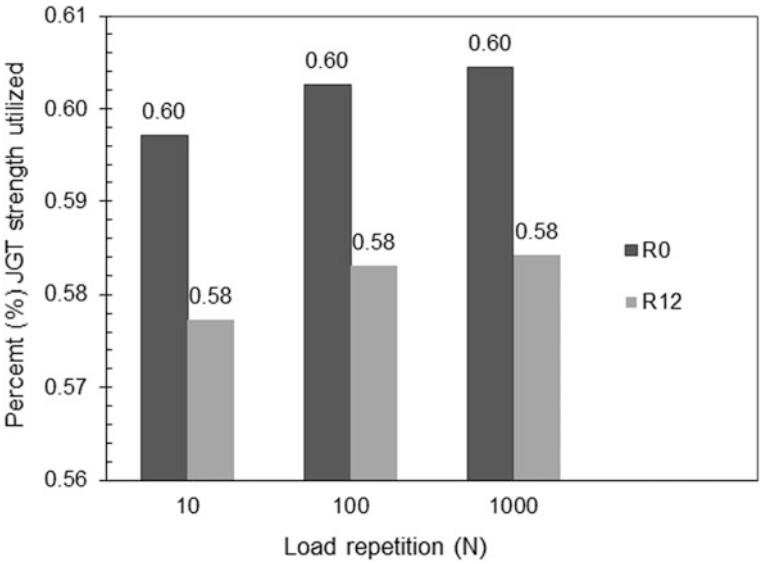

Fig. 5 Utilization of JGT strength under traffic loading

0.5% and exceed 1% only in extreme cases. Numerical study performed by Patra et al. (2016) also reported that the tensile mobilized in reinforcement is in the range 0.57–1.2% for reinforced rural road section. It may be suggested that as the subgrade soil gain strength with time which allows the JGT to serve its desired function at lower tensile strength.

3.4 Study on Usefulness of JGT on Subgrade Deformation Behavior of Rural Road Sections

Figure 6 represents the subgrade deflection taken at the top of the subgrade soil under the loading area for unreinforced and JGT reinforced rural road sections considered in the present study. It has been seen that the subgrade rut has been reduced in the range of 22–26% for the reinforced section R0 and reinforced section R12 with respect to the unreinforced section UR0 and unreinforced section UR12. In case of reinforced section R18 and reinforced section R24, after degradation of JGT subgrade rut depth has been reduced about 10–11% with respect to the unreinforced section UR18 and unreinforced section UR24. Based on the result of the present FE analysis, it has been clearly understood that the presence of JGT reduces subgrade deformation significantly under traffic loading and allows the rural road section to sustain on subgrade soil with low-CBR value due to membrane mechanism of the JGT. After degradation of JGT, subgrade soil already gains

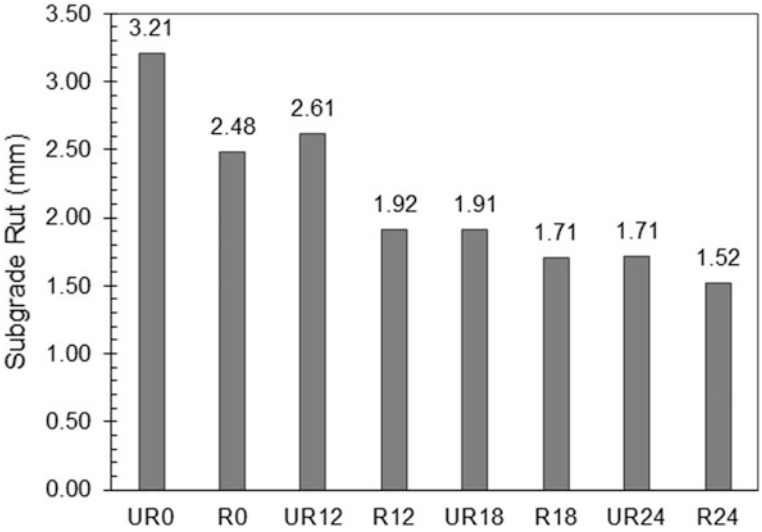

Fig. 6 Subgrade rut depth measured at top of subgrade soil beneath the loading area

sufficient strength to become independent of JGT. In this study, it has been also seen that after degradation of the fabric, although the unreinforced and reinforced rural road sections have same subgrade soil property, the subgrade deformation is reduced in reinforced section than the unreinforced section. Authors suggested that it is due to the presence of sand layers which allow the subgrade to face lower stress magnitude during traffic loading. In this present investigation, it has been observed that development of vertical compressive subgrade strain is reduced in the range of 16.96–35.73% in the JGT reinforced rural road section with respect to the unreinforced section.

4 Conclusions

Based on the present field investigation and FE analysis, following conclusions has been drawn.

- Reduction of subgrade rut depth of JGT reinforced rural road section than the unreinforced section is within the range of 22–26% and 10–11% before degradation of JGT and after degradation of JGT, respectively.
- In case of JGT reinforced rural road section, the vertical compressive subgrade strain has been reduced in the range of 16.96–35.73% with respect to the unreinforced section.

- Under traffic loading, only a small fraction of JGT strength around 0.58–0.6% has been mobilized.
- From the field investigation, the subgrade CBR value increases with increase in time under study.

Acknowledgements Authors express their sincere gratitude to National Jute Board (NJB), Kolkata, India, for their active support in the field investigation work. Authors also express their heartfelt thankfulness to Common Fund for Commodities (CFC), the Netherlands, for providing the facility of numerical analysis.

References

Ahlvin, R. G., & Ulery, H. H. (1962). Tabulated values for determining the complete pattern of stresses, strains and deflections beneath a uniform circular load on a homogeneous half space. *Highway Research Board Bulletin*, 342.

Al-Khateeb, L. A., Saoud, A., & Al-Msouti, M. F. (2011). Rutting prediction of flexible pavements using finite element modelling. *Jordan Journal of Civil Engineering, 5*, 173–190.

Basu, G., Roy, A. N., Bhattacharyya, K. S., & Ghosh, S. K. (2009). Construction of unpaved rural road using jute-synthetic blended woven geotextile—A case study. *Geotextiles and Geomembranes, 27,* 506–512. Technical Note, Elsevier.

Bera, A. K., & Roy, A. (2012). Engineering properties of jute geotextile and its efficacy to the consolidation of soil. *EJGE, 17,* 2631–2645.

Gupta, A., Kumar, P., & Rastogi, R. (2014, December). Performance evaluation and design criteria for low volume road. *Indian Highways*, 35–42.

Hufenus, R., Rueegger, R., Banjac, R., Mayor, P., Springman, S. M., & Bronnimann, R. (2006). Full scale tests on geosynthetic reinforced unpaved roads on soft subgrade. *Geotextiles and Geomembranes, 24,* 21–37.

Indian Road Congress 37 (2012). Giudelines for the design of flexible pavements (pp. 370–380). New Delhi, India.

Patra, S., Roy, S. K., Bera, A. K., Chakraborty, S., & Ghosh, A. (2016). Study on effectiveness of jute geotextiles reinforced rural road using ABAQUS. In *National Workshop on Jute Geotextiles* (pp. 17–18), Kolkata, India.

Perkins, S. W., & Edens, M. Q. (2002). Finite element and distress models for geosynthetic-reinforced pavements. *International Journal of Pavement Engineering, 3*(4), 239–250. Taylor & Francis.

Ramaswamy, S. D. & Aziz, M. A. (1989). Jute geotextiles for roads. In *International Workshops on Geotextile* (pp. 137–143), India.

Rao, A. S. (2003). Jute geotextile application in kakinada port area. In *Proceedings, National Seminar on Jute Geotextile & Innovative Jute Products*.

Saad, B., Mitri, H., & Poorooshasb, H. (2006). 3D FE analysis of flexible pavement with geosynthetic reinforcement. *Journal of Transportation Engineering* 402–415. ASCE.

Saha, P., Roy, D., Manna, S., Adhilkari, B., Sen, R., & Roy, S. (2012). Durability of transesterified jute geotextiles. *Geotextiles and Geomembranes, 35*, 69–75. Elsevier.

Taskiran, T. (2010). Prediction of California bearing ratio of fine grained soil AI methods. *Advances in Engineering Software, 41*, 886–892. Elsevier.

Parametric Study on the Behavior of Combined Pile Raft Foundation Founded on Multi-layered Soil Using PLAXIS 3D

Riya T. Johnson, Renjitha Mary Varghese and Jerin Joseph

Abstract The uses of pile raft foundations are common in recent years. The combined effect of pile and raft as foundation can lead to the reduction in total and differential settlements in problematic soil conditions. Many researchers have been done studies to predict the effect of combined pile raft foundations (CPRF) on the response of soil under heavy loads. But most of the numerical studies were done by considering soil as a single layer. The present study aims to find out the effect of pile raft in multi-layered soil using a three-dimensional finite element software PLAXIS 3D. The current parametric study includes the effect of diameter and spacing of piles with varying raft thickness on settlement. It is observed that raft foundation undergoes more settlement than pile raft foundation. The effect of raft thickness has a very little effect on reducing total and differential settlements. The effect of pile diameter and pile spacing was also given useful insight into the behavior of multi-layered soil.

Keywords Combined pile raft foundation · PLAXIS 3D analysis
Multi-layered soil

1 Introduction

The scarcity of land for the future construction has made the man to build high-rise buildings. These buildings will impart huge axial and lateral loads to the soils underneath their foundations. The load transfer mechanism from superstructure to

R. T. Johnson · R. M. Varghese · J. Joseph (✉)
Department of Civil Engineering, Albertian Institute of Science and Technology, Kalamassery, Kochi, Kerala, India
e-mail: jerinjoseph@aisat.ac.in

R. T. Johnson
e-mail: riya.rosemary93@gmail.com

R. M. Varghese
e-mail: renjithamv@aisat.ac.in

B. Adimoolam and S. Banerjee (eds.), *Soil Dynamics and Earthquake Geotechnical Engineering*, Lecture Notes in Civil Engineering 15,
https://doi.org/10.1007/978-981-13-0562-7_24

substructure is usually done by providing suitable foundations. The foundation is the first element of the building where construction starts, but when it fails, it can cause many defects in the building including failure or collapse of the building. The repair of defect in the foundations is most difficult and very costly, so it is most important to design foundation to avoid such failure of building. There are different types of foundations to enhance load transfer mechanism. Raft foundations are one among them to carry the loads from columns and distribute the load in the whole base area of building. When allowable soil pressure is low, or the building loads are heavy, the use of spread footings would cover more than one-half of area and it may prove more economical to use raft foundation. The raft foundation can satisfy the bearing capacity requirement but fails to keep differential as well as total settlement below the maximum allowable limit. Another alternative to the huge load transfer is giving deep foundations. Pile foundation may be adopted instead of a raft foundation where no firm bearing strata exist in any reasonable depth and the loading is uneven. The coastal region of India is found mainly by soft soil, and pile foundations are adopted as the best solution to overcome the low bearing capacity of soft soils. The pile foundation is a deep foundation in which the loads are taken to deeper level. Sometimes the length of the pile foundations will be very large to achieve the load-bearing capacity. The challenges from raft or pile foundation alone can be avoided using the combination of both which is generally known as the combined pile raft foundation (CPRF) system. In piled rafts, the raft directly interacts with soil and it is supported by group of piles of various configurations. The recent projects proved that the pile raft foundation will give most economical length of piles with minimum differential settlement.

2 Review of Literature

Burland et al. (1977) studied the CPRF system and found that pile is the only load-bearing part. But later studies showed that the raft system also takes load. The load sharing by the pile and the raft was studied by many researchers (Shukla et al. 2013; Davids 2008; Randolph 1994) and made designs according to that. Recent studies carried out by Nirmal et al (2014) reported that CPRF is best to provide larger diameter piles to reduce the maximum and differential settlement. Few researches have done studies on the behavior of combined pile raft foundations in layered soils which is very common in the field. Gopinath et al (2010) presented that the increase in raft thickness decreases the overall settlement of pile raft foundation when it is found on layered soils. While it is mentioned that even though the raft thickness does not have any significant effect in layered soils, the raft thickness has a major contribution in reducing the differential settlement (Oh et al. 2008). So this particular paper tries to give more insight into the response of CPRF on layered soil using finite element method.

3 Soil Model

The general stratum of subsoil consists of two soil layers mainly a loose sand layer of 15 m deep overlaid by the next layer of stiff clay of thickness 15 m. The properties of soil layers taken for the model studies are given in Table 1. The groundwater table was at 3 m below ground surface. Extensive parametric studies were carried out by varying surface loads of intensities 200, 400, 600, and 800 kN/m^2 to simulate the loads coming from high-rise buildings.

4 Finite Element Modeling in PLAXIS 3D

The combined response of sand and clay layer was analyzed using finite element method. Three-dimensional analysis was conducted using the software PLAXIS 3D AE. The soil behavior of soil was captured by Mohr–Coulomb model which is an elastic perfectly plastic model. The piles were modeled as linear elastic models. The length and width of the soil model were taken as 50 m, and the thickness was given as 30 m. The boundary conditions were fixed in such way that the boundary effects to the model should be minimal. The sides of the model were allowed to move freely in vertical direction but restrained in both *X* and *Y* directions. The bottom was fixed in all direction, and top of the soil layer was free to displace according to the external loads. The finite element model was analyzed with total stress approach.

5 Validation of the Model

The model was validated for various spacing between the piles under 200 kPa surface load. The model includes five layers of soil. The spacings of pile were taken as 3*d*, 4*d*, 5*d,* and 6*d* with pile diameter as 1 and 0.8 m thick raft. The results obtained from the present studiy matches well with results reported by Oh et al. (2008). Figure 1 shows the validation of the model by plotting the variation of pile spacing with settlement under surface load of 200 kN/m^2.

Table 1 Properties of subsoil used for model studies

Properties	Loose sand	Stiff clay
Thickness (m)	15	15
Unit weight (kN/m^3)	15	16
Saturated unit weight (kN/m^3)	18	19
Undrained cohesion (kN/m^2)	0	80
Friction angle (°)	28°	0
Young's modulus (kN/m^3)	6000	20000
Poison's ratio	0.3	0.35

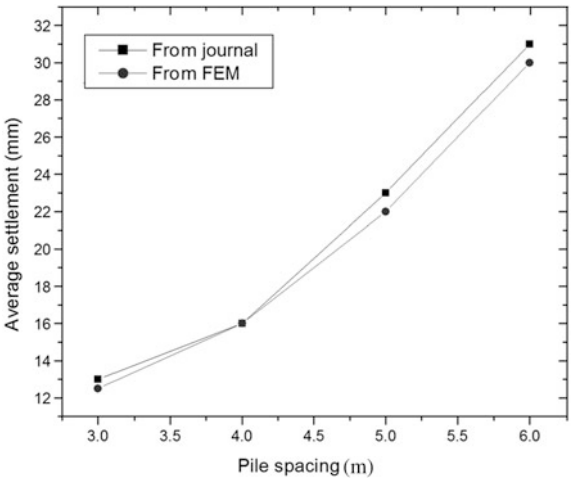

Fig. 1 Average settlement versus pile spacing

6 Parametric Studies

Parametric studies were planned to investigate the settlements of piled raft under the changes in parameters such as diameter of pile, spacing of piles, and raft thickness. The raft was modeled as concrete element, while piles are modeled as series of concrete embedded piles. Various case studies were taken into consideration to analyze the exact behavior of pile raft foundation system. The area of pile raft foundations and length of piles were fixed as 20 m $\times$ 20 m and 18 m, respectively. All studies were carried out considering the two soil strata. The details are listed below:

- Case 1: The effect of raft thickness was analyzed in Case 1 with a constant pile spacing of 4*d*, where diameter (*d*) of the pile was taken as 0.6 m. In this case, piled rafts with varying raft thickness as 0.3, 0.4, 0.6, 0.8, 1 m were modeled and found out the maximum and differential settlements under the surface loads ranging from 200 to 800 kN/m^2 with an increment of 200 kN/m^2.
- Case 2: Case 2 is mainly focused to find out the effect of pile spacing under different loading intensities. In Case 2, pile raft with raft thickness of 0.8 m was modeled by varying the pile spacing as 3*d*, 4*d*, 5*d*, 6*d*, 7*d*. The same surface load increments, and pile diameter was taken as that of Case 1.
- Case 3: Case 3 was included to study the influence of pile diameter on the response of CPRF systems. The other parameters were adopted as the same as that of Case 1.

7 Results and Discussions

The influence of various parameters such as the raft thickness, pile spacing, and pile diameter in a CPRF system is described in detail in the following sections.

7.1 Effect of Raft Thickness

The results obtained from Case 1 analysis are shown in Fig. 2 which shows the variation of maximum settlement with respect to raft thickness. There was a significant increase in both the settlements with increase in surface loads. The maximum settlement was found to be 20 cm under all surface loads except at the maximum surface load of 800 kN/m^2. It can be concluded that the maximum settlement decreases as the raft thickness increases in all loading cases (Fig. 2). On the other hand, the comparison of raft thickness on maximum settlement shows that there was little effect on the maximum settlement when raft thickness was varied from 0.3 to 1 m. In addition to that, the construction becomes uneconomic if raft thickness increases beyond 1 m. In view of these reasons, it can be summarized that the increasing the raft thickness does not have much significant influence in combined pile raft foundation and it is uneconomical after certain limits. The maximum and differential settlements were increased with increase in surface loads under multiple layers of soils (Figs. 2 and 3). Figure 3 also defines the variation differential settlement with raft thickness.

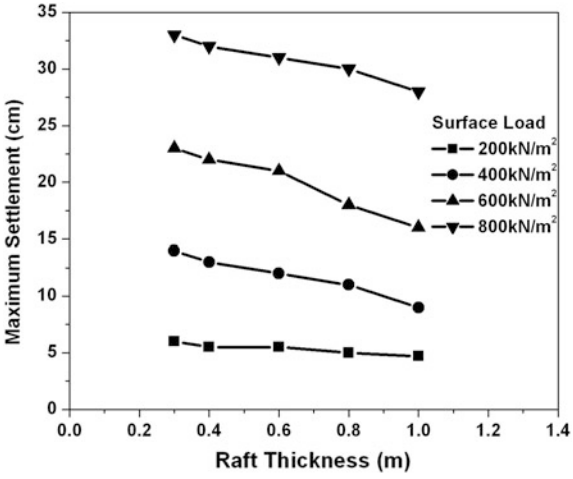

Fig. 2 Maximum settlement with varying raft thickness

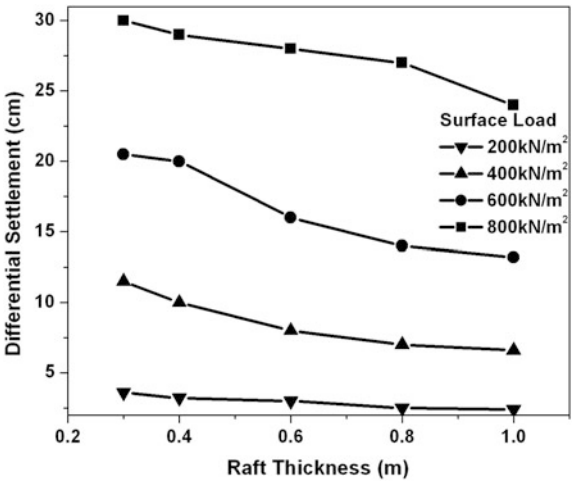

Fig. 3 Differential settlement with varying raft thickness

7.2 *Effect of Pile Spacing*

The variations in settlement due to different pile spacing are shown in Figs. 4 and 5. When the intensity of loading greater is than 200 kN/m^2, the increase in pile spacing has an adverse effect on the maximum and differential settlement under various loads.

The results showed that for 200 and 400 kN/m^2, both settlements were less than 10 cm, while the spacings between the piles were taken as 3*d* and 4*d*.

The differential settlements were found to be less than the maximum settlement in all cases. When the surface loads were increased from 200 to 800 kN/m^2, the

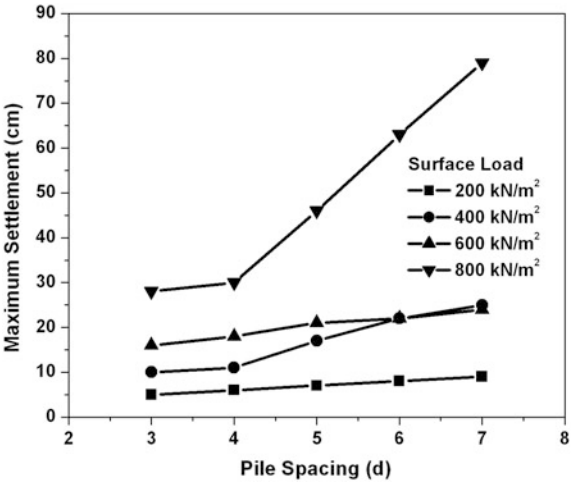

Fig. 4 Maximum settlement with varying pile spacing

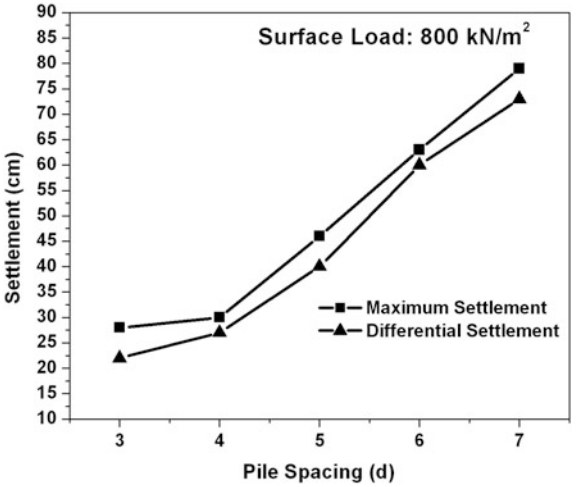

Fig. 5 Differential settlement with varying pile spacing

analysis with multi-layer soil strata has proved that the difference between the total settlement and differential settlement was decreased significantly (Fig. 5).

7.3 Effect of Pile Diameter

The diameter has a major effect on reducing the settlements. Figure 6 depicts the variations of settlement under various pile diameters and surface loads. It was found that both differential and total settlements of structure increase drastically at high values of vertical load intensity. The variation is found to be nonlinear (Fig. 7).

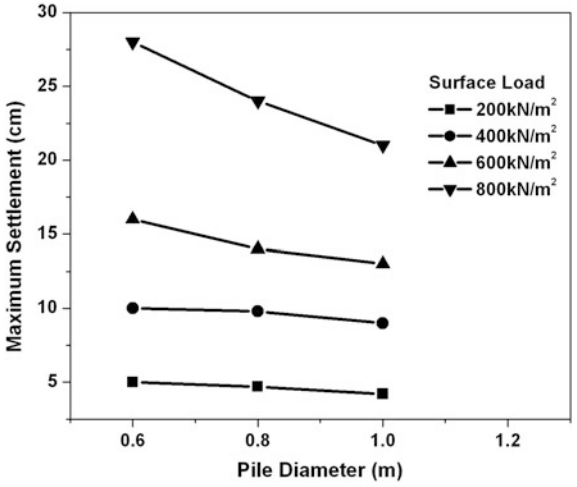

Fig. 6 Maximum settlement with varying pile diameter

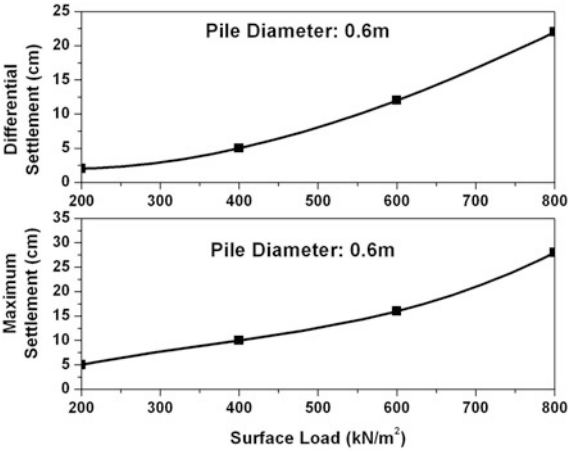

Fig. 7 Nonlinear variation of settlement with load

When pile diameter increased from 0.6 to 1 m, the reduction of both settlements was less than 20% for all vertical load intensities except 800 kN/m^2. The surface load of 800 kN/m^2 gave very high value of both maximum and differential settlements.

8 Conclusions

A set of studies were conducted on pile raft foundation in multi-layered soil to measure the soil response. The following conclusions can be drawn from the present studies.

- The raft thickness does not have significant effect on maximum and differential settlements.
- Pile spacing has important role in the performance of piled raft foundation. Both maximum settlement and differential settlement reduce with decrease in pile spacing.
- The pile diameter also plays an important role in reducing the settlements. Increase in pile diameter shows a decrease in maximum and differential settlements under all loading intensities.

References

Burland, J. B., Broms, B. B, & Demello, V. (1977). Behavior of foundation and structures. In *Proceedings of 9th ICSMFE*, Tokyo (pp. 495–546).

Davids, A. (2008). A postcard from Dubai design and construction of some of the tallest buildings in the world. In *Proceedings of the CTBUH 8 the World Congress*, 3–5 March, Dubai.

Gopinath, B., Junija, A., & Agarwal, A. (2010). Numerical modeling of piled raft foundation in soft clays. In *Indian Geotechnical Conference*, December 16–18, 2010, IIT Bombay.

Nirmal, J. J., & Hashifa, H. (2014). 'Study on settlement characteristics of combined pile raft foundation founded on sands with various arrangements of piles using Plaxis 3D. *International Journal of Emerging Technology and Advanced Engineering, 4*.

Oh, E. Y. N., Buli, Q. M., Surarak, R., & Balasubramaniam, B. (2008). Finite element modeling for piled raft foundation in sand. In *Eleventh East Asia-Pacific Conference on Structural Engineering & Construction*, November 19–21, Taiwan.

Randolph, M. F. (1994). *Design methods for pile groups and piled raft* (S.O.A. Report, 13 ICSMFE, New Delhi) Vol. 5, pp. 61–82.

Shukla, S. J., Desai, A. K., & Solanki, C. H. (2013). A dynamic behavioral study of 25 storey building with piled raft foundation with variable subsoil. *International Journal of Advance Research in Science and Engineering, 2*(1), 119–130.

Numerical Analysis of Seismic Response of a Piled Raft Foundation System

Ramon Varghese, A. Boominathan and Subhadeep Banerjee

Abstract Piled raft foundation is gaining popularity as a composite foundation system economizing foundation design for tall, heavy structures. The seismic response of a piled raft foundation would involve complex raft–soil–pile interaction as well as pile–soil–pile interaction, which cannot be estimated efficiently by existing methods available for pile groups. This paper discusses the development of a numerical model to study the seismic response of piled raft foundation system by substructure method-based seismic soil-structure interaction (SSSI) analysis using SASSI 2010 program. The flexible volume substructure method is used to analyze SSSI problem. Published data from a centrifuge test to study earthquake response of a piled raft system in soft clay was selected for the simulation. Results from the analysis are compared with experimental data.

Keywords Soil-structure interaction · Piled raft · Substructure method
Flexible volume method · SASSI

1 Introduction

The concept of a piled raft foundation that shares load between raft and pile is not new. Several papers published during the 1970s threw light onto the behavior and analysis of piled raft (PR) systems. Over the years, the use of piled raft foundation systems for buildings has gained popularity owing to an increase in the availability of case histories and guidelines. In regions where seismic activity is high, the design

R. Varghese (✉) · A. Boominathan · S. Banerjee
Department of Civil Engineering, Indian Institute
of Technology Madras, Chennai 600 036, India
e-mail: ramonvarghese@gmail.com

A. Boominathan
e-mail: boomi@iitm.ac.in

S. Banerjee
e-mail: subhadeep@iitm.ac.in

B. Adimoolam and S. Banerjee (eds.), *Soil Dynamics and Earthquake Geotechnical Engineering*, Lecture Notes in Civil Engineering 15,
https://doi.org/10.1007/978-981-13-0562-7_25

of any foundation system has to be done keeping in mind the seismic response characteristics. Ignoring soil-structure interaction effects could potentially lead to unsafe design or even may cause failure. For composite foundation systems like the piled raft particularly founded in multi-layered soil system, dynamic analysis cannot be done by simple analytical techniques. However, a seismic response analysis requires the use of numerical tools like the finite element or finite difference methods for reliable results. This study aims to develop a 3D model to estimate the seismic response of a piled raft system considering both inertial and kinematic interactions.

2 Literature Review

Several methods of static analysis of PR foundation systems have been published in the literature. Soil-structure interaction becomes significant for heavy structures, which may significantly interact with the ground. Hence, the practice of using ground surface acceleration for seismic analysis cannot be deemed safe. Research on horizontal/seismic loads on piled rafts is limited. In comparison to pile groups, piled rafts usually have lesser number piles. This can result in higher loads on piles, under seismic loading compared to a pile group. To better understand the performance of piled rafts under seismic loading, several researchers including Yuksekol et al. (2015) have performed 1-g shake table tests. They observed an increase in horizontal load resistance and the influence of vertical displacement due to horizontal loads on the vertical resistance of piles.

Centrifuge studies to evaluate seismic response of piled rafts were carried out by Sawada and Takemura (2014) and Horikoshi et al. (2002). They observed settlement of the piled raft during horizontal loading and shaking table tests, as well as reduction in raft resistance to horizontal load compared to a raft alone. Banerjee (2009) investigated the response of piled raft in soft clay subjected to seismic excitation. The piles used were of short nature, and the finding suggests that surrounding soil imposed an inertia load to the piled raft structure, thereby lengthening its resonance period. The 3D numerical simulation performed by the author could replicate the centrifuge model reasonably well.

Seismic response of a single degree of freedom superstructure on an idealized piled raft foundation was studied by Saha et al. (2015) using a simplified numerical model involving Winkler foundation concept. Mayoral et al. (2009) compared actual seismic response of an urban bridge support system on soft clay with computed results using SASSI 2000 program by flexible volume method.

A review of the literature suggests that there is limited understanding of the seismic behavior of piled raft foundation systems. Given the capabilities of modern computational facilities, it is feasible to study the seismic response of piled raft systems using numerical simulations. The present study was aimed at developing a numerical model for a substructure-based seismic analysis of a piled raft foundation system using SASSI 2010.

3 Details of Piled Raft System

Experimental data from the centrifuge study on seismic response of a piled raft foundation in system in soft clay by Banerjee (2009) was chosen for the numerical simulation. The PR foundation considered for modeling in the present study has a raft dimension of 12.5 m × 7.5m × 0.5m, and four piles with diameter 0.9 m and length of 13 m. These prototype dimensions were modeled in the centrifuge test using a rigid steel plate of 25 cm × 15 cm × 1 cm and the four solid steel piles of 1.8 cm diameter and 26 cm long with the test being performed at 50 g. The vertical load applied on the raft in prototype scale would be 605 tonnes.

4 Flexible Volume Substructure Method

The flexible volume substructuring method is based on the concept of partitioning the total soil structure system into three substructures (SASSI 2010) as presented in Fig. 1. The first substructure consists of free-field site, second substructure consists of excavated soil volume, and third substructure consists of structure, of which the foundation represents excavated soil volume.

The three substructures together form the soil-structure interaction system. The flexible volume method considers interaction between free-field site and excavated soil volume at the boundary as well as within the excavated soil volume.

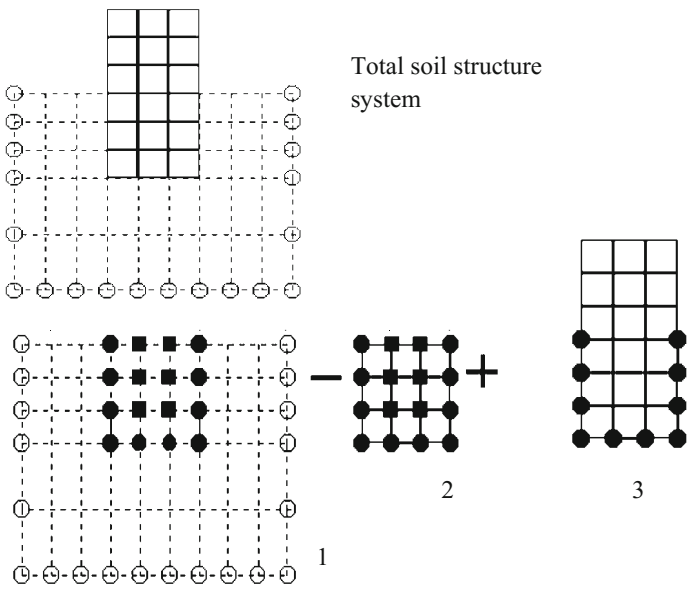

Fig. 1 Substructuring in the flexible volume method (Ostadan and Deng 2010)

The substructuring in the SASSI code is formulated using the complex response method and finite element technique. Free-field soil is modeled using horizontal layers of viscoelastic material, resting on a viscoelastic half-space. Both horizontal layering and viscoelastic material property are inherent limitations of the SASSI code. It should also be noted that analysis in frequency domain is several times faster than an analysis using the direct method.

5 Description of Numerical Model

5.1 Foundation

The raft is modeled using four-noded brick elements with stiffness property similar to that of steel used in the experiment. Material properties of structural elements used in the analysis for the PR system are presented in Table 1. The load of 605 tonnes was applied uniformly on the top surface of the raft. There are several techniques of modeling piles including the use of beam elements, volume elements, and inter-pile elements available in the SASSI finite element library. Beams could be used for modeling piles owing to their flexural characteristics; however, due to their inability to simulate actual soil resistance, the model is predicted to be less accurate. Nakaia et al. (2004) suggest that beam element modeling underestimates impedance functions and overestimates foundation input motions.

In the present study, piles in the piled raft system were modeled using brick elements. Flexural rigidity of the prototype pile dimension is 10,308,351 kN m^2 (Banerjee 2009). The modulus of elasticity of pile was then back-calculated using the flexural rigidity and moment of inertia of the pile section. Figure 2 shows the finite element mesh of the piled raft system with both raft piles modeled using four-noded brick elements. The total number of interacting nodes in the model was 1550.

5.2 Soil Properties

The modeling of soil layers using viscoelastic layers makes it a linear model, which cannot predict the cyclic changes in dynamic soil properties. In order to account for modulus reduction and damping increase, due to shear strain developed as the shear wave propagates, an equivalent linear ground response analysis is first performed

Table 1 Material properties used for structural elements

Component	Modulus of elasticity (GPa)	Poisson's ratio	Unit weight (kN/m^3)
Raft	200.0	0.25	78.5
Pile	320.1	0.25	78.5

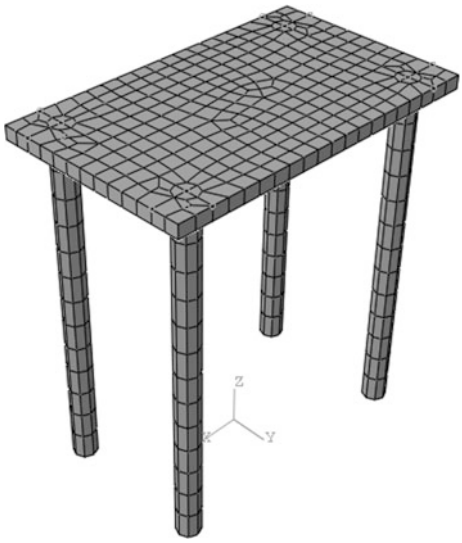

Fig. 2 Finite element mesh of the piled raft foundation

using the program SHAKE 2010. The soft kaolin clay used in the laminar shear box for the centrifuge test had a bulk unit weight of 16 kN/m^3, water content of 66%, liquid limit of 80%, and plastic limit of 35%. Initial modulus and damping values are taken from the results of dynamic tests on the kaolin clay as reported in Banerjee (2009). The variation of G_{max} with depth (or mean effective stress p') was calculated based on Eq. (1) suggested by Banerjee 2009. The resulting s-wave velocity, V_s, p-wave velocity, V_p, and damping ratio, ξ, for each layer are then used in the SASSI analysis.

$$G_{max} = 2060p'^{0.653} \tag{1}$$

The dynamic soil properties obtained from ground response analysis for the earthquake motion are presented in Table 2. In short, non-linearity of soil is accounted for partially by using soil properties that that will result after a seismic event. A total of 15 soil layers were defined in addition to the half-space below the 15th layer. Viscous boundary developed by Lysmer and Kuhlemeyer (1969) is used in the SASSI program.

5.3 Input Motion

The earthquake motion used in the centrifuge test as reported in Banerjee (2009) was used in the present study. The time history of acceleration was synthetically developed using typical response spectra of Sumatran earthquakes measured at rock sites in Singapore. The input motion time history with peak ground acceleration

Table 2 Dynamic soil properties used in the analysis

Layer no.	Thickness (m)	V_s(m/s)	V_p(m/s)	ξ
1	0.5	45.71	76.56	0.001
2	1	64.53	108.08	0.006
3	1	75.30	126.12	0.009
4	1	83.53	139.90	0.011
5	1	90.19	151.06	0.012
6	1	95.83	160.50	0.013
7	1	100.84	168.89	0.013
8	1	105.40	176.53	0.013
9	1	109.60	183.56	0.014
10	1	113.51	190.11	0.014
11	1	117.19	196.28	0.014
12	1	120.68	202.12	0.014
13	1	124.00	207.68	0.014
14	1	127.17	212.99	0.014
15	0.5	124.94	201.86	0.056

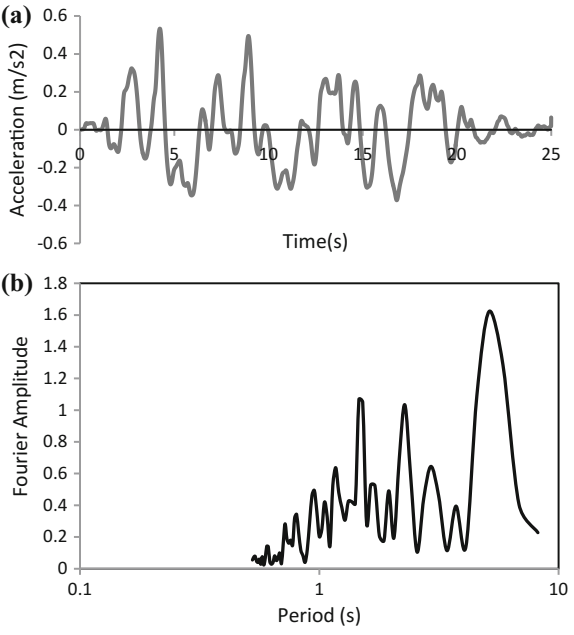

Fig. 3 **a** Time history of acceleration and **b** Fourier amplitude spectrum of input motion

(PGA) of 0.053 g is presented in Fig. 3a along with its Fourier spectrum in Fig. 3b. The earthquake has typical characteristics of far-field events including long periods and long durations.

6 Results and Discussion

The results extracted from the program after analysis presented in this paper include time history acceleration and response spectrum at the top of raft. The time history of acceleration is obtained at the top of raft along with time history obtained from the centrifuge test and presented in Fig. 4. The peak acceleration value recorded at the top of raft in the centrifuge test was 0.69 m/s^2, while the simulation produced a peak acceleration of 0.57 m/s^2.

Fourier spectra of acceleration recorded at the top of raft from both experiment and the simulation are presented in Fig. 5. The simulation has been able to reproduce most of the predominant frequencies, however, with some variation in Fourier amplitude. It is observed from the Fourier spectra that in the simulation the amplitude is de-amplified by about 10–20% at the range of period from 2 to 3 s, whereas at a period of around 5 s the amplification is about 23%. Response spectra obtained at the top of raft from both experiment and simulation are presented in Fig. 6. For the simulation, the highest peak spectral acceleration is observed near a period of 1.46 s, which is close to the peak from centrifuge test.

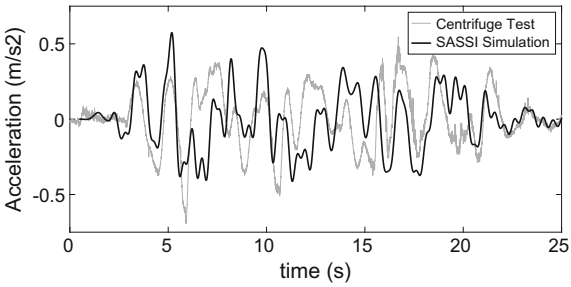

Fig. 4 Comparison of time histories of acceleration at top of raft for second earthquake

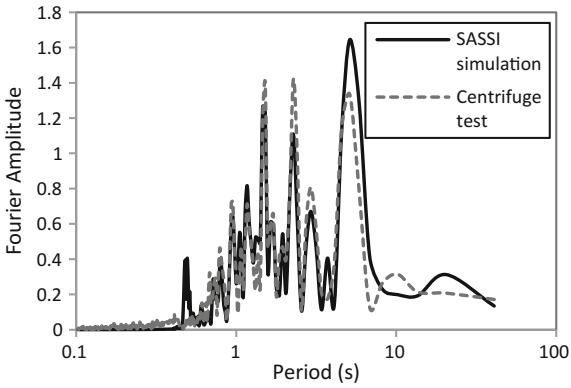

Fig. 5 Fourier spectra of acceleration at the top of raft

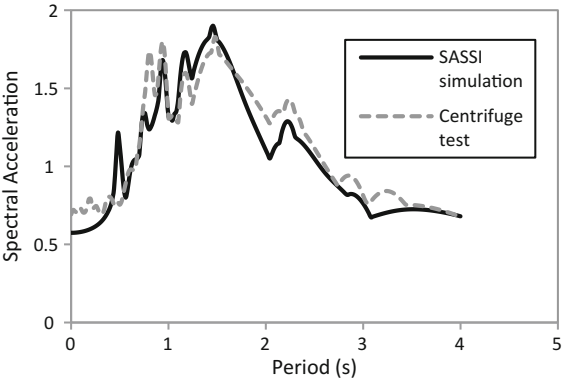

Fig. 6 Response spectra at the top of raft

7 Conclusion

A model to study seismic response of piled raft foundation is developed in the substructure-based soil-structure interaction program SASSI 2010. Published data from a dynamic centrifuge test on a piled raft system in soft clay subjected to an earthquake excitation was selected for the simulation. A pile raft foundation system with four piles in homogeneous soft clay was subjected to earthquake excitation, and its behavior was studied. Degraded soil properties from a one-dimensional ground response analysis were used in the SSSI analysis. The results in terms of time history of acceleration, Fourier spectrum, and response spectrum are compared with data from the centrifuge test. The simulation was found to be in reasonable agreement with measured data. The applicability of the model needs to be further verified by analysis using different input motions.

References

Banerjee, S. (2009). *Centrifuge and numerical modelling of soft clay-pile-raft foundations subjected to seismic shaking*. PhD dissertation, National University of Singapore.

Horikoshi, K., Matsumoto, T., Watanabe, T., & Fukuyama, H. (2002). Performance of piled raft foundations subjected to seismic loads. In *Foundation design codes and soil investigation in view of international harmonization and performance* (pp. 381–389).

Lysmer, J., & Kuhlemeyer, R. L. (1969). Finite element model for infinite media. *Journal of Engineering Mechanics Division, 95,* 859–877.

Mayoral, J. M., Alberto, Y., Mendoza, M. J., & Romo, M. P. (2009). Seismic response of an urban bridge-support system in soft clay. *Soil Dynamics and Earthquake Engineering, 29*(5), 925–938.

Nakaia, S., Katoa, H., Ishidaa, R., Manob, H., &Nagatac, M. (2004). Load bearing mechanism of piled raft foundation during earthquake. In *Proceedings of 3rd UJNR Workshop on Soil-Structure Interaction*, March 29–30.

Ostadan, F., & Deng, N. (2010). *SASSI 2010, User's Manual*. Berkeley: Geotechnical Engineering Division, Civil Engineering Department, University of California.

Saha, R., Dutta, S. C., & Haldar, S. (2015). Seismic response of soil-pile raft-structure system. *Journal of civil engineering and management, 21*(2), 144–164.

Sawada, K., & Takemura, J. (2014). Centrifuge model tests on piled raft foundation in sand subjected to lateral and moment loads. *Soils and Foundations, 54*(2), 126–140.

Yuksekol, Y. U., Matsumoto, T., & Shimono, S. (2015). Shaking table tests of piled raft and pile group foundations in dry sand. In *Proceedings of 6th International Conference on Earthquake Geotechnical Engineering*, 1–4 November, Christchurch, New Zealand. ICEGE.

Ultimate Pullout Capacity of Isolated Helical Anchor Using Finite Element Analysis

P. Ghosh and S. Samal

Abstract In this paper, the ultimate pullout capacity of single isolated helical anchor resting in homogeneous soil deposit with different helix configurations is determined using finite element analysis. The anchor is pulled to its ultimate failure controlling the displacement. Eight different types of anchor configuration are considered in the analysis, where mainly the number of helical plates, the depth of upper- and lowermost helical plates, and the ratio of spacing between the helical plates to the diameter of the plate are varied. The variation of load–displacement curve for each anchor configuration is obtained, and subsequently, the ultimate uplift capacity of each anchor is determined by using double-tangent method. The soil is assumed to follow Mohr–Coulomb failure criteria. The present theoretical observations are generally found in good agreement with those theoretical and experimental results available in the literature.

Keywords Finite element analysis · Helical anchor · Homogeneous soil Plasticity · Pullout capacity

1 Introduction

The anchor is a foundation system generally designed and constructed to transmit any uplift force and overturning moments coming from a structure to the underlying soil. Anchors are important for many engineering applications such as transmission towers, suspension bridges, tall chimneys, high-rise structures which experience lateral load like wind load, buried pipelines under water, offshore structures as well as tunnel construction. As compared to the installation of conventional plate anchor, helical anchor is quite easy to install and is quite cost-effective, which may be used both in tensile and compressive loading condition. Basically, helical anchors are

P. Ghosh (✉) · S. Samal
Department of Civil Engineering, Indian Institute of Technology Kanpur, Kanpur 208016, India
e-mail: priyog@iitk.ac.in

B. Adimoolam and S. Banerjee (eds.), *Soil Dynamics and Earthquake Geotechnical Engineering*, Lecture Notes in Civil Engineering 15,
https://doi.org/10.1007/978-981-13-0562-7_26

geotechnical foundations consisting of central steel shaft and number of helical plates welded along the shaft. These helical plates are generally made up of steel and are formed with a definite pitch. The anchor shaft is used to transmit torque during installation and to transfer loads to the helical plates. A number of investigations have been performed by several researchers to predict the uplift resistance of the plate anchor with the help of different numerical as well as experimental investigations. However, the work on the helical anchor is still scarce. From the literature, it has been seen that few research works (Ghaly et al. 1991; Rao and Prasad 1993; Ghaly and Clemence 1998; Hanna et al. 2007; Lutenegger 2011; Mittal and Mukherjee 2013; Nazir et al. 2013; Wang et al. 2013; Demir and Ok 2015) have been carried out to determine the ultimate uplift capacity of helical anchor theoretically as well as experimentally. From the reported investigations, it can be clearly understood that the ultimate uplift capacity of helical anchor depends upon the number of helical plates, the depth of upper- and lowermost helical plates, the ratio of spacing between the helical plates to the diameter of the plate, and embedment depth.

In the present investigation, a numerical study on the pullout capacity of single isolated helical anchor embedded in homogeneous soil layer has been carried out using finite element method developed in the framework of three-dimensional failure domain in ABAQUS 6.13.

2 Definition of the Problem

A single isolated helical anchor with multiple helical plates of diameter, D, is embedded in a homogeneous soil layer with an embedment ratio, $\lambda = H/D$, where H is the embedment depth of the uppermost helical plate (Fig. 1). The helical anchor is made up of steel, and the surface is assumed to be perfectly rough. The soil is assumed to obey Mohr–Coulomb failure criteria. The objective is to determine the magnitude of uplift capacity of the helical anchor, where the anchor is pulled with an incremental velocity in the upward direction for calculating the uplift loading capacity. Full failure domain is considered for the analysis as the helical anchor is not truly an axi-symmetric member.

3 Material and Geometry

3.1 Material

To determine the uplift capacity of the helical anchor, a single-layer homogeneous soil deposit is considered. The properties of the soil deposit have been taken from

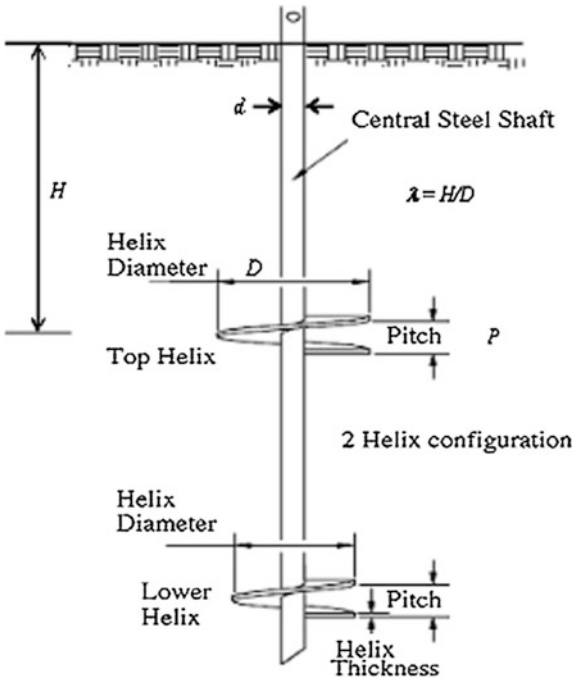

Fig. 1 Schematic diagram of helical anchor

Table 1 Properties of soil deposit (Wang et al. 2013)

Young's modulus (E) (kN/m^2)	Undrained cohesion (c_u) (kN/m^2)	Unit weight (γ) (kN/m^3)	Poisson's ratio (υ)	Angle of internal friction ($\phi°$)
12.75×10^3	12.75	16	0.4	0

Table 2 Properties of steel anchor

Young's modulus (E) (kN/m^2)	Density (ρ) (kg/m^3)	Poisson's ratio (υ)
2.1×10^8	7800	0.25

Wang et al. (2013) and are mentioned in Table 1, whereas the properties of steel anchor used in the analysis are given in Table 2.

3.2 Anchor Configuration

Eight different anchor configurations have been considered for the analysis (Fig. 2) whose geometric specifications (Table 3) are taken from Wang et al. (2013). It can

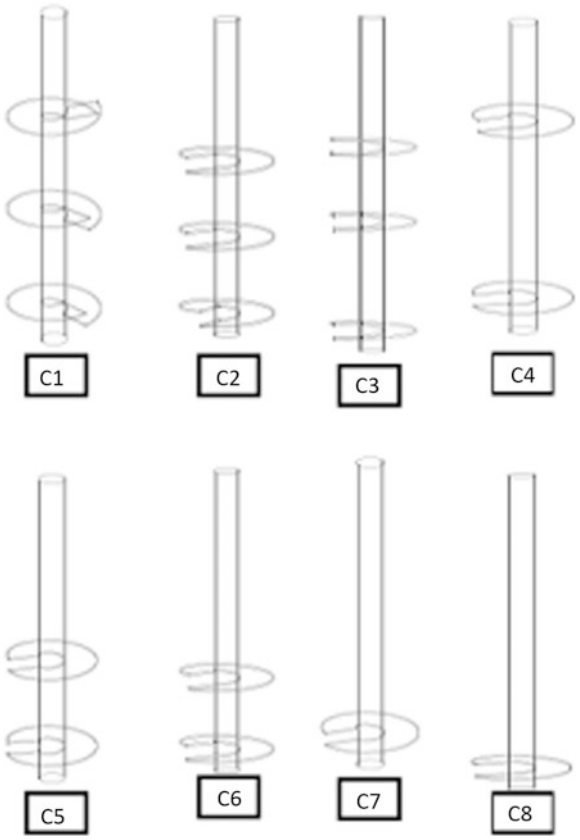

Fig. 2 Configuration of helical anchors

be seen from Fig. 2 that C1–C3 consist of three helical plates, C4–C6 consist of two helical plates, and C7–C8 comprise of single helical plate. For any particular anchor, the spacing between two plates (S_p) is kept constant except C3, where the spacing is unequal among the plates. The diameter of the helical plate and the central shaft is considered as 2.4 and 0.4 m, respectively, whereas the pitch of the helix (P) is taken as 0.46 m. The thickness of the helical plate is assumed as 0.1 m, which is considered to be negligible as compared to the diameter of the helical plate.

4 Analysis

The present finite element analysis has been performed using commercially available software ABAQUS 6.13. The numerical analysis has been carried out in 3D model. The whole soil domain is assumed to be at undrained condition. The soil

Table 3 Geometric details of different anchor configuration (Wang et al. 2013)

Configuration	Number of helical plates	Depth of uppermost plate, H (m)	Depth of lowermost plate (m)	Spacing between plates, S_p (m)	S_p/D
C1	3	2.65	9.85	3.6	1.5
C2	3	2.65	7.45	2.4	1.0
C3	3	2.65	8.65	2.4, 3.6	1, 1.5
C4	2	2.65	9.85	7.2	3
C5	2	6.25	9.85	3.6	1.5
C6	2	5.05	7.45	2.4	1
C7	1	6.25	6.25	–	–
C8	1	9.85	9.85	–	–

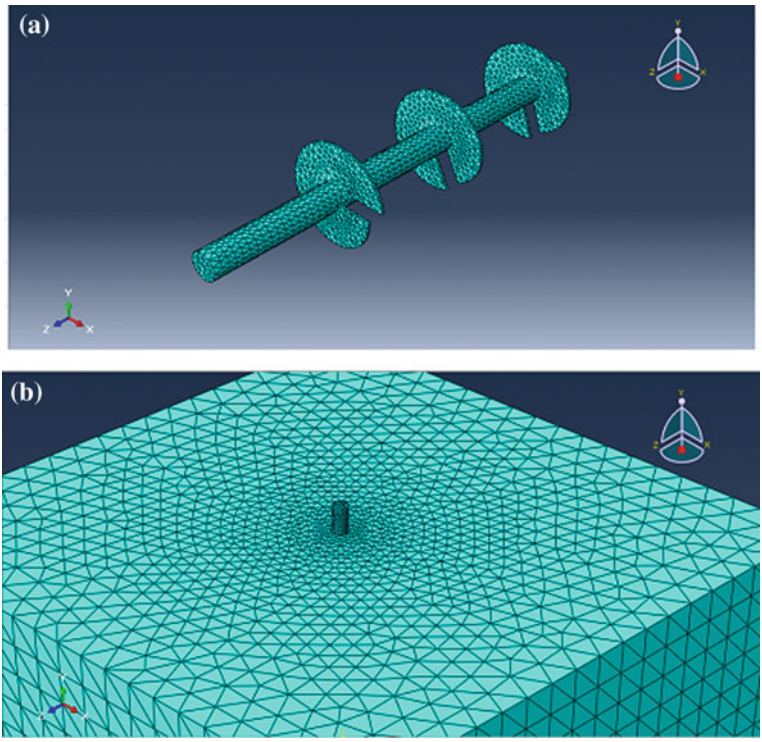

Fig. 3 Overview of **a** AutoCAD drawing and finite element meshing of C1 anchor, **b** finite element meshing of soil domain

deposit is assumed to follow Mohr–Coulomb failure criteria available in ABAQUS. Due to complicated geometry, the helical anchor is first designed in AutoCAD and then imported to ABAQUS. The finite element meshing has been done using four

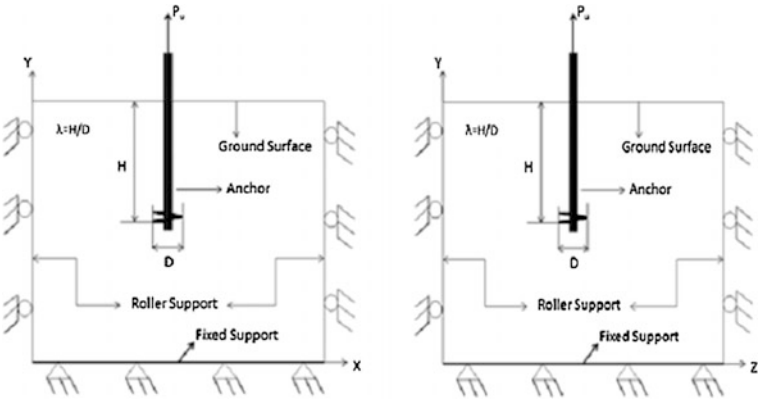

Fig. 4 Boundary conditions along XY and YZ plane

nodded tetrahedral elements. The AutoCAD drawing of helical anchor and the details of finite element meshing are shown in Fig. 3. In the analysis, general contact properties are used to simulate the interaction among all the surfaces. All the interacting surfaces are considered as penalty for tangential behavior and hard for normal behavior. The penalty behavior denotes that there is a finite coefficient of friction value between the surfaces and no slip occurs. In this analysis, the penalty value is taken as 0.1 as the soil is cohesive one (Table 1). The following boundary conditions are considered in the present analysis (Fig. 4).

- Displacements along X-axis, u_X are set to zero on the vertical boundaries parallel to YZ plane.
- Displacements along Z-axis, u_Z are set to zero on the vertical boundaries parallel to XY plane.
- All displacements are set to zero on the bottom boundary, i.e., $u_X = u_Y = u_Z = 0$.

Sensitivity analysis has been performed in order to determine the optimum domain size. For finding out the optimum domain size, anchor C1 and anchor C8 are chosen. The main reason behind choosing these two configurations is that C1 anchor configuration is having three helical plates with uniform spacing between the plates, and the lower plate is embedded at a depth of 9.85 m, which is the maximum depth considered in the present analysis, whereas C8 configuration is having single helical plate with embedment depth of 9.85 m. In this study, the depth of the soil deposit is fixed at 12.5D. It is found that beyond 7D in the horizontal direction, no significant change in the ultimate uplift capacity gets observed, and hence, the optimum domain size in the horizontal direction is selected as 7D from the center of the anchor.

5 Results and Discussion

In Figs. 5 and 6, the normalized load–displacement curves for isolated helical anchor placed in single-layer homogeneous soil deposit are shown for different configurations from C1 to C8, where P is the uplift capacity and is the vertical displacement of the anchor. The ultimate uplift capacity (P_u) of the anchor has been obtained by considering double-tangent method. It can be seen from Fig. 5a that for the same embedment depth of the lowermost helical plate, the anchor having three helical plates provides higher uplift capacity as compared to that with double and single helical plates. It can be observed from Figs. 5b and 6a that with the same number of helical plates, the uplift capacity increases with increase in S_p/D ratio. It can be also noticed from Fig. 6b that for the anchor with single helical plate the uplift capacity increases with increase in embedment depth ($\lambda = H/D$). The variation of ultimate uplift capacity for different anchor configurations is shown in Fig. 7. It can be seen that the magnitude of P_u increases with increase in S_p/D and the depth of lowermost helical plate.

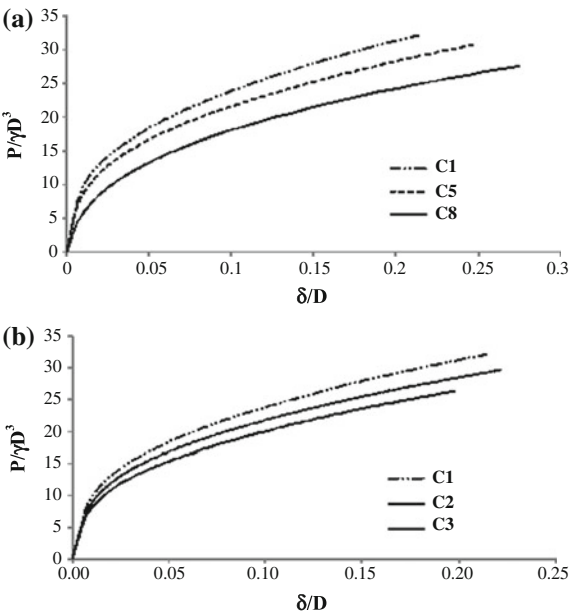

Fig. 5 Normalized load–displacement curve for isolated helical anchor with **a** same depth of lowermost helical plate, **b** three helical plates

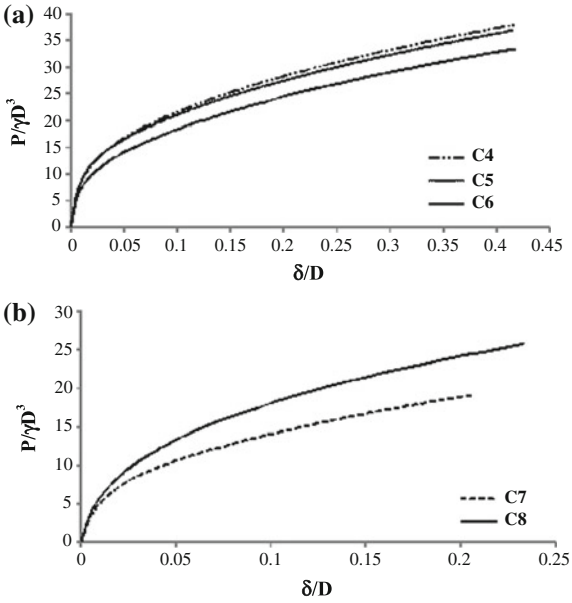

Fig. 6 Normalized load–displacement curve for isolated helical anchor with **a** two helical plates, **b** single helical plate

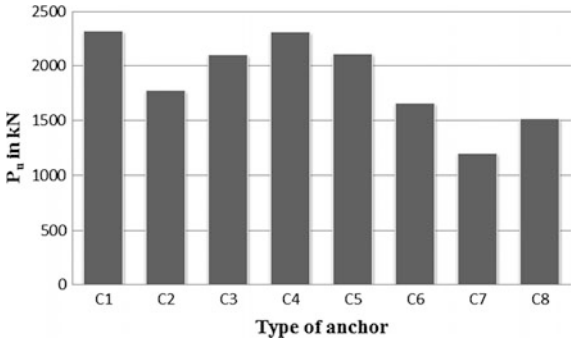

Fig. 7 Variation of P_u for different anchor configurations

6 Comparison

In Table 4, the magnitude of P_u for different anchor configurations obtained from the present finite element analysis is compared with the values reported by Wang et al. (2013). It can be seen that the present values compare reasonably well with the experimental and numerical results proposed by Wang et al. (2013).

Table 4 Comparison of P_u for different anchor configurations

Configuration	P_u (kN)		
	Present analysis	Wang et al. (2013)	
		Experimental analysis	Numerical analysis
C1	2320	1987	2381
C2	1775	1780	1755
C3	2100	2003	2068
C4	2310	1971	2343
C5	2110	1930	2166
C6	1660	1513	1666
C7	1200	1351	1171
C8	1520	1715	1504

7 Conclusions

In the present study, the ultimate uplift capacity of single isolated helical anchor is determined using finite element analysis. Eight different configurations of helical anchor are considered in the analysis. The uplift capacity of helical anchor is found to increase with increase in S_p/D ratio and λ. The magnitude of P_u is found to increase with increase in S_p/D and the depth of lowermost helical plate. The present results compare well with the results available in the literature.

References

Demir, A., & Ok, B. (2015). Uplift capacity of multi-plate helical anchors in cohesive soil. *Geomechanics and Engineering, 8*(4), 615–630.

Ghaly, A., Hanna, A., Ranjan, G., & Hanna, M. (1991). Helical anchors in dry and submerged sand subjected to surcharge. *Journal of Geotechnical Engineering, ASCE, 117*(10), 1463–1470.

Ghaly, A. M., & Clemence, S. P. (1998). Pullout performance of inclined helical screw anchors in sand. *Journal of Geotechnical and Geoenvironmental Engineering, ASCE, 124*(7), 617–627.

Hanna, A., Ayadat, T., & Sabry, M. (2007). Pullout resistance of single vertical shallow helical and plate anchors in sand. *Geotechnical and Geological Engineering, 25*(5), 559–573.

Lutenegger, A. J. (2011). Behavior of multi helix screw anchor in sand. In *Pan-Am CGS Geotechnical Conference*.

Mittal, S., & Mukherjee, S. (2013). Vertical uplift capacity of a group of helical screw anchors in sand. *Indian Geotechnical Journal, 43*(3), 238–250.

Nazir, R., Chuan, H. S., Niroumand, H., & Kassim, K. A. (2013). Performance of single vertical helical anchor embedded in dry sand. *Measurement, 49,* 42–51.

Rao, S. N., & Prasad, Y. V. S. N. (1993). Estimation of uplift capacity of helical anchors in clays. *Journal of Geotechnical Engineering, ASCE, 119*(2), 352–357.

Wang, D., Merifield, R. S., & Gaudin, C. (2013). Uplift behaviour of helical anchors in clay. *Canadian Geotechnical Journal, 50,* 575–584.

Part III
Geohazards: Analysis, Mitigation and Management

Landslide Risk Assessment and Mitigation—A Case Study

A. R. Amashi, A. M. Hulagabali, C. H. Solanki and G. R. Dodagoudar

Abstract Landslides are defined as down slope movement of rock, debris and earth under the influence of gravity. Slide is one of the most common types of hazards on slopes, which might lead to considerable casualties and economic loss. The study and analysis of slope is essential in understanding their performance and, in particular, their stability, reliability and deformations. The aim of the present study is to analyse the typical slope by varying different soil parameters like cohesion, angle of internal friction, water table and also slope geometry such as slope angle and slope height. The stability of the slope is analysed based on numerical simulation using three geotechnical software namely Slope/W, SV-Slope and Plaxis 2D. The study further is directed towards the assessment of stability of landslide along State Highway-72, near Mahabaleshwar, Maharashtra. The analysis of slope is carried out using Slope/W and Plaxis 2D. It was found through the analysis that the slope was unstable under the saturated condition. In an attempt of suggesting suitable remedial measures for the same, soil nailing is provided for the slope and simulation is carried out using Geo-5/Nailed slope software. As a result, the slope was found stable after the application of soil nailing.

Keywords Landslide · Numerical simulation · Factor of safety
Remediation

A. R. Amashi (✉) · A. M. Hulagabali
Department of Civil Engineering, Basaveshwar Engineering College, Bagalkot, Karnataka, India
e-mail: ashwini.amashi@gmail.com

A. M. Hulagabali
e-mail: anandmhulagabali@gmail.com

C. H. Solanki
Applied Mechanics Department, SVNIT Surat, Surat, Gujarat, India
e-mail: chs@amd.svnit.ac.in

G. R. Dodagoudar
Department of Civil Engineering, IIT Madras, Chennai, Tamil Nadu, India
e-mail: goudar@iitm.ac.in

B. Adimoolam and S. Banerjee (eds.), *Soil Dynamics and Earthquake Geotechnical Engineering*, Lecture Notes in Civil Engineering 15,
https://doi.org/10.1007/978-981-13-0562-7_27

1 Landslide

1.1 Introduction

Landslides are a serious geologic hazard that involves all varieties of mass movements of hill slopes resulting from the failure of the materials such as rock, soil, debris, artificial fills driven by the force of gravity. These landslides not just cause an extensive damage to the property but also cause loss of lives. The triggering factors responsible for landslides are rainfall, rapid snowmelt, earthquakes and anthropogenic activities. A comprehensive evaluation of slope stability has an essential theoretical and practical significance. Analysis of slope stability has always been an important research content in the field of geotechnical engineering. It develops in an endless stream in the analysis method currently.

1.2 Methodology

Present study deals with analysis of slopes using Limit Equilibrium Method (LEM)-based software namely Geostudio (Slope/W), Geo-5 as well as Finite Element (FE)-based numerical tool Plaxis 2D. The study has been carried out in two parts. First part deals with analysis of a general homogeneous slope by varying different soil parameters and the second part includes the analysis of case study with slope failure. Suitable remedial measures are also recommended and demonstrated for the slope. The input data required to analyse the case study with slope failure is obtained from previously published paper that is mentioned in the later part. Analysis gives a single value of factor of safety (FOS) which is a ratio of available shear resistance to that required for equilibrium.

2 Parametric Study

2.1 Introduction

Based on the principles of soil mechanics, there are three general groups of parameters which determine the strength or instability of slope such as strength of a soil, geometry of a soil and pore water pressure which includes seepage forces. In this study, our approach is to keep some of the parameters constant and to investigate effects of remaining parameters such as slope geometry, cohesion, friction and variation in groundwater table on slope stability. In this manner, we can understand the effects of various parameters on the stability of slopes.

2.2 Simulation

Series of investigations are performed considering slope having simple homogeneous geometry as shown in Fig. 1. The parametric analysis has been carried out using Slope/W, SV-Slope and Plaxis 2D with phi-*c* reduction approach. To validate and obtain more accurate results, three software was used. The variations of FOS values with different soil parameters are shown in Figs. 2, 3, 4, 5 and 6.

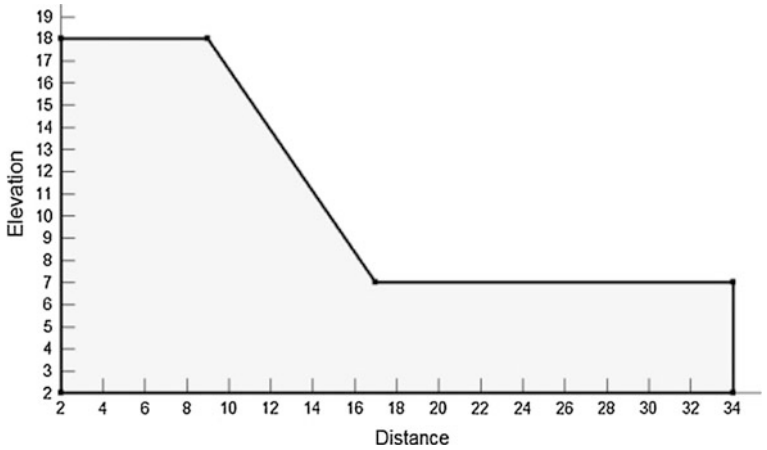

Fig. 1 Slope adopted for parametric analysis

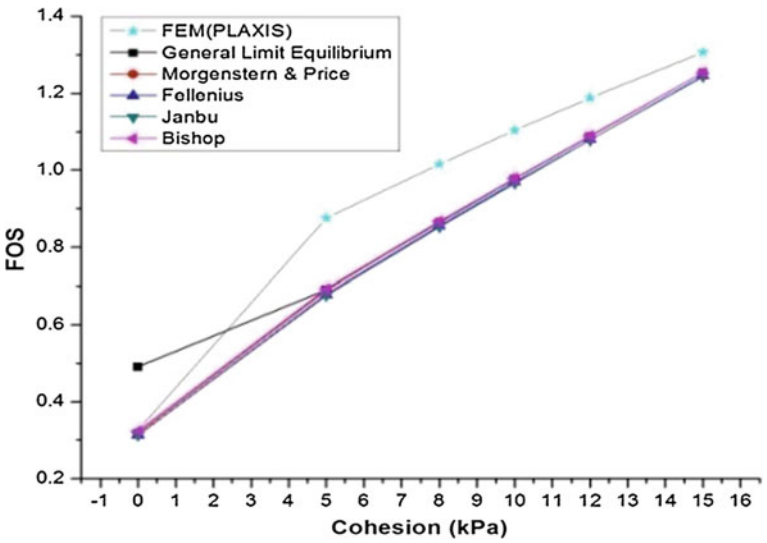

Fig. 2 Variation of cohesion with constant friction angle $\varphi = 25°$ using Slope/W and Plaxis 2D

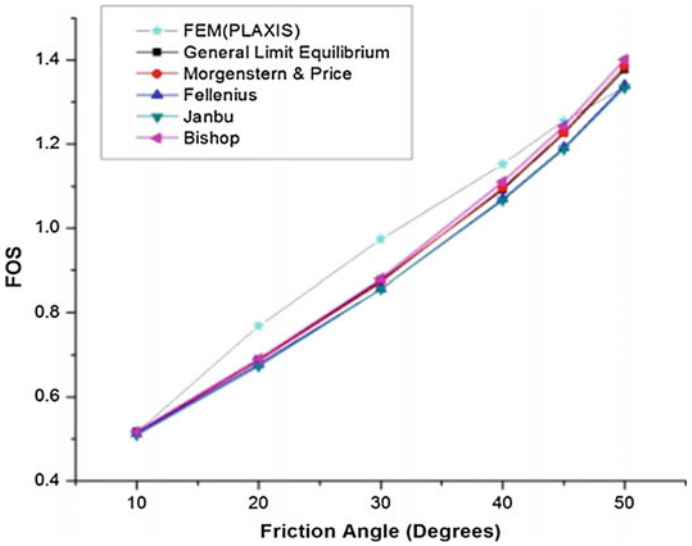

Fig. 3 Variation of friction angle with constant cohesion c = 5 kPa using Slope/W and Plaxis 2D

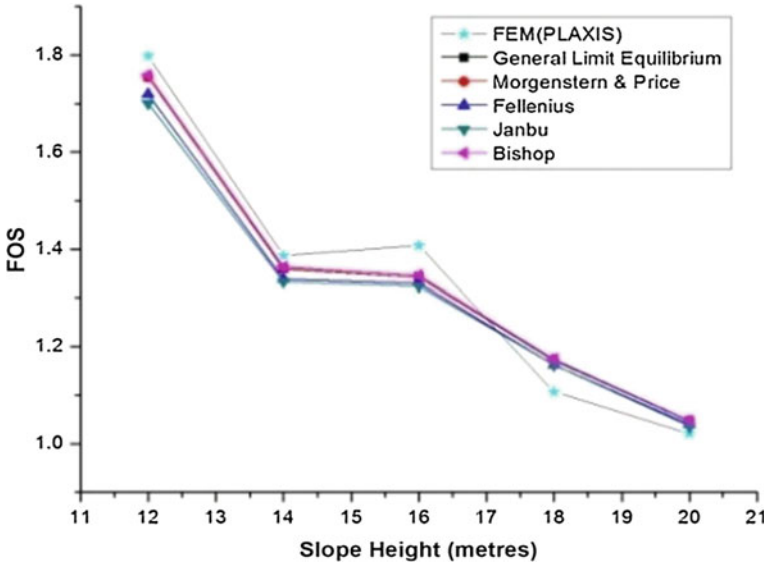

Fig. 4 Variation of slope height with c = 10 kPa, φ = 30° using Slope/W and Plaxis 2D

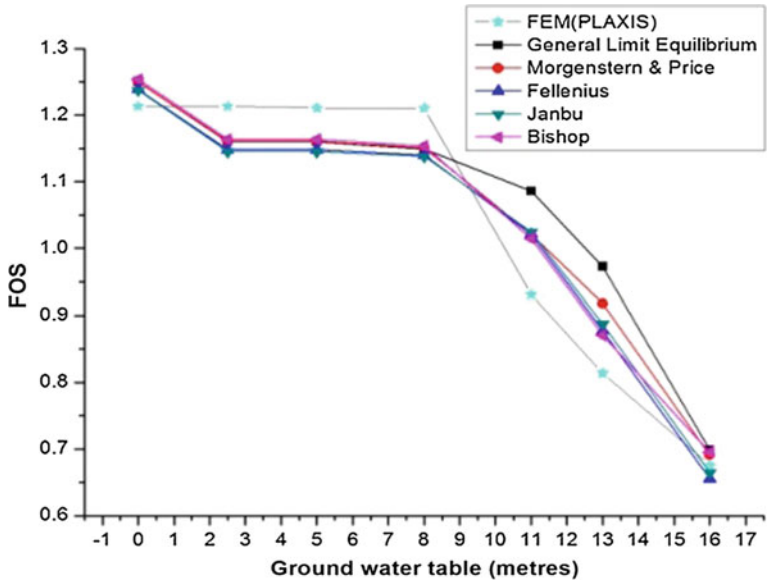

Fig. 5 Variation of groundwater table using Slope/W and Plaxis 2D

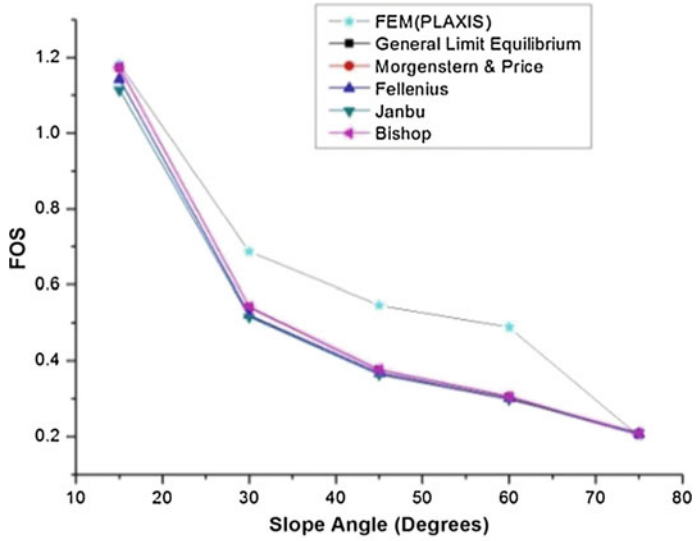

Fig. 6 Variation of slope angle with c = 2 kPa, φ = 15° using Slope/W and Plaxis 2D

The parametric study shows that as the cohesion and internal friction increase, FOS increases but as water table, slope height and slope angle increase the FOS decreases. The FOS varies linearly as the cohesion increases but it is not the same with other parameters like slope height, slope angle, water table and friction angle. The values of FOS obtained from different LEMs such as Bishop, Fellinius, Janbu and Morgesteron price (M-P) methods showed almost same results with less than 10% variations, whereas General Limit Equilibrium (GLE) method tends to over-estimate the FOS. The analysis was also carried out using SV-Slope, and the results were within acceptable limits.

3 Case Study SH72 Mahabaleshwar

3.1 Study Area

The study area is chosen from the previous research work by M. Ahmad et al. 2013, which was focused on State Highway (SH-72) between Poladpur and Mahabaleshwar which is a part of the Deccan traps. The SH-72 connects the famous hill station in Mahabaleshwar, located in Satara district of Maharashtra and lies at a distance of about 120 and 285 km from Pune and Mumbai, respectively. The study area falls between latitude 17° 52′ 30″–18° 00′ 00″ and longitude 73° 26′ 15″–73° 41′ 15″ (Ahmad et al. 2015). The area is prone to weathering action, formation of soils and presence of bole beds in between two consecutive basaltic flows; in addition to this, joints, sub-vertical-to-vertical slopes, heavy rainfalls, etc., lead to slope instability. The area falls under Seismic Zone III. The basalts found in this area are fine-grained, massive and jointed in nature (Kainthola et al. 2012).

3.2 Numerical Simulation

The data required to carry out the analysis of this area is obtained from the previous paper published by Ahmad et al. (2013). They carried out the slope stability analysis using Slide-6 numerical tool. The details are as follows; five different types of soil have been identified on the basis of physical nature and colouration. Through field survey, they have considered a general slope having maximum height as 15 m above the road and the average slope angle of 70°. To assess the impact of five different soils, 4.5 m soil bed on the top of the slope and about 3 m soil layer has been taken above the slope in their study (Ahmad et al. 2015). The five different geo-engineering soil properties are independently applied on the slope as shown in Fig. 7 and analysed using Geostudio and Plaxis 2D. The aim of this study is to analyse the stability of the slope having basaltic soil formations and the effect of these soil on slope stability (Tables 1 and 2).

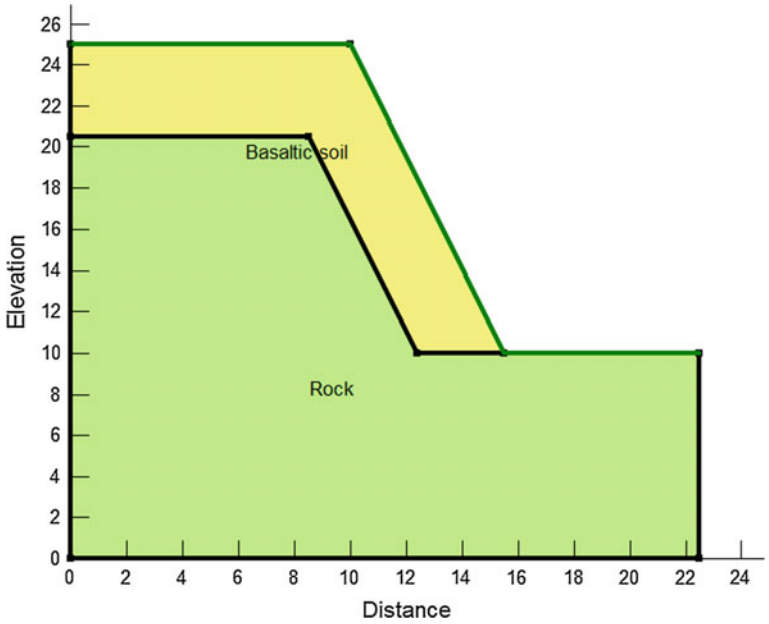

Fig. 7 Geometry of slope

Table 1 Properties of soil

Soil sample	Cohesion (kPa)		Friction angle (°)		Density (kN/m^3)	
	Dry	Wet	Dry	Wet	Dry	Wet
S1	70	35	23	18	18	19.5
S2	44	27	17	13	17.5	18.5
S3	62	83	18	17	19	20
S4	88	52	27	22	22	24
S5	60	31	19	16	19.5	22.5

Table 2 Rock soil sample details

Parameters	Dry	wet
Average density (kN/m^3)	27	28.5
Average cohesion (MPa)	11.6	8.4
Average friction angle (°)	37	30
Average Young's modulus (GPa)	40.1	36.3
Average Poison's ratio	0.24	0.22

3.2.1 Simulation Using Slope/W and Plaxis 2D

The results of slope stability analysis along SH-72 Mahabaleshwar by using Slope/W and Plaxis 2D under dry and saturated condition are given in Figs. 8 and 9.

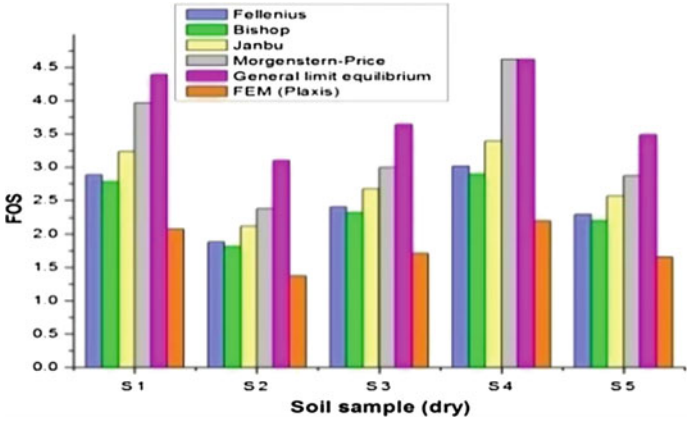

Fig. 8 Simulation using Slope/W and Plaxis 2D under dry condition

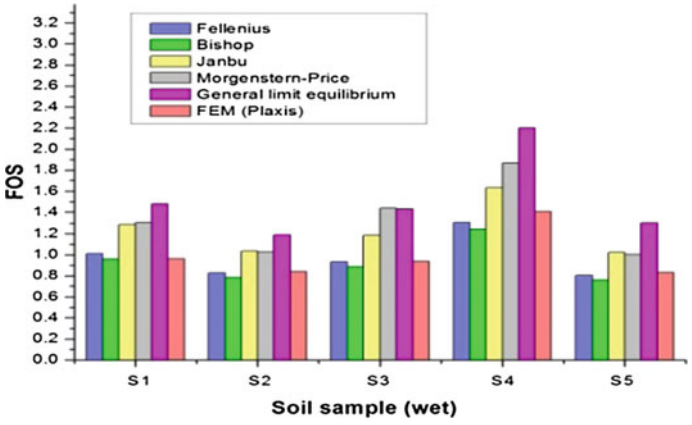

Fig. 9 Simulation using Slope/W and Plaxis 2D under wet condition

The results obtained through the analysis say that the LE methods such as Fellenius, Bishop and FE method showed FOS values with less variation whereas Janbu, GLE and M-P overestimated the FOS values. It is observed that the resultant FOS obtained from the stability analysis is more than 1 for all 5 soil samples under dry condition which implies the slope is stable. In wet condition, the FOS obtained is less than 1 for soil samples S2, S3, S5 which indicates that they are unstable and FOS values are nearly equal to 1 for sample S1 which says it is critically stable. The FOS obtained for soil sample S4 is greater than 1 and is found to be stable.

3.3 Remediation

The highway that is part of study area remains closed due to frequent landslides that occur in small and large slopes during monsoon caused due to heavy rainfall and vibrations produced by the traffic. In the present study, an attempt is made to demonstrate the application of remedial measure (soil nailing) for the mitigation of landslide using LE-based software tool Geo-5 (Nailing). Soil nailing is provided to stabilize the slope with different types of basaltic soils formed due to weathering on the surface of hills. The analysis is carried out for three field conditions, i.e., under dry condition, wet condition and simulation of earthquake (pseudo-static) in dry and wet condition. The horizontal and vertical acceleration coefficients considered for pseudo-static analysis are k_h = 0.15 and k_v = 0.075. Properties of soil nails are nail diameter 25 mm, spacing 1.2 m, yield strength 0.28 MPa, ultimate bond 120 kPa, length 1.5 m. The variation of results for different LE methods for soil samples 1–5 is shown in Fig. 10.

The resultant FOS obtained from slope stability analysis using Geo-5 (Nailing) tool with Bishop Method is around 2–3 after providing soil nailing. The provision of soil nailing is shown in Fig. 11.

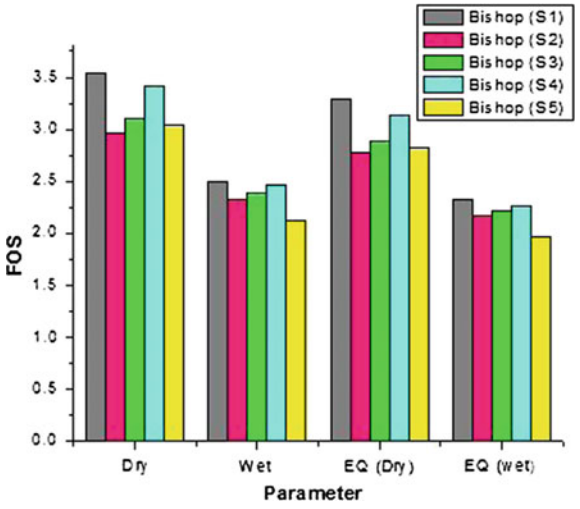

Fig. 10 FOS values after remediation

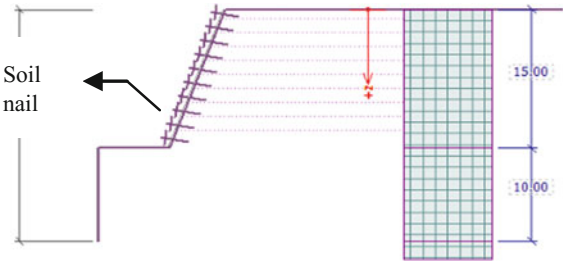

Fig. 11 Provision of soil nailing

4 Conclusions

- The parametric study shows that as the cohesion and internal friction increase, FOS increases, but as the water table, slope height and slope angle increase the FOS decreases. The FOS varies linearly by increasing the value of cohesion, whereas for the other parameters, the FOS does not vary linearly.
- When we compare FOS values using Limit Equilibrium Method and Finite Element Method, later method gives higher FOS values.
- The FOS obtained from Bishop Method and Ordinary Fellinius Method is almost similar, whereas GLE, Janbu's and M-P methods overestimate the FOS values.
- From the analysis of case study, it was found that the slope was unstable or on the verge of failure. Hence to increase the stability of the slope, suitable remedial measure was demonstrated.
- The FOS values obtained after providing remediation were around 2–3 and slopes were found stable.

References

Ahmad, M., Ansari, M. K., & Singh, T. N. (2015). Instability investigations of basaltic soil slopes along SH-72, Maharashtra, India. *Geomatics, Natural Hazards and Risk, 6*(2), 115–130.

Chakraborty, D., & Choudhury, D. (2009). Investigation of the behavior of tailings earthen dam under seismic conditions. *American Journal of Engineering and Applied Sciences*, pp. 559–564.

Fawaz, A., Farah, E., & Hagechehade, F. (2014). Slope stability analysis using numerical modeling. *American Journal of Civil Engineering, 2,* 60–67.

Hamdhan, N., & Schweiger, H. F. (2013). Finite element method-based analysis of an unsaturated soil slope subjected to rainfall infiltration. *International Journal of Geomechanics, ASCE, 13* (5), 653–658.

Kainthola, A., Singh, P. K.,Wasnik, A. B., & Singh, T. N. (2012). Distinct element modelling of Mahabaleshwar road cut hill slope. *Geomaterials, 2*, 105–113.

Rabie, M. (2014). Comparison study between traditional and finite element methods for slopes under heavy rainfall. *Housing and Building National Research Center Journal*, pp. 160–168.

Xue, D., Li, T., & Wei, Y. (2013). Numerical modeling of Giant Badu landslide reactivated by excavation in China. *Journal of Earth and Science Engineering, 2,* 109–115.

A Catastrophe Theory for Planar Sliding Slope

S. Bala Padmaja, G. V. Narasimha Reddy and E. Saibaba Reddy

Abstract For safe design of man-made or natural slopes, stability analysis of slopes is carried out using various conventional methods. In these methods, factor of safety is considered to be greater than or equal to one for stable slopes. Natural disasters like landslides are caused due to sudden and discontinuous phenomenon of slopes failures. But in practice, the failures may occur even when the factor of safety is greater than 1, as in the case of landslides. To overcome these situations, catastrophe theory can be used where conventional stability analysis methods have certain limitations to analyze these types of slope failures. In the present paper, the stability analysis of landslides using catastrophe theory for a mathematical model with planar sliding slope is carried out. Instability mechanism of slope is based on the material stiffness along the sliding slope. Critical factor of safety of the slope depends on the stiffness of the soil medium.

Keywords Catastrophe theory · Stiffness · Landslides

1 Introduction

Landslide is a natural disaster that threatens the human life, property, and restricts socioeconomic development of a local region. Landslide evolution mechanism has been studied to satisfy the increasing demand for disaster mitigation and control. In addition to geologic and geomorphologic conditions, it is the rainfall that was the meteorological cause for landslides or debris flow to occur in many cases.

S. Bala Padmaja (✉) · G. V. Narasimha Reddy
Department of Civil Engineering, JNTUH College of Engineering, Hyderabad 500085, India
e-mail: s.balapadmaja@gmail.com

G. V. Narasimha Reddy
e-mail: gvnreddy@jntuh.ac.in

E. Saibaba Reddy
VSS University of Technology, Burla 768018, Odisha, India
e-mail: esreddy1101@gmail.com

B. Adimoolam and S. Banerjee (eds.), *Soil Dynamics and Earthquake Geotechnical Engineering*, Lecture Notes in Civil Engineering 15,
https://doi.org/10.1007/978-981-13-0562-7_28

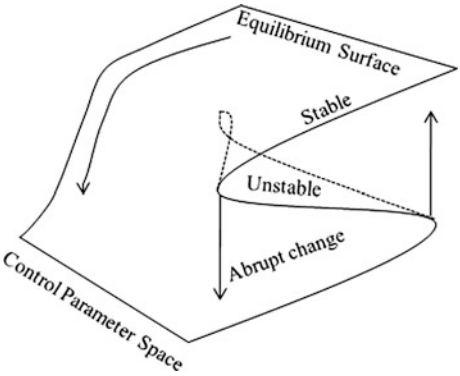

Fig. 1 Cusp catastrophe model

Many methods have been developed for slope stability analysis, but are unable to predict mechanism of catastrophic failures like landslides. Two strange cases of landslides are reported by Qin et al. (2001) where landslide occurs when the factor of safety is greater than one and landslide does not occur when factor of safety is less than one. Catastrophe theory (Rene Thom, 1960) is one of its kinds which describe the sudden and dramatic failure of slopes as in the case of landslides. This mathematical theory studies and classifies the small sudden changes which occur at unpredictable timing and also the magnitude of a landslide. Catastrophe theory can reflect the real situation (Yang et al. 2008) when compared to the limit equilibrium methods. In rock mass stability analysis, the application of catastrophe theory is vastly carried out (Li and Ping 2005; Zhang et al. 2014). The effect of local precipitation and human activity on intensity of landslides is studied using cusp catastrophe theory (Tao et al. 2013). The cusp catastrophe model which is one fundamental type of catastrophe theory was characterized by sudden and smooth changes, divergent and bimodal behaviors, hysteresis, and stability of structure. Among various applications, the cusp catastrophe theory plays a vital role in landslide analysis. In Fig. 1, the cusp model is presented where gradual potential decrease takes place along the smooth equilibrium surface and the control space consists of two control parameters. It is understood from the model that the failure does not occur instantly as soon as the displacement occurs along the failure slope. But, it fails at certain displacement which is defined in the potential function equation of the mechanical model.

2 Landslide Model

A mechanical model of planar sliding slope is considered, which is an inhomogeneous intercalation composed of two media with different strengths, where one media is elastic medium and the other is elasto-plastic medium. Assuming that the

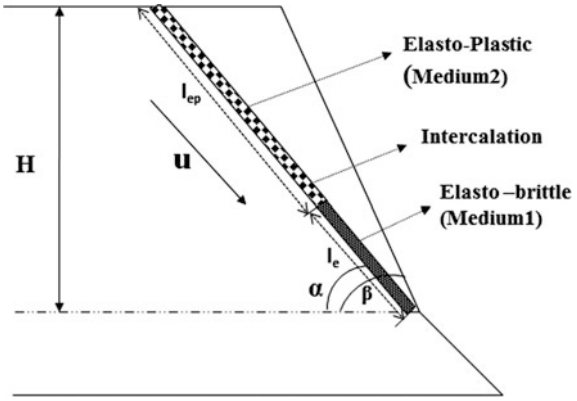

Fig. 2 Landslide mechanical model of planar sliding slope

sliding slope surface is inclined at β with horizontal and the soil mass above a sliding surface is a rigid mass (Fig. 2).

The potential function equation for the mechanical model is developed based on governing equations given by Qin et al. (2001), in which the inhomogeneous intercalation is composed of strain softening medium. In the present paper, instead of strain softening it is considered as elasto-plastic to stimulate a different field condition. The overall potential energy (V) of the system is given by,

$$V = l_{ep} \int_0^u G_{ep} \frac{u}{h} e^{-\left(\alpha \frac{u}{u_o}\right)} du + \frac{1}{2} \frac{G_e l_e}{h} u^2 - mgu \sin\beta \tag{1}$$

where G_{ep} is the initial shear modulus; G_e is the shear modulus; u is displacement; u_o is the displacement value at peak stress (Fig. 3); α is the displacement factor; l_{ep} and l_e are lengths of the sliding surface for the elasto-plastic medium and

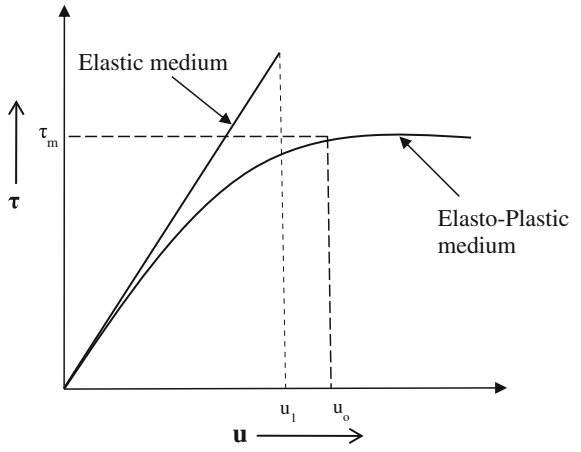

Fig. 3 Shear stress versus displacement curve for two media

elasto-brittle medium, respectively; H is the height of the rock mass, h is the thickness of the intercalation; β is the failure slope angle, and mg is the weight of the rock mass.

From Eq. (1), the necessary cusp condition is derived for displacement ratio (u/u_o) in terms of displacement factor (α) to define the stiffness ratio (k). The stiffness ratio is defined as the stiffness of elastic media to the stiffness of the elasto-plastic media. Stiffness of the soil medium is based on the shear modulus of soil and the lengths of the medium.

$$k = \frac{G_e l_e}{G_{ep} l_{ep} e^{-(\alpha \frac{u}{u_o})}} \tag{2}$$

Stiffness ratio ($k \leq 1$) is the required condition for catastrophic landslide occurrence according to cusp theory. At cusp, the displacement ratio (u/u_o) is assumed to be 2. The critical factor of safety (FS_c) defined by the ratio of the resisting force to the driving force at displacement u is:

$$FS_c = \frac{\left(1 - \sqrt{2}(1-k)^{1/2}/2\right)\left(e^{\sqrt{2(1-k)}} + k\right)}{1 + k - \frac{\sqrt{2}}{3}(1-k)^{\frac{3}{2}}} \tag{3}$$

The factor of safety is based on the stiffness property of soil at failure. The failure mechanism of landslides with critical factor of safety greater than one is discussed in the proceeding section.

3 Results and Discussions

The critical factor of safety (FS_c) depends on the stiffness ratio (k) and the displacement ratio (u/u_o). The effect of various parameters such as lengths' ratio (l_e/l_{ep}) and displacement factor (α) on k is analyzed. Hence, parametric study has been carried out to know the effect of various parameters on critical factor of safety (FS_c).

The displacement factor (α) is used in evaluation of the shear stress of medium 2, to predict soil behavior under various loading conditions, and describes the behavior of the curve after peak stresses. This stress distribution will be more relevant in landslide analysis for field stimulation. In Fig. 4, the variation of shear stresses (t) versus displacement ratio (u/u_o) for different displacement factors (α) is plotted. From Fig. 4, it is observed that as α is increasing the shear stress is decreasing gradually and also decreases with increase in u/u_o. As u/u_o is increasing, it implies that the strain softening of the soil increases, thus increasing the percolation of rainwater affecting the shear stresses.

Figure 5 shows the variation of stiffness ratio with respect to length ratio for various displacement factors (α). The stiffness ratio increases linearly with length ratio and displacement factor. The lengths' ratio (l_e/l_{ep}) depends on the planar

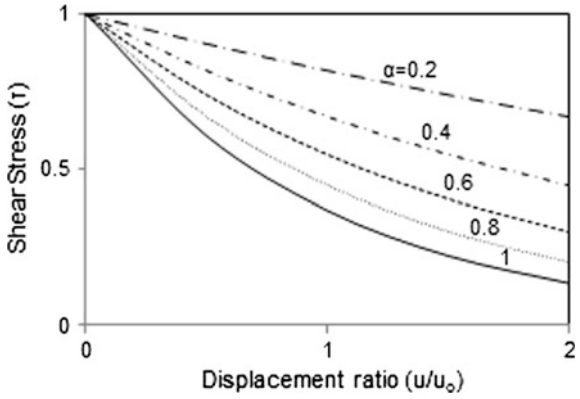

Fig. 4 Shear Stress variation with respect to displacement ratio (u/u_o) with different displacement factors

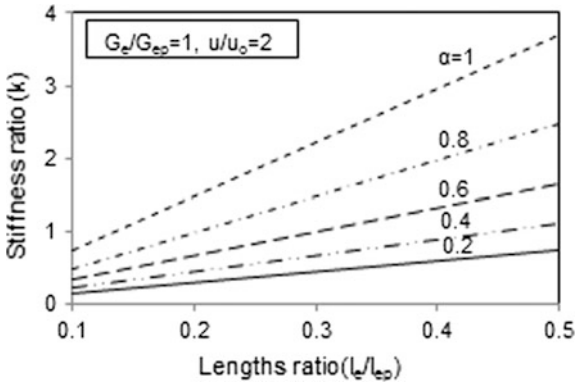

Fig. 5 Variation of stiffness ratio with lengths' ratio for various displacement factors

sliding slope of inclination (b). The increase in l_e/l_{ep} ratio results in increase of stiffness ratio along the sliding plane. According to cusp theory, if $k \geq 1$, the slope is stable. In this graph, $k \geq 1$ at certain l_e/l_{ep} ratio, still slope fails due to seepage of rainwater. In such rainfall-induced landslides, the shear modulus of soil media varies based on the pore water pressure resulting decrease in $k \leq 1$.

Figure 6 shows the variation of stiffness ratio (k) with displacement factor for various length ratios (l_e/l_{ep}) at shear modulus ratio ($G_e/G_{ep} = 1$) and displacement ratio ($u/u_o = 2$). It is understood that as α increases the stiffness ratio decreases nonlinearly and also with decrease in length ratio. The l_e/l_{ep} ratio decreases with increase in length of medium 2 along the intercalation plane making the slope prone to a landslide. The stiffness ratio is directly dependent on l_e/l_{ep} ratio, that is why landslide occurs only when $l_e < l_{ep}$.

The critical factor of safety (FS_c) variation with displacement ratio (u/u_o) for varying α value is shown in Fig. 7. The critical factor of safety decreases with increase in displacement ratio (u/u_o) and α. The increase in displacement ratio is possible when the shear stress along the sliding plane decreases due to various loading conditions. The displacement factor (α) is high for dense soil which

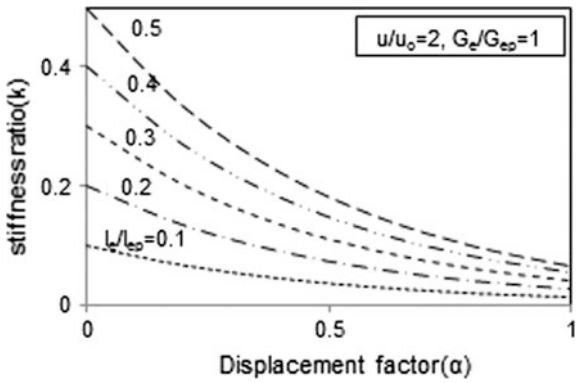

Fig. 6 Variation of stiffness ratio with displacement factor for varying lengths' ratio values

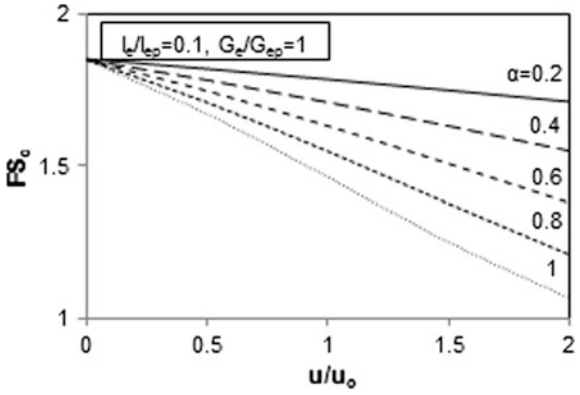

Fig. 7 Critical factor of safety versus displacement ratio for different displacement factor (α) values

indicates that the displacement increases along the failure slope and decreasing the critical factor of safety. Even though the $FS_c = 1.37$, for $\alpha = 0.6$ and $u/u_o = 2$, there is a probability of landslide occurrence according to cusp theory.

In Fig. 8, the effect of length ratio on critical factor of safety for varying displacement factor is studied. It is analyzed that the critical factor of safety (FS_c) is decreasing with increase in length ratio (l_e/l_{ep}) and displacement factor (α). The slope is assumed to be unstable up to an $FS_c = 1.71$ at $l_e/l_{ep} = 0.1$ and $\alpha = 0.2$. But when $l_e/l_{ep} = 0.5$ and $\alpha = 0.2$, the $FS_c = 1.06$, which says that the slope is stable, if $FS_c \geq 1.06$. As the l_e length increases, the maximum shear stresses also increase resulting decrease in the critical factor of safety. The length of the elastic medium (l_e) on the failure plane will increase when the percolation of rainwater is less due to less porosity.

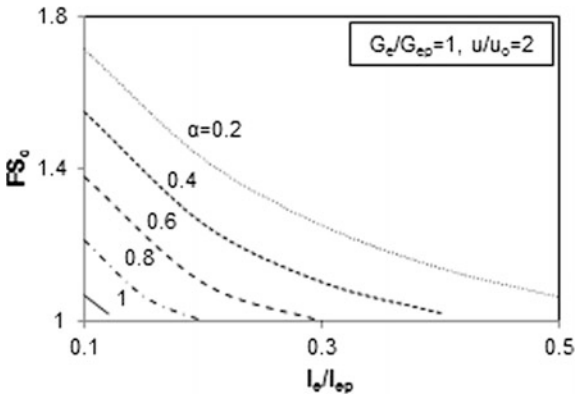

Fig. 8 Critical factor of safety versus length ratio for different displacement factors (α)

4 Conclusions

- The instability mechanism of a landslide using cusp theory gives insight of critical factor of safety, which is based on stiffness ratio and displacement of the sliding plane.
- Using the cusp mathematical model, the displacement criterion is more relevant to field conditions to determine the instability mechanism of the planar sliding slope.
- This method is used to predict the instability of landslides with critical factor of safety greater than one.
- The stiffness ratio increases with increase in l_e/l_{ep} ratio and displacement factor (α). As stiffness ratio is increasing, the critical factor of safety decreases gradually with increasing the stability of the slope structure.

Acknowledgements We are thankful to Professor M. R. Madhav who moderated this technique and guided in carrying out research work.

References

Gilmore, R. (1993). *Catastrophe theory for scientists and engineers*. New York: Dover Publications Inc.

Li, J-T., & Ping, C. A. O. (2005, August). Cusp catastrophe model of instability of pillar in asymmetric mining. *Applied Mathematics and Mechanics, 26*(28). ISSN 0253-4827.

Qin, S. Q., Jiao, J. J., Wang, S. J., & Long, H. (2001). A nonlinear catastrophe model of instability of planar-slip slope and chaotic dynamical mechanisms of its evolutionary process. *International Journal of Solids and Structures, 38,* 8093–8109.

Tao, Y., Cao, J., Hu, J., & Dai, Z. (2013). A cusp catastrophe model of mid-long-term landslide evolution over low latitude highlands of China. *Geomorphology, 187*, 80-85.

Yang, K., Shi, C., & Wang, J. F. (2008). Applying catastrophe theory to slope reliability analysis. In *Boundaries of rock mechanics*. London: Taylor & Francis. ISBN 978-0-415-46934-0.

Zhang, J., Shu, J., Zhang, H., Ren, X., & Qi, J. (2014). Study on rock mass stability criterion based on catastrophe theory (Vol. 2015, Article ID 850604, 7 pages). Hindawi. http://dx.doi.org/10.1155/2015/850604.

Properties of Sand–Rubber Tyre Shreds Mixtures for Seismic Isolation Applications

B. R. Madhusudhan, A. Boominathan and Subhadeep Banerjee

Abstract Disposal of scrap rubber tyres is a big challenge and a serious environmental problem. In India, it is estimated that one waste tyre per person is produced annually. The percentage of recycling is very less when compared to the stockpiling every year. It is widely known that the rubber is a good damping material. Consequently, there is a big scope for the usage of this scrap rubber for earthquake engineering purposes. The present study involves the characterization of sand–rubber tyre shreds mixtures for the application in seismic base isolation of low-rise buildings. The sand–rubber tyre shreds mix is characterized with respect to dynamic properties for various percentages of rubber tyre shreds such as 0, 10, 30, 50 and 100% by weight. In this regard, a series of cyclic triaxial tests were carried out to evaluate strain-dependent moduli and damping of the mixtures. It was found that 10% sand–rubber tyre shreds mixture yielded satisfactory dynamic properties required for seismic isolation of low-rise buildings.

Keywords Sand–rubber tyre mix · Seismic isolation · Shear modulus
Damping ratio

1 Introduction

Since the existing methods of seismic isolation of buildings are very expensive for their use in low-rise buildings, it becomes very important to find alternative ways. Study on sand–rubber mixtures was carried out by various researchers for various

B. R. Madhusudhan (✉) · A. Boominathan · S. Banerjee
Department of Civil Engineering, Indian Institute
of Technology Madras, Chennai 600036, India
e-mail: mssimha1990@gmail.com

A. Boominathan
e-mail: boomi@iitm.ac.in

S. Banerjee
e-mail: subhadeep@iitm.ac.in

B. Adimoolam and S. Banerjee (eds.), *Soil Dynamics and Earthquake Geotechnical Engineering*, Lecture Notes in Civil Engineering 15,
https://doi.org/10.1007/978-981-13-0562-7_29

geotechnical applications like usage as backfill materials in retaining structures (Humphrey et al. 1997; Lee et al. 1999), as construction or fill materials (Edil and Bosscher 1994; Foose et al. 1996; Bosscher et al. 1997; Zornberg et al. 2004). Few studies on this material were carried out keeping in view the protection of buildings from earthquake-induced vibrations (Tsang 2007; Anastasiadis et al. 2011; Senetakis et al. 2011, 2012). As far as dynamic soil properties such as shear modulus and damping ratio are concerned, previous researches are not conclusive on optimum percentage of sand–rubber tyre shreds mixtures yielding satisfactory strain-dependent shear moduli and damping ratios. Hence, it is imperative to find the behaviour of these mixtures under dynamic loading. This paper presents the results of strain-controlled cyclic triaxial tests. The strain-dependent shear moduli and damping ratios for various percentages of rubber shreds mixed with sand are presented. The rubber content which yields better results at large strain levels is also presented.

2 Materials Tested and Testing Equipment Used

2.1 Materials

River sand which is widely used for construction purposes was utilized for experimental investigation. The rubber shreds were derived from scrap tyres of vehicles. The size of shreds adopted was 2 mm and down. The percentages of rubber content adopted were 0, 10, 30, 50 and 100%. These percentages are gravimetric. Particle size analyses were carried in accordance with IS 2720 (Part 4)—1985. The materials are classified as poorly graded in accordance with Unified Soil Classification System and can be denoted by SP. Figure 1 shows the particle size distribution of the materials. Figure 2 shows the rubber shreds.

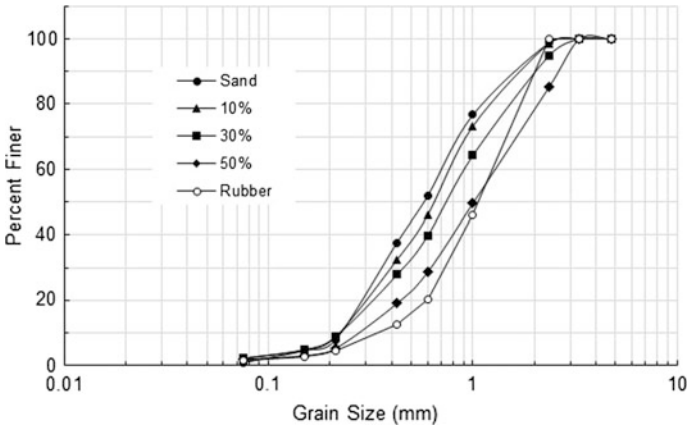

Fig. 1 Particle size distribution curves for sand–rubber tyre shreds mixtures

Fig. 2 Rubber tyre shreds

Table 1 Properties of sand–rubber tyre shreds mixtures

Sand–rubber tyre shreds mixture percentage (by weight)	Property		
	Specific gravity	γ_{dmax} (kN/m^3)	γ_{dmin} (kN/m^3)
0	2.68	17	15
10	2.30	14.1	12
30	1.90	9	7.2
50	1.56	7.5	5.1
100	1.14	5.1	2.7

The specific gravity, the maximum and minimum unit weights of the materials were found in accordance with IS 2720 (Part 3)—1980 and IS 2720 (Part 14)—1983, respectively, and the results are summarized in Table 1.

2.2 Testing Equipment

The cyclic triaxial tests were carried out on sand–rubber tyre shreds mixture specimens using Wykeham Farrance, UK, make servo-controlled advanced cyclic triaxial apparatus available at the Soil Dynamics and Earthquake Engineering Laboratory, IIT Madras (Fig. 3).

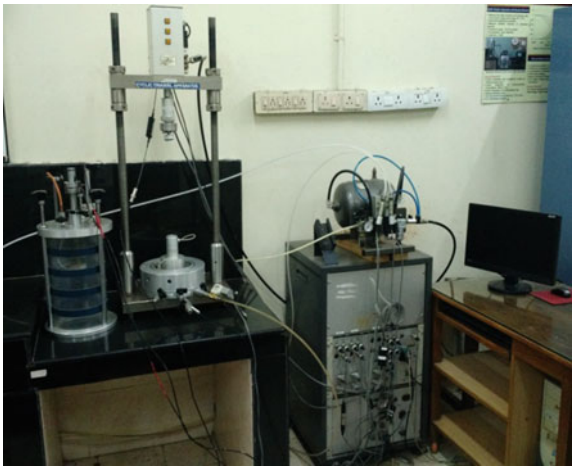

Fig. 3 Cyclic triaxial apparatus

3 Sample Preparation and Testing Methodology

3.1 Preparation of Sample

The samples were prepared by dry deposition and tamping method. The relative density adopted was in the range of 75–85%. The samples were prepared in five layers with each layer given equal number of blows. Since the materials are cohesionless, a vacuum pressure of up to 10 kPa was used as aid for preparing samples. The diameter and height adopted were 50 and 100 mm, respectively, by using vacuum split mould. Figure 4 shows the specimen prepared using the above-mentioned procedure.

3.2 Testing Procedure

The samples prepared were saturated till Skempton's pore pressure coefficient (B-Value) greater than 0.95 was achieved. Then, consolidation was done under an effective confining pressure of 100 kPa. A series of strain-controlled cyclic triaxial tests were carried out under undrained conditions in accordance with ASTM D3999/D3999M-11 (2011). All the tests were carried out at a frequency of 1 Hz with 25 number of loading cycles.

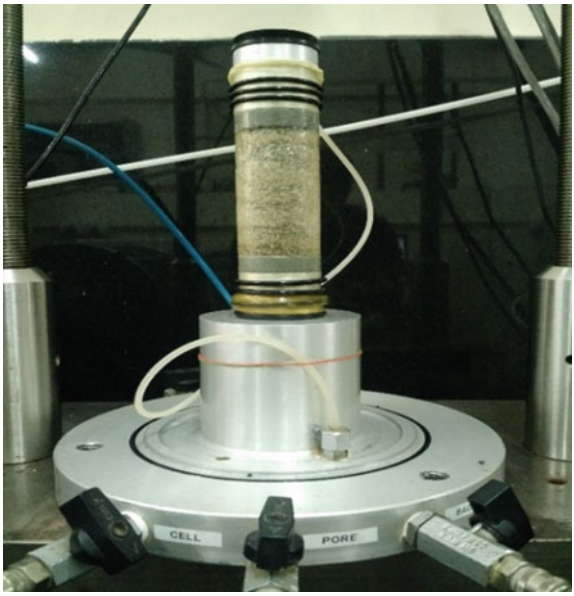

Fig. 4 Specimen prepared from sand–rubber tyre shreds mixture

4 Results and Discussion

Typical hysteresis loops obtained from the cyclic triaxial tests carried out on 50% sand–rubber tyre shreds mixture are shown in Fig. 5. The shear strain (γ) is calculated from the axial strain (ε) using the formula:

$$\gamma = \varepsilon(1 + \mu) \tag{1}$$

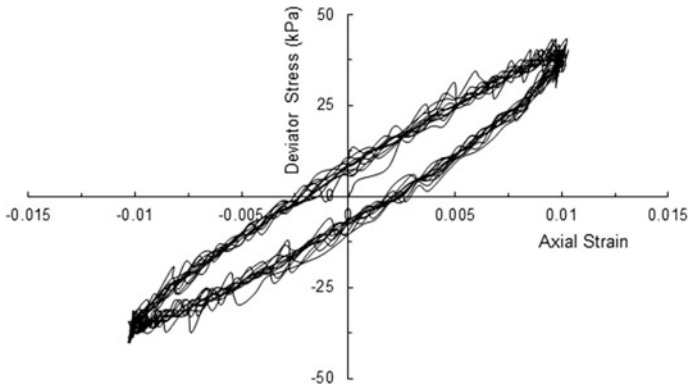

Fig. 5 Typical hysteresis loops for 50% rubber content showing 25 number of cycles at 1% strain

where μ is Poisson's ratio and its value is 0.5 for undrained conditions. The secant modulus (E_{sec}) is calculated by taking the slope of the line joining the ends of the loops. The secant shear modulus (G_{sec}) is calculated by using the formula:

$$G_{sec} = \frac{E_{sec}}{2(1+\mu)} \tag{2}$$

The damping ratio is calculated by using the formula:

$$D = \frac{1}{4\pi}\frac{A_{loop}}{A_{triangle}} \tag{3}$$

where A_{loop} is the area of the hysteresis loop, and $A_{triangle}$ is the area of the triangle (area of the shaded portion in Fig. 6). The shear moduli and damping ratios for all the mixtures were calculated for the fifth cycle.

Figure 7 shows the plot of shear modulus versus shear strain for all the mixtures. As shear strain increases, the shear modulus decreases for all the rubber contents. The modulus reduction is highest for the pure sand and least for the pure rubber. The sand–rubber shreds mixture with 10% rubber content shows higher value of shear modulus in comparison with other mixtures but less than that of pure sand. Figure 8 plots the damping ratio versus shear strain for all rubber contents. It can be observed that the damping ratio increases with shear strain. At any shear strain level, with increase in the percentage of rubber, the damping ratio is decreasing. It is only for the 10% rubber content, the maximum damping ratio is observed at all strain levels. It is intriguing to note that the pure rubber is showing the least damping ratio at all the strain levels. Authors believe that at 10% rubber content, the interaction between the soil and rubber particles is highest and this may be due to the size of the sand and rubber particles adopted for experimental investigation which is very small.

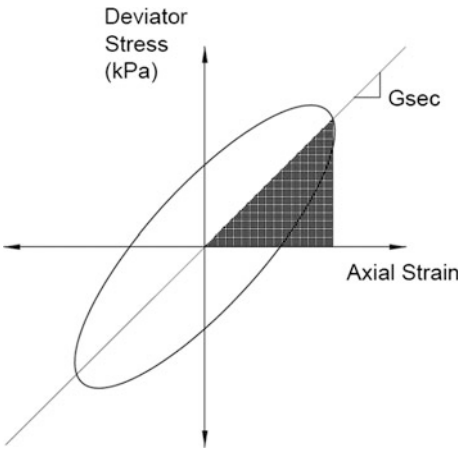

Fig. 6 Schematic diagram of hysteresis loop

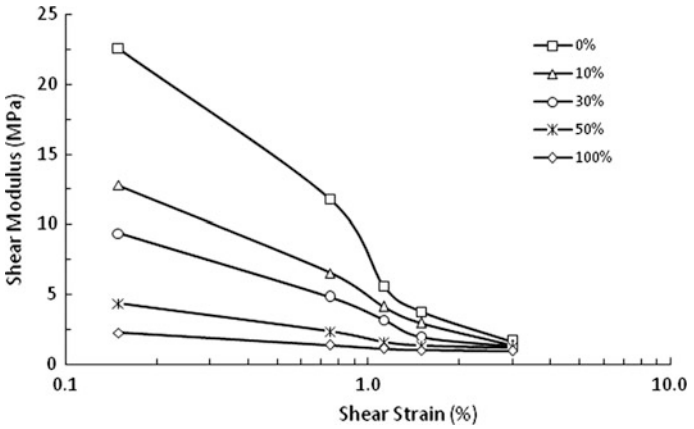

Fig. 7 Plot of shear modulus versus shear strain for sand–rubber tyre shreds mixtures

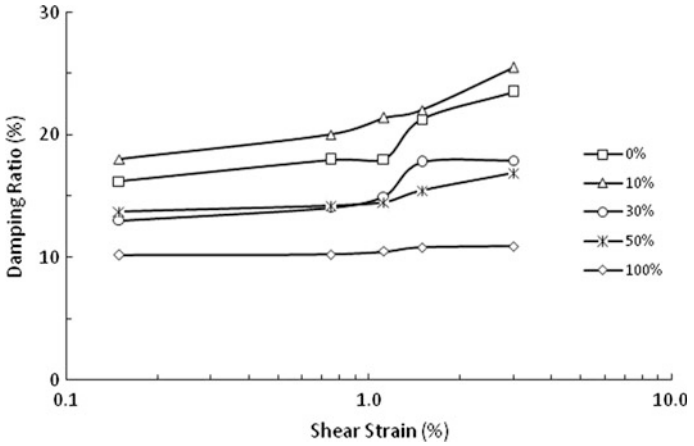

Fig. 8 Plot of damping ratio versus shear strain for sand–rubber tyre shreds mixtures

5 Conclusions

From the experimental study, the following conclusions can be made:

With increase in shear strain, the shear modulus reduces for all the percentages of rubber in sand–rubber tyre shreds mixtures.

The modulus reduction increases with a decrease in percentage of rubber. The modulus reduction is highest for the sand and lowest for the rubber.

The damping ratio increases with increase in strain levels. Lesser damping ratios are observed for higher percentages of rubber. The pure rubber shows least

damping ratio. This behaviour is mainly due to the size of the sand and rubber particles adopted for experimental investigation.

The 10% rubber content by weight shows higher shear modulus and damping ratio values compared to all other percentages. Hence, 10% rubber content possesses satisfactory shear moduli and damping ratios at large strain levels and may be effectively used as a material for seismic base isolation applications.

References

Anastasiadis, A., Senetakis, K., Pitilakis, K., Gargala, C., & Karakasi, I. (2011). Dynamic behavior of sand/rubber mixtures. Part I: Effect of rubber content and duration of confinement on small-strain shear modulus and damping ratio. *Journal of ASTM International, 9*(2).

ASTM D3999/D3999M-11. (2011). Standard test methods for the determination of the modulus and damping properties of soils using the cyclic triaxial apparatus. In *Annual Book of ASTM Standards*. West Conshohocken, PA: ASTM International.

Bosscher, P. J., Edil, T. B., & Kuraoka, S. (1997). Design of highway embankments using tire chips. *Journal of Geotechnical Engineering, 123*(4), 295–304.

Edil, T. B., & Bosscher, P. J. (1994). Engineering properties of tire chips and soil mixtures. *Geotechnical Testing Journal, 17*(4), 453–464.

Foose, G. J., Benson, C. H., & Bosscher, P. J. (1996). Sand reinforced with shredded waste tires. *Journal of Geotechnical Engineering, 122*(9), 760–767.

Humphrey, D., Cosgrove, T., Whetten, N. L., & Herbert, R. (1997). Tire chips reduce lateral earth pressure against the walls of a rigid frame bridge. In *ASCE Technical Seminar on Renewal, Rehabilitation and Upgrades in Civil and Environmental Engineering*.

IS 2720 (Part 3). (1980). *Methods of test for soils: Determination of specific gravity*. New Delhi, India: Bureau of Indian Standards.

IS 2720 (Part 4). (1985). *Methods of test for soils: Grain size analysis*. New Delhi, India: Bureau of Indian Standards.

IS 2720 (Part 14). (1983). *Methods of test for soils: Determination of density index (relative density) of cohesionless soils*. New Delhi, India: Bureau of Indian Standards.

Lee, J. H., Salgado, R., Bernall, A., & Lovell, C. W. (1999). Shredded tires and rubber-sand as lightweight backfill. *Journal of Geotechnical and Geoenvironmental Engineering, 125*(2), 132–141.

Senetakis, K., Anastasiadis, A., Pitilakis, K., & Souli, A. (2011). Dynamic behavior of sand/rubber mixtures. Part II: Effect of rubber content on G/Go-γ-DT curves and volumetric threshold strain. *Journal of ASTM International, 9*(2).

Senetakis, K., Anastasiadis, A., & Pitilakis, K. (2012). Dynamic properties of dry sand/rubber (SRM) and gravel/rubber (GRM) mixtures in a wide range of shearing strain amplitudes. *Soil Dynamics and Earthquake Engineering, 33,* 38–53.

Tsang, Hing-Ho. (2007). Seismic isolation by rubber-soil mixtures for developing countries. *Earthquake Engineering and Structural Dynamics, 37,* 283–303.

Zornberg, J. G., Cabral, A. R., & Viratjandr, C. (2004). Behaviour of tire shred-sand mixtures. *Canadian Geotechnical Journal, 41,* 227–241.